David André Cabrita Nora

The role of lithic raw materials on tool performance and use:

The efficiency and durability on stone tools edge.

A importância das matérias-primas líticas no seu desempenho e uso:

Eficiência e Durabilidade no gume das ferramentas em pedra lascada.

UAlg FCHS
UNIVERSIDADE DO ALGARVE
FACULDADE DE CIÊNCIAS HUMANAS E SOCIAIS

Faro, 2021

David André Cabrita Nora

The role of lithic raw materials on tool performance and use:

The efficiency and durability on stone tools edge.

A importância das matérias-primas líticas no seu desempenho e uso:

Eficiência e Durabilidade no gume das ferramentas em pedra lascada.

Master in Archaeology

Work carried out under the supervision of:

Doctor: Vera Aldeias

Doctor: João Marreiros

UAlg FCHS
UNIVERSIDADE DO ALGARVE
FACULDADE DE CIÊNCIAS HUMANAS E SOCIAIS

Faro, 2021

The role of lithic raw materials on tool performance and use: The efficiency and durability on stone tools edge.

A importância das matérias-primas líticas no seu desempenho e uso: Eficiência e Durabilidade no gume das ferramentas em pedra lascada.

Declaration of authorship of work

I declare to be the author of this work, which is original and unpublished. Consulted authors and works are duly cited in the text and are included in the list of references included.

ABSTRACT

Understanding and identifying the use of stone artifacts found in the archaeological record has long been one of the main focus on the study of lithic technology. Thus, investigating the use of stone tools is critical for interpreting and reconstructing the prehistoric subsistence and behavioural patterns in archaeological investigation.

The evaluation of the physical and mechanics principles underlying the question of why a particular rock type is preferred over another for the production and use of stone tools, or questions regarding the interaction between the acquisition of a particular type of lithic raw material to obtain a flake with a sharper edge was one of the main daily decision-making processes of past hominins. So, this type of action suggests predisposed know-how of lithics raw materials behave.

Although not fully understood, several studies have shown that the relationship between the properties of lithic raw material and the use of stone tools has been shown to be directly related.

The aim of this master's thesis is therefore to explore the interaction between the use of stone tools by prehistoric populations and their adaptability to different raw materials, using two distinguished groups coarse-grain and fine-grain rock types as main evidence. All lithic raw materials were evaluated by an experimental design regarding their efficiency and durability. At the same time, a methodology combining experimental replication and material analysis to address this issue will be presented and proposed.

The controlled experimental program conducted in this thesis was designed to determine the efficiency and durability of four lithic raw materials - quartzite, flint, obsidian, and dacite. This work builds on a preliminary experiment by Pedergnana et al., 2019, which investigated the use of flint and obsidian in scraping movements. Following the initial observations made by Pedergana and colleagues, the present study aims to take the next step by introducing greater variability of raw materials and a new motion, cutting against a new contact material (wood). The experiment is conducted using a mechanical device (SMARTTESTER®) that mimics the human cutting motion, in this particular case a bidirectional longitudinal movement. The experimental plan is divided into three phases: 1) Characterization of the raw material, 2) Experiment that mimics the cutting process and quantifies the number of variables, 3) Data

analysis to nullify the null hypothesis "*efficiency does not vary according to the different lithic raw materials*".

The ability to bring new quantifiable data to consider efficiency and durability of stone tools shows that the methodology used is suitable to address these issues and can be expanded to other research questions. The results presented show that all lithic raw materials reveal their efficiency in performing a cutting movement in pine wood in the first 250 strokes. Flint proved to be the most resistant lithic raw material tested in this experiment, being the most durable and efficient after 1000 strokes. Quartzite showed a fragmentation pattern, while obsidian, being a very brittle raw material, likely shows a relationship with a technological feature in his reduction when performing bidirectional movements in wood. Dacite proved to be a good substitute for flint due to its homogeneous hardness values and consistent performance after passing through all cycles.

The development of the work described in the above phases will allow to understand and quantify the efficiency and durability of each lithic raw material. These data can contribute to various topics in lithic studies, such as edge durability, reduction sequences, retouch intensity, and raw material sourcing and optimization strategies. Furthermore, this study aims to integrate a free database on an open-access platform to compare the obtained results with stone tools from other archaeological sites. As a possible case study, Kalavan 2 a Middle Paleolithic open-air site with an assemblage composed of obsidian, chert, basalt, limestone, and welded tuff associated with woodworking by use-wear studies is included in the discussion of this thesis as an example of continuous work on this topic.

Keywords: Experimental Archaeology, Controlled experiments, Lithic raw materials, Stone Tool Edge Performance, Efficiency, Durability.

RESUMO

Compreender e identificar os desígnios dos artefatos em pedra lascada recuperados do contexto arqueológico têm sido ao longo do tempo o objetivo principal para os especialistas em tecnologia lítica. O estudo do uso das ferramentas em pedra, é um processo fundamental para a construção de inferências sobre o passado pré-histórico, seja na compreensão de padrões de subsistência de uma comunidade ou apenas como identificação de padrões comportamentais gerais do passado.

Na avaliação das características físicas e mecânicas acerca das matérias-primas líticas estão subjacentes questões como o porquê de certo tipo de pedra ter sido escolhido em detrimento de outra, para a produção e o uso, ou questões sobre a interação da aquisição de um tipo específico de matéria-prima para a obtenção de uma lasca com um gume cortante. Todo este tipo de ação pressupõe um exercício mental lógico, este exercício é interpretado pelos arqueólogos como um testemunho direto do desenvolvimento do comportamento humano.

Especificamente, uma relação direta tem vindo a ser construída entre o comportamento humano do passado e as propriedades das matérias-primas, contudo, esta nem sempre é compreendida, por falta de testagem e de quantificação que permita construir inferências com base uniformitárias.

De tal modo, o objetivo desta dissertação passa por contribuir para o tópico da interação entre o uso das ferramentas em pedra e as populações do passado, e a sua adaptabilidade, por meio da eficiência e durabilidade de quatro matérias-primas líticas, quartzito, sílex, obsidiana e dacito. Este trabalho assenta os seus alicerces num trabalho experimental preliminar elaborado por Pedergana et al., 2019. O estudo preliminar procurou caracterizar a performance do sílex e da obsidiana em movimentos de raspagem em osso sintético. Com base nas observações construídas por Pedergana e colegas (2019), o presente estudo foi desenvolvido como intuito de testar uma maior variabilidade de matérias-primas e um novo movimento, a ação de cortar, bem como a matéria de contato, madeira. O trabalho experimental, têm como principal eixo o uso de um aparelho mecânico (SMARTTESTER®), desenhado especificamente para imitar a ação humana, neste caso particular a ação de cortar num movimento linear bidirecional. O plano experimental para compreender a influência das matérias-primas neste tipo de ação foi divido em três fases: a) Caraterização das matérias-primas, b) Plano Experimental c) Analises de

dados. Este plano experimental tem como principal objetivo a falsificação da hipótese nula "*eficiência varia de acordo com as diferentes matérias-primas líticas*".

A capacidade desta dissertação ao introduzir novos dados quantitativos para a perceção de como a eficiência e a durabilidade, podem ser abordadas no estudo das ferramentas em pedra, é indicativo de que a metodologia aplicada, pode ser considerada como valida. Os resultados indicam que todas as matérias-primas se revelam eficazes ao executar um movimento bidirecional linear na madeira nas primeiras 250 repetições. Contudo o sílex revela ser a matéria-prima mais resiliente testada neste plano experimental, mantendo a durabilidade e eficiência após aplicadas 1000 repetições. O quartzito demonstrou um alto padrão de fragmentação, enquanto a obsidiana sendo a matéria-prima mais quebradiça, revelou uma possível relação com uma estratégia de redução do gume, na interação com a madeira. O dacito revelou ser um bom substituto do sílex, devido à sua homogeneidade da dureza bem como a consistência da performance ao concluir todo o ciclo experimental.

O desenvolvimento deste estudo, possibilita um melhor entendimento referente à durabilidade e eficiência as matérias-primas líticas bem como quantificar as variáveis em estudo. Este tipo dados quantitativos e qualitativos tem a possibilidade de contribuir para o entendimento de toda a cadeia operatória das ferramentas em pedra, tais como performance dos gumes, esquemas de redução, graus de retoque, estratégias de aquisição e otimização de matérias-primas, marcas de uso bem como estudos funcionais, ou descarte.

Não sendo o objetivo principal desta dissertação, um possível caso de estudo é apresentado na discussão como um exemplo de aplicação deste tipo de trabalho experimental. Kalavan 2 é um sítio de ar livre do Paleolítico Médio composto por um conjunto lítico em obsidiana, sílex, dacito, calcário e tufo soldado, associado ao trabalho em madeira por estudos de uso e desgaste. Este trabalho pretende incorporar este tipo de dados numa base de dados de acesso livre, para possíveis comparações com artefatos em pedra de diferentes sítios arqueológicos.

Palavras-Chave: Arqueologia Experimental, Experimentação Controlada, Matérias-Primas Líticas, Eficiência, Durabilidade, Ferramentas em Pedra, Performance dos Gumes.

Table of Contents

List of Figures

List of Tables

Chapter1 INTRODUCTION

Stone implements are the most diverse, and abundant artifact from the paleolithic archaeological record, and are the majority body of information about the origins and developments of prehistoric technological systems. Stone tools recovered from archaeological sites give primary information about raw material acquisition, tool production, design, and use. Therefore, the characteristics coming from these implements make the possibility to infer about major processes that marked the evolution of human behavior through time. For instance, the variability of lithic raw materials present in the archaeological record, in general, are associated and seen as a reflex of different human behavioral strategies, such as environmental adaptations (Robinson & Sellet, 2018), cultural actions (Bordes, 1971), cognition (Mcbrearty & Brooks, 2000), and function (Semenov, 1964).

It is argued that raw material is a crucial variable in the production and use of stone tools, influencing technological variations and thus the composition of the assemblage. The development of more accurate analyses of prehistoric technology and tool performance requires a better knowledge of key physical/mechanical properties. This is particularly true for the study of use-wear traces, the intensity of retouch, or even reduction sequences, where knowledge and description of the physical variability of lithic raw materials are fundamentally linked to the origin and interpretation of features identified on stone tools. For example, identifying and quantifying different types of rock properties that are likely to affect the formation of particular forms of damage could provide greater insight into the formation of use marks and improve interpretation.

Hence, the last decades have seen an effort by the research community to come with methodologies towards quantification, standardization, and calibration for identifying mechanical properties of the lithic raw materials to better understand their variability in the archaeological context. These include internal properties (hardness, brittleness, density, microstructure, grain size), and external properties, give reference to the tools' shape, size, surface, among others (Brantingham et al., 2000; Domanski et al., 1994; Goodman, 1944; Goudie, 2006).

However, the question of why humans produce, design, and use different types of stone tools in the past (raw materials and forms) is still not totally understand. Primarily, the choice of different raw materials may be limited by their availability and frequency in the landscape

(Andrefsky, 1994; Brantingham et al., 2000; Goodyear, 2021; Hiscock, 1986; Kuhn, 1992). Secondly, different raw materials are known that behave differently in a given task and against a given worked material due to their specific mechanical properties. Nevertheless, material properties and physical characteristics are rarely tested and considered when designing experiments in functional research, even though they are often considered a crucial element (Evans, 2014).

However, few studies aim to answer scientific questions about the performance, efficiency, and durability of stone tools and the direct relationship between the different lithic raw materials and the outcome. For example, a mechanized experimental study on raw material as a functional variable showed significant differences in resistance to edge abrasion for different raw material properties. For isotropic and microcrystalline materials, use-wear was found to occur by regular edge scarring, whereas for granular materials, gradual use-wear of individual grains was observed (Greiser, 1979). Or to quantify efficiency based on different edge morphologies and angles (Collins, 2008; Key & Lycett, 2015). However, few studies aim to answer scientific questions about the performance, efficiency, and durability of stone tools and the direct relationship between the different lithic raw materials and the outcome. For example, a mechanized experimental study on raw material as a functional variable showed significant differences in resistance to edge abrasion for different raw material properties. For isotropic and microcrystalline materials, wear was found to occur by regular edge scarring, whereas for granular materials, gradual wear of individual grains was observed (Greiser, 1979). Or to quantify efficiency based on different edge morphologies and angles (Collins, 2008; Key & Lycett, 2015).

Terms such as performance, efficiency, and durability are frequently mentioned in this study, so an explanation of these terms must be established before further examination. Several connections can be made between the three terms, which is the reason why they usually occur together in the literature. Performance can refer to the successful completion of an action and this is where the first link is found, as performance can be measured by two factors, effectiveness and efficiency, although effectiveness is not synonymous with efficiency. Effectiveness (also known as efficacy) is a metric that describes the theoretical relationship between goal achievement and a predefined objective. Efficiency is more of a practical relationship between output and outcome (benefits and costs), an indicator of the resources used to achieve a goal. Related to efficiency comes durability, an indicator of the usefulness of a

product over time. The concept refers to the ability of an object or an induvial to maintain a function over time. Durability can be affected by wear and tear or natural factors such as age, environmental exposure factors, and others (Collins, 2007; Schunk, 2021).

So, these concepts can be used in this study as follows: Performance refers to how well the sample performed the task, in this case cutting pinewood, measured by efficiency and durability. Efficiency is measured by comparing two factors: the time (cycles) and the depth of penetration of each sample into the pine wood. Durability is measured by the depth of penetration compared to the edge damage of each sample when it makes a bidirectional movement into the pinewood under the same conditions.

So is the purpose of this dissertation to investigate the differences in efficiency and durability of different lithic raw materials representatives of the two main groups of rocks identified in the archaeological record: fine and coarse-grained. To address these two issues in an experimental approach, the falsification of the null hypothesis "efficiency does not change according to changes on lithic raw material" was considered.

Therefore, to understand the suitability and how different types of rock behave on a given action it is fundamental to develop experimental replications. This exercise will also help to understand how rocks differentiate from each other, in terms of stone tool use, and how this could have influenced past human decisions.

This study builds on a preliminary experiment designed by Pedergana et al. 2019, which looked at flint and obsidian used on scraping movements.

Pedergana and colleagues conclude as preliminary results that obsidian have a superior efficiency compared to flint in terms of material removal. There is also an increase in edge reduction due to microfracturing, which gives obsidian the ability to remove target material up to 1300 strokes. Edge reduction in flint is considered minimal, which could indicate better durability, but the authors found overall target material removal to be worse than obsidian, suggesting that flint dulls more quickly and is, therefore, less efficient.

These preliminary results and their possible interpretations, showing that microfracturing affects the durability of the cutting edge and, directly, efficiency in obsidian and that flint, for example, behaves differently, were the basis for further research on this topic, not only to quantify the events but also the introduction of more raw materials.

Therefore, the present study aims to take the next step by introducing a wider variability of raw materials and a new movement, cutting. The experiment was performed with the support of a mechanical device (SMARTTESTER®), created to mimic human actions of cutting, in this particular case, a longitudinal bidirectional movement. The experimental design is organized in three stages:

1 - Characterization of the raw materials regarding variables such as hardness, sample morphology, and a macroanalysis.

2 – Controlled Experiments; mimic replication of the cutting action, quantifying the number of movements, velocity, direction, vertical weight, and sample morphology (edge angle, edge topography, removed material).

3 – All the collected data and results will be imported to a statistic program to test the null hypothesis, "*efficiency does not vary according to the different lithic raw materials"*.

The development of the work described above is divided into 6 main chapters. Following this chapter, the state-of-the-art (Chapter 2), starts with a narrative about experimental archaeology and its division into experiments (first generation, second generation, and third-generation experiments). This is followed by an account of the importance of lithic raw materials in experimental approaches, introducing topics such as efficiency, durability, and edge reduction, and ending with a brief description of the framework of the thesis.

Chapter 3 is considered one of the most important chapters of this thesis, as it provides a detailed explanation of all the methods used in the three phases of the study, as well as a reference to the samples used in the experiments and an explanation of the experimental design.

The description of the results is given in Chapter 4, where all the graphical results of the tridimensional procedure are introduced and explained, as well as the values of all the sensors selected for this experiment.

The discussion takes place in Chapter 5. Here the results presented in the previous chapter are compared with each other and correlations between cause and effect of efficiency and durability of each raw material are shown as far as possible. Also, the falsification of the null hypothesis "efficiency does not change according to changes on lithic raw material".

Furthermore, this study aims to integrate a database on a freely accessible platform to compare the obtained results with stone tools from archaeological sites. In advance of this study, although it is not the main objective, an attempt is made to treat an archaeological site, Kalavan

2 (Malinsky-Buller et al., 2021) as an example of the possibilities that a study of this type can contribute to the understanding of some, unexplained events of the *chaîne-opératoire* of stone tools.

Kalavan 2 is a Middle Paleolithic open-air site that preserves evidence of multiple occupations by Middle Paleolithic hunter-gatherers (ca. 60-45 ka.) at 1640 m asl in the northern slopes of Areguni Mountains, ca. 8 km north of the northern shore of Lake Sevan and 70 km northeast of Yerevan, Armenia in Figure 1. These archaeological site counts with high-resolution analyses, from chronology based on X-Ray Fluorescence (pXRF) elemental analyses, tephra and luminescence (pIRIR) dating analyses, to paleovegetation proxies - pollen and leaf waxes - analysis to better characterize the environment during Middle Paleolithic occupation. In terms of lithic analysis, two points were key to the selection of this archaeological site as a possible case study. It was noted that in all units obsidian artifacts outnumber non-obsidian ones and that the non-obsidian components show a wide variety, including basalt, dacite, welded tuff, chert, and limestone. The other reason is what the authors called shaping flakes. These types of flakes are < 2 cm in size and are categorized by the scars on their backsides that remove the previous stages of retouch. The authors have therefore attempted to come with possible solutions, one of which states that shaping flakes were likely diverse and may reflect part of the initial stages of retouch or secondary retouch after use when the edge has become dull, jagged, or uneven. These technological signatures reflect maintenance behaviors intended to extend tool use life. In addition, obsidian retouched points and shaping flakes show signs of use-wear that may indicate activities associated with woodworking (Malinsky-Buller et al., 2021)

As explained above, the experimental work conducted in this thesis aims to test a variety of lithic raw materials (including some of the rock types presented in Kalavan 2) in a control setup to address edge efficiency and durability against a contact material (pinewood). Therefore, the results of this experiment can help build a more consistent argument about the use of lithic raw materials in Kalavan 2 and understand patterns of damage that may cause past hominins to adopt different technological solutions.

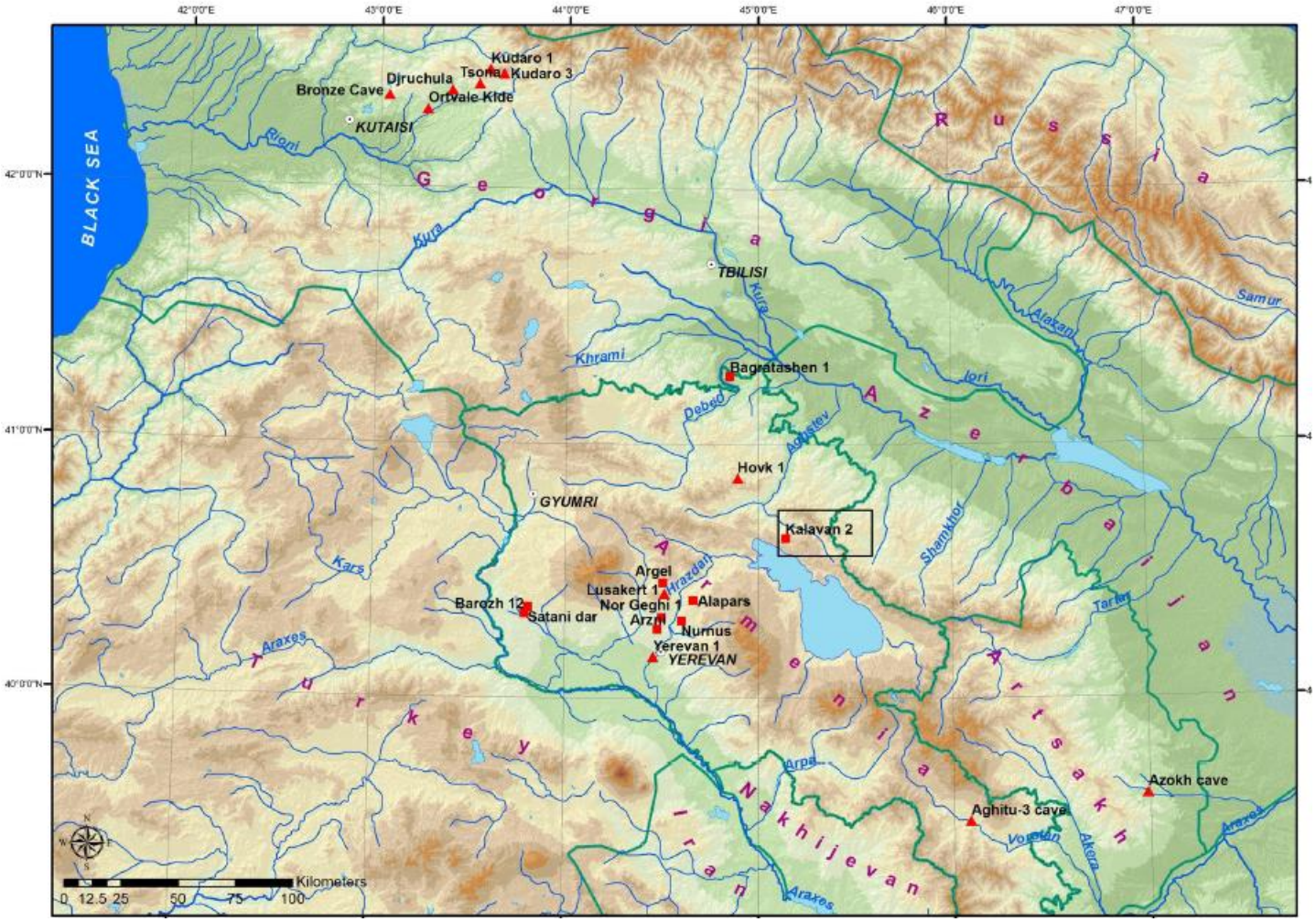

Figura 1: Location map of Kalavan 2 within southern Caucasus and north-eastern Armenian highlands showing main Lower, Middle, and Upper Paleolithic sites

Chapter2 STATE-OF-THE-ART

2.1 Experimental Archaeology

One of the main goals of archeology as a science is to analyze and understand the evolution of human behavior by formulating inferences that allow us to reconstruct the past. The assumptions of archeologists mostly depend on definitions, concepts, and interpretations obtained from ethnographic or empirical observations as well as hypothesis testing (Binford, 2019). As a result, when analyzing the archaeological record, the body of evidence used to explain the evolution of human behavior is largely based on experimental replication of possible past human actions (Eren et al., 2016; Lin et al., 2018; Miller, 1982).

The introduction of a combined series of events on the theoretical and conceptual discussion on the archaeological research, such as the introduction of the "New Archaeology" Caldwell (1959), the revision of Ascher (1961), on how to conduct experiments, the logic of science presented by Popper (1959), and the paper "The Structure of Scientific Revolutions" presented by Kuhn (1962), lead to the emergence of the so-called hypothetico-deductive approach in archaeology. In this case, experiments are conducted in which a hypothesis is developed and then tested to determine whether it can be proven or disproven. If a hypothesis proves to be false, it must be replaced by a new, possibly better hypothesis, which is also aimed to be tested. A hypothesis can be considered valid if it cannot be falsified and is supported by the results of the experimental replication. However, in this context, the term "valid" does not mean "true," but rather that the principles of the hypothesis can be used until they are disproved and replaced by a better set of principles (Lin, 2014).

The use of experiments as the main proxy for archaeological interpretation is not a new concept. Archaeological experimentation have been applied to a wide range of topics, but they all revolved around two main themes: determining whether certain objects were natural or man-made, and determining the use of certain artifacts or types of artifacts. Barnes (1939), Clark (1958), Moir (1912), and Warren (1914) are names associated with the onset of experiments focused on the distinction between natural objects and anthropic artifacts, while Sonnenfeld (1962) and Semenov (1964) are names associated with tool use. Ascher (1961) referred to the latter type of experiments as 'imitative experiments," which are conducted with the intention

that the researcher imitates the behavior of the archaeological assemblage under study and thus contribute to the interpretation of the archaeological material.

In recent decades, several researchers have emphasized the primary limitations of archaeological experiments, which can be summarized and grouped as follows (Eren et al., 2016; Lin, 2014).

(a) Lack of clear research questions, including hypothesis and assumptions to be tested;

(b) Alternative hypotheses are rarely tested;

(c) Insufficient information about the material and methods used;

(d) Lack of clear identification, organization, and definition of the control samples and manipulation of the different variables;

(e) Coexistence of confounding variables related to the presence of multiple variables;

(f) Insufficient information about the material and methods used;

While some of these limitations in experimental replication should be addressed to improve the discipline, others can only be attributed to different hierarchical levels of experiments based on the main objective and research questions, which strongly influence the organization, planning, and design of experiments. Structuring and planning experimental designs is crucial not only to distinguish between strong and weak abductive conclusions but also to serve as a basis for others. Experiments should employ controlled and repeatable methods to evaluate the validity of a hypothesis from a scientific standpoint. Experiments are considered reliable (high internal validity) if they can be repeated and their parameters and variables can be controlled and changed as needed and in a variety of ways. (Lin, 2014; Marreiros, et al., 2020).

From this discussion, the distinction of different ways of thinking in experimental archaeology created space for new classifications of experiments, such as "actualistic", "pilot" or "exploratory", and "controlled", "second generation" or "laboratory" experiments. For simplification, Marreiros and colleagues (2020) advocate the use of first and second-generation experiments, respectively, and add a third-generation, which aims at testing the models created in the second-generation experiments, taking into account the human variability on the design of the experiment and its expected outcome. The use of this terminology should allow a better perception of the different levels, but also the complementary nature of all approaches, which should be combined when planning and designing experiments.

2.1.1 First-Generation Experiments

First-generation experiments are critical for generating new hypotheses and concepts, and for determining the most important factors to test as individual predictors of the outcome. In addition, these tests are critical in gaining initial insights into the efficiency and durability of tools and in evaluating the suitability of particular tools for performing a particular task. Since experiments require time and resources, these insights are also crucial for optimizing planning, cost, and schedule, as key issues can be selected and prioritized, and experiments can be merged. In this situation, first-generation experiments are expected to provide valuable insights into our understanding of the technology to date. Mechanical devices are largely neglected in first-generation experiments where researchers reproduce potential past technologies and evaluate archaeological tool reproductions. In this situation, it is crucial to evaluate the variability of the archaeological record by inferring, for example, the suitability of different raw materials for a particular function (Marreiros et al., 2020). Studies such as (Gibaja et al., 2011; (Aldeias et al., 2019) are examples of first-generation-experiments.

2.1.2 Second-Generation Experiments

Second generation experiments use more elaborate designs. This is due to the nature of the multiple variables used to try to answer more fundamental questions about some key elements of the archaeological record, such as the variety of rocks used to make stone tools. This strategy does not aim to provide a direct answer to the entire perspective of a research project, but rather to construct units of analysis and measurement. Unlike first-generation experiments, second-generation experiments, are based on concepts that are not only independent of the archeologist's interpretations but also on uniformitarianism laws, i.e., physical principles that behave uniformly in space and time. Since most experimental designs incorporate multiple variables, and first-generation experiments aim to identify the most significant factors, they must be examined independently in order to evaluate and analyze their influence and correlation with other variables in the experiment. Accordingly, second-generation studies often employ mechanical or automated technologies that significantly reduce human variability while monitoring and manipulating system variables. Several studies as e.g., (Aldeias et al., 2016; Astruc et al., 2003; Calandra et al., 2020; Collins, 2008; Dibble & Rezek, 2009; Eren et al.,

2014; Iovita et al., 2014; Keller, 1966; Lerner, 2014; Paixão et al., 2021; Pereira et al., 2017; Pfleging et al., 2019; Yonekura et al., 2006) are examples of second-generation experiments.

Thus, second-generation experiments, unlike first-generation experiments, generally do not attempt to directly reproduce human actions or even real-life activities. Instead, they use what are called expert systems (mechanical devices) (Grace et al., 1985). Expert systems develop fundamental principles by isolating, regulating, and evaluating the cause-effect relationship of variables, from which a more detailed and accurate understanding of the process can be derived (Marreiros et al., 2020).

2.1.3 Third-Generation Experiments

A third step is proposed by Marreiros and colleagues (2020) in the design of experiments, which they call "third-generation" experiments. The recognition of a fundamental principle in the application of a second-generation design must be juxtaposed with an archeological-like design, created and used by archeologists, but still independent of archaeological interpretations. Any models and patterns created can be tested in this environment, which is a "naturalistic" man-made world with human variability, and tools and behaviors can be tested that are comparable to those discovered in archaeological records. To evaluate the patterns discovered, these studies should include both standardized and archeologically reproduced tools, the latter of which can be tested on objects from the archaeological record. Human variability can be tested and quantified if technologies such as multisensor gesture recognition systems are included in the experimental design, which should include not only the reproduction of potential past technologies but also testing and measurement of human variability.

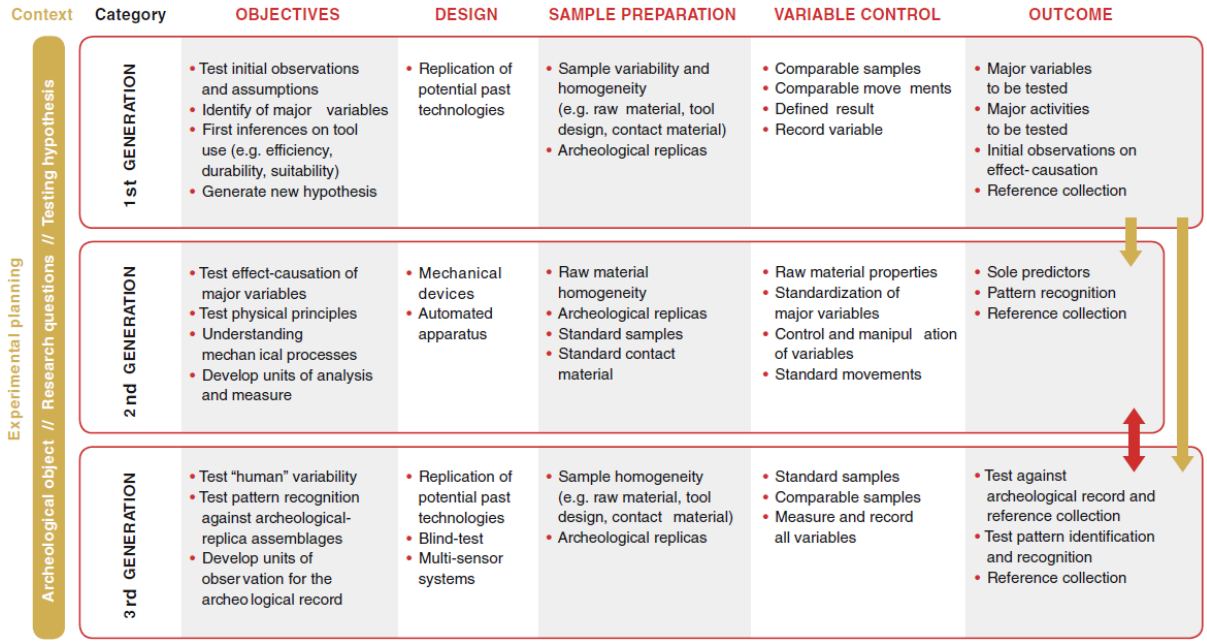

Figure 2: Diagram representing the different categories included in the experimental planning. For each category, different aspects are discussed, concerning its objectives, design, sample preparation protocols, variable control, and outcome (Marreiros et al., 2020).

2.2 The Role of Lithic Raw Materials - Experimental approaches.

Lithic raw materials played an important role in prehistory since they were used to create tools for more than two million years (Harmand et al., 2015). It was the ability to collect rocks and transform them into tools that gave an advantage to the human species to overlap environmental difficulties, adapt, and evolve (Ambrose, 2001; Foley & Lahr, 2003)Lithic raw materials played an important role in prehistory since they were used to create tools for more than two million years (Harmand et al., 2015). It was the ability to collect rocks and transform them into tools that gave an advantage to the human species to overlap environmental difficulties, adapt, and evolve (Ambrose, 2001; Foley & Lahr, 2003).

Studies of lithics assemblage have the potential to answer a wide range of questions, including mobility (Braun et al., 2008), landscape use (Pereira & Benedetti, 2013), site use variability (Goldman-Neuman & Hovers, 2012; Harmand, 2009; Stout et al., 2005), and, more specifically, the individuality that marked major technological and cultural dynamics on human behavioral evolution. Flaking predictability, sharpness, durability, quality, usefulness, and decision-making in prehistoric populations have been related to studies that aim to identify how much

past humans were aware of the characteristics of lithic raw materials used to produce implements (Hovers et al., 2009).

Following this, studies on raw material variability have been focused on the dichotomy notion of quality, which may be categorized by, high or low; good or bad. Apart from the subjectivity of the term "quality," most lithic analysts have highlighted the significance of the role that lithic's raw material "quality" implies in artifact form. The quality of raw materials is expected to exhibit a direct effect on the lithic technical organization (Andrefsky, 1994). It is presumed that a degree of low-quality raw materials and scarcity lead to informal technologies, and stone tool production made from higher quality raw materials were easier to manipulate and achieve the requirements of the stone knapper (Andrefsky, 1994; Brantingham, 2000), but the archaeological record also shows the opposite (see (Moník & Hadraba, 2016)for a different perspective).

Therefore, the raw material is considered to constrain the design, manufacture, and use of artifacts in many ways. The nature of each raw material outcrop, which includes differences in “internal” (i.e., fracture predictability, elasticity, brittleness, hardness, homogeneity, granularity, and isotropy (Andrefsky, 2005; Eren et al., 2014; Goodman, 1944) and “external” properties (i.e., size, shape, surface regularity, cortex presence, cleavage plans (Eren et al., 2011, 2014). This variance will have a direct influence on artifact "quality", matching properties of lithic raw materials with certain activities, suggesting a link between raw material and function. Therefore, the raw material is considered to constrain the design, manufacture, and use of artifacts in many ways. The nature of each raw material outcrop, which includes differences in “internal” (i.e., fracture predictability, elasticity, brittleness, hardness, homogeneity, granularity, and isotropy (Andrefsky, 2005; Eren et al., 2014; Goodman, 1944) and “external” properties (i.e., size, shape, surface regularity, cortex presence, cleavage plans (Eren et al., 2011, 2014). This variance will have a direct influence on artifact "quality," matching properties of lithic raw materials with certain activities, suggesting a link between raw material and function.

To understand how raw material properties impact the use and production of stone tools first is needed to identify and separate the variables involved in this process. With the development of controlled laboratory studies, it became simpler to isolate such variables as well as quantify and reproduce the results (Braun et al., 2009; Braun et al., 2008; Calandra et al., 2020; Collins, 2008; Marreiros et al., 2020; Marreiros et al., 2020; McPherron et al., 2014; Pereira et al., 2017).

In 1944, Goodman was the first to develop an experimental methodology that linked raw material properties with research on lithic technology and typology. Goodman drew attention to the diversity of stone tool types seen in the archaeological record and proposed three possible explanations:

1. The craftsman's personality, (Costa, 2010; de la Torre, 2011), also imply this argument, calling "artificial forces" by Costa and de la Torre called "technical incompetence". All suggested that raw materials influenced the end result of stone tools manufacturing because the hominis did not possess the knowledge, manual dexterity, skills, or incentive to tackle "challenging" raw materials);
2. Cultural transmission from generation to generation;
3. The physical environment in which the artisan lived.

Costa and de la Torre (2011) also mentioned another aspect that could be linked to the last explanation of Goodman, which is "natural forces" and "raw material constraints" respectively. They expanded on this hypothesis by stating that, rather than the interaction of behavioral and cultural factors with physical/geological factors, the dominant source of artifact morphology (or stone tools production) is entirely within the raw material itself, i.e., there are natural raw material constraints that "dictate" artifact morphology (or manufacture and use) (Eren et al., 2014).

Goodman also proposed that all options are linked and that when considering environmental issues and constrains, the availability of raw materials is of fundamental relevance. His theoretical reasoning linked raw material selection to cultural tradition, but also to an argument that environmental resources could be fully explored. In the past materials were chosen based on utility, giving the impression that background knowledge of how rock properties behaved was present in prehistoric populations during raw material selection (Goodman, 1944). This idea was later highlighted by (Manninen & Knutsson, 2014) “when lithic technological organization is viewed as an intersection of many varying dimensions, the properties, and availability of raw materials can be considered the most important determinants in how these dimensions intersect within any organizational context.”

The introduction of the Goodman 1944 study reaches a line of study that had previously been confined from, Geology research, and was now beginning to emerge in Archaeology, which advocates that the perspective of how the properties of lithic raw materials impact the manufacture of stone tools. Goodman states, "(...), the major interest of the archaeologist

naturally lies in such characteristics of the rocks as may be expected to affect the ways in which they can be shaped into tools and the peculiar utility and durability of such tools".

To dissect the term "physical properties," Goodman defines it as a range of characteristics performing different types of operations under specified conditions, mentioning the hardness test as an example, where the normal procedure is defined as scratching the unknown material with a material of known hardness value, the principle being the Mohs scale.

Goodman's study intended to identify and quantify the properties of raw materials such as obsidian, silicified volcanic tuff, fossil wood, flint, chert, quartzite, and limestone using a variety of tests, the majority of which were utilized in industrial engineering and geological research. Hardness was measured by the penetration method, this method was chosen because of the similarities that results can show when compared to the behavior of flaking pressure. The next method used was to measure density (gravimetric method), followed by toughness (standard hammer testing device) to address the workability and durability properties of a tool, and the last one was resiliency by rebound tester, also to monitor the workability, but with the acquaintance of the principle of elasticity explored by Francis Birch (Goodman, 1944).

The main contribution of the previous research was to emphasize the significance of understanding the influence of stone's physical properties on the mechanics of stone tool usage and manufacturing. If one can determine which properties of stone influenced raw material selection by early hominins, one may be able to understand the significance of certain types of rocks in different lithic toolkits.

In his conclusion, Goodman stated that his work did not have a reasonable value due to the low measurements that were recorded, but it was a revolutionary approach that should be refined and extended to the study of all rocks and minerals used in toolmaking.

Following Goodman 1944 publication, few studies addressed the quantitative approach to understanding stone tool implements and their mechanical properties. Among these studies, (Domanski et al., 1994; 2009) investigate flaking properties of rock types used in stone tool manufacture, by using mechanical parameters such as modulus of elasticity, compressive strength, tensile strength, and fracture toughness. This approach aimed to investigate the changes in the mechanical properties of stone tool materials after intentionally heated.

In his papers from 2006, 2008 Yonekura applied the same principle as Goodman. Citing Clark, 1980 and Domanski et al., 1994, this study points out that the evaluation and quantitative

assessment of lithic raw materials in the field of archaeology was not fully established, because studies of prehistoric lithic materials were done based on petrological classifications and qualitative descriptions by macro-observations. Yonekura methodology focused on artifacts quantitative examination based on mineral composition, microstructure, and mechanical properties, which could have directly influenced their applicability for developing various tools, to obtain fundamental data on Paleolithic materials for archaeological studies. Also, what Yonekura aimed to present is a different perspective on studying lithic assemblages by replacing the conventional approaches (descriptive, qualitative, and petrological) with a "modern" approach based on new methods for obtaining uniformitarian data to construct better inferences from the archaeological record.

2.2.1 Durability and Edge Efficiency of Lithic Raw Materials - Experimental approaches.

Concerning the mechanical properties of archaeological lithic raw materials, other studies start to investigate an optimum method regarding the research question, applying statistics to estimate the quality of stone implements, by using mechanical tests and controlled experimentation to understand for example durability and edge performance of stone tool made on each type of rock. (Braun et al., 2009;Collins, 2007; Key et al., 2020).

Braun and colleagues (2009) focused their research on understanding the importance of raw material quality on Oldowan technology. Investigations have found that Oldowan hominins favored specific kinds of stone for artifact production. Previous research on the artifact assemblage from the early Pliocene Oldowan location of Kanjera South (South Rachuonyo District, Kenya) indicates that raw material selection and transportation were critical elements on Late Pliocene human adaptations. However, the exact characteristics of the raw material that had a major impact on the decision-making of the early hominins were unknown. They focused on durability and fracture predictability as two important features to access raw material characterization, and these were applied to investigate why past hominins selected particular types of rocks. To evaluate stone durability and flake predictability, a series of actualistic experiments on edge attrition are combined with additional mechanical testing (hardness test) of diverse lithologies. To quantify edge durability from each raw material, Braun et al., focused on digital images from a specific area of the flake, captured before and after each experiment. The lost material from the lithic sample was calculated with the support of imaging compare software (Image J 4.0.1). This study demonstrated that, by applying different mechanical tests

combined with actualistic experiments, it is possible to draw new information regarding the assemblage. It is stated that Oldowan toolmakers at Kanjera South, were probably selecting lithic raw materials, based more on durability than fracture predictability. ´

To assess edge reduction between coarse- and fine-grained materials, Pereira and colleagues (2017) used high-resolution methods and mechanical experimental devices. Their work focuses on their use in an experimental program specifically designed to compare the edge reduction of quartzite and chert when cutting pinewood. Their experimental program was conducted to shed light on issues such as raw material choice and past human use that may be relevant to raw material performance. The result of the experiment showed that quartzite edges performed worse than chert edges when all factors were tightly controlled in the task of cutting wood across the veins. Based on the results, the authors believe that the most likely reasons for the simultaneous use of fine-grained and coarse raw materials such as chert and quartzite at the same time and place are related to their complementary use for different tasks due to their different physical properties, which on a larger scale may have significance for local cultural patterns and ultimately for cognitive abilities.

A similar study was done by Key and colleagues 2020 exploring raw material selection decisions during Olduvai's Early Stone Age by combining controlled experiments with raw material performance. Force, work, and material deformation were the variables chosen to measure the changes while performing cutting movements in a controlled setting. By cutting movements, they refer to the separation of materials by means of fracturing, a broad definition presented by (Atkins, 2009). To address raw material optimization, a comparison between three raw materials was investigated through reduction in performance across the duration of a known task. For each sample, a longitudinal cutting stroke was processed resulting in what Key et al called a durability condition (i.e., condition one was a fresh flake, condition two was after one cut, and condition three was after two cuts, etc.) (Key et al., 2020). Also, sharpness was measured from the initial phase of knapping and after each movement recording force, work, and material deformation.

The relative differences in performance throughout the six controlled cutting tests were used to assess raw material durability. First, the percentage changes in mean force, work, and material deformation from each flake's initial controlled cutting test to their sixth. Following that, statistical tests were used to determine if individual abrasive cutting strokes were sufficient to

produce significant decreases in performance in durability conditions one through six, and how this differed across the three raw materials (Key et al., 2020).

In this study, the authors refer that every stone tool manufactured in ESA (Early Stone Age) in Olduvai Gorge required a selection of each raw material to be utilized. The performed experiments show that edge sharpness and durability, as well as functional performance, differ considerably across chert, basalt, and quartzite. These differences had the potential to influence raw material selection-related behaviors at Olduvai during the ESA. Quartzite was the sharpest raw material in this experiment, requiring much less effort and energy on using than basalt. Chert has edges that are nearly as sharp as quartzite but are more durable. Basalt has proven to be much more durable than both chert and quartzite, although it has a significantly lower initial edge sharpness.

Both studies mentioned above are good examples of the extension of Goodman's work. The first study is dedicated to a more actualist perspective using local knappers to manufacture the flakes samples and the activities performed. As the other is more focused on second-generation experiments, where they used most likely engineering testing on flakes knapped by an experienced flintknapper.

2.2.2 Lithic Raw Materials Efficiency - Experimental approaches.

In archaeological lithic studies, the term efficiency is assumed to be fundamental to the technological design and production of stone implements. although, without specifying what efficiency is and what concepts archaeologists claim to evaluate efficiency (Collins, 2007).

Collins, 2007 emphasizes that, despite the lack of a clear definition of the concept used in archaeology, artifacts have a direct association with increased efficiency when procurement and resource exploitation activities are carried out. This is accomplished by lowering the cost of time and energy while boosting the returns.

At this point, efficiency is imposed by an economic model, where the definition depends on the ratio of output to input (Output/Input=Efficiency) (Christenson, 1982).

Different input/output configurations provide various levels of efficiency. Each may be changed to evaluate total energy efficiency (all inputs, independent of the source) or only the cost inputs, known as total factor efficiency/productivity (measure the efficiency evolution

within a food system). Finally, labor efficiency is defined as the amount of product generated per unit of human labor input. Although output per person-hour is the most often used metric of labor efficiency, the input may also be quantified in units of work energy (kcal) to obtain labor's energy efficiency.

Christenson in his study also presented different types of ratios to access tool efficiency, one being the "net energy acquisition rate", which measures energy profit as the denominator being time. Key and Lycett (2015) applied a variation of this ratio to assess the impact of edge angle on human stone tool users by measuring the efficiency of a cutting task while considering the relationship between edge angle, loading, and flake size. The last-mentioned ratio is the "marginal cost", which is the same as marginal efficiency in economics, where an increase is expected in the total production over time by the allocation of inputs (Christenson, 1982).

Due to the presence of a number of ratios used to address efficiency, the concept has become diffused in the literature, generating misunderstanding between efficiency and other aspects of human behavior (Christenson, 1982). To consider a behavior, as action, or as artifact as efficient, is needed to determine specific goals of each activity, and identify variables that can minimize or maximize efficiency. In artifact performance variables such as edge-angle, shape (profile, section,), size and length, raw material and weigh, use action, contact material, and hardness, are known to affect the output of the ratio (Christenson, 1982; Collins, 2007).

In this perspective, Keller's (1966) performed an experiment relating to the development of edge-damage with use action and its implications on utility. This study was one of the first systematic investigations on replica of artifact performance. The study kept raw material and contact material constant but varied modes of use to allow estimations of the relative efficiency of different edges in different uses to be determined from measurements of edge dullness.

2.2.3 Edge Reduction

Reduction in lithic technologies is seen as a means of understanding the technological variability present in the archaeological record. The analysis of reduction can address a variety of strategies, such as retouching. The concept of retouching as re-sharpening, necessarily links retouch to use, the more intensely an artefact has been reduced, the more use is attributed to it. Many studies estimating reduction sequences for traditional archaeological 'types' have demonstrated this concept, claiming that the type of each object class represented in the deposit depends on the degree of reduction the object has suffered during use (Dibble, 1995; 1984; Kuhn, 1990).

To enable comparisons between different artefact morphologies and the extent of reduction demonstrated, the relationship between use and retouch must be assumed to be fixed. This has allowed artefacts with comparable levels of retouch to be associated with comparable levels of use, meaning that the researcher only needs to identify the intensity of reduction at a site in order to also capture the intensity of use. The rates of use and reduction are assumed to be constant. However, this constant has yet to be proven, creating a knowledge gap that prevents valid conclusions from being drawn about prehistoric technology (Collins, 2008).

For example, following the work of Lin & Marreiros, (2021) Quina technology, more specifically Quina scrapers, is considered to be a result of intensive reduction with the presence of stepped fractures and also intensively retouched on successive occasions. This work focuses on understanding the relationship between the intensity of reduction, the thickness of the blank, and the edge angle in Quina scrapers. To explore these issues, a linear modeling approach was used to investigate the effect of the variables. In doing so, they conclude that Quina retouching has no clear effect on maintaining the angle of retouched edges during reduction. Thus, the occurrence of Quina retouching is likely related to other factors, some of which are related to the economic and functional requirements of these tools.

Studies such as the previous one, recognize that any reduction process is subject to a large number of extraneous variables. The reduction intensity has been found to necessarily depend on the size of blanks produced for use, function, and economic factors such as quality of raw material or accessibility.

2.2.4 Thesis Framework

As mentioned in the previous sections, research has not been conducted systematically in terms of the quality of raw material and experimental approaches. Much less when issues such terms as efficiency and durability and function are associated with lithic raw materials.

This study uses the methodological framework outlined by Pedergana and colleagues (2019), which focuses on testing how different raw materials perform under similar constraints. They use "no difference in raw material and mode attrition performance" as the null hypothesis for the experiment, and "significant difference between raw materials" as the alternative. Also, the preliminary results, mentioned above about the efficiency and durability of obsidian and flint, lead to the development of this work, applying new motions, raw materials, and sensor readings, such as tool force, friction, velocity, and penetration depth.

The experimental design in this dissertation attempts to address the same principle by holding constant the edge morphology, contact material, and other variables that affect edge performance but use four lithic raw materials as testing variables to estimate their efficiency in executing a cutting motion.

This study also seeks to clarify the differences in edge performance (through efficiency and durability) between coarse - and fine-grained raw materials representative of stone tools present in archaeological studies. Furthermore, this work aims to complement how reduction evolves across the cutting-edge during a given function and motion in the four raw materials tested. By understanding how reduction occurs in the different lithic raw materials, new assumptions can be made about the intensity of retouch or the morphology of retouch. Finally, this work contributes with a standardized and controlled methodology to study the durability and efficiency of lithic raw materials. Further sequences of the same methodology but with different active samples (lithic raw materials) and passive samples (contact materials) should be carried out to achieve a more uniformitarian knowledge of stone tools.

In this study, a possible connection is made, as an example of how important this type of work is to archaeological studies, Kalavan 2, assemble the essential data to test the questions about how the properties of lithic raw materials can influence decision making when the acquisition or use of raw materials is a primary function.

Chapter3 MATERIALS AND METHODS

This chapter presents the methods of the experimental design and the materials used in this thesis, that will be used to systematically test a range of four lithic raw materials, and consequently quantify their effect on the performance (efficiency and durability) of cutting pine wood. Edge durability, as well as the ability to constantly maintain a cutting performance for extended periods, have also been included as potential contributors to the overall edge efficiency of the lithic raw materials.

"True scientific experiments do not try to replicate real life: instead, they isolated and control a small number of variables to assess how they interacted in specified conditions" (Sillar, 2003 p. 178). In the same perspective, this experimental design focuses on acquiring quantitative data to contribute to the development of interpretive principles and link inferential physical properties of artifacts to behavioral processes that archaeologists wish to answer.

3.1 Materials

The raw materials selected for this study were Obsidian, Flint, Quartzite, and Dacite, chosen from the TraCEr reference collection at MONREPOS-RGZM. Each raw material has a unique geological outcrop coordinated, being Obsidian and Dacite from Armenia, Quartzite from Germany, and Flint from Belgium in Figure 3.

Figure 3: Lithic raw materials collection: A - Dacite; B - Obsidian; C - Top (Quartzite) Down (Flint).

Two main aspects lead to the choice of these raw materials: 1) the widespread use in archaeology sites; and 2) the contrast between fine and coarse-grained rocks.

The fine-grained samples are flint as a representative of a microcrystalline sedimentary rock and obsidian as an igneous rock with a high content of silica. Fine-grained samples are characterized by their homogeneity, which means that flakes produce a better and sharper edge and have the best properties to perform specific operations (Collins, 2008). On the other hand,

in coarse-grained samples, quartzite as a metamorphic rock is very rich in quartz and sandstone grains, and dacite has a felsic rock with a porphyritic structure and a high content of feldspar, silica, and quartz grains. According to Morrison, 1994, coarse-grained rocks are harder than fine-grained rocks and therefore have a more efficient edge (Pereira et al., 2017). Even within the same rock type, there is a degree of internal diversity, evident in different microstructures and hardness (Domanski et al., 1994)

To ensure uniformity on the morphology and length of the edges, all specimens were cut with a length of 3 cm, a width of 2.5 cm, a thickness of 1 cm, and a 45° edge (Figure 4). The entire collection consists of three specimens of each lithic raw material, for a total of 12 specimens.

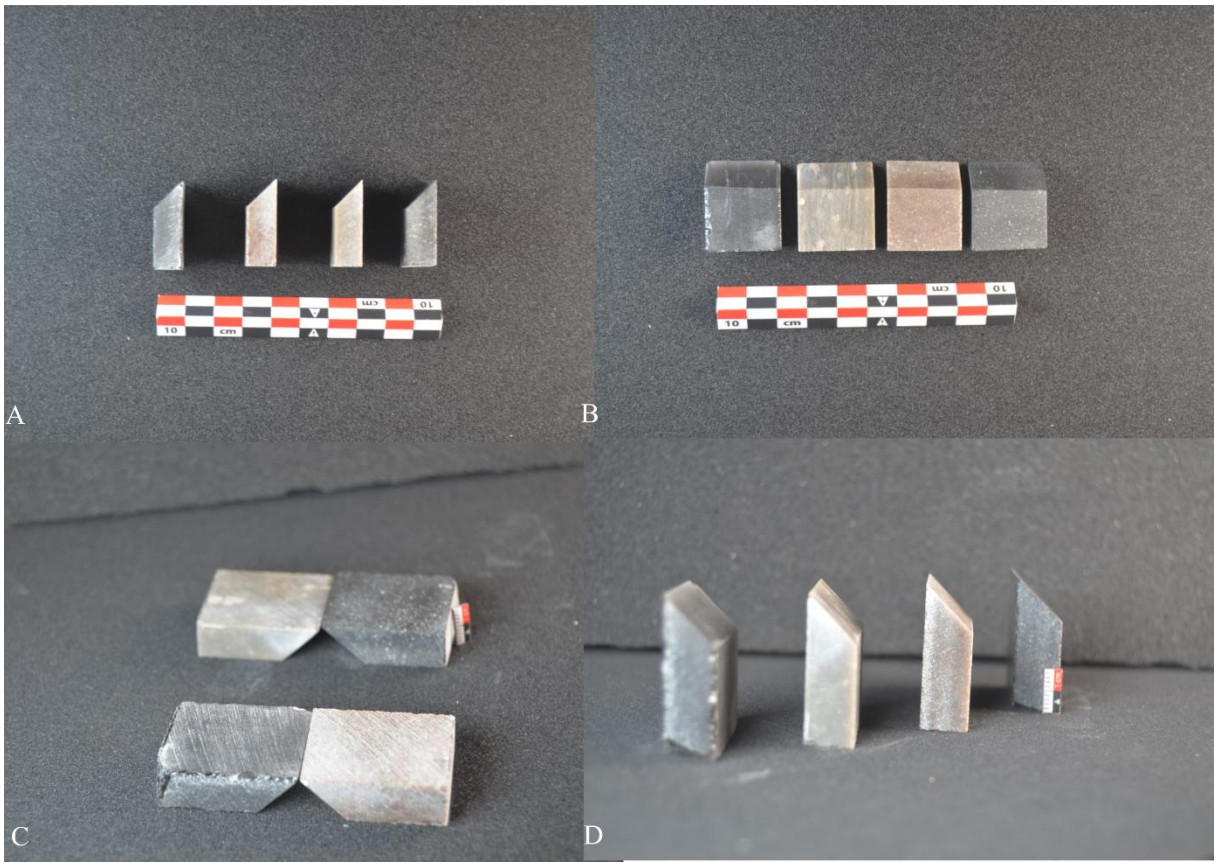

Figure 4: Lithic raw materials samples: A - Profile view; B - Plan view; C - Section view; D - Profile view.

To carry out the experiment, a variety of contact materials such as bone, wood, and horn were available. Among these alternatives, wood was the better choice because the same plank could be used to perform all the samples with the same applied force without changing the contact material. Variations from the internal and external properties could affect the final results of each raw material, and this would result in an uncontrollable variable.

For commercial purposes, wood hardness is universally tested using the Janka hardness test, which involves measuring the force required to push a steel cylinder with a diameter of 11.28 millimeters (produce a circle with an area of 100 square millimeters) into the wood to a depth of half the cylinder's diameter. The output data are exported in pressure units, which are then converted to kgf (kilograms force) (Doyle & Walker, 1985; Hirata et al., 2001).

Pinewood plank was obtained from the Bauhaus commercial bricolage center in Germany. European Pine Wood has an average density of 255 kgf (2.5 kilonewtons) and a moisture content of 12 to 15% (https://jp.europeanwood.org/en/living-with-wood/selected-european-woodspecies/pine/). The planks were selected with a standard dimension of 20 cm in length. The presence of growing glue-laminated timber was considered in the selection of the timber, so only non-glued timber was selected (Figure 5).

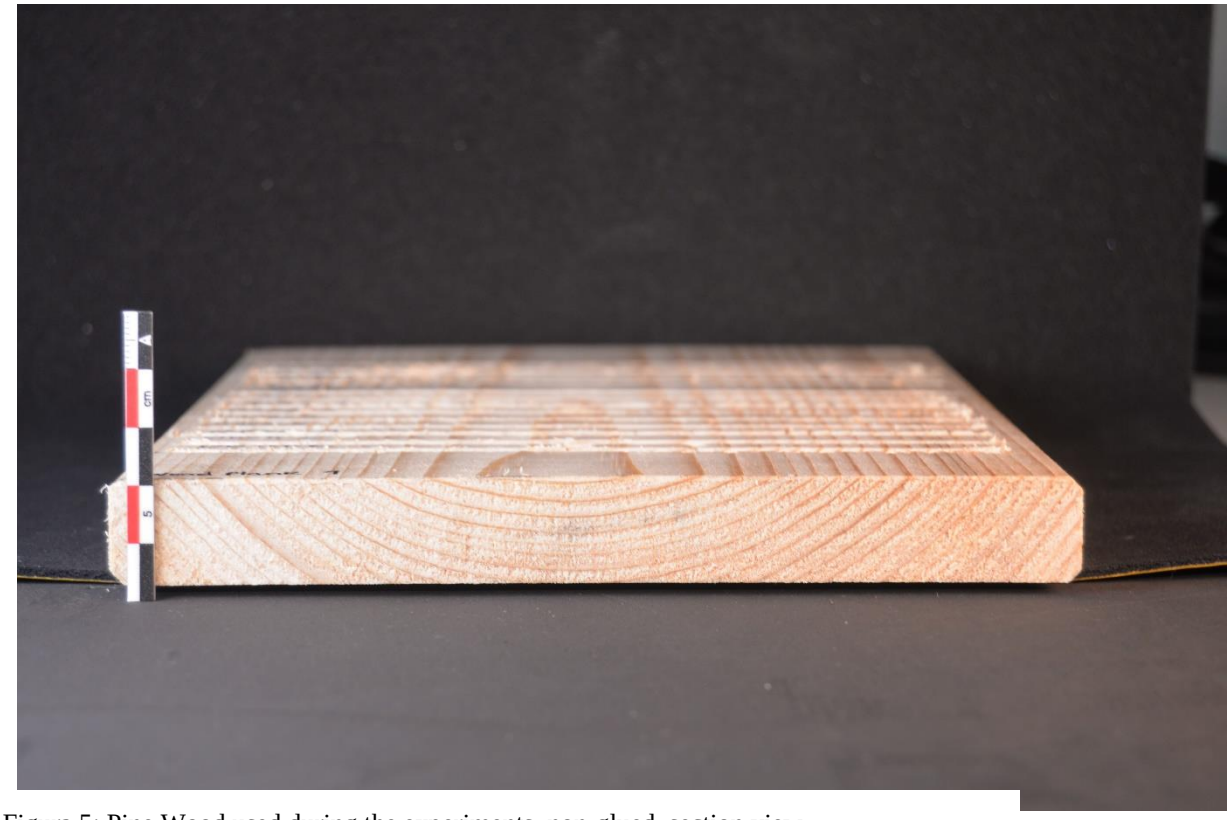

Figura 5: Pine Wood used during the experiments, non-glued, section view.

3.2 Experimental Design – Introduction

This study specifically attempts to develop a model that explains stone tool durability and efficiency by examining the cutting action (linear and bidirectional motions) against pine wood.

Sample preparation, controlled variables recording, and contact material are utilized to carry out the lithic experiments in a standard setting. The experimental design is therefore divided into three sections, illustrated in the figure below.

Figure 6: Experimental design workflow.

3.3 PRE-EXPERIMENTS

3.3.1 Controlled and measured variables

Previous studies, namely by Collins (2007), have shown that several variables can have either a direct or indirect impact on the performance of stone tool efficiency. These variables are: Edge-angle, profile plan, and section shape, size and length, raw material and weight, use action, and contact material type and hardness are all variables to consider (Collins, 2007, pp. 93).

For this study and considering its goals and time available to perform the experiment, I have selected the following setting.

Variables that kept constant throughout the experiment:

- Force Applied: 5 kg
- Velocity: 600 mm/s (max)
- Travel distance: 15 cm
- Edge angle: 45º in the first stage (0 – 125cycles).
- Angle of Work: 90º
- Edge plan: Straight
- Contact material: Pine wood
- Duration: 250x strokes, 500x until 1000x strokes
- Action: Cutting in a bi-directional movement.

Variables that vary during the experiments:

- Raw material: Flint, Obsidian, Dacite, and Quartzite.
- Edge morphology
- Edge angle (after the first cycle of strokes)

Variables measured during the experiment:

- Force against the contact material
- Friction
- Platform depth

- Position
- Velocity
- Sample Edge morphology
- Sample weight

3.3.2 Sample preparation / Raw Material characterization

The first step (pre-experiment) aims to standardize and characterize the lithic raw materials used. After the selection of the blanks, the pieces were cut by an industrial saw machine at the selected measurements for the experiment, yielding three specimens from each block. Each specimen was then placed in a diamond band saw to obtain a 45-degree cut on the edge (see appendix). Once all specimens were cut, each specimen was assigned a unique ID with a bar code (Figure 7). Each piece was weighted, and the instrument used was a balance accurate to the first decimal digit.

Figure 7: ID representation of the samples.

Identifying the internal structure of raw materials is a crucial step in experimental archaeology for quantification and replication. As a result, several recent and controlled studies (Braun, 2009; see references) have already isolated archaeologically relevant variables for measuring raw material quality that can be replicated, including hardness (Goudie, 2006).

An Equotip Leeb Impact Device C with probe serial number IC51-004-0185 was used for the hardness measurements (see Appendix C, for more information). This is an instrument used in industry, but its configuration software allows calibration for different hard materials, so a configuration for lithic raw materials was developed. The configuration is determined by the outline dimensions of the sample (length, width, and thickness) and the weight of the sample. The analyses were carried out in TraCEr, the Laboratory for Traceology and Controlled Experiments in Monrepos, RGZM.

To ensure the accuracy of the tests, all samples were previously inspected and registered for macroscopic internal and external defects to determine if there was any deviation that could affect the final result (e.g., sample DAC3-5, which had a surface-to-surface void, but this did not affect the final result). For each sample, the instrument Leeb Impact Device was used in an accurate vertical position (Yaşar & Erdoğan, 2004). To reduce possible measurement errors (e.g. proximity of corners or 45º slope, slippage, or cracking during testing) and test internal variability each rock was measured ten times. The result values were then exported to a .csv file for further statistical analysis and a .pdf report (see appendix D) for each sample, which also included the Leeb instrument reference and all additional information.

3.3.3 Imaging acquisition workflow

Following the experiment sequence, each sample was scanned with a portable scanner (Figure 8), HP 3D Structured Light Scanner Pro S3 DAVID SLS-3. For a macro-scale comparison, a 3D digital automated microscope ZEISS Smartzoom 5 (equipped with a PlanApo 1.6/0.1x objective, and an integrated segmented LED ring light) was used to image larger areas with low magnification. To get the images, a program (ZEISS Zen Core) was utilized, which included the usage of the image Extended Depth of Focus (EDF) stacking module to create in-focus images. A digital camera (Nikon DSLR camera, model D610 with a Nikon AF-S Nikkor 50mm f/1.8g lens) was utilized to capture a broad morphological depiction of the samples.

A Structured Light Scanner, which is a combination of a projector, a camera, and a computer, was used to scan the samples. A series of parallel and perpendicular lines are projected upon a calibration panel by the projector. After the calibration from 120/60/30 mm is completed, the representative lines will meet the sample, and the camera will capture the object's distortion pattern and send it to the HP 3D software running on the control station computer. Once in the program, the algorithms compute surface information using the triangulation approach.

Multiple scans from different angles must be collected to produce a tridimensional representation of the item. In this work, the lithic samples were put on a manual rotating table and produce 8 single scans of each surface with a field of view (FOV) of up to 60 mm and a resolution of up to 0.06mm. Using HP software, 10 separate acquired images were aligned and combined. The 3D model was exported in a polygon file format at the end of this procedure (.PLY and .STL).

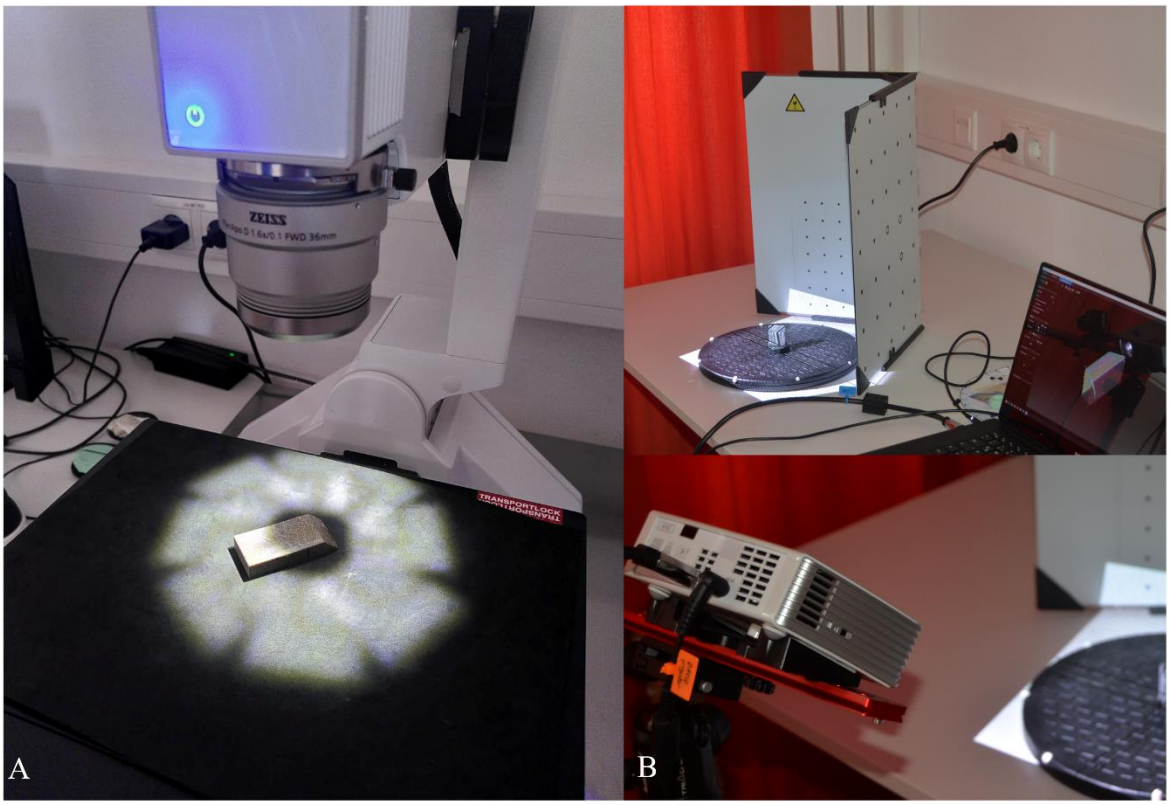

Figure 8: A, ZEISS Smart zoom 5; B, 3D scanning (HP 3D Structured Light Scanner Pro S3 DAVID).

3.4 EXPERIMENT

A methodological and controlled approach were the ground basis to ensure the experiment validity by keeping constant as many variables as possible.

In this investigation, the (SMARTTESTER®, manufactured by Inotec AP GmbH with modifications made by Walter Gneisinger) (Figure 9 and 10) equipment was utilized to conduct controlled experiments (see details in Calandra et al., 2020). The SMARTTESTER® hardware system is composed of drives and sensors connected to a centralized controlling/computing unit. A graphical operating system is included in the operating system. The touchscreen is mainly used to program the machine: programming components (drive and sensor actions, loops, conditions, etc.) may be dragged into the scripting window to create a testing experiment. Each experiment can control up to five drives and five sensors in parallel or at the same time measuring force, platform depth, torque, and distance sensors.

This mechanical equipment allows for the control and measuring of a large number of variables throughout the tests, namely, velocity, applied force, angle of work, number of movements, position, and travel distance to automatically reproduce the tests.

The versatility of the Inotec Smarttester allows to explore different setups (linear, rotary, percussion, and oscillating) (Calandra et al., 2020). For this experiment, the linear setup was used, which consists of three linear drives mounted in this configuration to move the tool and worked material to be moved in three directions: linear drive #1 moves the tool along the X (horizontal) axis, linear drive #2 moves the worked material along the Y (horizontal) axis, and linear drive #3 raises and lowers the tool along the Z (vertical) axis (Calandra et al., 2020).

To automize the machine and the experiment, a configuration script was written resulting in the steps from Figure 11.

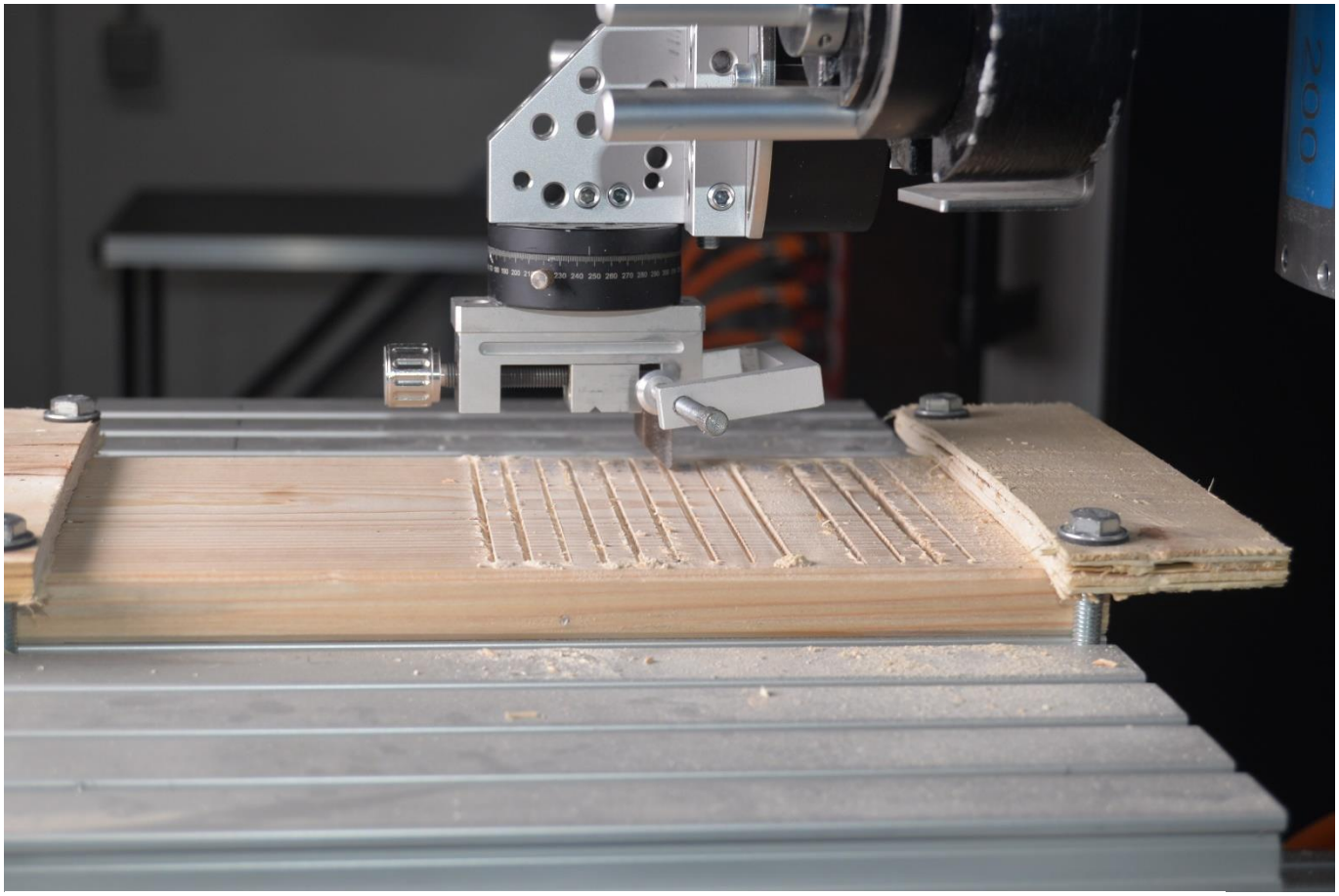

Figure 9: Linear setup: flint flake cutting a pine board in unidirectional movements. Overview of the setup

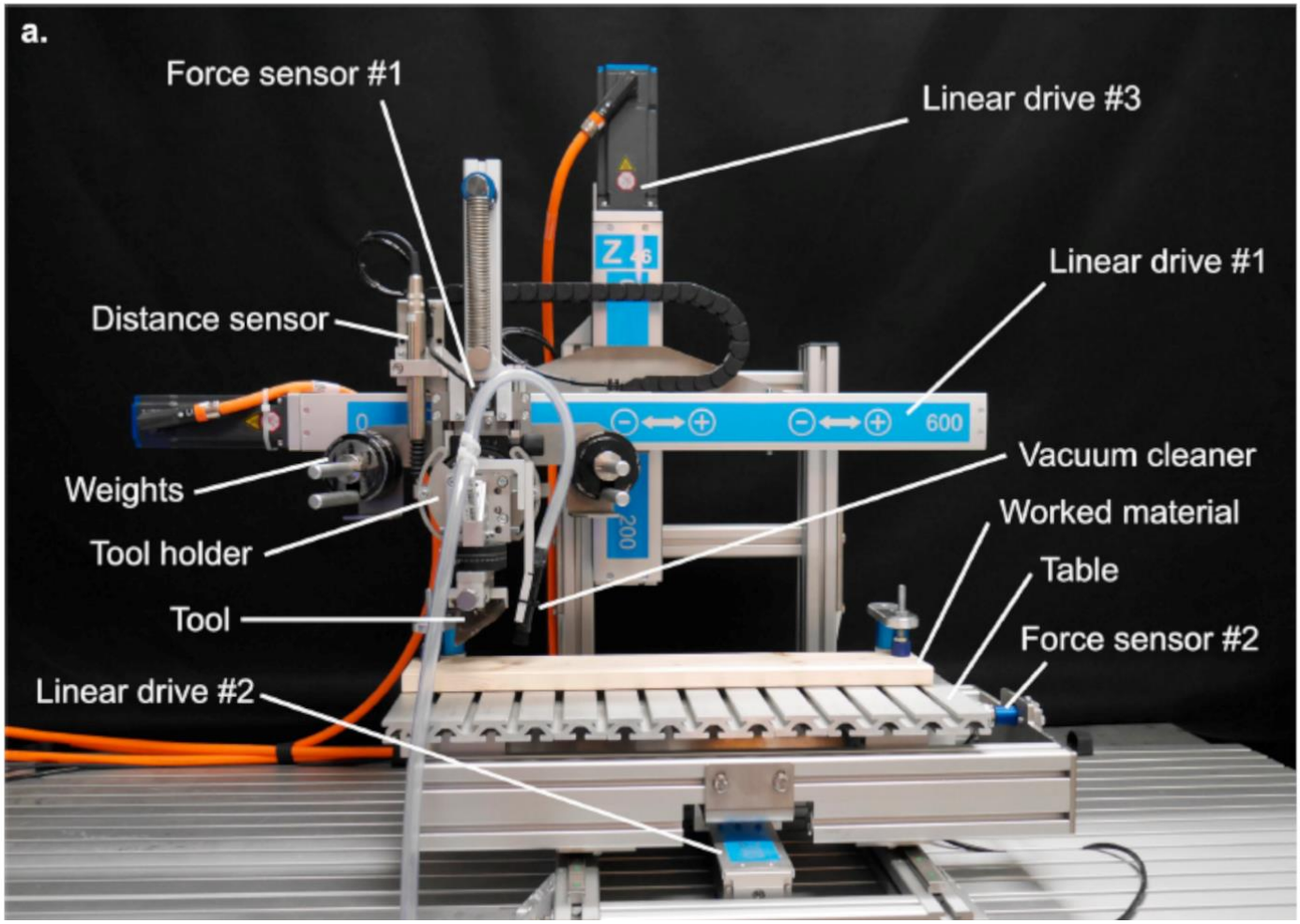

Figure 10: A- ZEISS Smart zoom 5 B-3D scanning (HP 3D Structured Light Scanner Pro S3 DAVID.

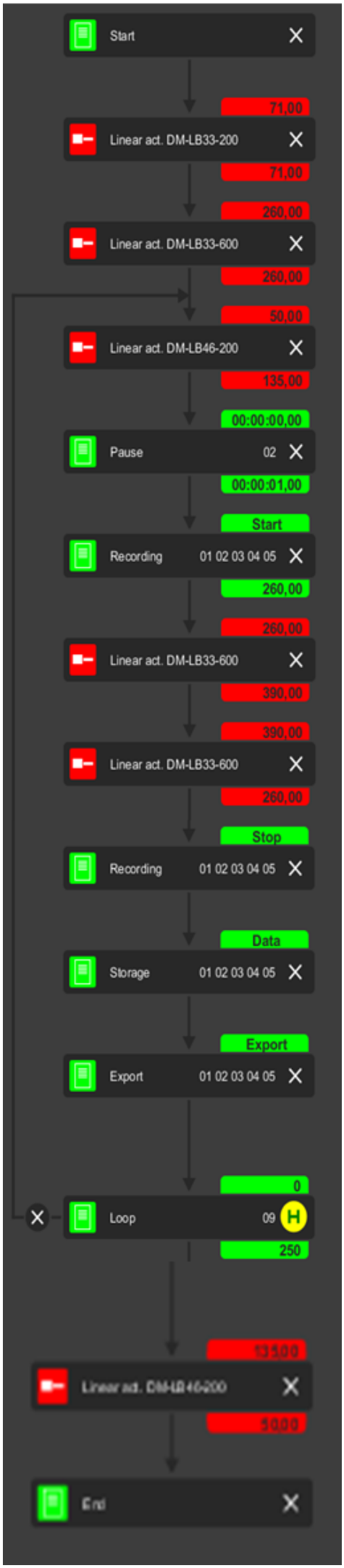

Figure 11: Screenshot from the setup to conduct the experiment.

The workflow from Figure 11 was the one used to perform the experiment. The first procedure of the experiment is to attach the sample to the machine, which includes measuring the sample (3 cm), setting a safety zone on the Z-axis (50 cm), and achieving the point of contact with the contact material (130 cm), as well as the maximum penetration depth (14 cm) (Figure 13). To execute a clean and straight cut at the start of the experiment, all samples were exactly aligned with the contact material's surface. All samples in this experiment went through three running stages (0-250 strokes; 250-500; 500-1000). In this experiment, each stroke was counted from point A to point B as one stroke, a linear bidirectional movement, but the drive measurements are recorded in cycles, thus 1 cycle equals the path length from point A to point A Figure 12. From the cycle path, up to 20 points are recorded, and then all the points are exported to a .txt file with the measurements for each sensor selected.

Imaging recording of 3D scan from stage to stage and a low magnification picture was also obtained, as previously described.

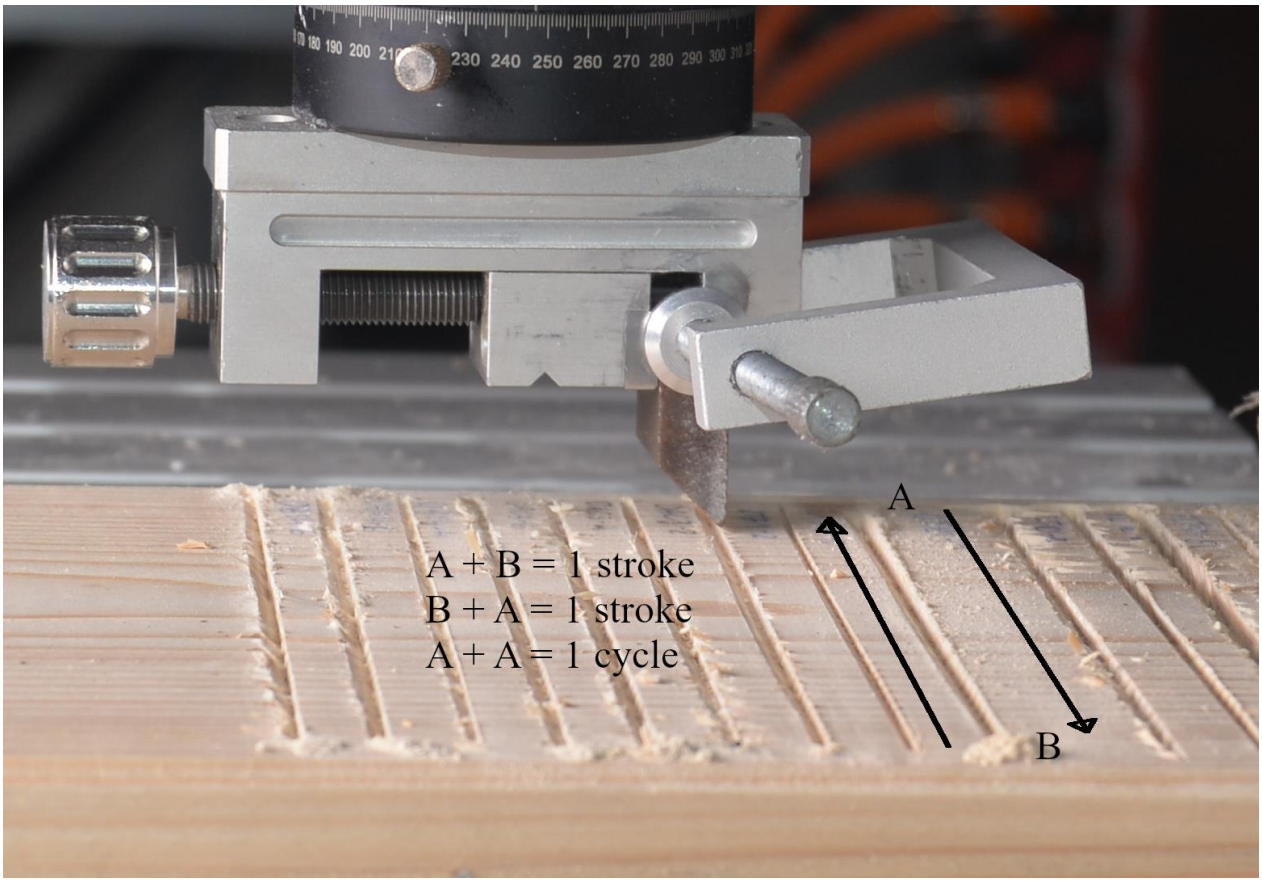

Figura 12: Cycle illustration.

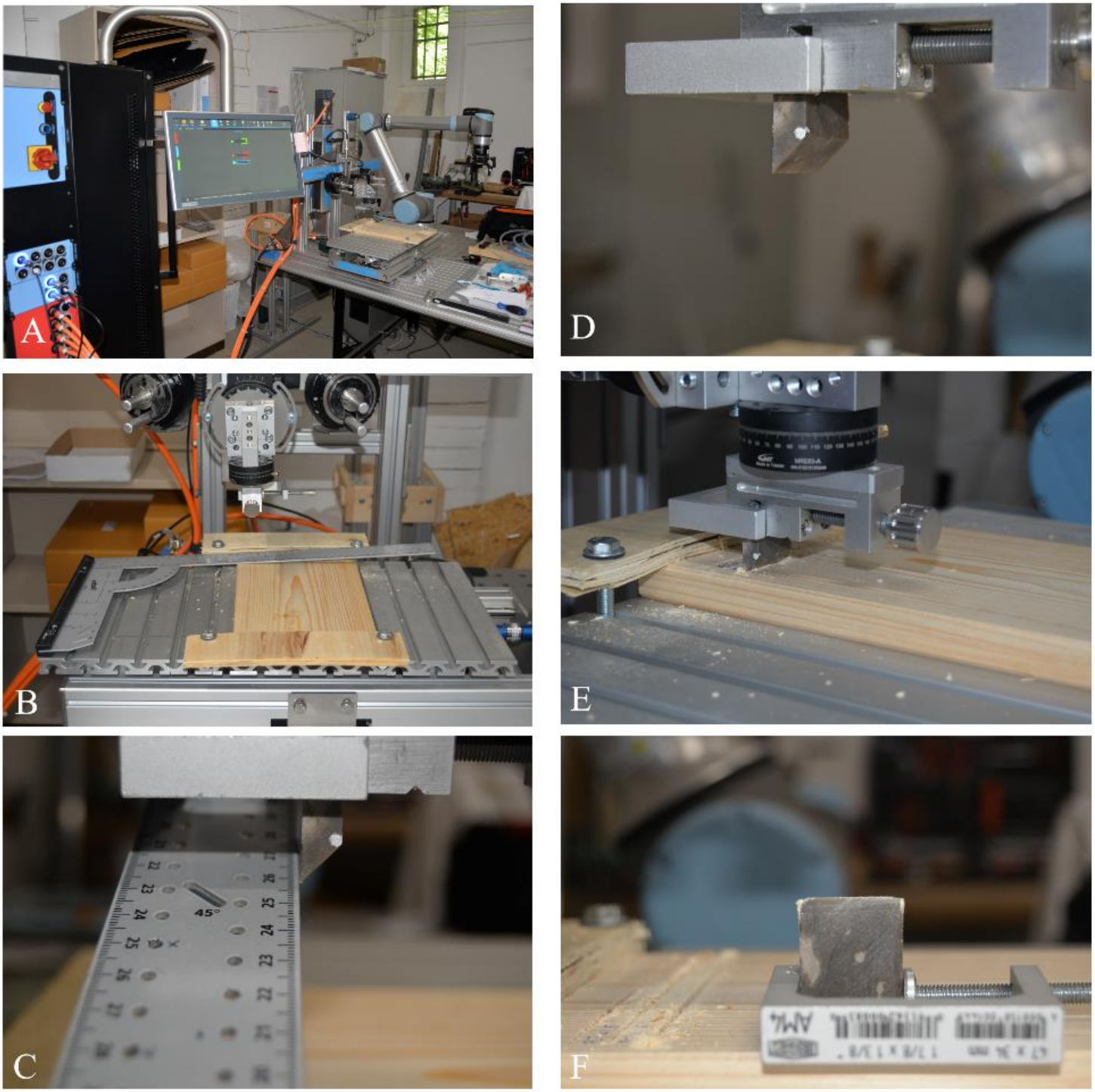

Figure 13: Inotec experiments set: A) Overview of the setup; B) Alignment of the plank; C) Alignment of the sample; D) Sample ready for performing the experiment; E) Sample performing the experiment bidirectional linear movement; F) End of the Experiment.

3.5 ANALYSIS

3.5.1 3D Model preparation and process

Tridimensional data must be prepared before any analysis can be performed. The preparation consists of three major tasks, the first two are related to the mesh treatment and the other with model alignment. GOM inspect v2.0.1 software was used for this operation. The.PLY or.STL file was imported into this software, and then the mesh operation, mesh errors removal, and hole repair was utilized to clean the raw model (see GOM Inspect workflow). Following that, the manual alignment operation was performed to place the tool in the orientation of the longitudinal axis. To overlap the models, a pre-alignment and a best-fit alignment were performed in addition to the manual alignment. Subsequently, the model was trimmed to the edge of the 45º slope for a more accurate computation and display of the edge damage.

3.5.1.a Surface comparison

Surface comparisons between meshes were performed using two software techniques.

CouldCompare is a software for processing 3D point clouds (and triangle meshes). It was originally developed for comparison between two dense 3D point clouds (such as the ones acquired with a laser scanner) or between a point cloud and a triangular mesh.

In this study, I use the “C2M” tool, which is used to compare surface deviation from mesh to mesh. The comparisons were made for all lithic samples following the combinations of 0 to 125, 125 to 250, and 250 to 500 cycles. Additionally, for a clearer visualization of how much the edges were reduced in total, a comparison was made between cycles 0 and 500 cycles.

The results were exported as a csv file to quantify the loss material and plotted as two images. One image is referred to as the histogram with the intervals of edge damage, as the second is an image of the computation of the mesh for visualize the edge reduction between cycles.

To follow all steps used in this thesis for C2M comparisons, see CloudCompare Workflow in appendix C.

A different strategy was used for the analysis of the pinewood plank. As mentioned earlier, the contact material stayed attached throughout the experiment, causing the impossibility of a scan between the cycles. So, a different methodology had to be used to determine how deeply the

lithic raw materials penetrated and how straight the cut was. For this reason, a GIS technique was employed.

3.5.1.b GIS analysis

Following mesh treatment in GOM Inspect, the model was exported as an. ASCII file (American Standard Code for Information Interchange). This comprises a table containing thousands of points, each with a distinct coordinate (XYZ) that exactly represents the object's surface. This file provides all information required to load the model point cloud into the GIS program.

QGIS Version 3.14.16 was utilized to conduct the GIS study. Our data file was imported as a delimited text layer as the initial step. This file provides the information required to project the points cloud that depicts the object's topography. The points must be transformed into a triangulated surface before the surface analysis can begin based on Digital Surface Models (DSM). The Triangulated Irregular Network (TIN) method was employed to do this, and the resulting surface was stored as a raster file. The following computations were then performed:

3.5.1.c Convex Hull

Given that the initial 3D scan of the pinewood plank was not processed, the easiest way to evaluate surface deformation is to establish the vertical datum for the elevation variable used to inspect the piece and compute additional variables such as depth. Because there are sections of the surface of the contact material that stay undisturbed during the experiment, the Z (vertical datum) was placed in that location. A 3D convex surface is generated in MeshLab with all 3D points as a reference to compute all the deformation in the Pine Wood using the coordinates of the datum. In the CloudCompare program, the depth was calculated between the convex hull and the 3D model (Benito-Calvo et al., 2018).

3.5.1.d Slope

This calculation generates a raster file containing information on a surface's slope and steepness. Slope can be expressed in degrees (0–90º). The slope of a raster cell is the steepest slope of a plane formed by the cell and its eight neighbors. The GDAL Digital Elevation Model (DEM) tool was used to create the computational method. This calculation generates a raster file containing information on a surface's slope and steepness. Slope can be expressed in degrees (0–90). The slope of a raster cell is the steepest slope of a plane formed by the cell and its eight

neighbors. The GDAL DEM tool was used to create the computational method (Paixão et al., 2021).

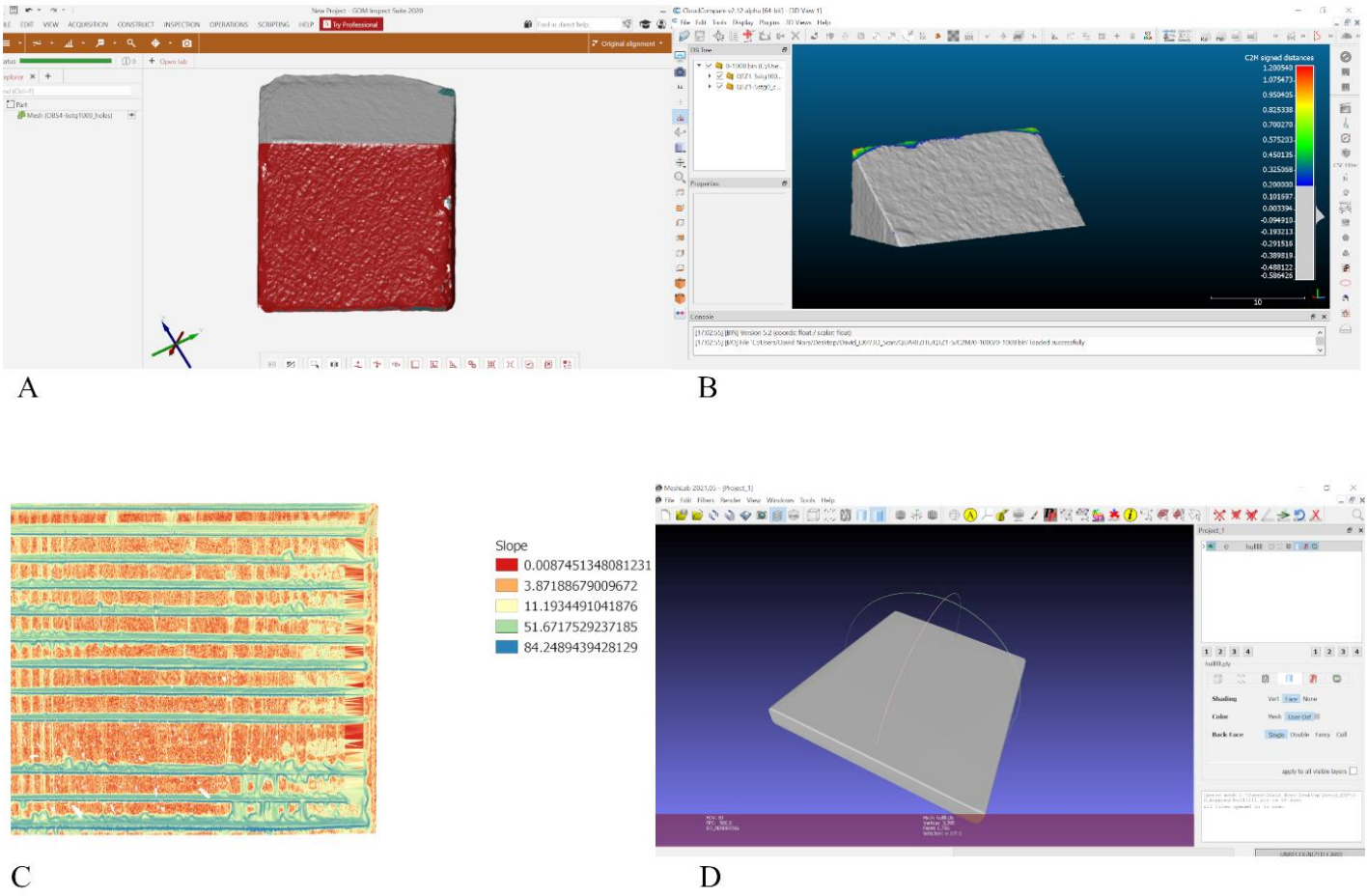

Figura 14 -Imaging Analysis: A) 3D model Cut through the surface in GOMI Inspect; B) Surface Comparisons in CloudCompare; C) Slope Analysis in Quantum GIS; D) Convex Hull in MeshLab.

3.6 Data processing and statistical analysis

As previously stated, all results from the five sensors are exported in an a.txt file in order to make the data readable and in a format that allows further statistical analysis. To achieve that, two R scripts (appendix B) were modified, one to import the data and the other to analyze it.

3.6.1 R Scripts, data import, analysis, and plotting:

Import/ Plot Inotec Script

https://github.com/jmmarreiros/rockEffandDurab

This script imports and merges all single .txt files (strokes + sensors) produced with the Inotec Smarttester. The experiment involved 12 samples (3 samples from every 4 raw materials) which have been used in four cycles (0-250, 250-500, and 500-1000 strokes) respectively. The script will:

1. Read in the original TXT-files
2. Format and merge the data for each sample
3. Combine the data from the 12 samples into one
4. Write an XLSX-file and save an R object ready for further analysis in R

The second script plots sensor data in order to visualize the measurements recorded throughout the experiment. Variables of interest are penetration depth, attrition, force, velocity.

Import/Plot Mesh .csv data from 3D models

https://github.com/jmmarreiros/rockEffandDurab

To treat the values of quantification of edge durability, two scripts were written, one to import and merge all the data produced from the mesh distances .csv files, and the second to plot the values to visualize edge damage from all stages of the experiment, a total of 48 scans are involved in the analysis.

3.7 Data analysis

To address the null hypothesis "*efficiency does not vary according to the different lithic raw materials*", two sets of analyses were performed; two simple linear regressions were established to assess efficiency and durability. In these two sets inter variability of each raw material was also tested.

In the first set, the variable platform depth was regressed against the number of strokes to assess efficiency: $Efficiency = \frac{Platform\ depth}{Number\ of\ strokes}$, this study employed the full experimental sample assemblage (n = 12) in all phases (48 replications).

The second set of studies used a similar approach, but with the variable platform depth regressed against edge reduction values to evaluate durability of a lithic raw material: $Durability = \frac{Platform\ depth}{Edge\ reduction}$, this was done with all samples to get a more homogeneous result.

I use two analytical methods to quantify edge reduction. One is based on the maximum distance in millimeters between cycles observed in the scanned samples. Comparing the first mesh (e.g., cycle 0) to the second mesh (e.g., cycle 125), the distance comparisons give an accurate measure of edge reduction. Although this is the maximum distance, it may be specific to a portion of the edge. To counter the maximum distance results, the second formula divides the edge into parts (this is possible due to the triangulation of the mesh) and counts the distance (mm) through the edge, which gives us the results of all edge reduction. This formula also allows us to determine if there is variability between samples of the same raw material.

In order to understand the hardness measures and what is the relation between raw materials One-way analysis of variance (ANOVA) and Tukey (posthoc test) with R were performed.

ANOVA objective: One-Way ANOVA is used to test the differences between at least three groups (or more) as the comparison between two groups can be done with the t-test. The analysis essentially aims to test whether there is a significant difference between the means and whether the factors influence a dependent variable. Testing for a significant difference allows for the simultaneous comparison of multiple groups. In this analysis, the chance is assumed to cause only small differences, with large differences being caused by real causes. To determine if there is a difference between means, hypothesis testing is used, where two options can be presented:

(1) Null hypothesis, i.e., the population means are the same - the sample means in terms of hardness are the same:

(2) Alternative hypothesis, the population means are different, or at least one of the means is different from the others - the sample means for hardness are different, or at least one of the means is different from all the others:

Assumptions: Like another hypothesis testing, ANOVA is based on assumptions that allow it to be used and maintained.

1) All observations must be independent;

2) The observations in each group must have an approximately normal distribution;

3) The variances in each group must be approximately equal;

4) The dependent variable is continuous.

The result shows that the distribution of at least one of the groups is different from the others, but it does not indicate between which groups the difference is significant. Therefore, it is necessary to perform multiple comparison tests, in this case, Tukey's test. This test is best for making comparisons between all pairs, but also because it is easy to apply.

When the sample sizes of the groups are equal, the Tukey's Test is exact, that is, for the set of all pairwise comparisons, the error rate of the set of tests is exactly α (significance level) and the confidence interval is also exactly 1 - α. It is worth noting that exact multiple comparison tests are rare because most do not control the assumed significance level.

Tukey's test consists of comparing all possible pairs of means and is based on the least significant difference considering the percentiles of the group. In calculating the D.M.S., the studentized range distribution, the mean square of the ANOVA residuals, and the sample size of the groups are also used.

Chapter4 RESULTS

Following the approaches and procedures outlined, and data obtained, results are presented in this chapter and organized according to the methods described earlier.

4.1 RAW MATERIAL CHARACTERISATION

Lithic raw materials can be distinguished from petrological classifications, which refer to the mineral composition of each raw material. In lithics analysis is common to establish two main groups: coarse-grained rocks, such as quartzite, and fine-grained as flint. Quartzite classification results from the presence of crystal quartz in the sample, which results in a rough texture. Fine-grained rocks, on the other hand, are associated with rocks that have a microcrystalline composition based on silica, for example, flint. This type of characteristic has implications for the predictability of fractures and the economy of raw materials.

Flint samples consist of heterogeneous nodules with a light to dark color and lighter-colored inclusions (<0.5-1 mm) with different silicification degrees in some areas of the nodule (Fiers et al., 2019). Quartzite was gathered from the Reno River (Germany) basin and consists of a homogeneous nodule with a light brown color, and a presence of microcrystals of quartz (Figure 16). Obsidian samples are original from Armenia outcrops, samples consist of a light black and translucid color at some regions of the samples, from figure 15, is possible to observe the vitric composition of the sample. Dacite also from Armenia, presents a dark color with some with microcrystals of quartz inclusions, in some samples is possible to verify crystallization holes (Figure 16).

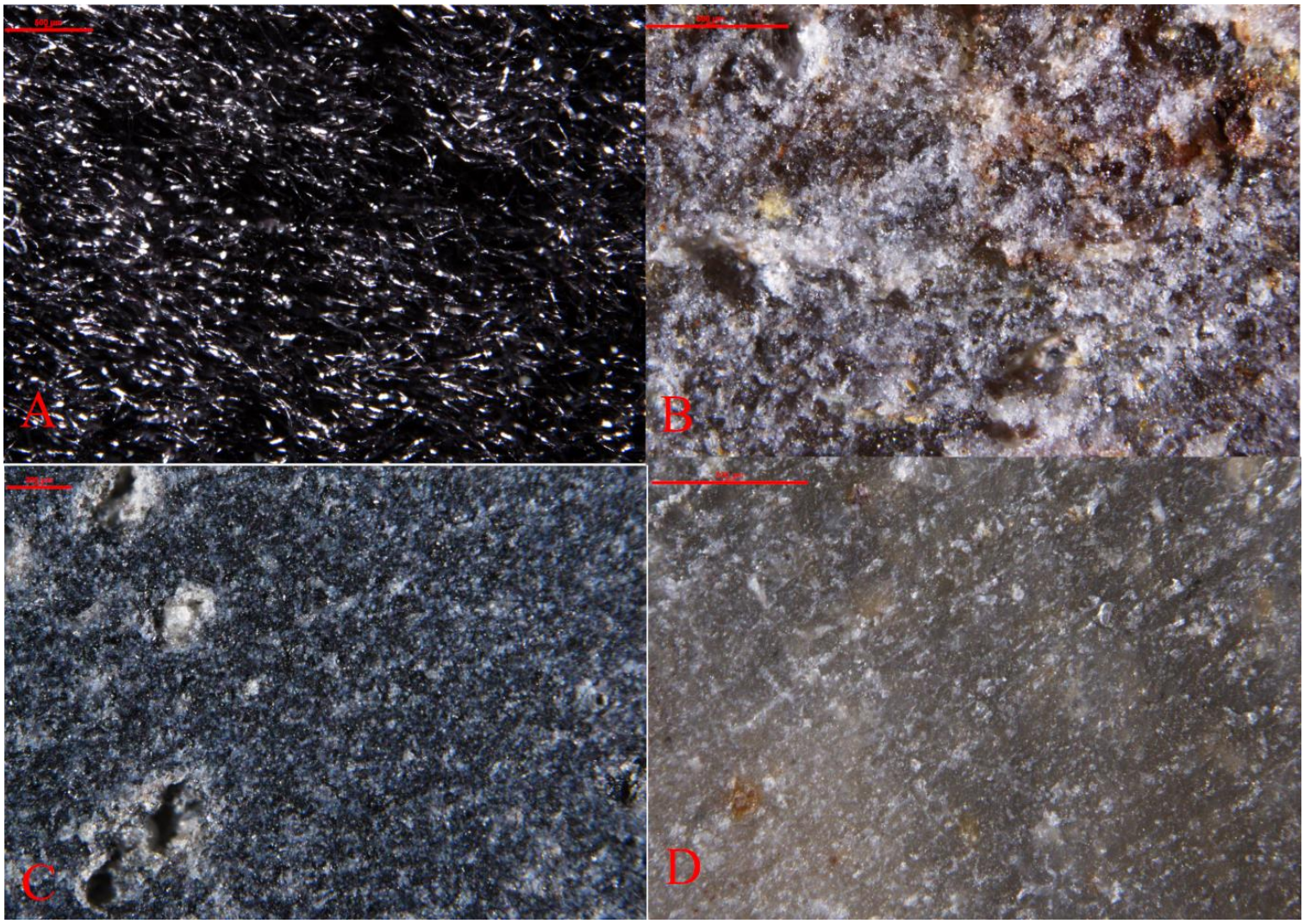

Figure 15: A - Obsidian (OBS4-2) B - Quartzite (QTZ1-5) C - Dacite (DAC3-6) D - Flint (FLT10-6).

As previously mentioned, the material properties of the four raw materials in this experiment were addressed by measuring the sample's hardness. Measuring properties such as raw material hardness allows for a better understanding and prediction of aspects of raw material physical properties, which are known to have a major impact on stone tool efficiency and durability. To test the null hypothesis "all mean values relative to hardness are equals", a total of 10 measurements in each sample from the four lithic raw materials, performing a total of 230 (FLT10-1 did not count to this analysis due to wrong measurements) measurements were acquired.

Table 1: ANOVA factors.

```
anovafactor

##                      Df Sum Sq Mean Sq F value Pr(>F)
## factor(rawmaterial)   3 213345   71115   119.8 <2e-16 ***
## Residuals           226 134128     593
## ---
## Signif. codes:  0 '***' 0.001 '**' 0.01 '*' 0.05 '.' 0.1 ' ' 1
```

The result of ANOVA shows with 95% confidence that the analysis of variance is significant because p=2×10-6 (p< 0.05), that is the null hypothesis “no significant differences between the hardness of the samples” was rejected. The confirmed differences between the hardness parameters of the samples are confirmed by the visual analysis of the boxplot (Figure 16). The comparative graphical projection allows confirmation and completes the rejection of the null hypothesis.

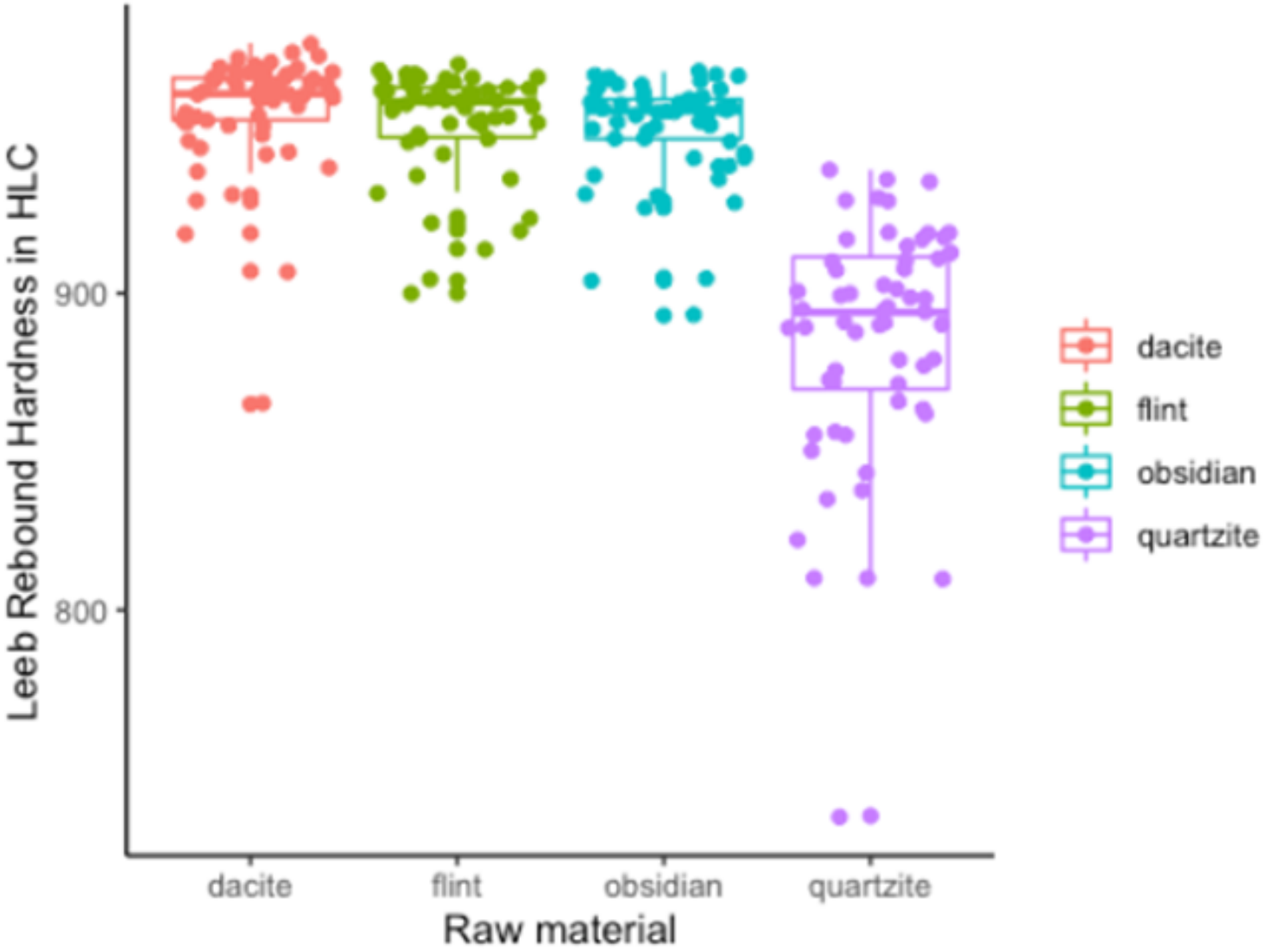

Figura 16: Boxplot Leeb Rebound Hardness, for dacite, flint, obsidian and quartzite.

From the graphic, is possible to see that at least one sample is different from the other. In this case, the differences can be seen from all quartzite samples, which also seems to show a higher internal variability. It is also possible to observe some atypical values (outliers) in quartzite and dacite samples, which are below the standard deviation limits. Also, in each raw material is possible to differentiate that dacite, flint, and obsidian compared to quartzite, have more homogenous values, while quartzite shows a more dispersed variability from the hardness values. After confirming the presence of differences in the hardness measurements, a posthoc test was performed, Tukey's test. This test allows us to statistically test which combinations between samples show significant differences.

The result of Tukey's test is presented in Table 2 below, where the mean differences in hardness, confidence interval, and p-value are given. The present test was interpreted according to the next confidence interval and p-value:

Table 2: Results of the Tukey multiple comparisons of means, with 95% family-wise confidence level.

```
  Tukey multiple comparisons of means
    95% family-wise confidence level

Fit: aov(formula = HLC ~ factor(rawmaterial), data = longdata)

$`factor(rawmaterial)`
                         diff       lwr        upr     p adj
flint-dacite         -4.556667 -16.63054   7.517202 0.7628076
obsidian-dacite      -5.800000 -17.31198   5.711983 0.5613191
quartzite-dacite    -72.566667 -84.07865 -61.054684 0.0000000
obsidian-flint       -1.243333 -13.31720  10.830536 0.9933580
quartzite-flint     -68.010000 -80.08387 -55.936131 0.0000000
quartzite-obsidian  -66.766667 -78.27865 -55.254684 0.0000000
```

After performing Tukey's test and the confidence values presented, it is possible to conclude with 95% confidence that the mean hardness values of the quartzite-dacite, quartzite-flint, and quartzite-obsidian samples are significantly different. Looking at the p-values is possible to see that the sample combinations quartzite-dacite, quartzite-flint, and quartzite-obsidian have low significance values (< 0,05). In this way, conclusions with 95% confidence values showed that quartzite hardness is different. Also, from another perspective, there is no significant difference between flint-dacite, obsidian-dacite, and obsidian-flint samples. These results can also be observed by the boxplot above.

4.2 CONTROLLED EXPERIMENT'S RESULTS

The outcomes of the so-called controlled experiments are discussed in the last section of the Results. The aim of these experiments was to determine the efficiency and durability of four raw materials when in contact material (pinewood) while performing a specified activity (in this case bidirectional linear movement, mimicking a bidirectional cutting movement). Results are presented in the next order: penetration depth, followed by sensors results and the could-to-mesh comparison (C2M), provided by the tridimensional scans.

The sensor's values were all plotted as can be seen below. For each sample force was registered, nominal values are shown in negative units as negative force is the force acting on the sample against the applied force, once the applied force is applied of 5kg is in the Z-axis, and the force sensor is registered in the axis of X. As explained in the methods section, the friction sensor is placed at the end of the x linear drive. Therefore, only the values going from step 2 to 10 are valid for analysis when the motion exerts a force on the sensor. Thus, the only nominal values that are valid for interpretation are the first cycle and all other cycles from steps 2 to 10. Velocity sensor attached at the same position as the friction, resulting in negative values when the opposite motion begins. The penetration depth sensor is attached at the Z-axis, above the platform, so as penetration values get closer to zero as each sample penetrates the pinewood.

As mentioned above, the contact material (pine wood) was submitted to a control experiment with an active material (lithic raw material). Each cycle corresponds to a travel distance separated by 20 steps (steps corresponds to drives measurement). The initial movement (point A to point B) corresponds to the first 10 steps and the return movement corresponds to the other 10 steps (point B to point A). (Figure 17).

From the edge reduction, cloud to mesh (C2M) analysis results in one graphic representation of the counts of edge damage per part. In the graphic is possible to see in the x-axis the distance in mm, and in the y axis the number of parts, by parts is meant the number of triangulations through the edge, higher values representative of more percentage of the edge affected by the damage.

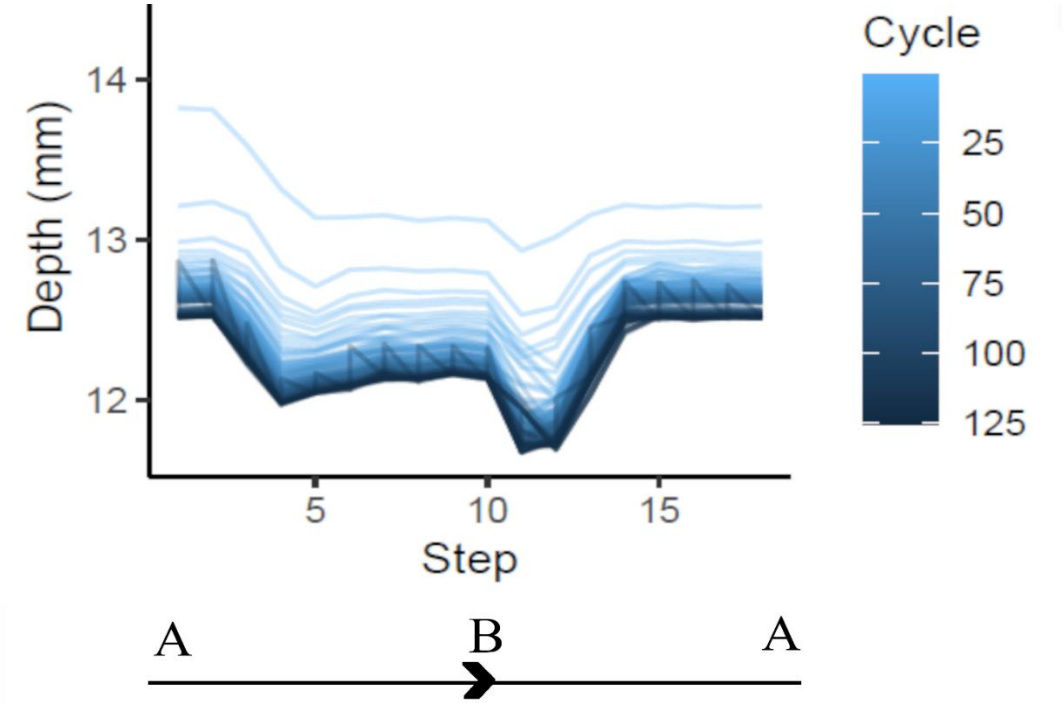

Figura 17: Graphical representation of the cycle setup.

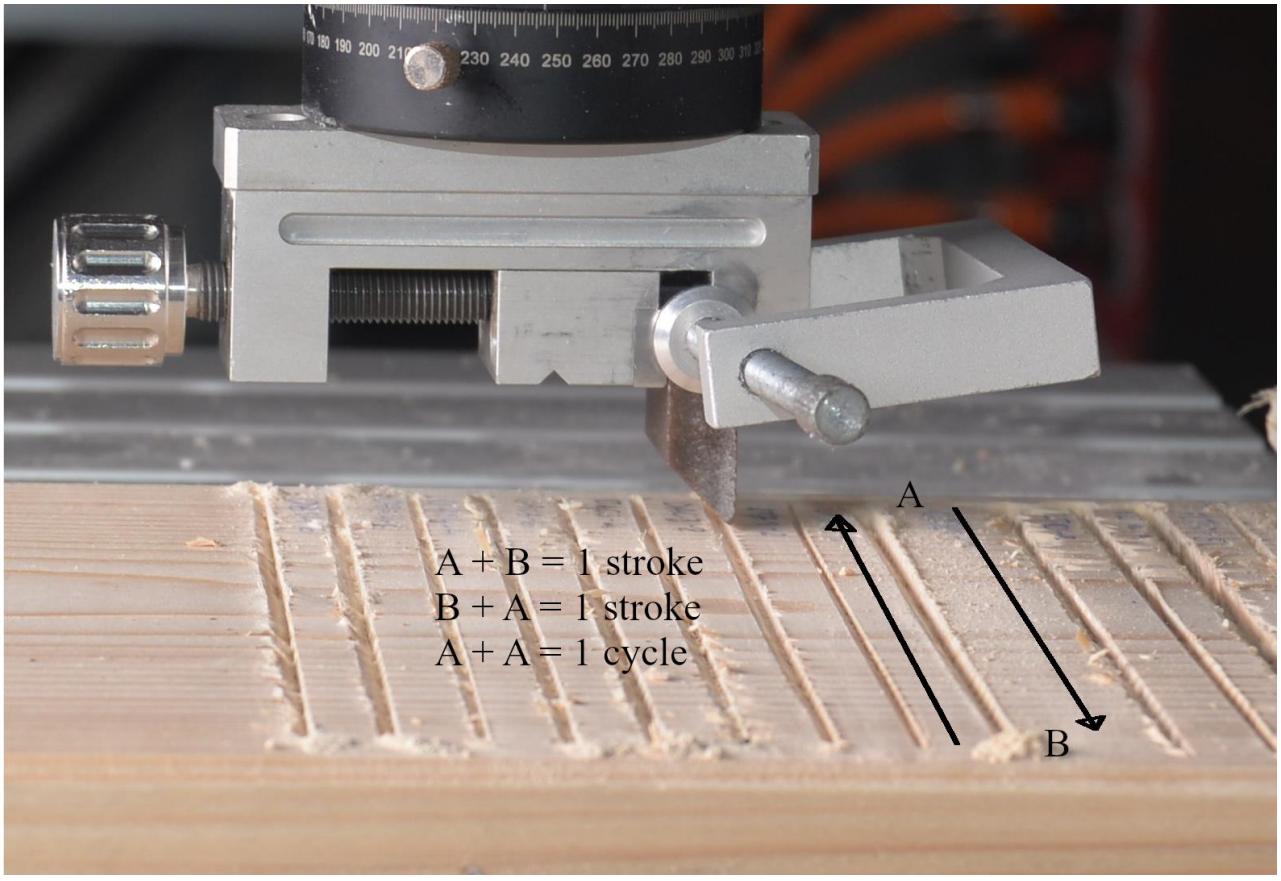

Figura 18: Cyycle ilustration..

4.2.1 QUARTZITE

4.2.1.a QTZ1-1:

From (Figure 18 A), the results are the following:

The first cycle begins with a penetration depth of 16.0 mm in the first ten steps and reaches a maximum of 14.4 mm in the return movement. In the 0 to 125 cycles, the maximum penetration of the sample in the pinewood was 1.5 mm. After the first cycle, the tendency is an increase in penetration. In the last cycles, the initial movement begins at 14.9 mm of penetration depth and crosses a maximum depth of 13.8 mm.

Following the previous values, the news cycle from 126 to 250, starts with a penetration depth of 15.1 mm and reaches a maximum of approximately 14.2 mm. In this cycle, the sample traveled an absolute total of 0,9 mm into the contact material.

After the 500 cycles, the same pattern is observed, lead to penetration of 1.0 mm. Sample QTZ1-1 reached a depth penetration of 13.9 mm at the end of the experiment.

Figure 18 B represents the sensors measure from Inotec, and the results are the following:

The results shown represent all cycles involved in the experiment (0 to 500). The force results range from -50 N to -70 N. In the first steps the force starts with homogeneous values of -48 N. When the movement starts, is possible to observe a multimodal distribution of the values with a maximum of -65 N and a minimum of -55 N. The measurements from step 6 to 11 show a uniform force applied to the sample, ranging from about -58N to -61N. The mean value of force in sample QTZ1-1 is -58 N (see table 3).

Friction values result in a maximum of -73 N. In the first step the initial movement begins at 0 N and is possible to observe a slight increase in the first two steps towards -20 N. The other registered cycles, the initial movement starts at constant values, the travel distance rapidly hit a high friction value, possible to see by the stepped line from step 2 to 3. During the motion is possible to check a decrease in step 5, 7 and 8, followed by an increase in step 4, 6, and 9. The velocity starts at 0 mm/s and has an exponential increase until the fourth step reaching 600 mm/s. From the step 4 to 7 the velocity decrease and achieve a constant linear velocity between 100 mm/s until it stops at step 10. The return movement represents the mirror values of the initial movement.

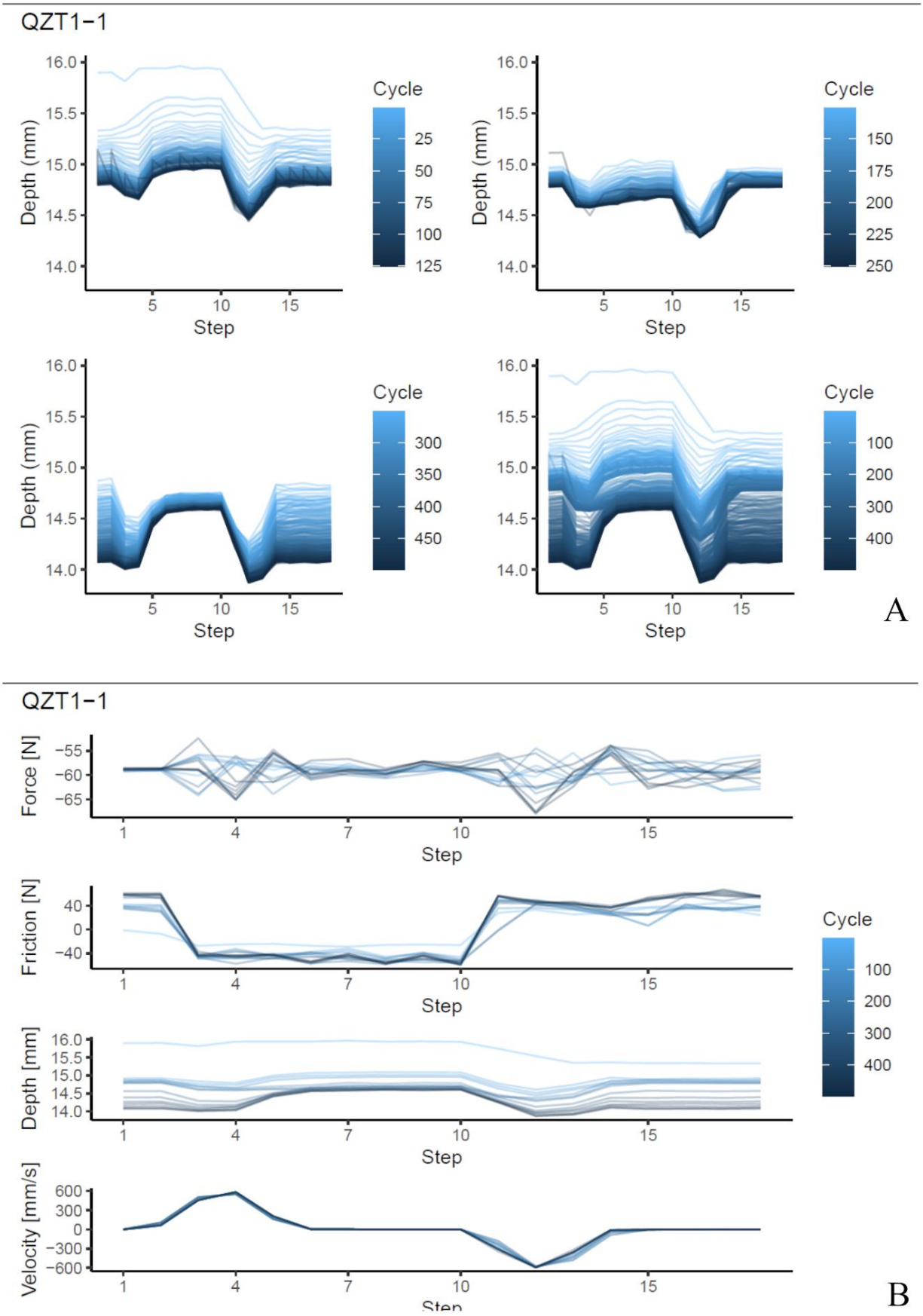

Figura 19: Graphic representation of the values recorded from Inotec from sample ID: QTZ1.1. A - Penetration depth (mm) results, B - Sensors results.

4.2.1.b QTZ1-1 Edge reduction, C2M Comparisons:

Figure 19 represents a graphical observation of the edge reduction from cycles 0 to 500, which corresponds to 1000 linear movements applied to the contact material. A maximum of 1.75 mm was deteriorated after the experiment, although this damage is confined to a specific area of the edge. Most of the damage was achieved in the first cycle (0 to 125) see figure 19, no other reduction is visible in this cycle. A minor reduction is verified from stage 126 to 250, with a range of 0.5 mm in this case affecting the other extremity of the sample. The C2M comparison from cycle 251 to 500 (Figure 20) shows a better distribution of the edge damage trough out the sample, but with low values (0.2 mm to 0.6 mm) when comparing with the previous cycles.

QTZ1-1:

C2M Comparison - Cycle 0 to 125.

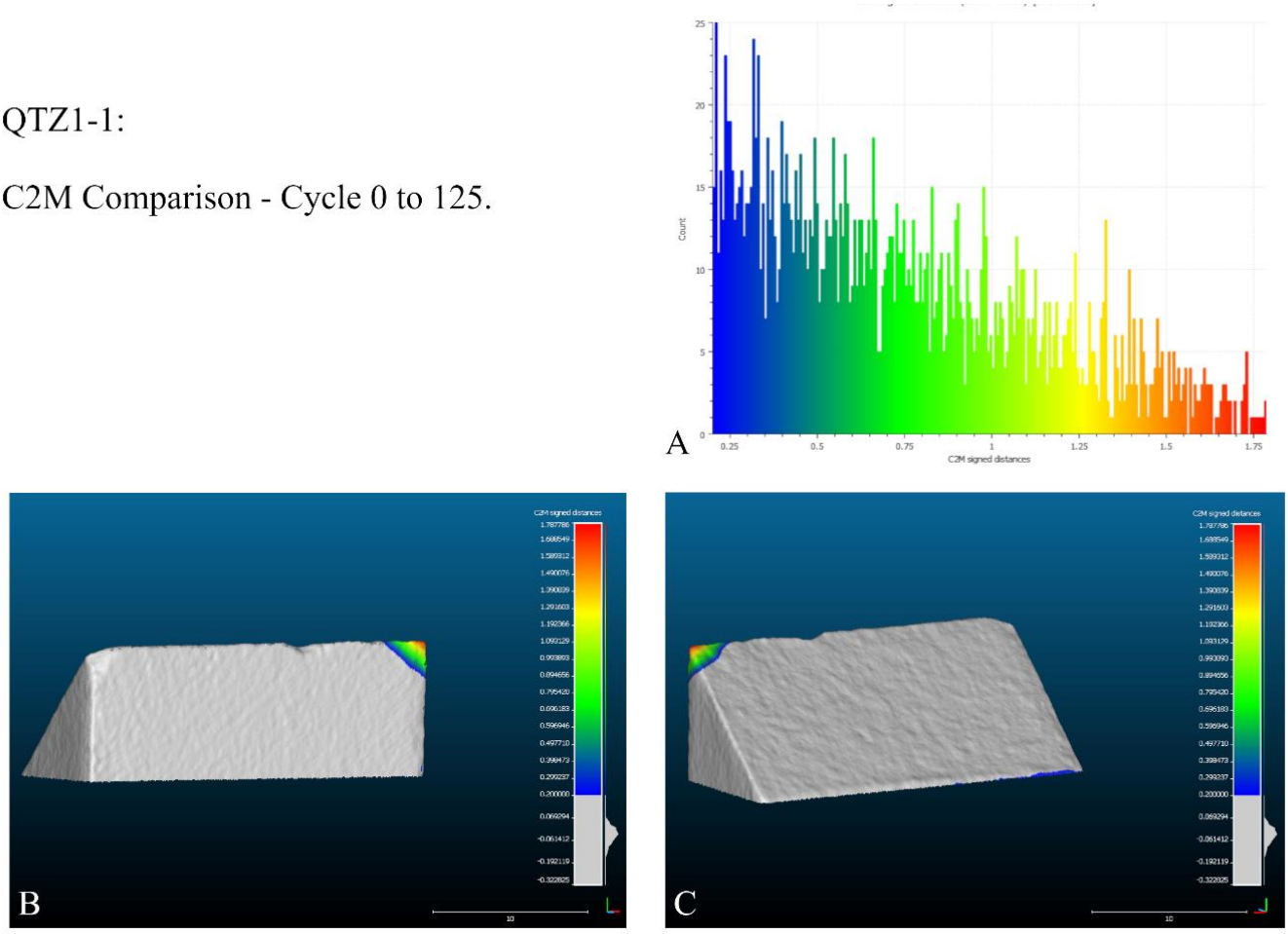

Figure 20: Cloud-to-Mesh edge reduction comparison, sample ID: QTZ1-1, Cycle 125-250. A - Edge damage histogram, B - Back view, C - Front view.

QTZ1-1:

C2M Comparison - Cycle 125 to 250.

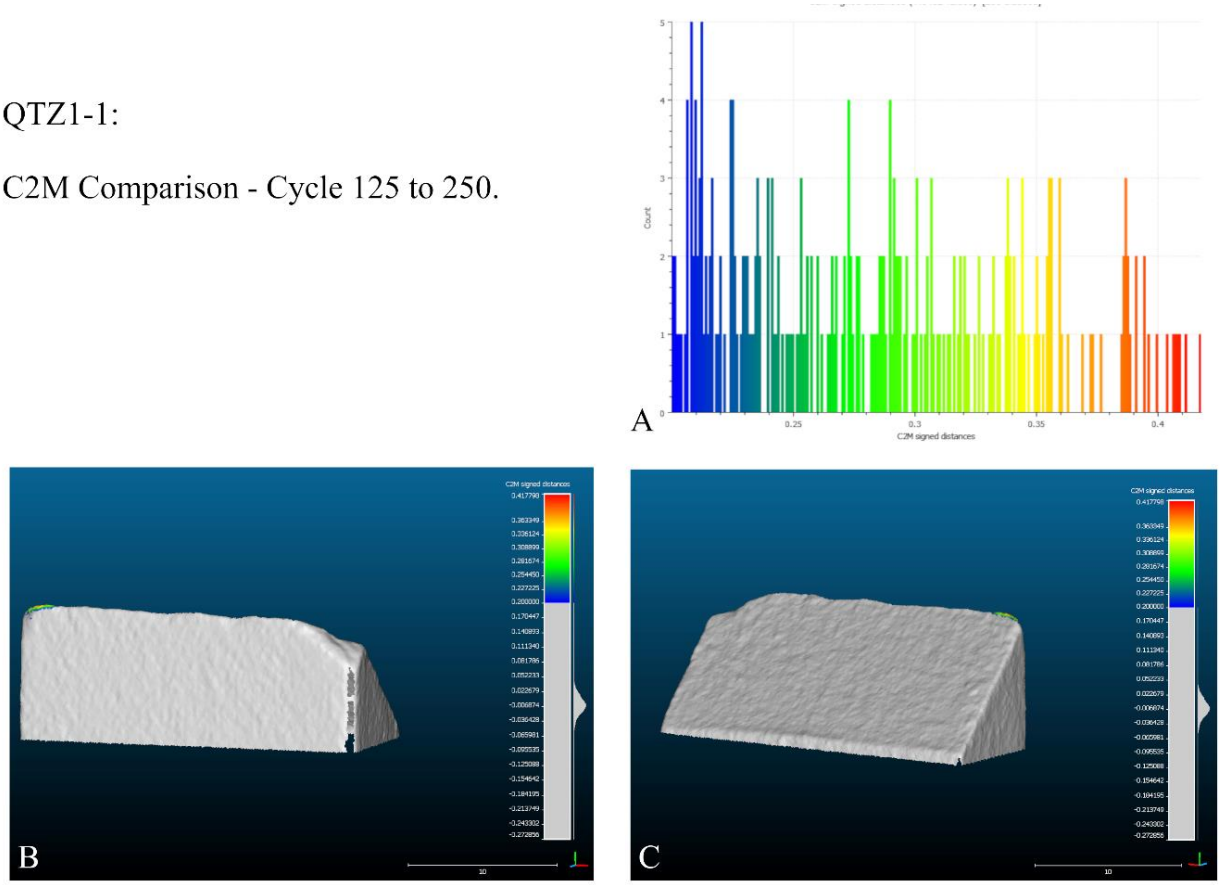

Figure 21: Cloud-to-Mesh edge reduction comparison, sample ID: QTZ1-1, Cycle 125-250. A - Edge damage histogram, B - Back view, C - Front view.

QTZ1-1:

C2M Comparison - Cycle 250 to 500.

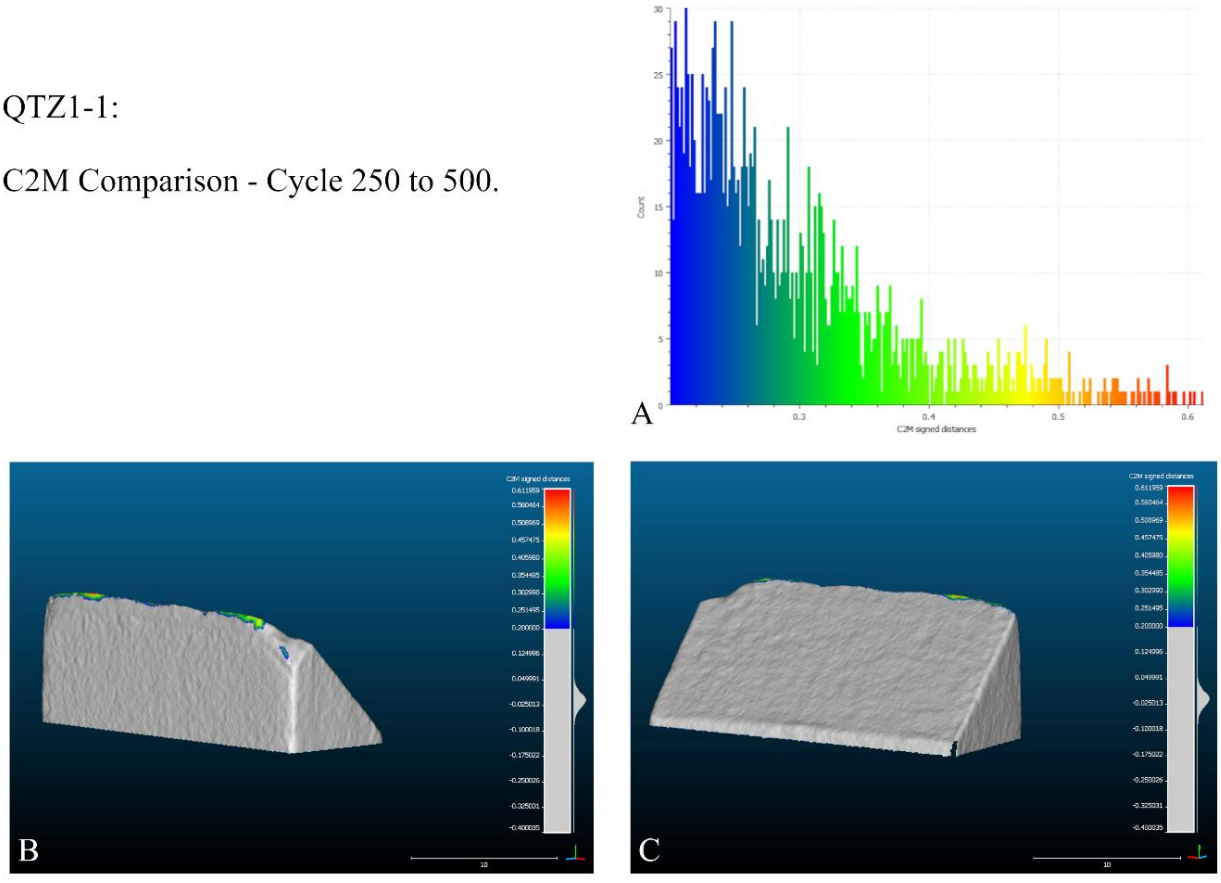

Figure 22: Cloud-to-Mesh edge reduction comparison, sample ID: QTZ1-1, Cycle 250-500. A - Edge damage histogram, B - Back view, C - Front view.

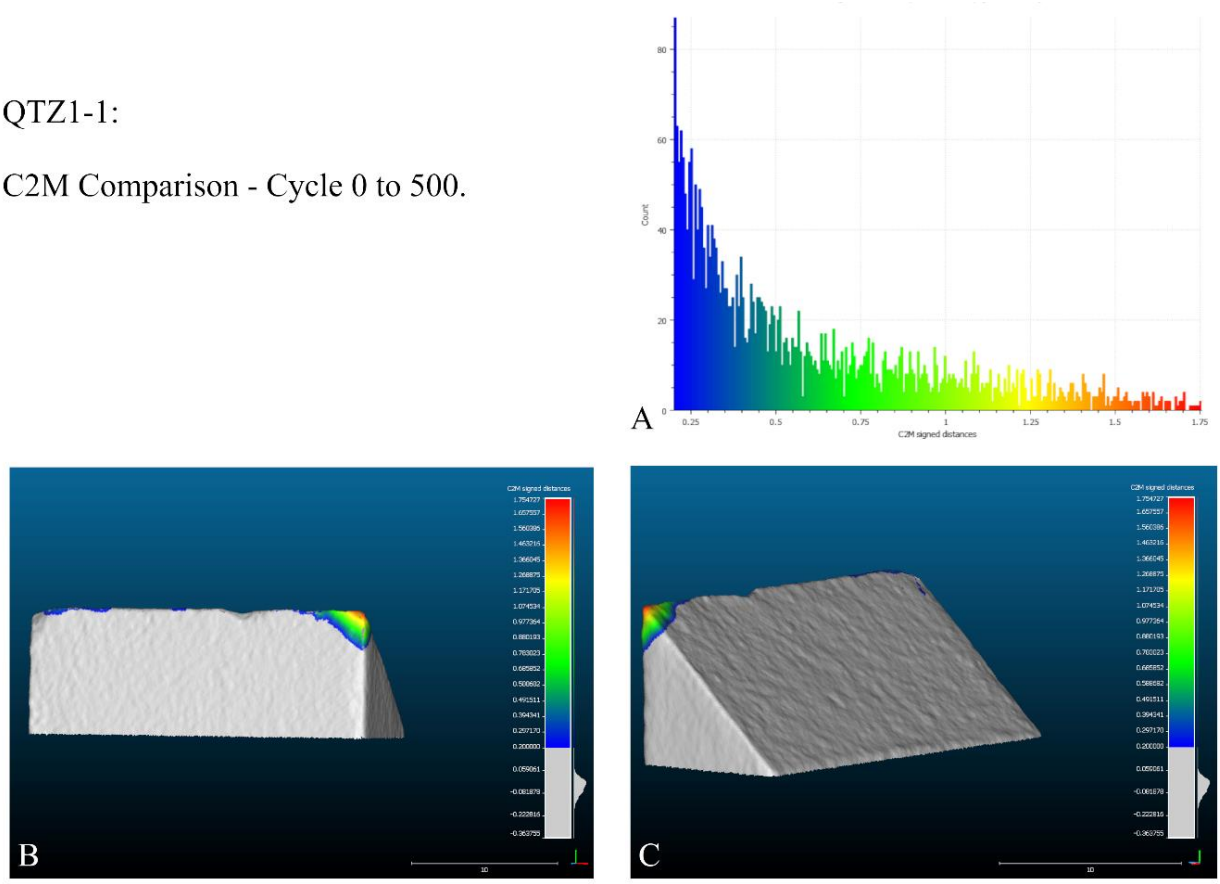

Figure 24: Cloud-to-Mesh edge reduction comparison, sample ID: QTZ1-1, Cycle 0-500. A - Edge damage histogram, B - Back view, C - Front view.

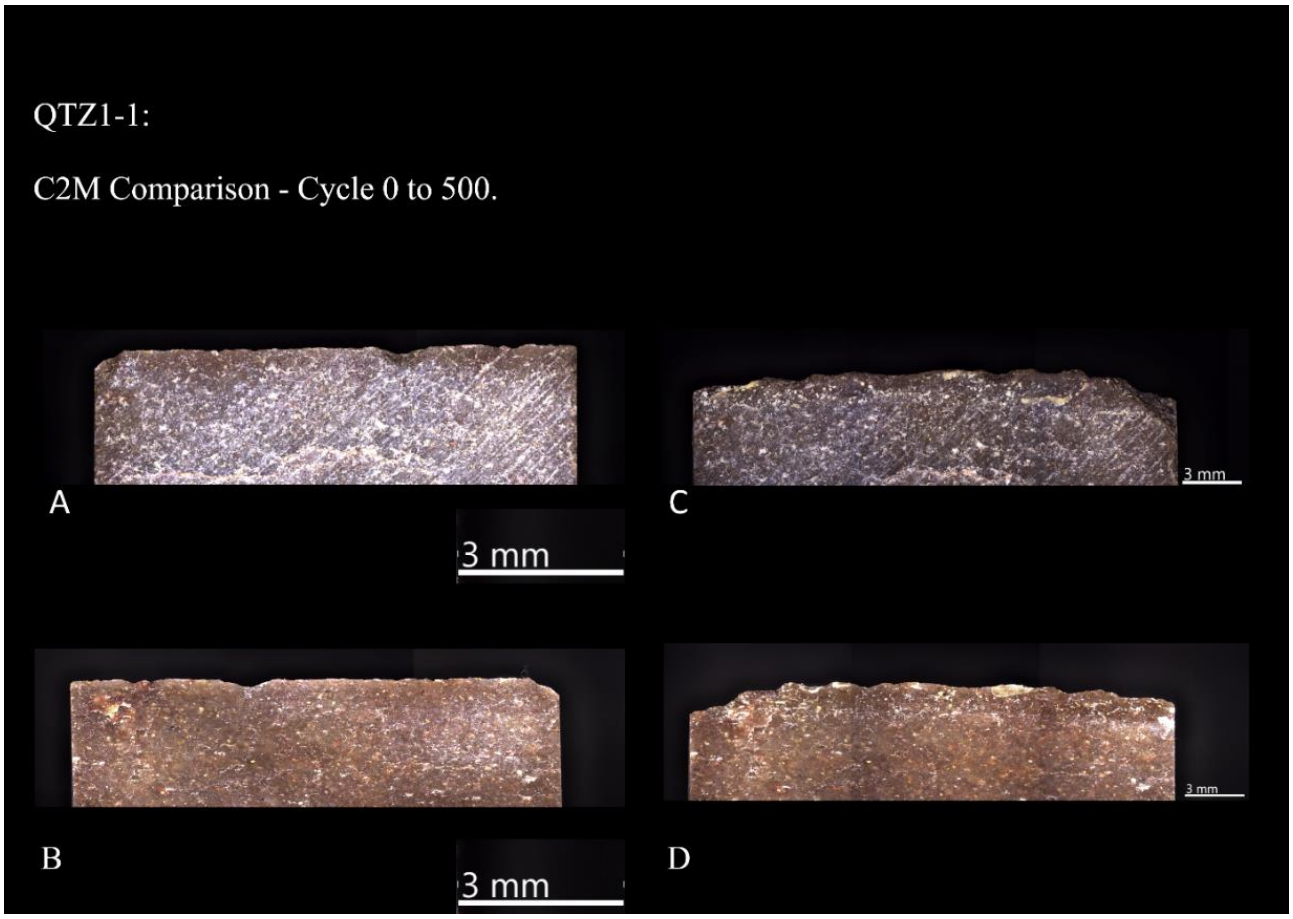

Figure 23: ZEISS Smart zoom images, A/B Cycle 0: A - Back view, B – Front view, C/D Cycle 500: C – Back View, D – Front view. Sample ID: QTZ1-1.

4.2.1.c QTZ1-5:

From Figure 24 A, the results are the following:

The first cycle begins with a depth penetration of 14.7 mm. During this cycle, there is a slight increase in mm of depth penetration over pinewood, with a maximum depth penetration of about 1.3 mm. The last cycles begin with a depth penetration of 13.8 to 14.0 mm with a slight increase over the first 10 steps of the cycles.

From cycle 126 to cycle 250, similar behavior can be observed. The cycles started with an approximation depth of 14.1 mm and have reached a depth penetration of about 13.2 mm in step 10.

The last cycles (cycles 251 to 500) start with a depth penetration between 13.9 and 12.5 mm it is possible to see an increase in depth penetration along with the first 3 steps with a maximum peak of around 12.3 mm. From step 10, the last cycle (cycle 500) shows a maximum depth penetration of 12.0 mm, in the return movement of the sample. The maximum penetration of the sample into the wood from the first stroke until the end of the experiment was 2.7 mm.

Figure 24 B represents the sensors measure from Inotec, and the results are the following:

The results shown represent all cycles involved in the experiment (0 to 500). The values from the force sensor have a distribution from -31 N to -93 N. High values are always followed by lower values, showing a multimodal distribution. This event can be seen at the stages when the sample is stopped, and movement begins (1-5 and 11-15). The mean value for the force registered in QTZ1-5 is -58 N.

The linear distribution of friction values shows a star at 0 N followed by a decrease to near -50 N, and then a balance during the travel distance to step 10. In all the other cycles when the movement begins a stepped decrease happens to -60 to -90 depend on the cycle. After step 3 to 10 is possible to observe a more constant movement, where the friction doesn’t change as much.

The velocity values are following the experiment, an increase of 0 mm/s to 600mm/s, the peak is reached in step 4 with an immediate deceleration until it stops in step 10 and starts again, with negatives values due to backward motion, but with the same pattern.

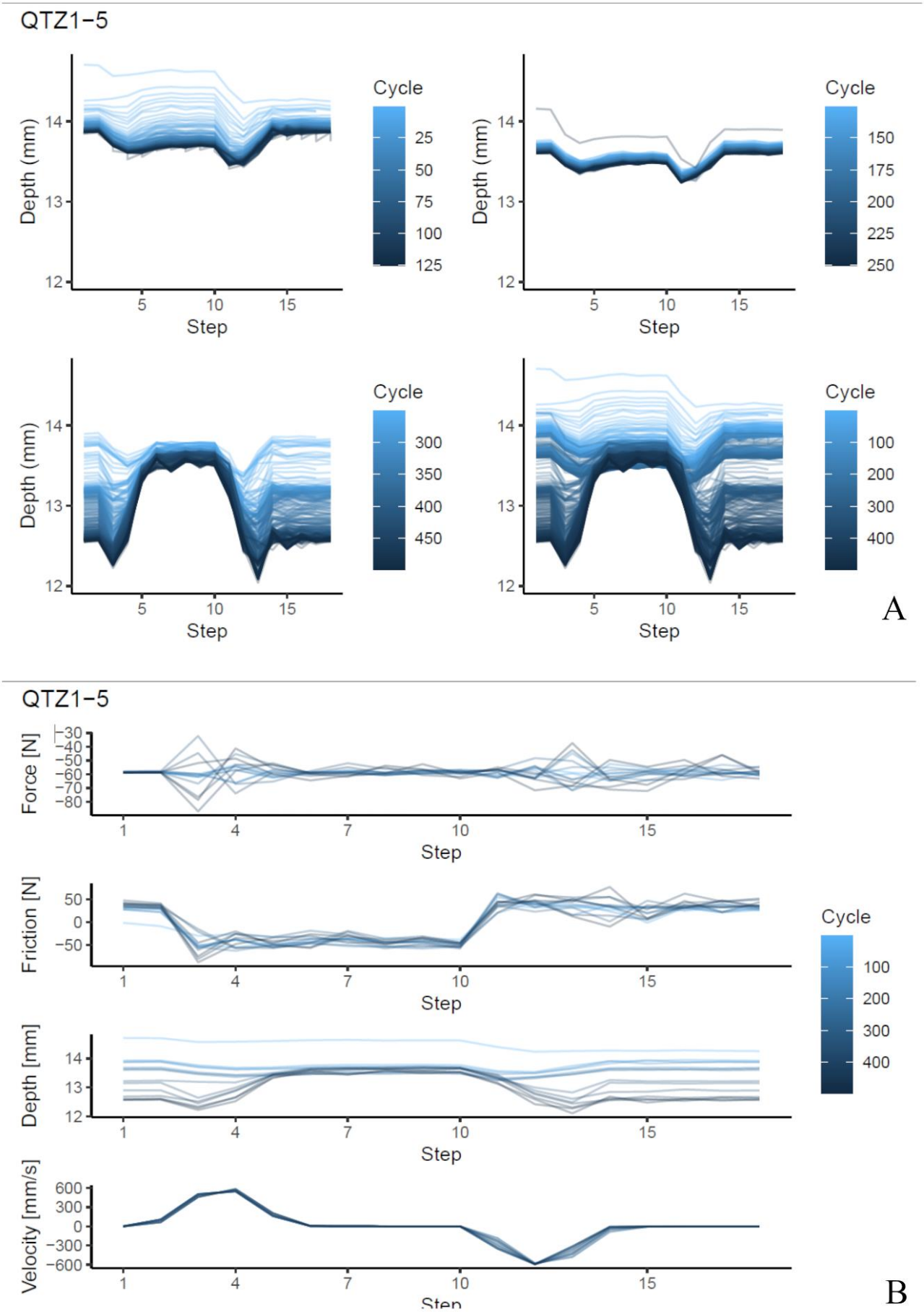

Figura 25: Graphic representation of the values recorded from Inotec from sample ID: QTZ1.5. A - Penetration depth (mm) results, B - Sensors results

4.2.1.d QTZ1-5 Edge reduction, C2M Comparisons:

Figure 25 shows the mesh comparison of cycles 0 to 500. After the 1000 strokes, a maximum of 1.2 mm of lithic raw material was destroyed from the edge of the sample. In QTZ1-5 comparison from the figure 25 reveal that all the edge was exposed to damage, but the extremities were the most damaged areas with values reaching 1.0 mm to 1.2 mm. From the cycles contrasts 0/125/250, the damage was superior in-depth and area on the first 250 strokes (Figure 25, A).

QTZ1-5:

C2M Comparison - Cycle 0 to 125.

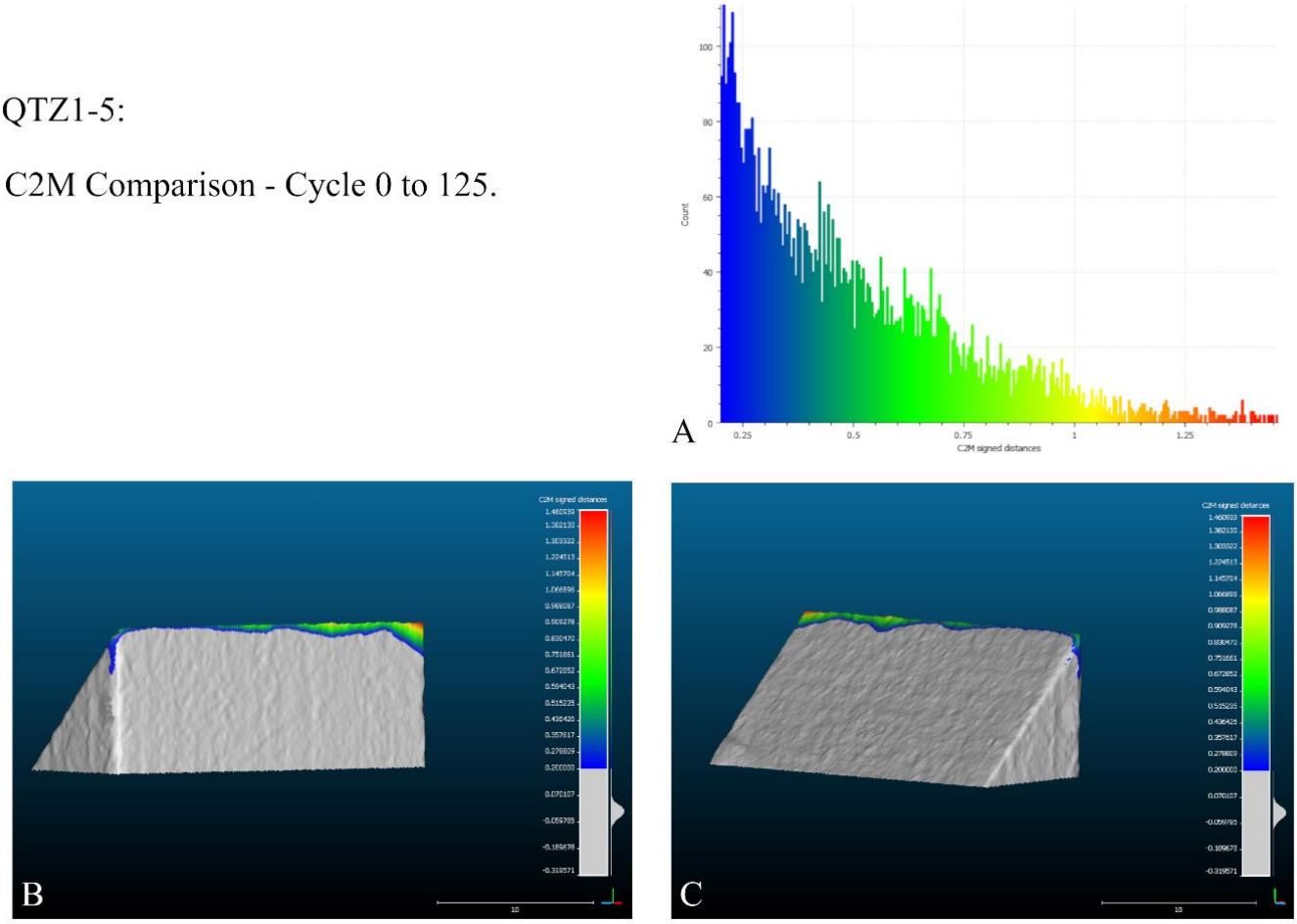

Figure 26: Cloud-to-Mesh edge reduction comparison, sample ID: QTZ1-5, Cycle 0-125. A - Edge damage histogram, B - Back view, C - Front view.

QTZ1-5:

C2M Comparison - Cycle 125 to 250.

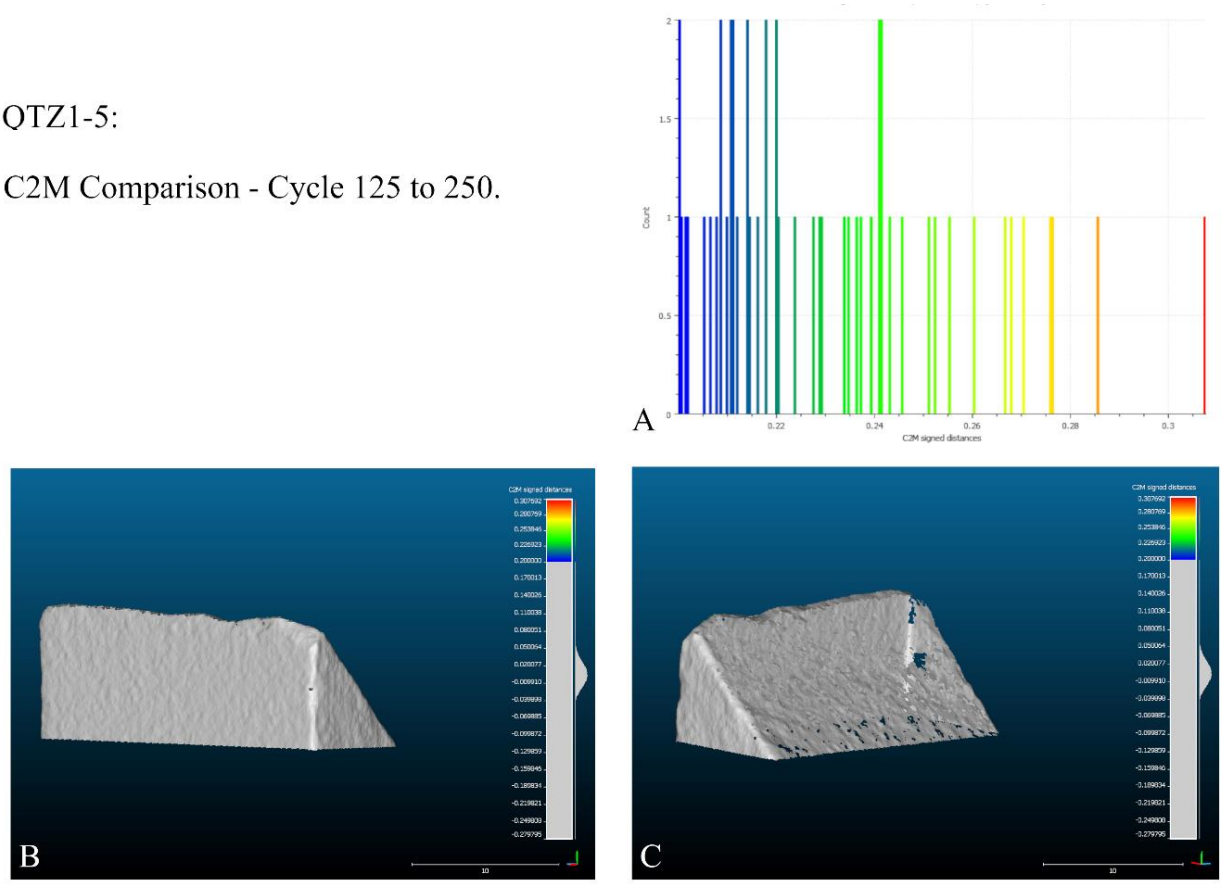

Figure 27: Cloud-to-Mesh edge reduction comparison, sample ID: QTZ1-5, Cycle 0-125. A - Edge damage histogram, B - Back view, C - Front view.

QTZ1-5:

C2M Comparison - Cycle 250 to 500.

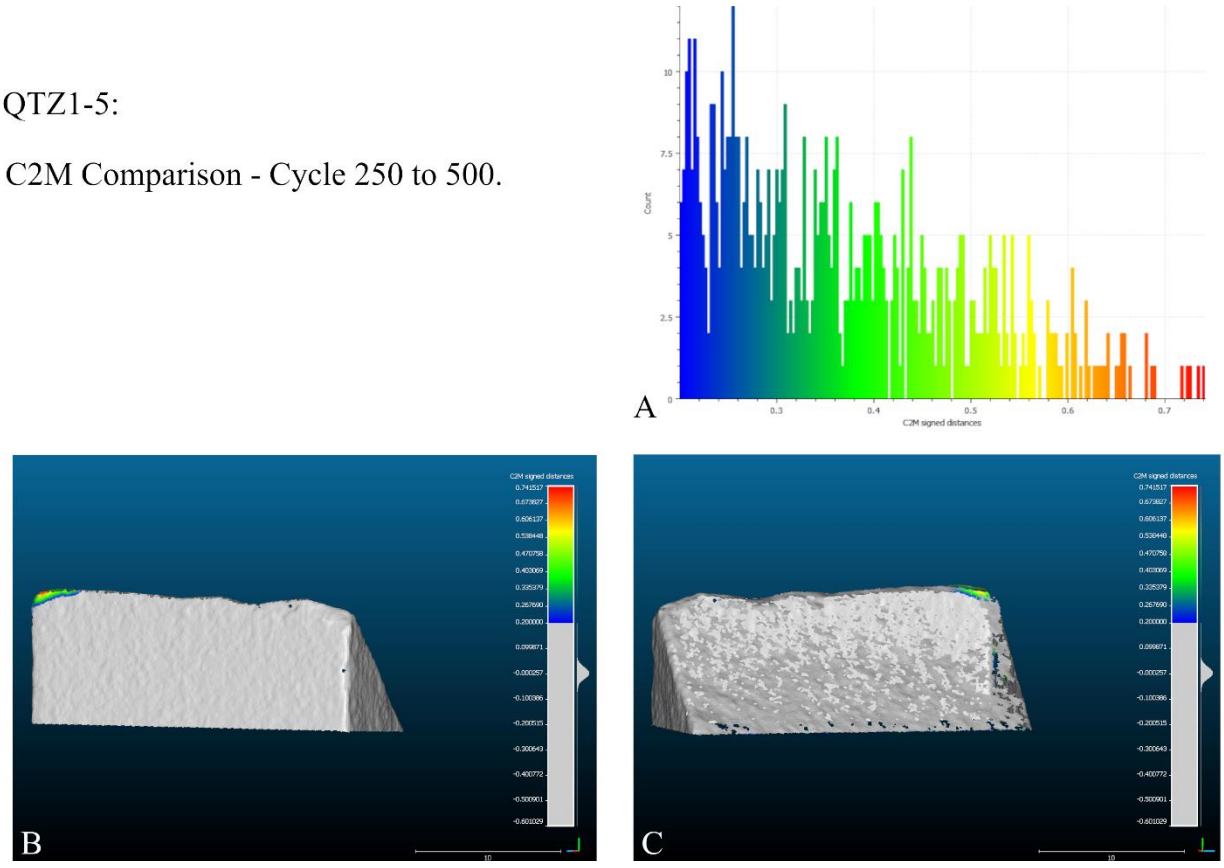

Figure 28: Cloud-to-Mesh edge reduction comparison, sample ID: QTZ1-5, Cycle 250-500. A - Edge damage histogram, B - Back view, C - Front view.

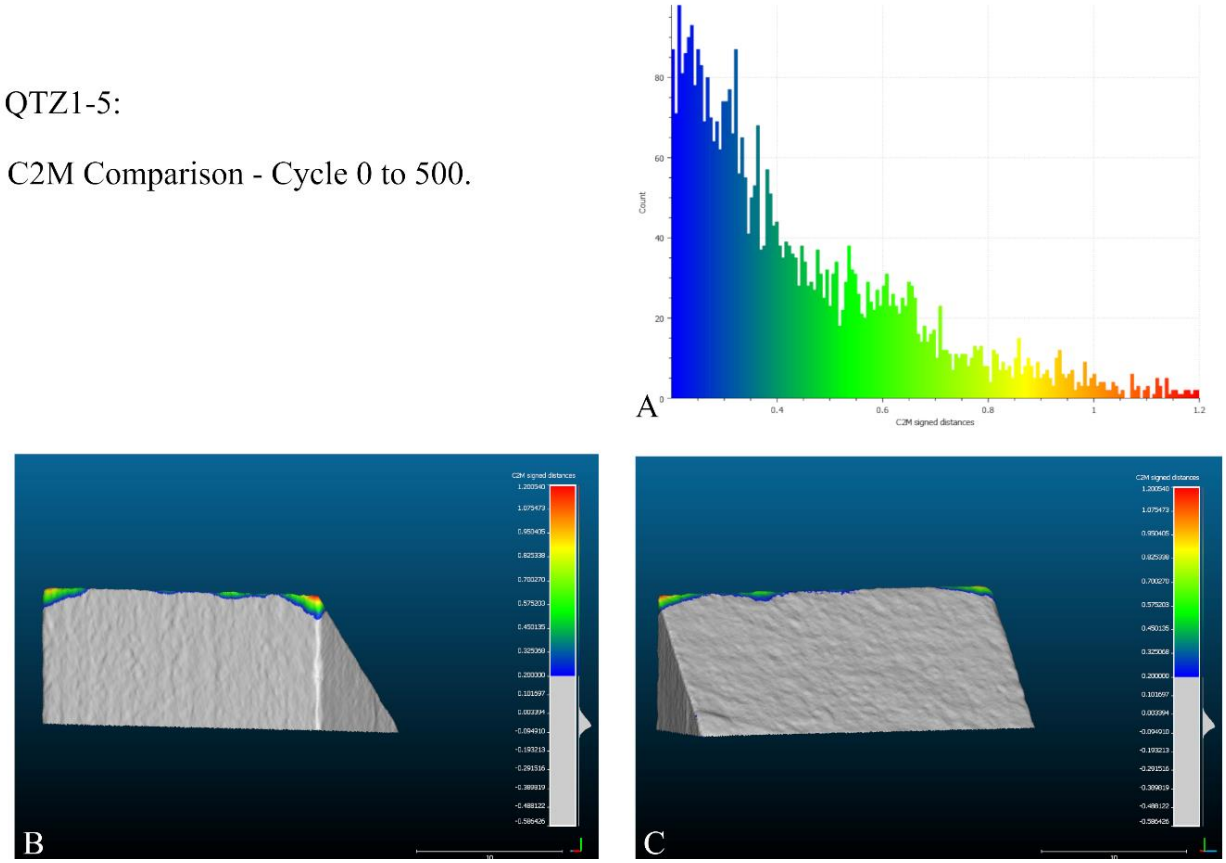

Figure 30: Cloud-to-Mesh edge reduction comparison, sample ID: QTZ1-5, Cycle 0-500. A - Edge damage histogram, B - Back view, C - Front view.

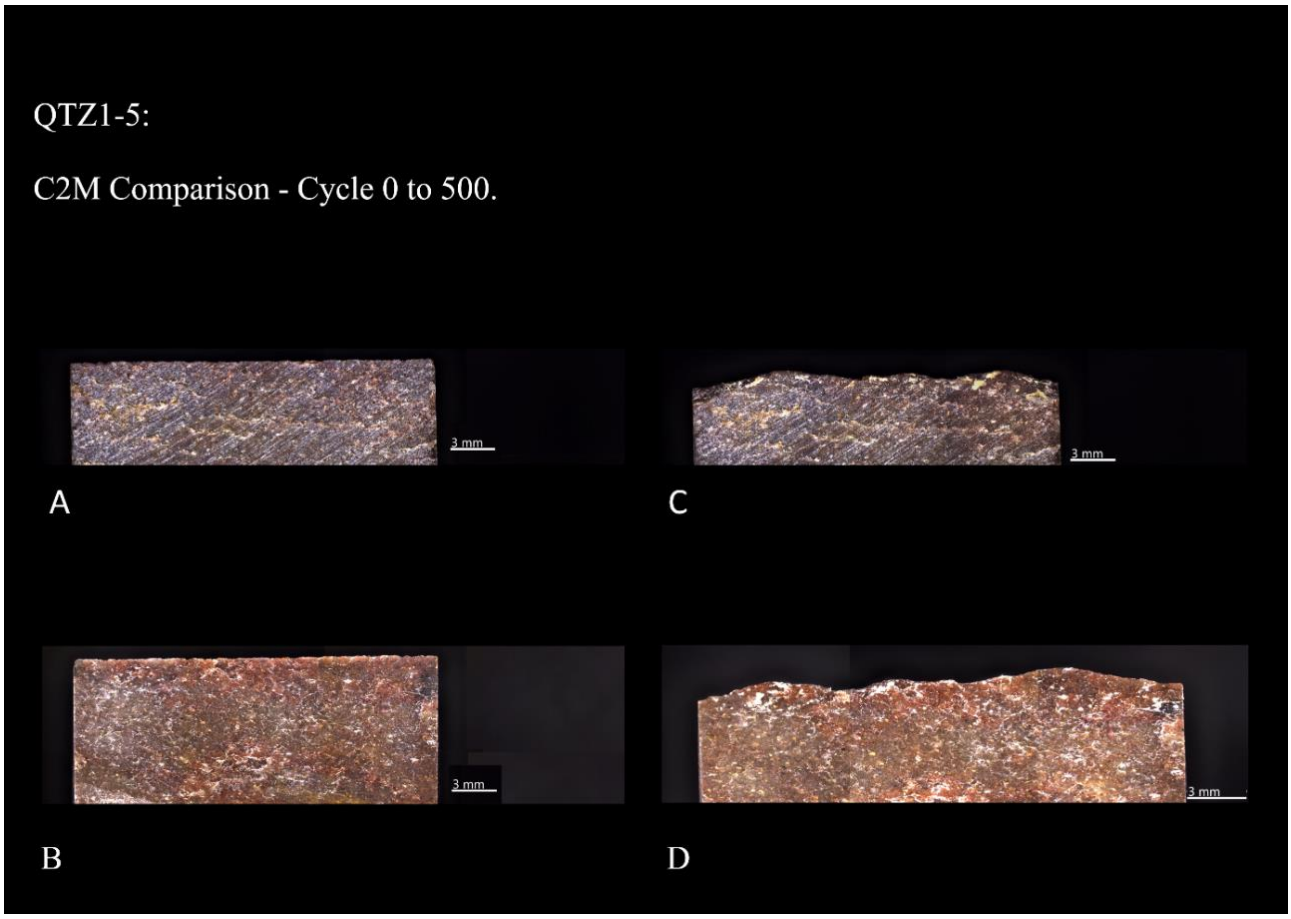

Figure 29: ZEISS Smart zoom images, A/B Cycle 0: A - Back view, B – Front view, C/D Cycle 500: C – Back View, D – Front view. Sample ID: QTZ1-5.

4.2.1.e QTZ1-2:

From Figure 30 A, the results are the following:

Sample QTZ1-2 begins the experiment by gradually penetrating the pinewood from a depth of about 14.3 mm in the first cycles (0 to 125), although a small gap is observed in the graph between the 50 and 75 cycles, this gap is representative of an abrupt penetration of approximately 0.5 mm when considering the other cycles. The next stage starts exactly at the deepest measure from the previous cycle, the next 250 moves behave similarly to the previous ones. Gradually, the sample reaches a maximum depth of 11.5 mm.

The last 250 cycles also maintain a constant depth until 1000 strokes are reached with a maximum penetration depth of 10.7 mm. In all the graphs, it can be observed that the sample reaches a lower depth in the steps related to the start of the movement, steps 1 to 4 and 11 to 14. QTZ1-2, have a maximum penetration of 3.6 mm into the contact material.

Figure 30 B represents the sensors measure from Inotec, and the results are the following:

All the cycles start the experiment with a force applied of -60 N, and most of the cycles maintain constant the same force. Only six cycles among the cycles 350 and 500 behave differently from the rest of the experiment, this event is recorded in steps 3 to 5, and 12 to 15, the values are between -40 N and -85 N.

The initial friction to which the QTZ1-2 sample is submitted reaches approximately -40 N, with a decrease in step 3, and oscillates between -40 and -80 N until it reaches the first stop in step ten. All the other cycles range between 0 and -40 N in the travel distance (step 3 to 10). Because is not possible to take the values of the first two steps as real values, what is possible to see is that an increase of friction exists in the firsts steps. Two lines values from cycles 2 to 125 correspond to grey-blue color registered the highest values of friction of -82 N.

From the velocity graph, is possible to observe constant values. The first 4 steps are equivalent to steps 10 to 14, representing the acceleration speed reaching 600 mm/s and -600 mm/s. From steps 10 to 14 exists a slight deviation of the constant velocity with a premature decrease in step 10 followed with the reverse behavior as ascending to point A.

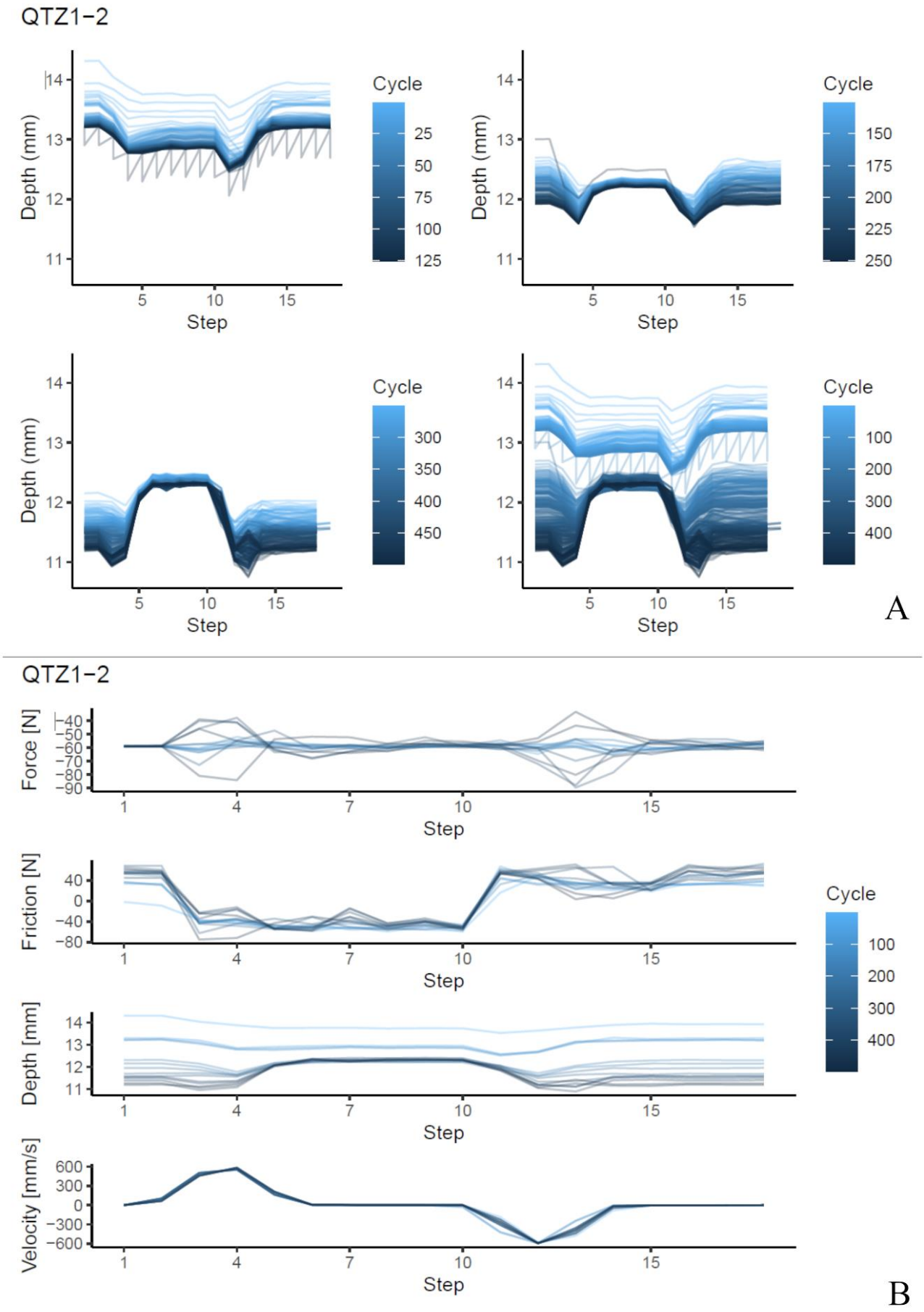

Figura 31: Graphic representation of the values recorded from Inotec from sample ID: QTZ1-2. A - Penetration depth (mm) results, B - Sensors results.

4.2.1.f QTZ1-2 Edge reduction, C2M Comparisons:

After 1000 strokes applied to QTZ1-2 against the contact material is possible to identify the damage through the sample's edge (Figure 34). The maximum damage of 1.3 mm is visible in one of the extremities of the sample. Damage of at least 0.5 mm is visible on all edges. More expressive damage is visible on the external side of the sample (Figure 34-C). The bigger percentage of reduction of quartzite material is visible at the first 250 strokes (Figure 31), the damage covers all the edges and goes until 1.0 mm through the sample.

QTZ1-2:

C2M Comparison - Cycle 0 to 125.

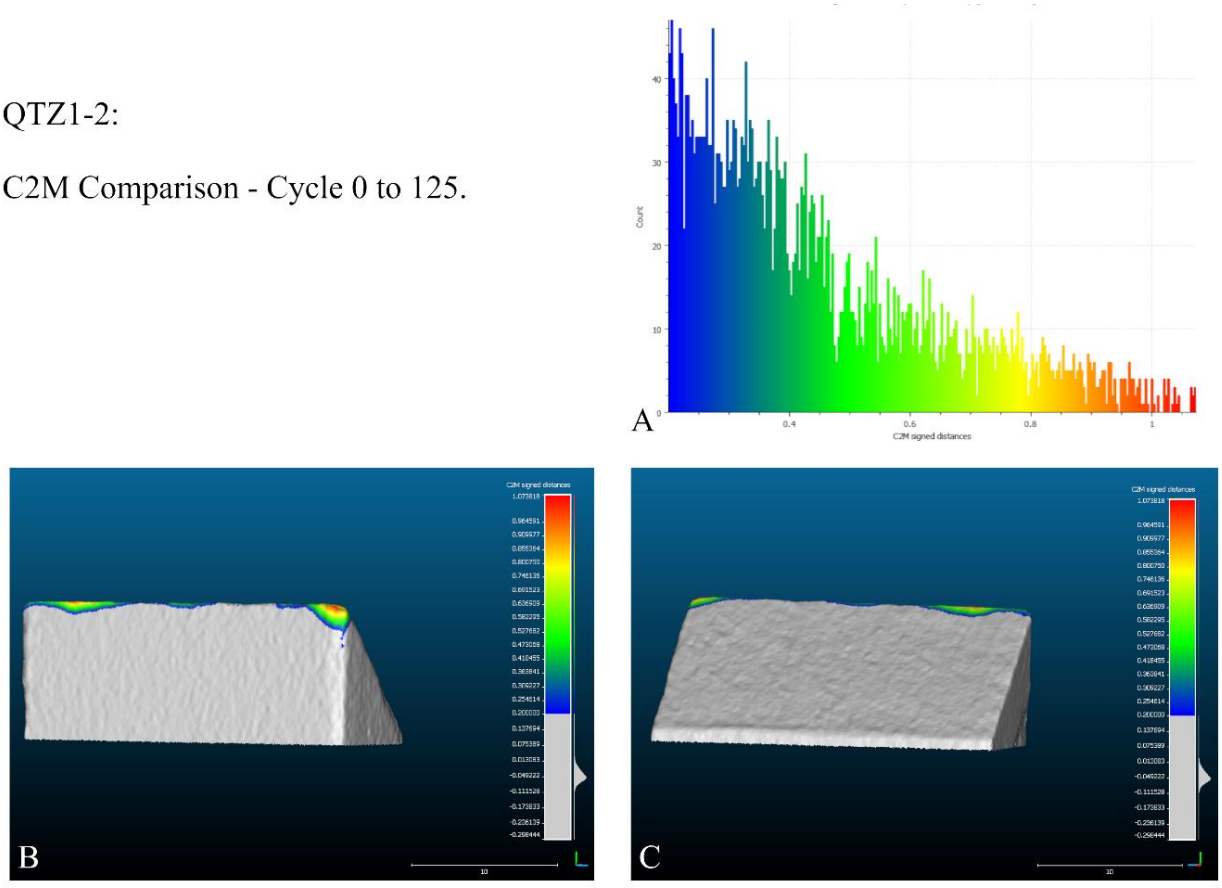

Figure 32: Cloud-to-Mesh edge reduction comparison, sample ID: QTZ1-2, Cycle 0-125. A - Edge damage histogram, B - Back view, C - Front view.

QTZ1-2:

C2M Comparison - Cycle 125 to 250.

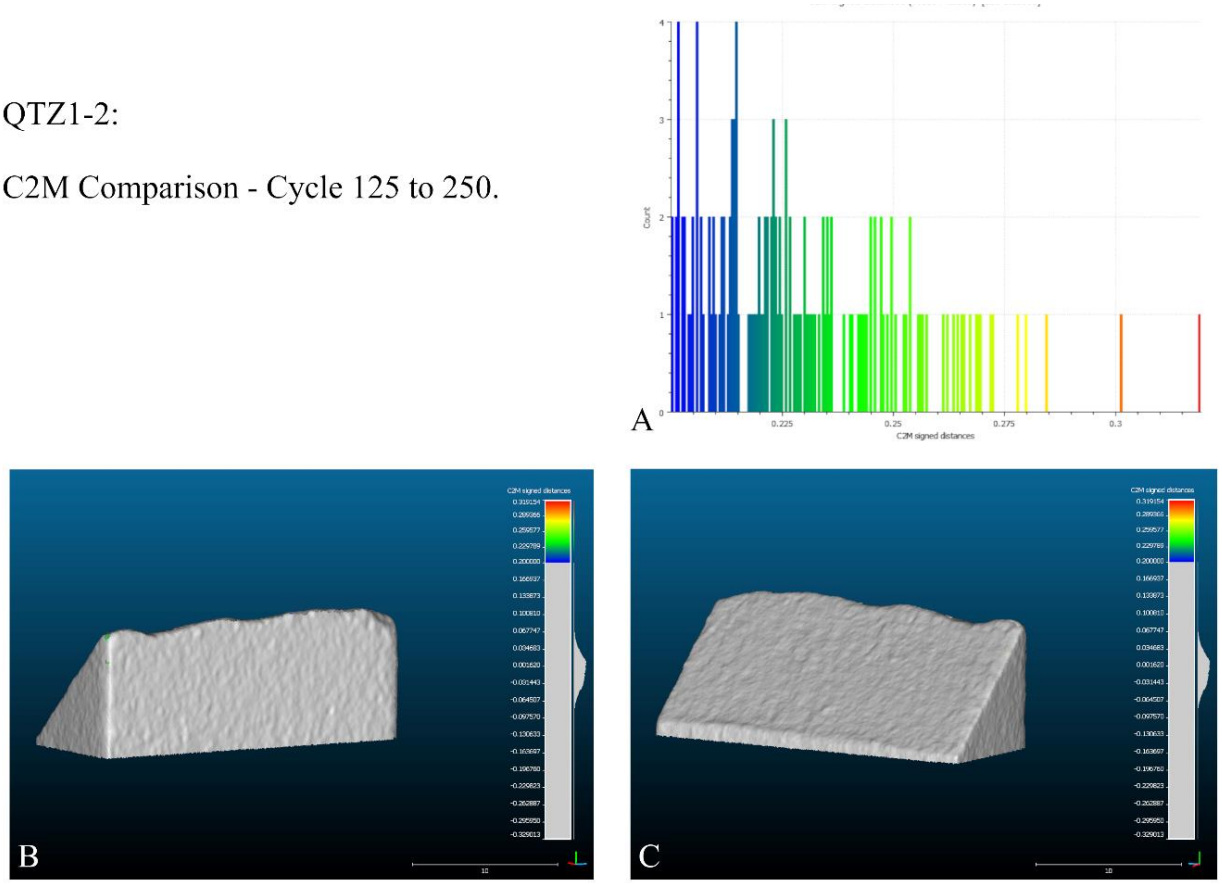

Figure 33: Cloud-to-Mesh edge reduction comparison, sample ID: QTZ1-2, Cycle 125-250. A - Edge damage histogram, B - Back view, C - Front view.

QTZ1-2:

C2M Comparison - Cycle 250 to 500.

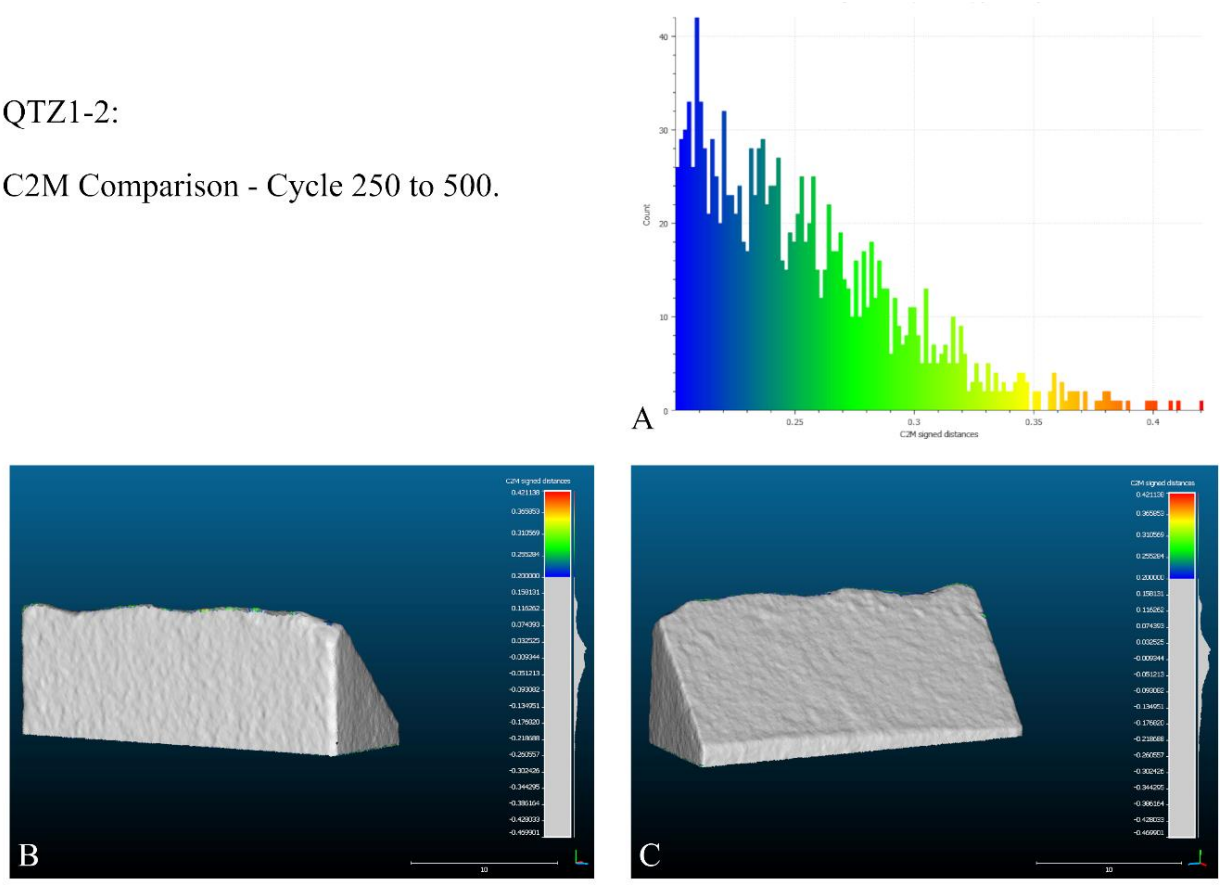

Figure 34: Cloud-to-Mesh edge reduction comparison, sample ID: QTZ1-2, Cycle 250-500. A - Edge damage histogram, B - Back view, C - Front view.

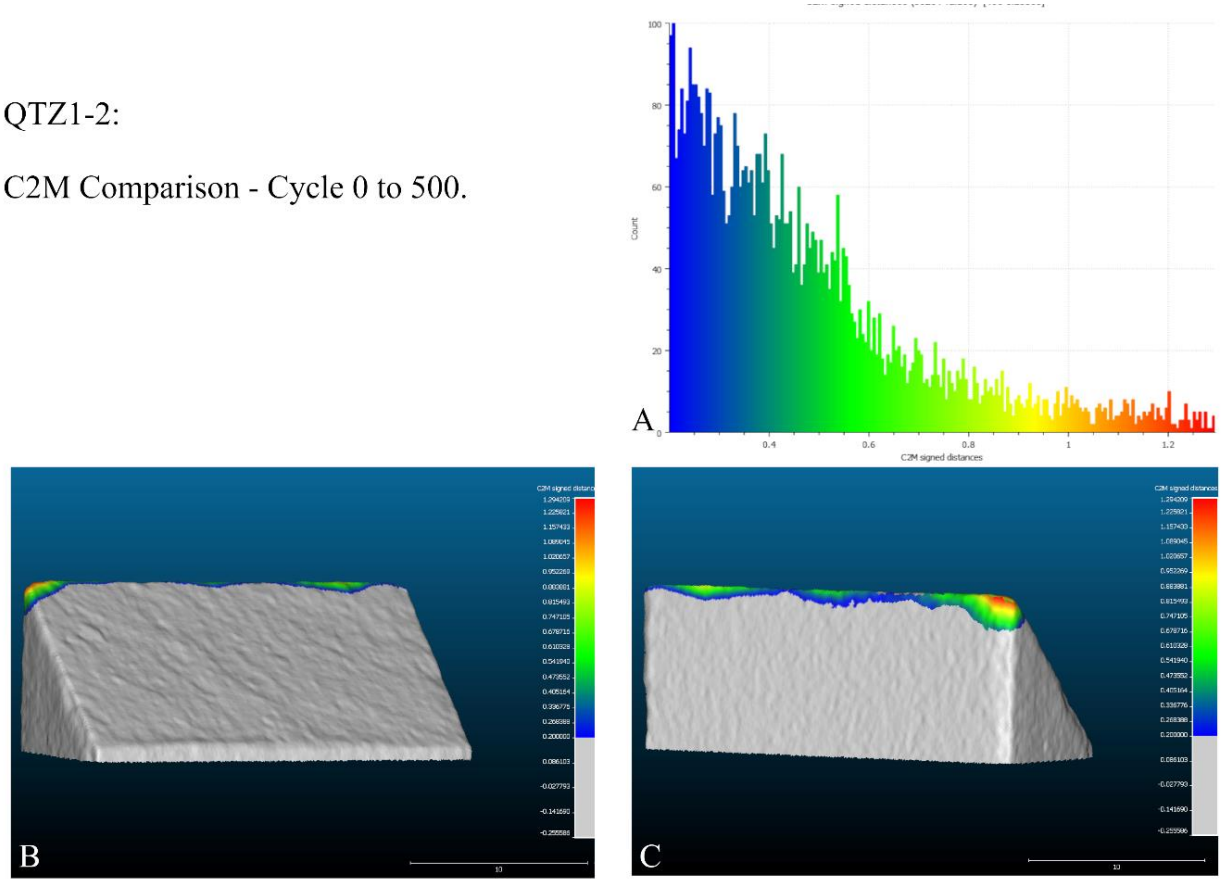

Figure 35: Cloud-to-Mesh edge reduction comparison, sample ID: QTZ1-2, Cycle 0-500. A - Edge damage histogram, B - Back view, C - Front view.

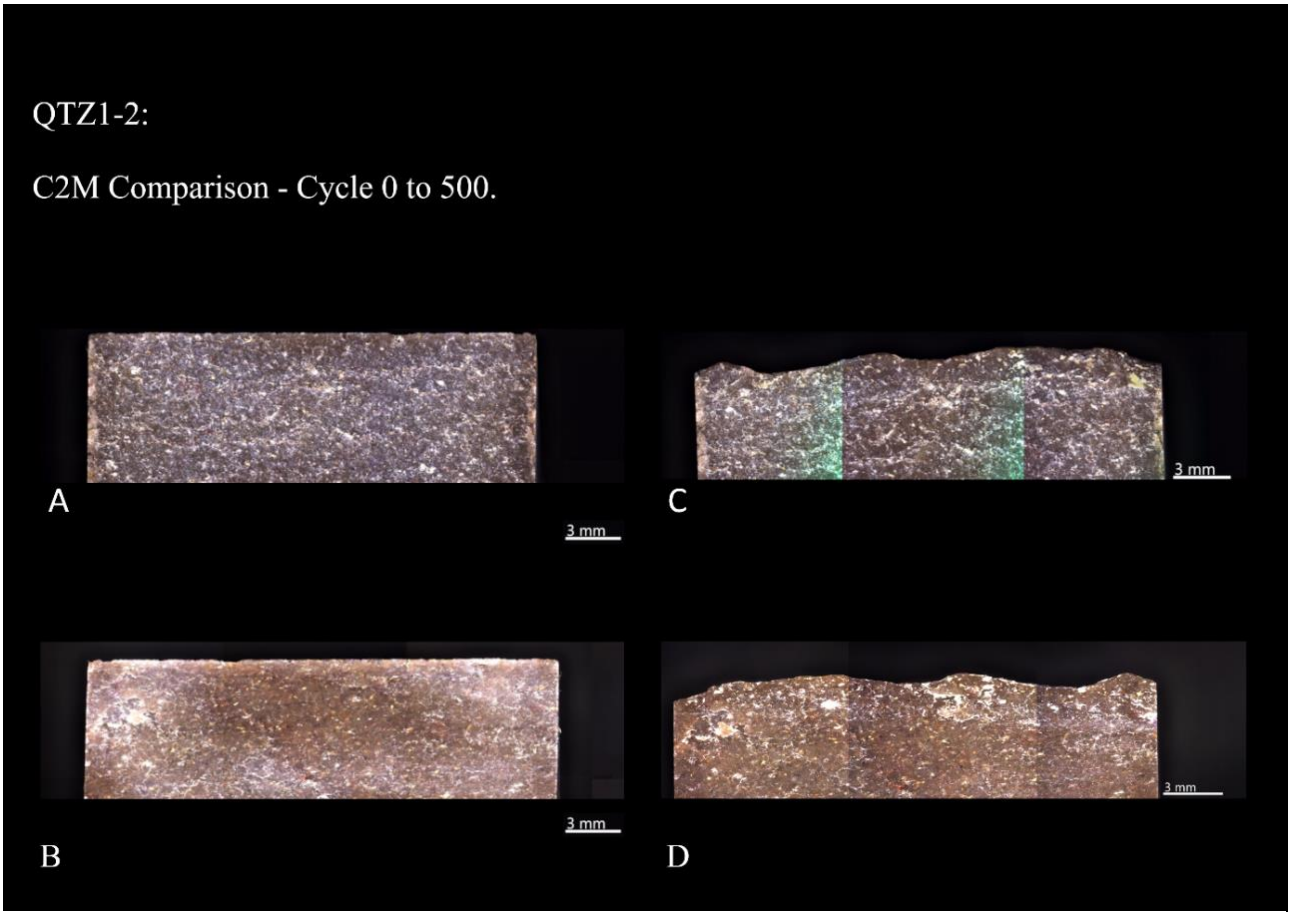

Figure 36: ZEISS Smart zoom images, A/B Cycle 0: A - Back view, B – Front view, C/D Cycle 500: C – Back View, D – Front view. Sample ID: QTZ1-2.

4.2.2 FLINT

4.2.2.a FLT 10-2

From Figure 36 A, the results are the following:

The first cycle, using the FLT 10-2 sample, starts with a depth penetration of 15.7mm. During this cycle it is possible to verify that the material penetrates the wood with higher incidence from step 13, reaching a maximum depth penetration of 13.4 mm. Increasing the number of cycles, it turns out that the depth penetration also increases. In cycle 124 the moves start with a depth penetration of about 13.5 mm and the maximum depth penetration of 13.4 mm, which is verified in step 13.

The same pattern is observed from cycle 126 to cycle 250. In these cycles, the moves start with a depth penetration close to 13.6 mm throughout the first 3 steps. From steps 4 to 12 the sample didn't penetrate as much as steps 13 to 20 with a maximum depth penetration around 13.5 mm.

As of cycle 251, the moves start with a very similar depth penetration. However, in cycles 251 to 258, it is observed that the depth penetration decreases from step 5 reaching 14.3 mm. From step 10 onwards, all cycles start the movement with a very similar depth penetration and reach the maximum penetration around 13.1 mm.

Figure 36 B represents the sensors measure from Inotec, and the results are the following:

All cycles start the movement with an initial force applied on the pinewood of about – 67 N. During the movements, the cycles behave in different ways, and by analyzing the force graph it is possible to verify that the 200 first cycles present a greater applied force of -65 N around step 3. The same behavior is verified again around step 13 but with cycles 300, 400, and 500. The first movement of sample FLT10-2 start at 0 N and the friction applied in this first cycle didn't exceed -50 N. The initial friction that the two bodies in contact suffer after cycle 1 is around 0 to -109 N from step 3 to 10. From step 5 on, friction starts to increase in the last cycles, with the maximum friction being reached – 110N. In the velocity graph, all cycles behave in the same way. The movement speed starts at 0 mm/s and reaches its maximum of around 600 mm/s in step 4 of all cycles. From step 10 onwards, all cycles start at 0 mm/s and reach a maximum speed of -600 mm/s, with minor diversions on the return movement in steps 10 to 14.

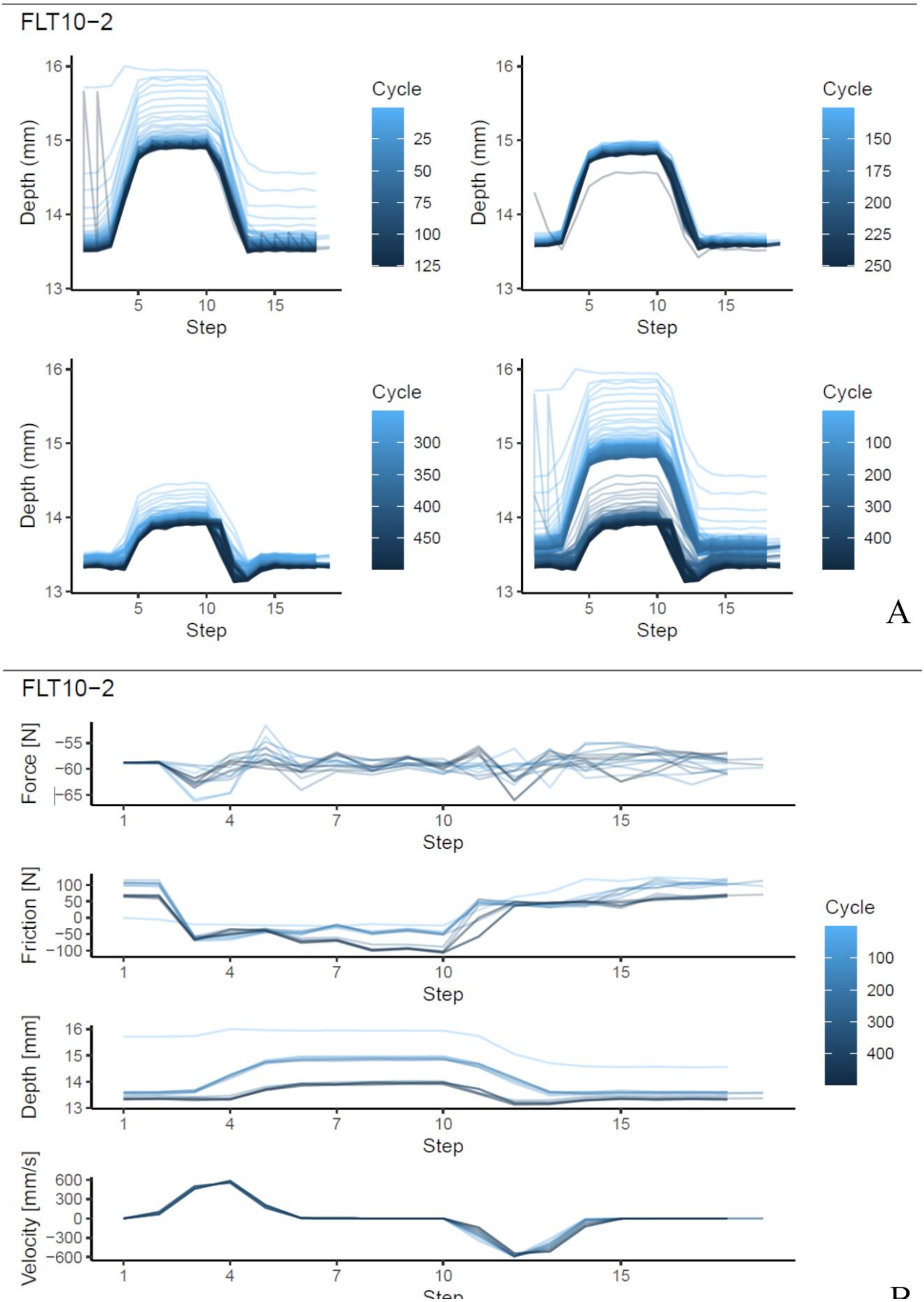

Figura 37: Graphic representation of the values recorded from Inotec from sample ID: FLT10-2. A - Penetration depth (mm) results, B - Sensors results.

4.2.2.b FLT10-2 Edge reduction, C2M Comparisons

FLT10-2 comparisons 0 to 500 cycles show little degradation of the edge. From the histogram in Figure 41, it can be seen that the damage in the edge is constant over several parts when the damage ranges from 0.2 mm to 0.3 mm, the same behavior is observed from 0.3 mm to 0.5 mm but in a lower part of the edge. In the other cycles, it is seen that the flint is slowly damaged from the first 250 blows and reaches its maximum damage of 0.5 mm, the next 250 strokes result in less damage, moreover one end of the edge was reduced to 0.5 mm. The last cycle witnesses the greater damage, the graph (Figure 39-A) shows that the damage is more concentrated from 0.3 mm to 0.5 mm.

FLT10-2:

C2M Comparison - Cycle 0 to 125.

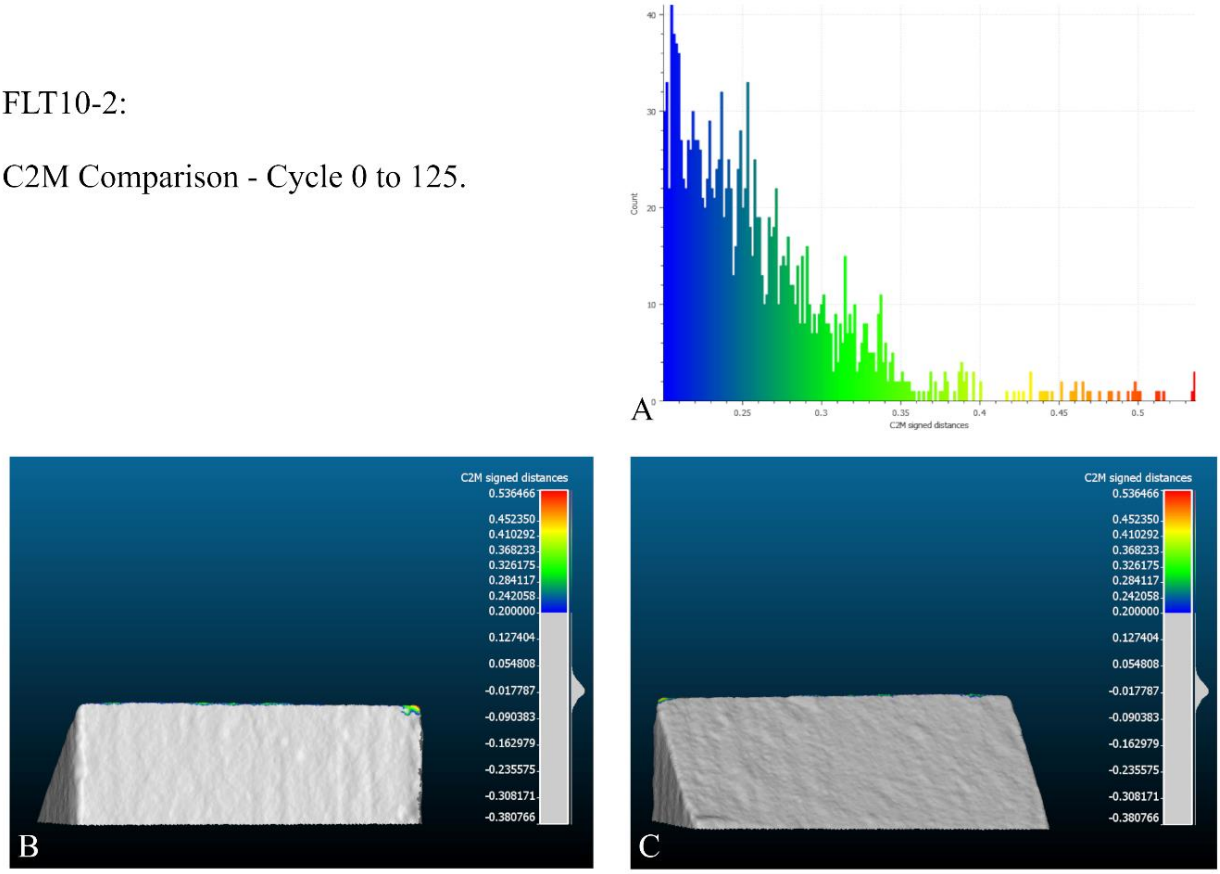

Figure 38: Cloud-to-Mesh edge reduction comparison, sample ID: FLT10-2, Cycle 0-125. A - Edge damage histogram, B - Back view, C - Front view.

FLT10-2:

C2M Comparison - Cycle 125 to 250.

.

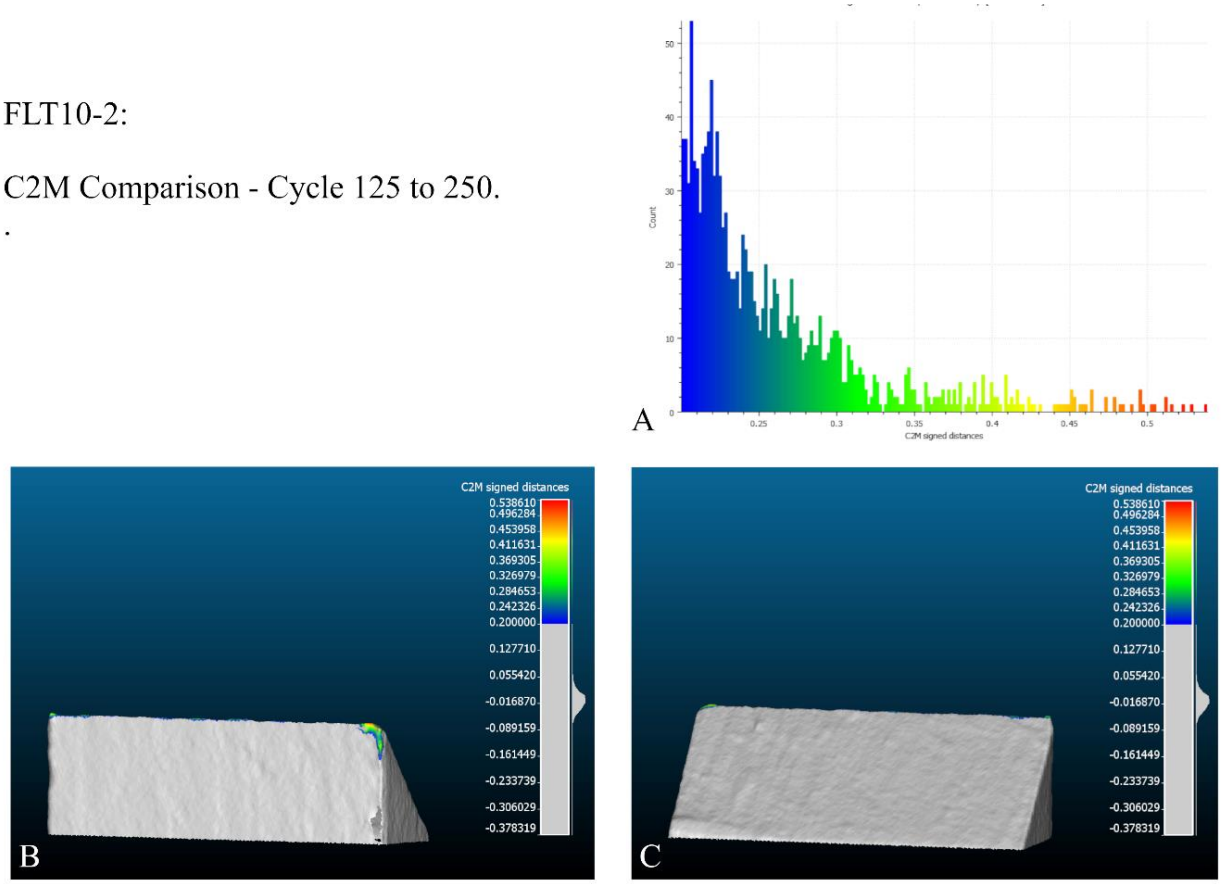

Figure 39: Cloud-to-Mesh edge reduction comparison, sample ID: FLT10-2, Cycle 125-250. A - Edge damage histogram, B - Back view, C - Front view.

FLT10-2:

C2M Comparison - Cycle 250 to 500.

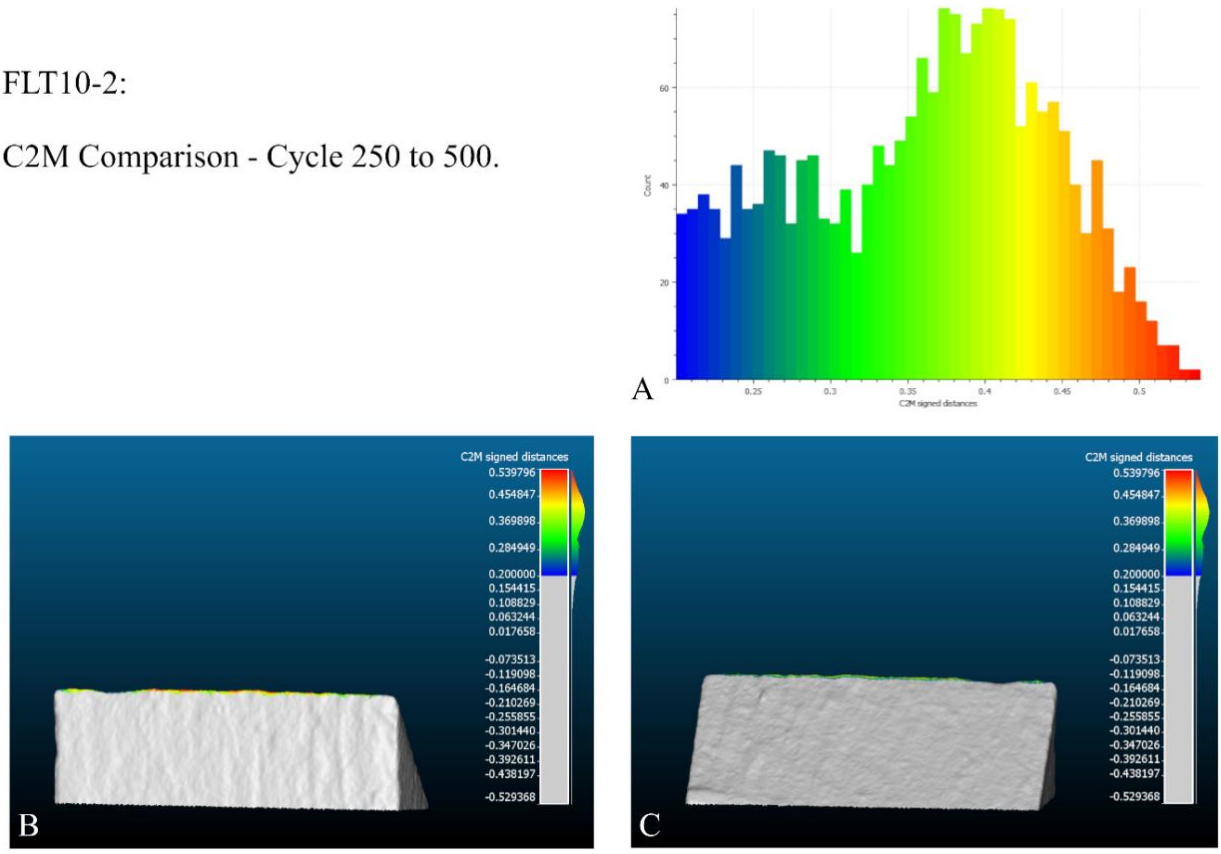

Figure 40: Cloud-to-Mesh edge reduction comparison, sample ID: FLT10-2, Cycle 250-500. A - Edge damage histogram, B - Back view, C - Front view.

FLT10-2:

C2M Comparison - Cycle 0 to 500.

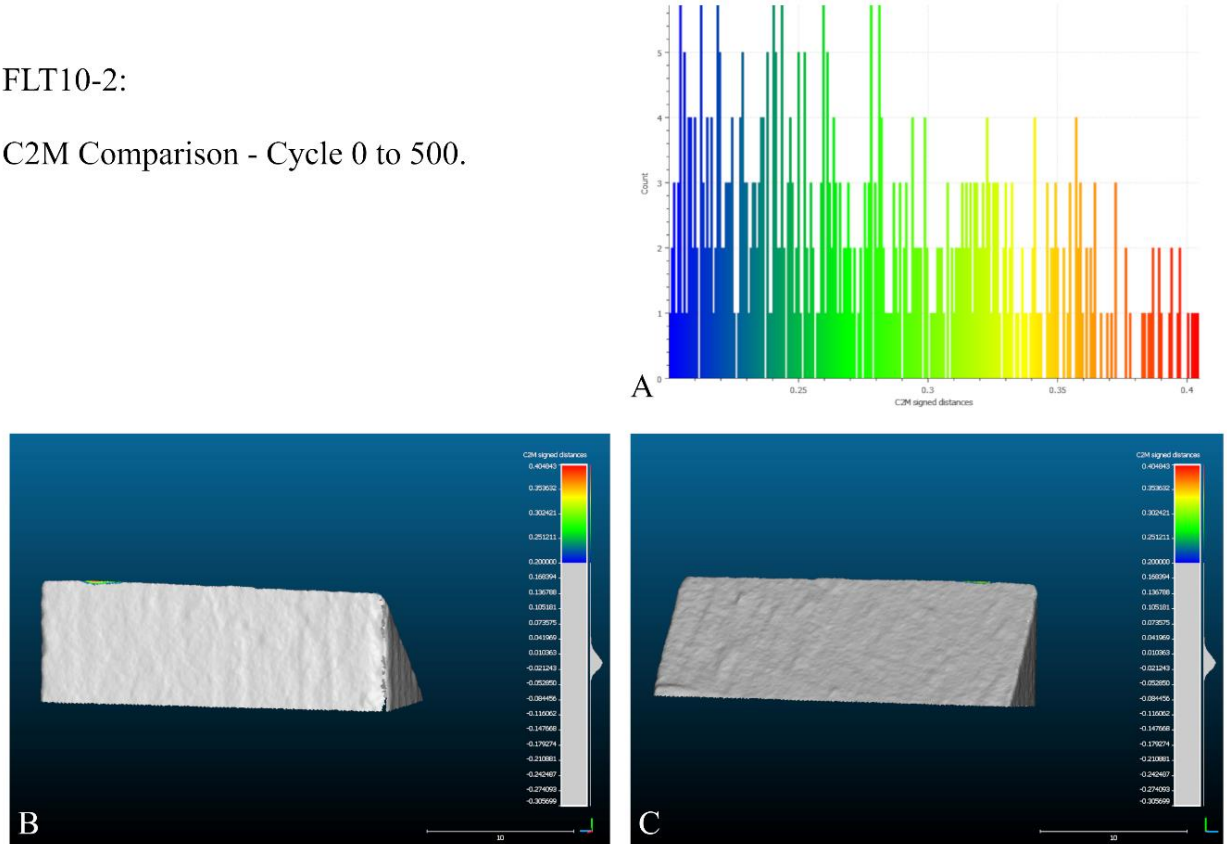

Figure 42: Cloud-to-Mesh edge reduction comparison, sample ID: FLT10-2, Cycle 0-500. A - Edge damage histogram, B - Back view, C - Front view.

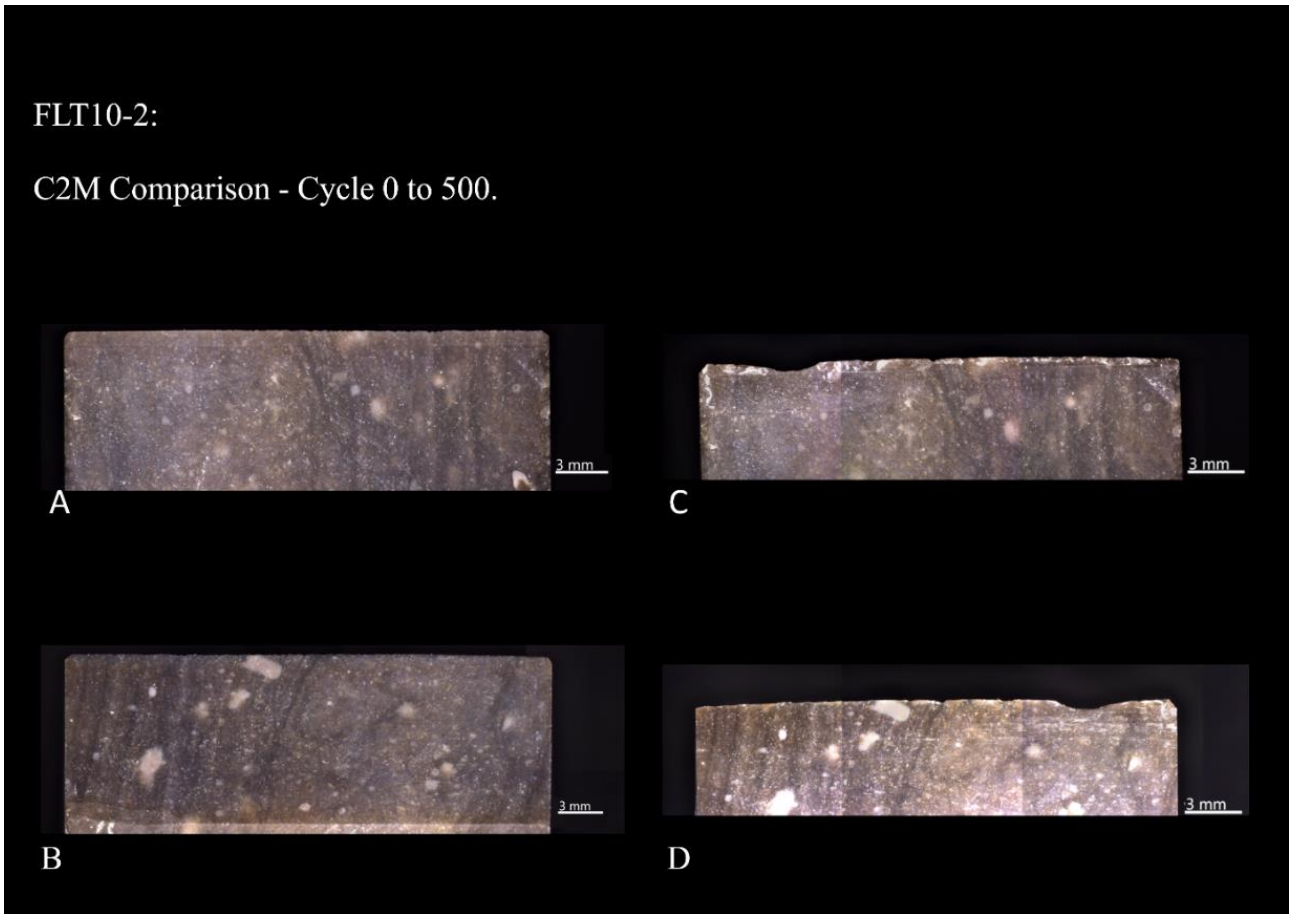

Figure 41: ZEISS Smart zoom images, A/B Cycle 0: A - Back view, B – Front view, C/D Cycle 500: C – Back View, D – Front view. Sample ID: FLT0-2.

4.2.2.c FLT10-5

From Figure 42 A, the results are the following:

FLT 10-5 sample, starts the first cycle with a depth penetration of 15.4 mm. During this cycle, a maximum depth penetration of 15 mm is observed in step 10. The remaining 124 cycles follow the same trend and have a maximum depth penetration of 13.7 mm.

In the following 126 cycles (124-250 cycles), the performance is very similar. The cycles start with a depth between 14.1 mm and 13.6 mm, and it is in cycle 250 that the deepest penetration is verified. In this cycle, the maximum depth reaches 13.3 mm in step 3 and 13 mm in step 13.

Cycle 251 starts with a depth of 13.7 mm over the pinewood. During the last few cycles, the penetration depth increases to 11.9 mm in step 3. From step 13, cycle 500 reached the maximum penetration depth of about 11.6 mm demonstrated in all cycles.

Figure 42 B represents the sensors measure from Inotec, and the results are the following:

The movement over the pinewood started with a force of -60N, which remained constant throughout the initial steps. Oscillations in the force parameter were verified from step 3 to step 5 and from step 12. The force graph of the backward movement (step 11 to 20) represents a wide distribution of the values with a range of -40 to -70 newtons.

The initial friction of 0 newtons in the first cycle shows an increase of friction at -50 N. It is possible to verify an increase in friction from step 3 and small successive decreases during the sample linear movement. The 200-500 cycles initial friction increase to near -60 N, and then reach high picks at step 4, 6, and 10, followed by a decrease on step 5, 7, and 9.

As expected, the initial velocity is 0 mm/s and gradually increases until it declines from steps 5 to 10. All cycles have demonstrated the same velocity through all cycles. There are slight differences in velocity between cycles from step 10 to 15 onwards. From this point onwards there is also a slowdown in velocity. A renewed increase in speed is registered between steps 12 and 14, after these steps the speed is constant.

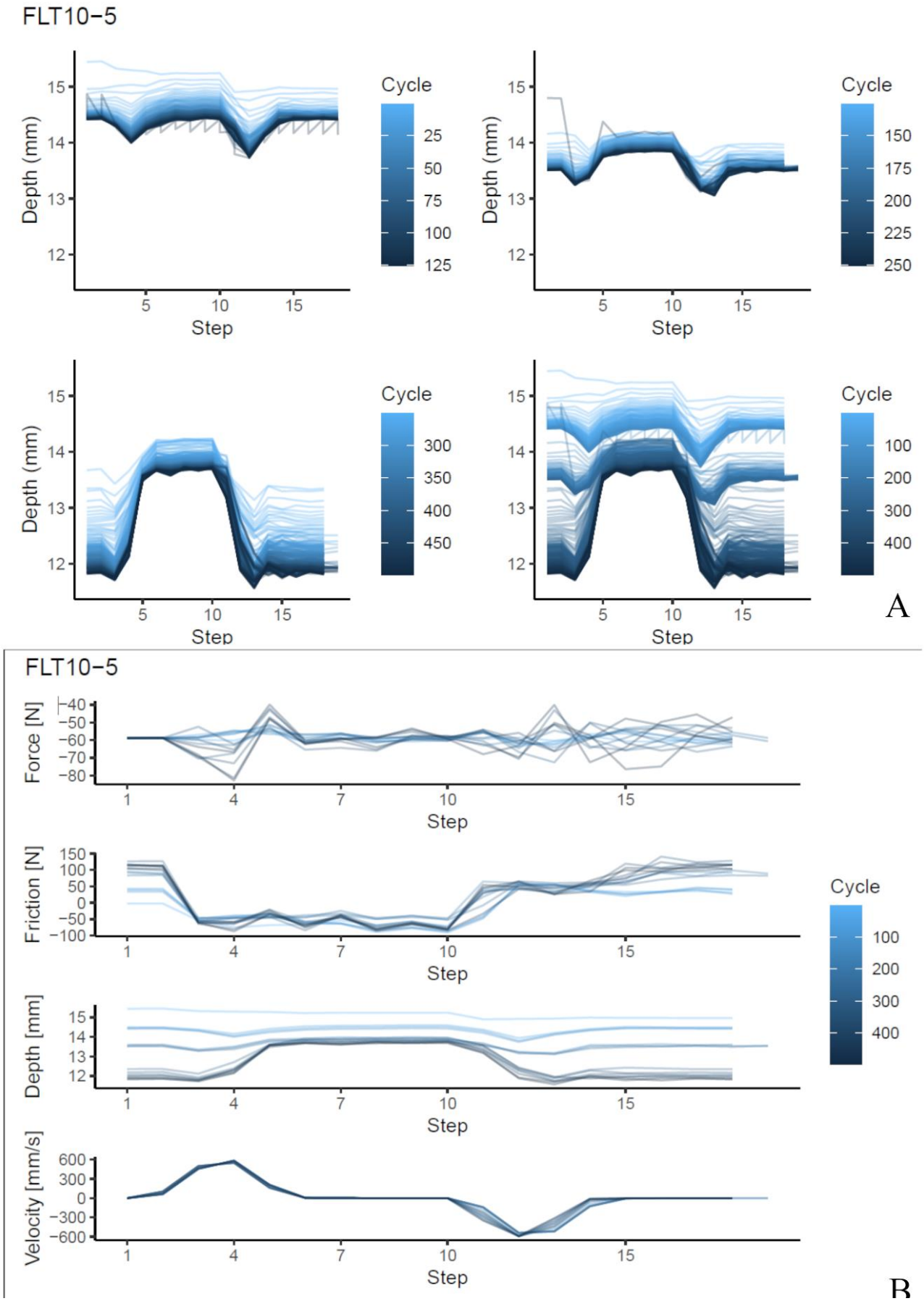

Figura 43: Graphic representation of the values recorded from Inotec from sample ID: FLT10-5. A - Penetration depth (mm) results, B - Sensors results.

4.2.2.d FLTT10-5 Edge reduction, C2M Comparisons

The sample FLT10-5 after crossing the three cycles of the experiment didn't result in expressive damage to the edge. From cycle 0 to 125, result in damage from 0.2 to 0.3 mm in an inferior number of parts. Throughout the cycle 125 to 250 the reduction of the active sample is 0.2 mm (Figure 45-A). The last cycle didn't result in major alterations to the edge sample.

FLT10-5:

C2M Comparison - Cycle 0 to 125.

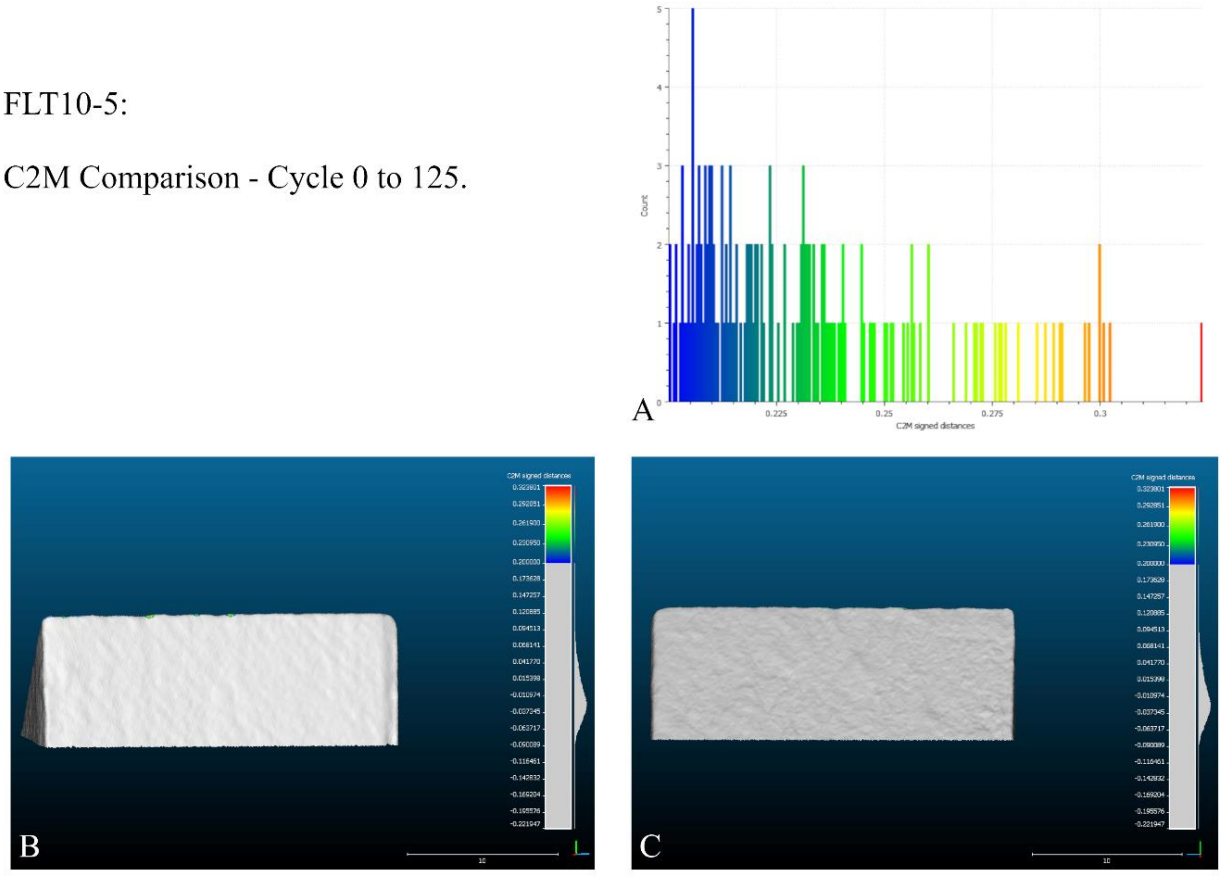

Figure 44: Cloud-to-Mesh edge reduction comparison, sample ID: FLT10-5, Cycle 0-125. A - Edge damage histogram, B - Back view, C - Front view.

FLT10-5:

C2M Comparison - Cycle 125 to 250.

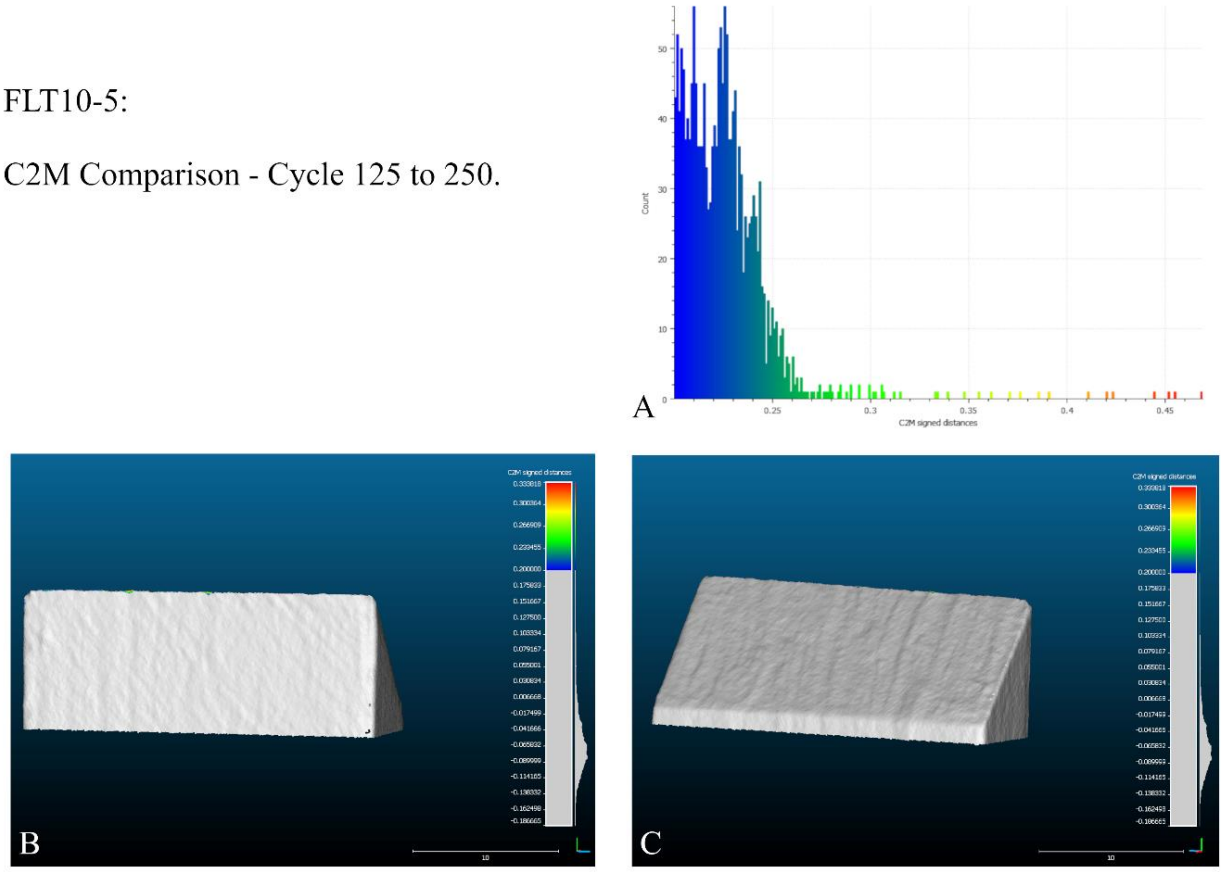

Figure 46: Cloud-to-Mesh edge reduction comparison, sample ID: FLT10-5, Cycle 125-250. A - Edge damage histogram, B - Back view, C - Front view.

FLT10-5:

C2M Comparison - Cycle 250 to 500.

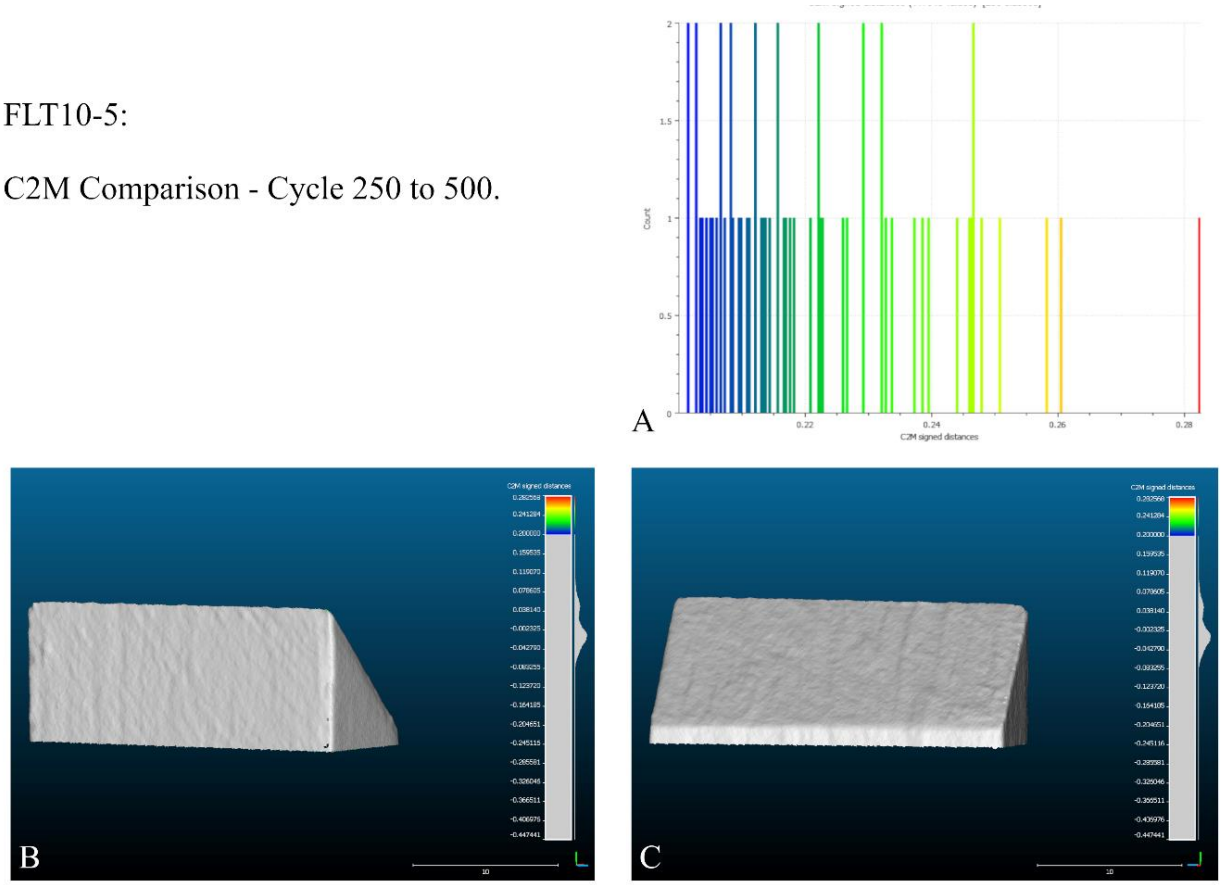

Figure 45: Cloud-to-Mesh edge reduction comparison, sample ID: FLT10-5, Cycle 250-500. A - Edge damage histogram, B - Back view, C - Front view.

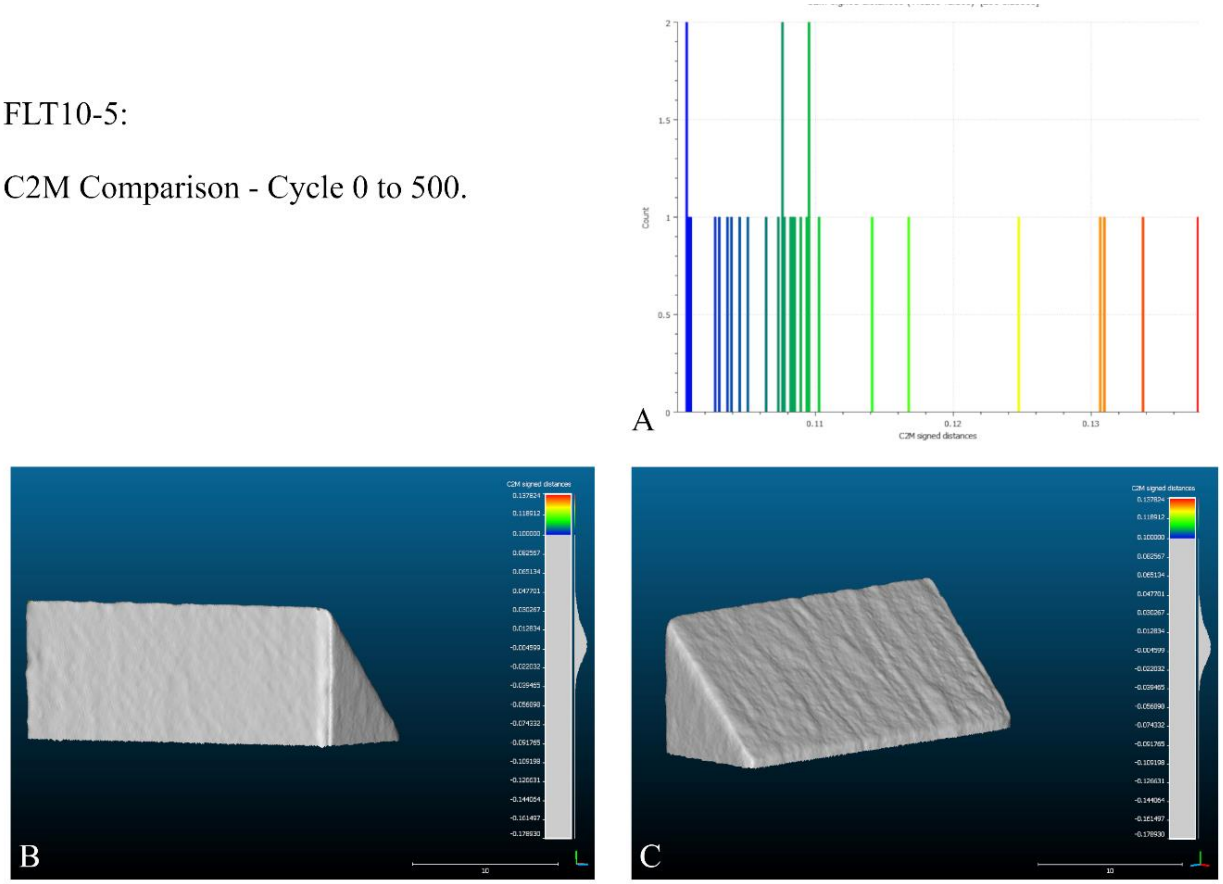

Figure 47: Cloud-to-Mesh edge reduction comparison, sample ID: FLT10-5, Cycle 0-500. A - Edge damage histogram, B - Back view, C - Front view.

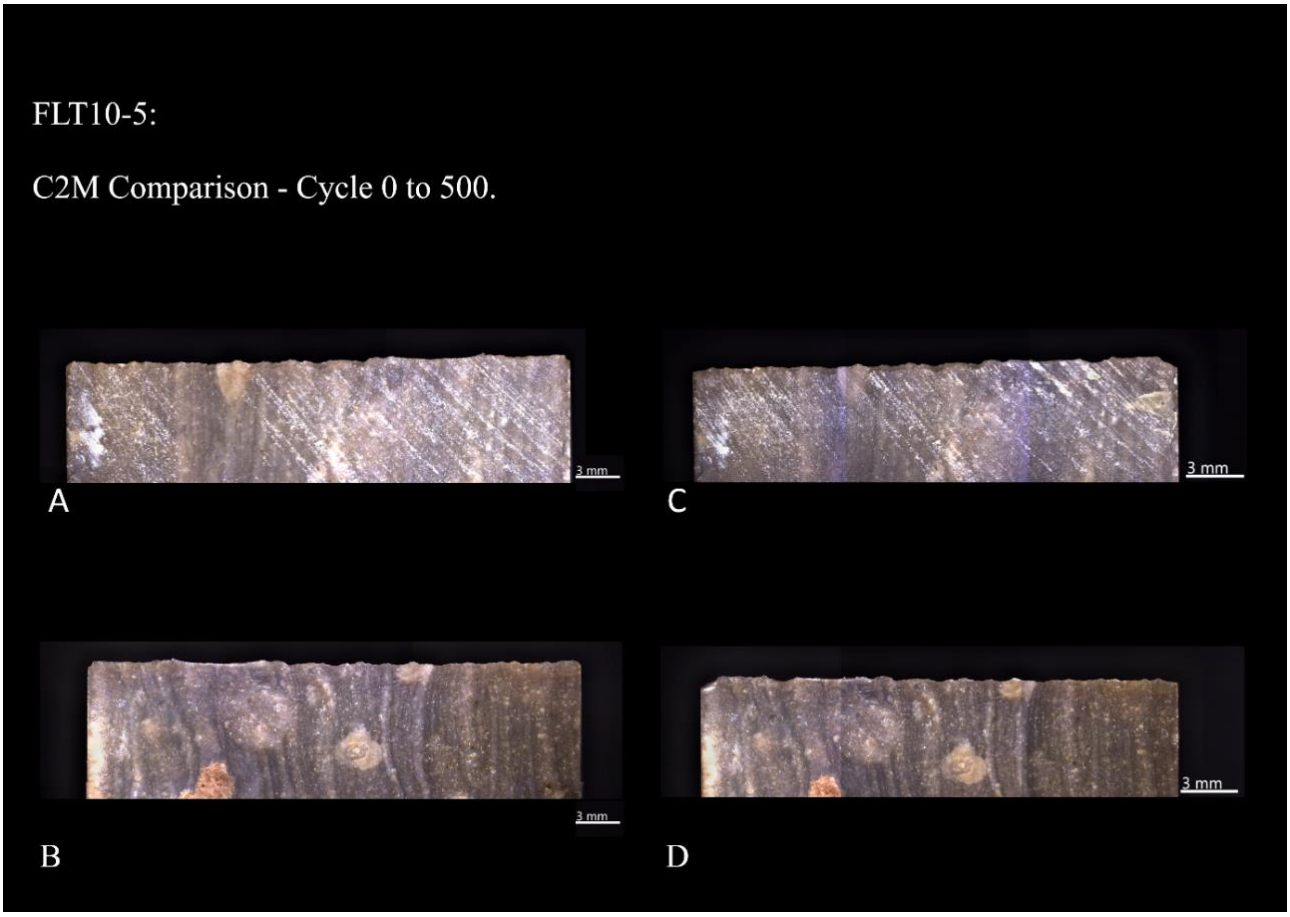

Figure 48: ZEISS Smart zoom images, A/B Cycle 0: A - Back view, B – Front view, C/D Cycle 500: C – Back View, D – Front view. Sample ID: FLT0-5.

4.2.2.e FLT 10-6

From Figure 48 A, the results are the following:

The movement of the first cycle using the FLT 10-6 sample started with a depth penetration of 15.3 mm and remained constant during the first steps. In the course of the linear movement, there was a sharp increase in depth penetration reaching its maximum in step 13 with 14.8mm. All the other 124 cycles started with a depth penetration of between 13.9 mm and 14.7 mm and recorded their maximum of 13.6 mm in step 13, just like the first cycle.

From cycle 126 up to cycle 250, it is observed that all cycles have the same action. These cycles start with a depth penetration between 14.2 mm and 13.8 mm with a maximum recorded in step 13 with 13.5 mm. Also, throughout cycles 251 to 500, it is verified that the movements have the same pattern. All these cycles start with a depth penetration of 13.2 mm to 13.5 mm and reach their maximum at 13.0 mm in step 13.

Figure 48 B represents the sensors measure from Inotec, and the results are the following:

The movement in this sample starts with a force of -60N and remains constant during the first 10 steps of all cycles. The differences and oscillations of the applied force start to be noticed after step 10 in the last cycles. This type of pattern is only verified in this sample.

As for the friction parameter, from cycle 2 all the cycles have a stepped increase in friction applied to the sample, and friction loss from step 3 onwards, which later remains constant until it stops.

The initial velocity starts at zero and behaves the same as the other FLT 10-2 and FLT 10-5 samples. There is a gradual increase in speed in all cycles, reaching the maximum speed near step 4 with 600 mm/s. Similar to the FLT 10-5 sample, speed fluctuations only occur in the last cycles. These differences are observed between step 11 and step 14.

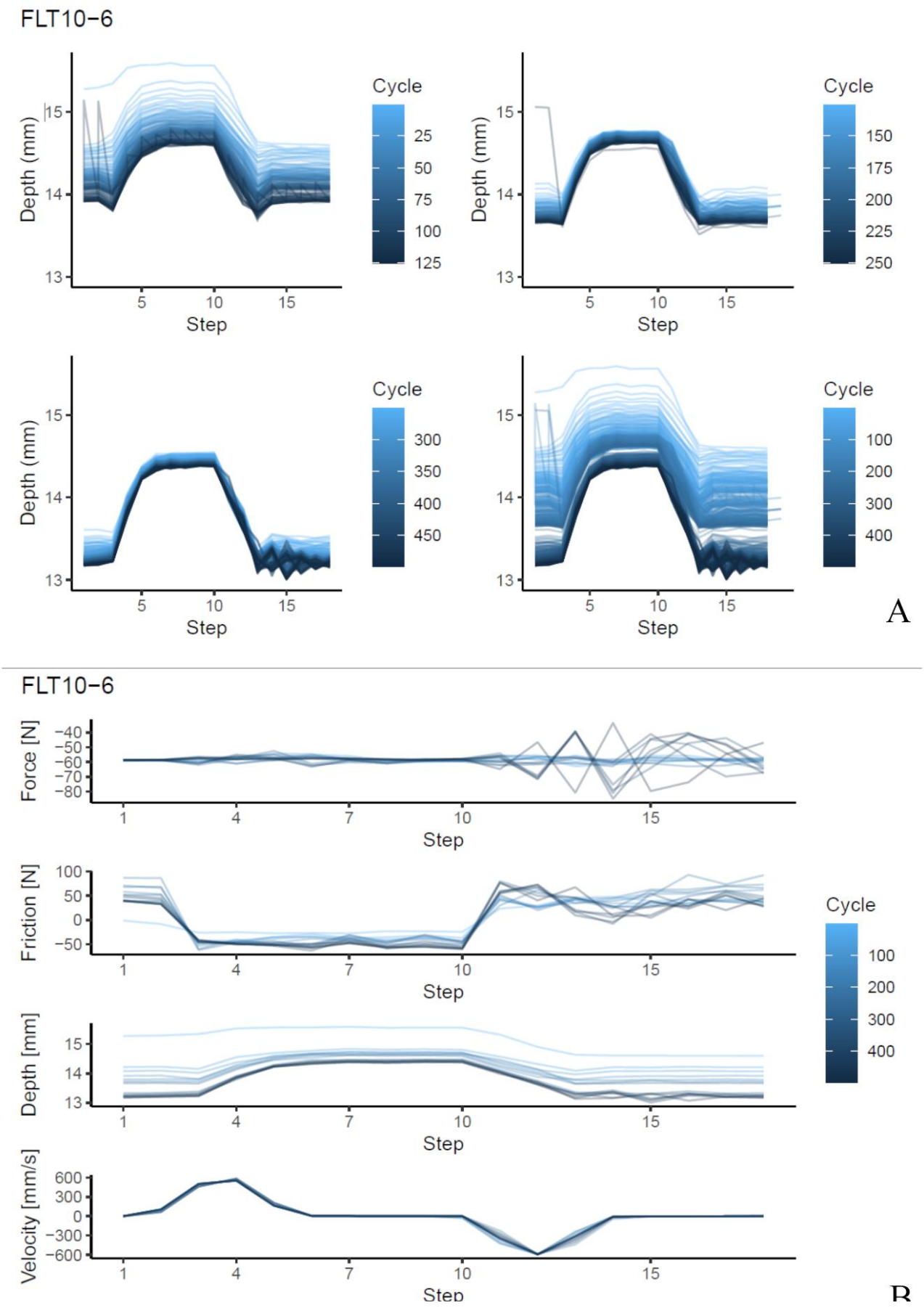

Figura 49: Graphic representation of the values recorded from Inotec from sample ID: FLT10-2. A - Penetration depth (mm) results, B - Sensors results.

4.2.2.f FLT10-6 Edge reduction, C2M Comparisons

The edge reduction of FLT10-6 can be seen in the first cycle Figure 49, the damage to the specimen was no more than 0.5 mm, throughout the edge, but with enhancement on the dorsal side of the sample Figure 49-B. For the other cycles (125→250→500), the reduction was between 0.2 mm and 0.4 mm. After the 1000 bidirectional linear movements into the pinewood, a slight reduction of 0.5 mm is visible in Figure 53.

FLT10-6:

C2M Comparison - Cycle 0 to 125.

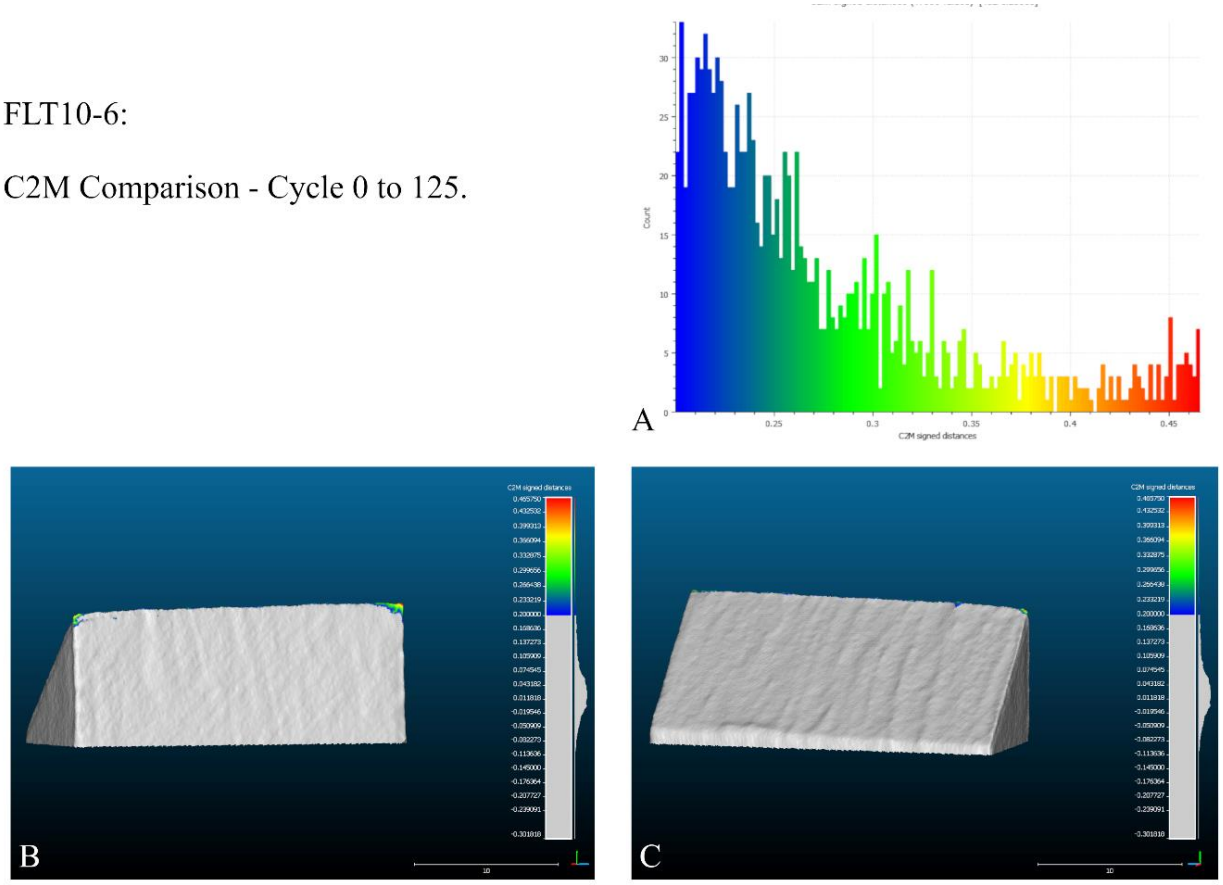

Figure 50: Cloud-to-Mesh edge reduction comparison, sample ID: FLT10-6, Cycle 0-125. A - Edge damage histogram, B - Back view, C - Front view.

FLT10-6:

C2M Comparison - Cycle 125 to 250.

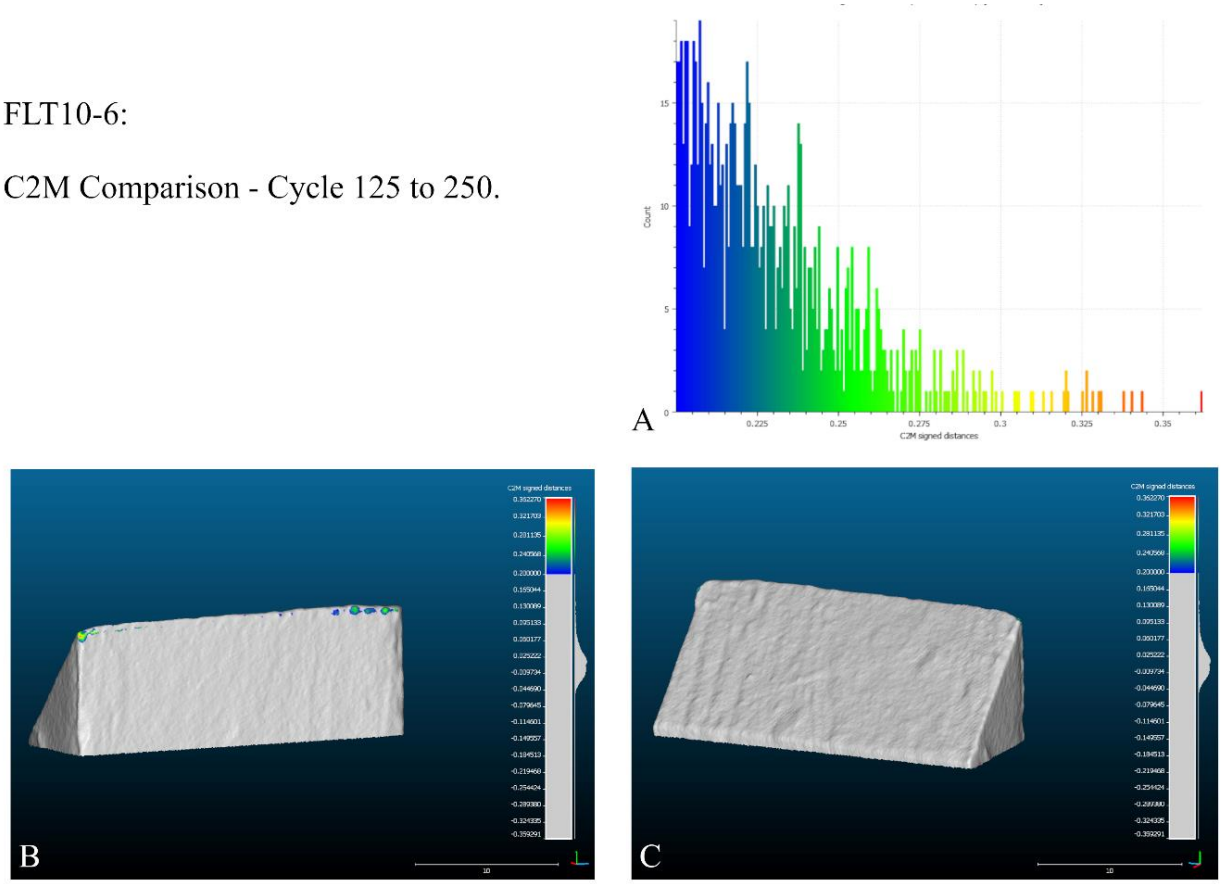

Figure 52: Cloud-to-Mesh edge reduction comparison, sample ID: FLT10-6, Cycle 125-250. A - Edge damage histogram, B - Back view, C - Front view.

FLT10-6:

C2M Comparison - Cycle 250 to 500.

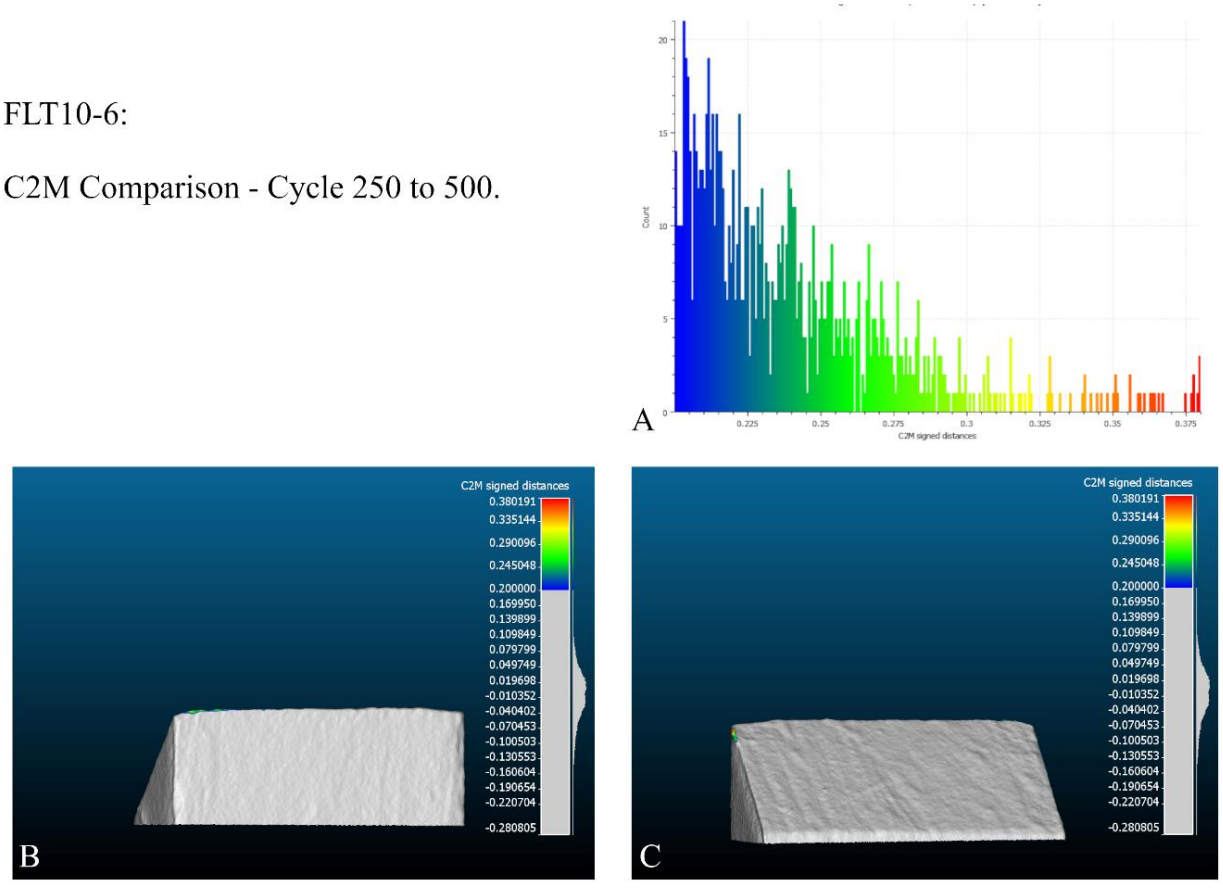

Figure 51: Cloud-to-Mesh edge reduction comparison, sample ID: FLT10-6, Cycle 250-500. A - Edge damage histogram, B - Back view, C - Front view.

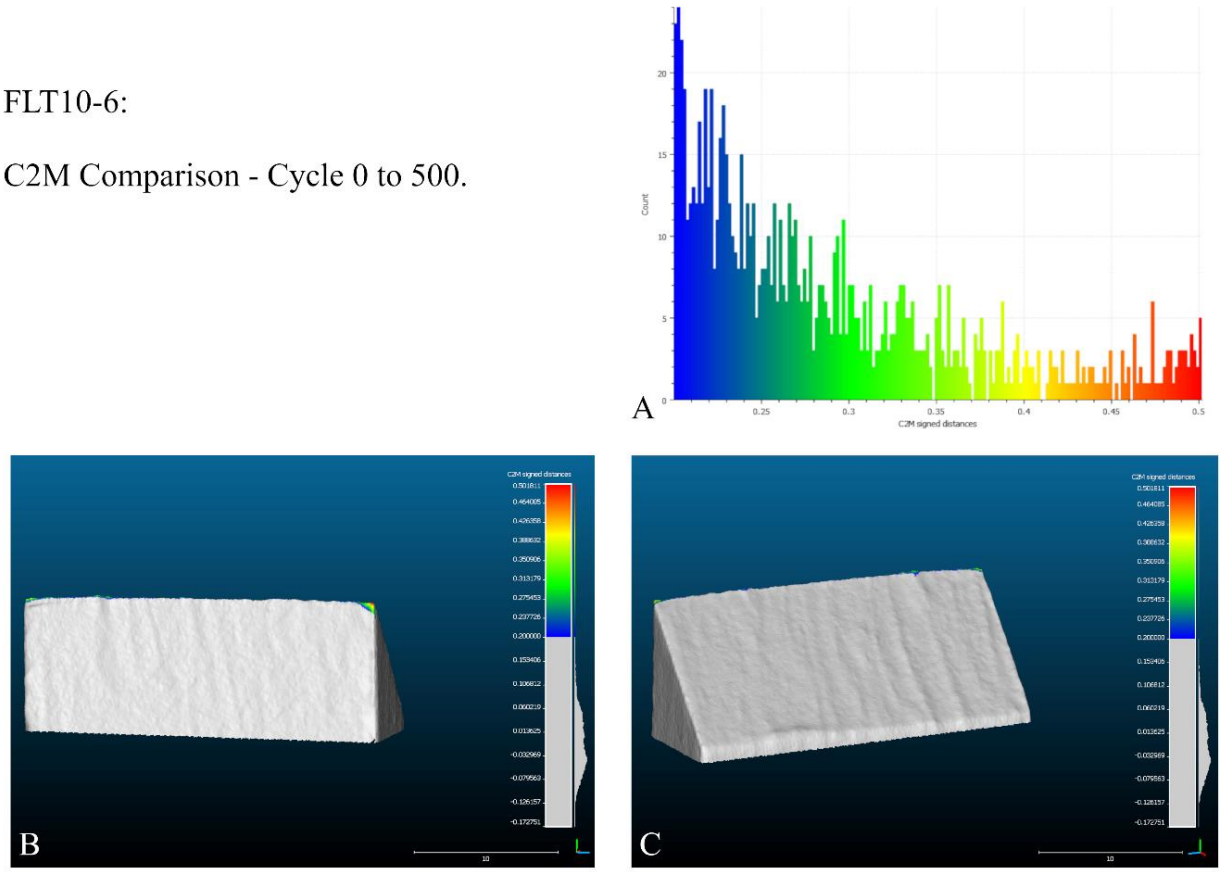

Figure 54: Cloud-to-Mesh edge reduction comparison, sample ID: FLT10-6, Cycle 125-250. A - Edge damage histogram, B - Back view, C - Front view.

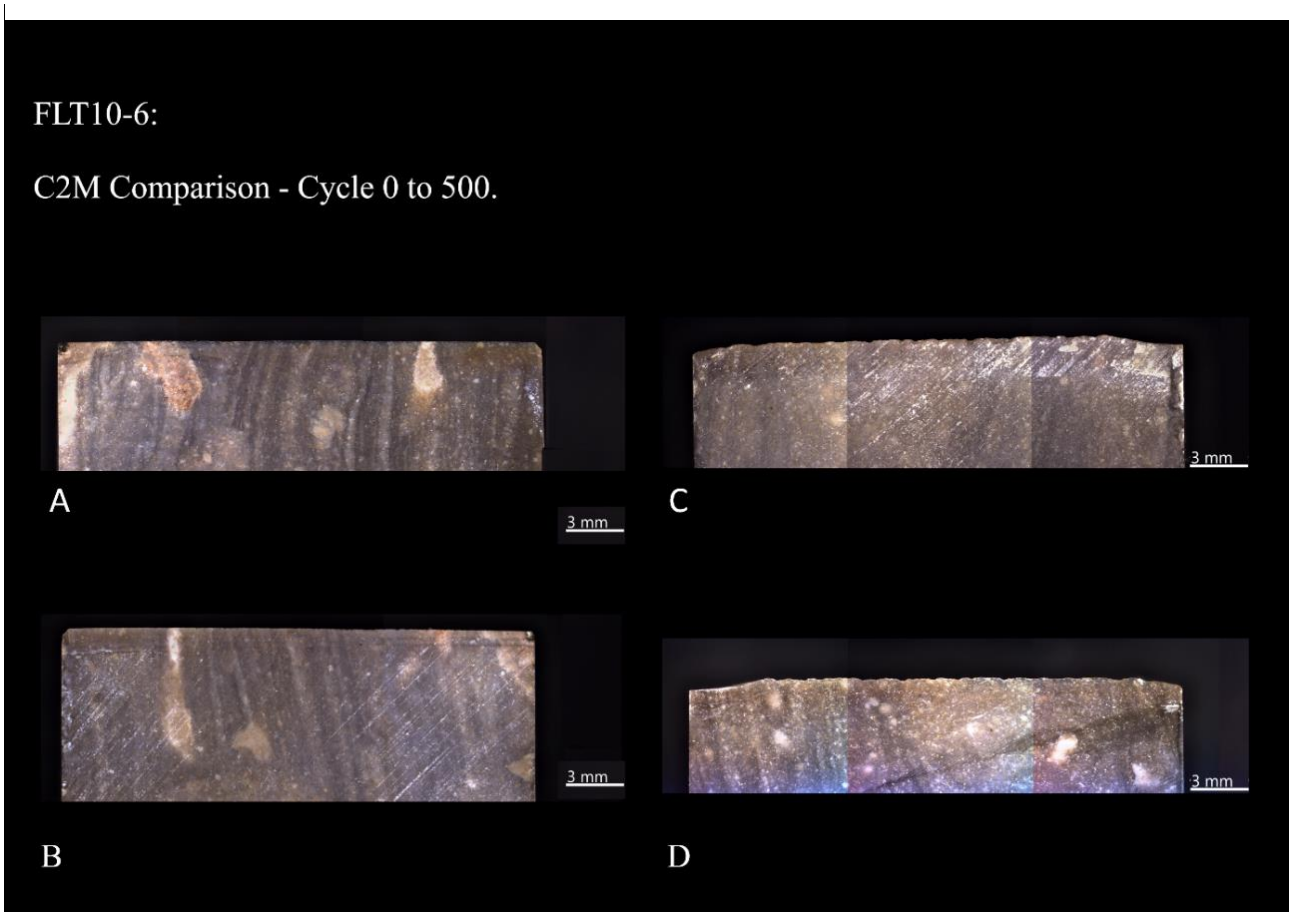

Figure 53: ZEISS Smart zoom images, A/B Cycle 0: A - Back view, B – Front view, C/D Cycle 500: C – Back View, D – Front view. Sample ID: FLT0-6.

4.2.3 DACITE

4.2.3.a DAC3-4

From Figure 54 A, the results are the following:

The penetration sensor records that DAC3-4 starts its movement at a depth of approximately 13.8 mm until it reaches point B, equivalent to step 10. In a backward movement of the sample, it goes deeper into the pinewood 1.3mm. After the abrupt initiation, a more constant movement takes place, between 13.5 mm and 12.0 mm, in the first 125 cycles. The ongoing movement from stroke 126 to 250, has also a distribution along with the contact material of 1.00 mm deep. For the last 250 cycles, the sample behaves constantly reaching maximum deep of 12.3 mm. From the plot of all cycle is visible that Dacite sample was constant trough out the experiment, starting in at 13.8 mm and reaching a deeper level of 11.4 mm a total of 2.4 mm.

Figure 54 B represents the sensors from Inotec, and the results are the following:

Results from the force sensor always start between -55 and 60 newtons. From step 2 to 6 in the first cycles is possible to observe a difference of force applied to the sample, with low values of -50 N and high values -63 N, after step 7 the values more or less stabilizes at the initial force, until it stops at step 10. The backward movement equivalent from steps 10 to 20, register more heterogeneous values between all cycles ranging from -50 to – 69 N.

The friction pattern is characterized by an increase in the initial steps 1 to 3 and a relative constant performance from steps 4 to 6. After step 7 a bimodal distribution is visible with values from 0 to -92 N.

Velocity values show a regular acceleration from step 1 to 4 at 600 mm/s, after reaching the pick, a deceleration occurs until it stops at step 10. The same pattern is verified but as a mirror result of the first 10 steps and with negative values due to the backward linear movement.

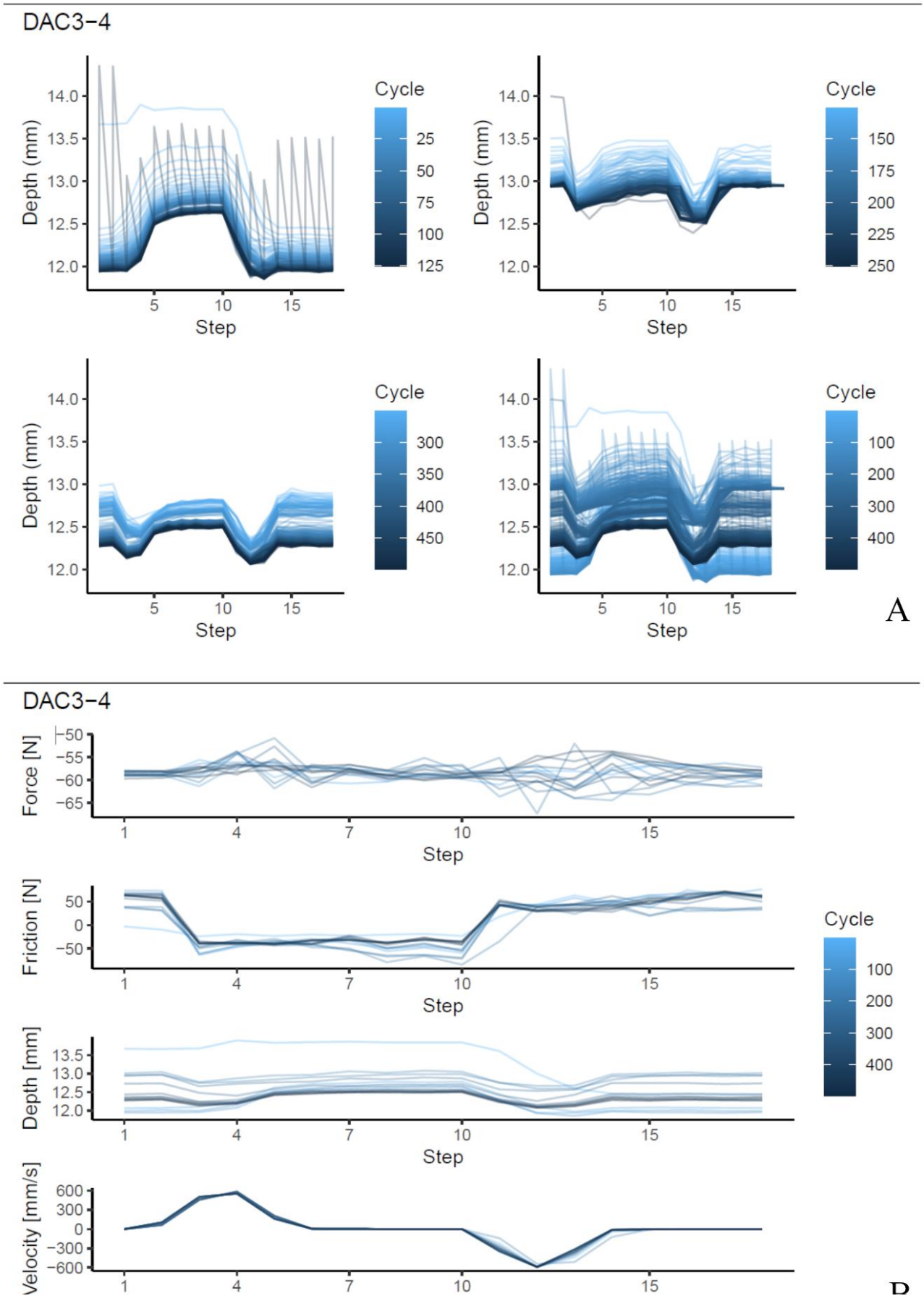

Figura 55: Graphic representation of the values recorded from Inotec from sample ID: DAC3-4. A - Penetration depth (mm) results, B - Sensors results.

4.2.3.b DAC3-4 Edge reduction, C2M Comparisons

After running the first cycle (0 to 125), DAC3-4 shows a minimum modification over the edge Figure 55. The opposite is verified when applied more than 250 moves into the contact material, besides a major break in one of the extremities reaching 1.0 mm, all the damage is located through all the samples with values range from 0.2 to 0.6 mm.

In the next cycle, the sample did not show linear damage, but instead, three small areas are affected. One near the previous removal from cycle 125 to 250, no more than 0.5 mm was removed. The two areas remaining are in the opposite direction, with the same values. These three removals are in the external part of the sample Figure 56-B. From the projection of the comparisons between 0 and 500 cycles, it's clear that the damage is concentrated at the two extremities of the sample.

DAC3-4:

C2M Comparison - Cycle 0 to 125.

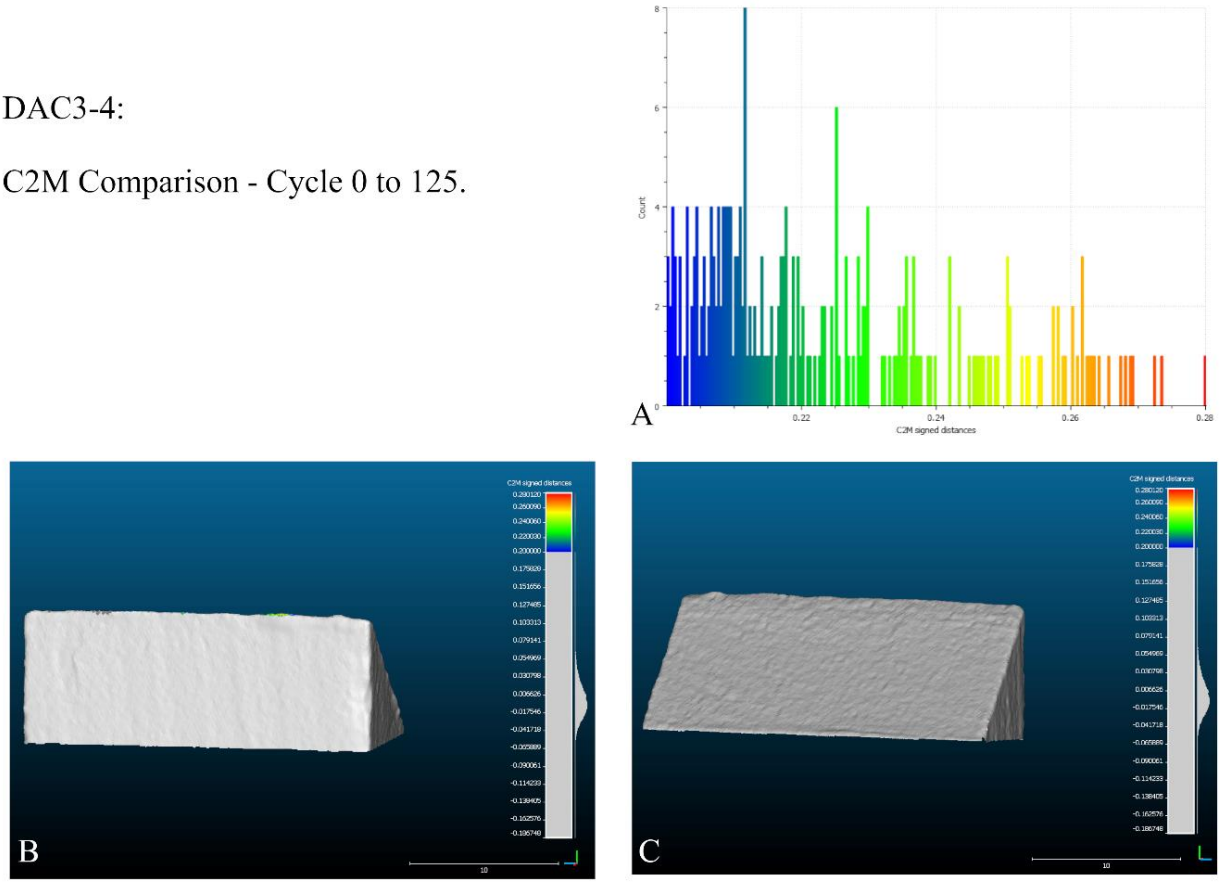

Figure 56: Cloud-to-Mesh edge reduction comparison, sample ID: DAC3-4, Cycle 0-125. A - Edge damage histogram, B - Back view, C - Front view.

DAC3-4:

C2M Comparison - Cycle 125 to 250.

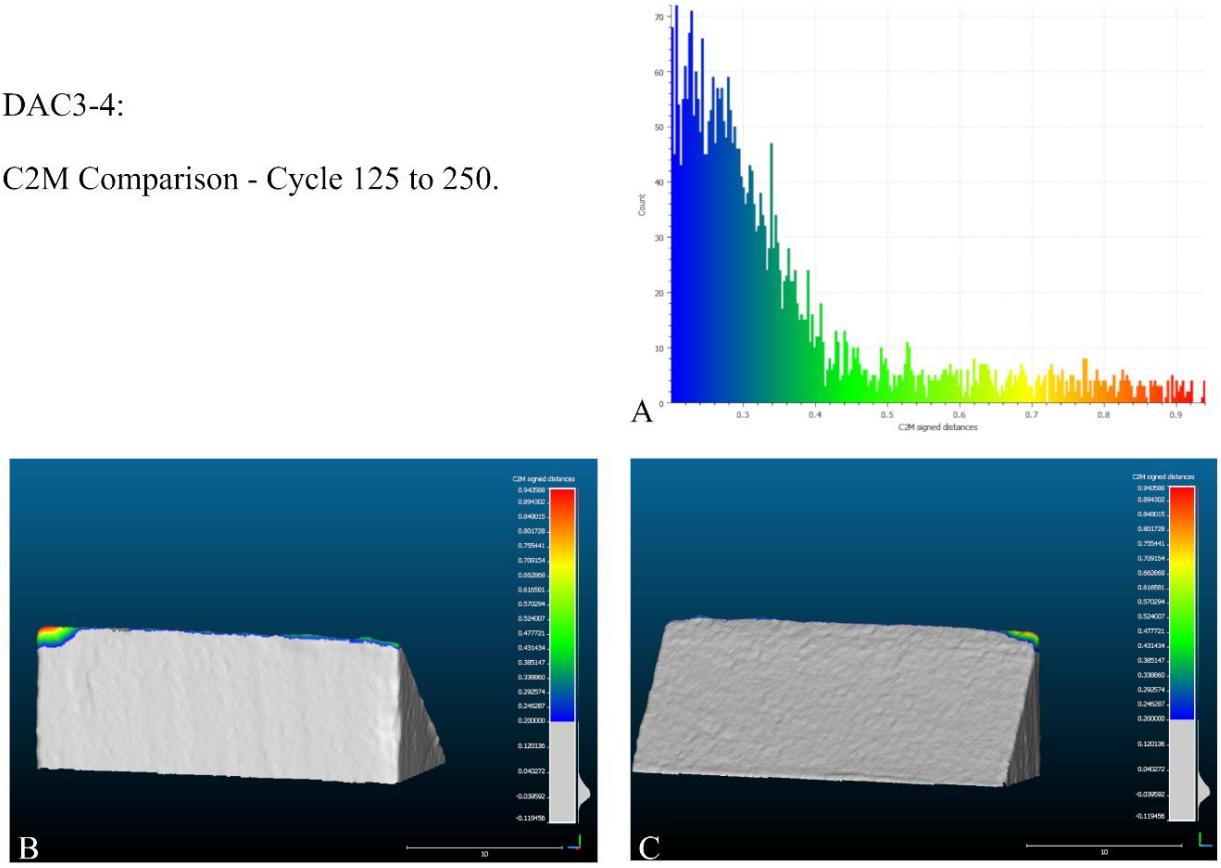

Figure 57: Cloud-to-Mesh edge reduction comparison, sample ID: DAC3-4, Cycle 125-250 . A - Edge damage histogram, B - Back view, C - Front view.

DAC3-4:

C2M Comparison - Cycle 250 to 500.

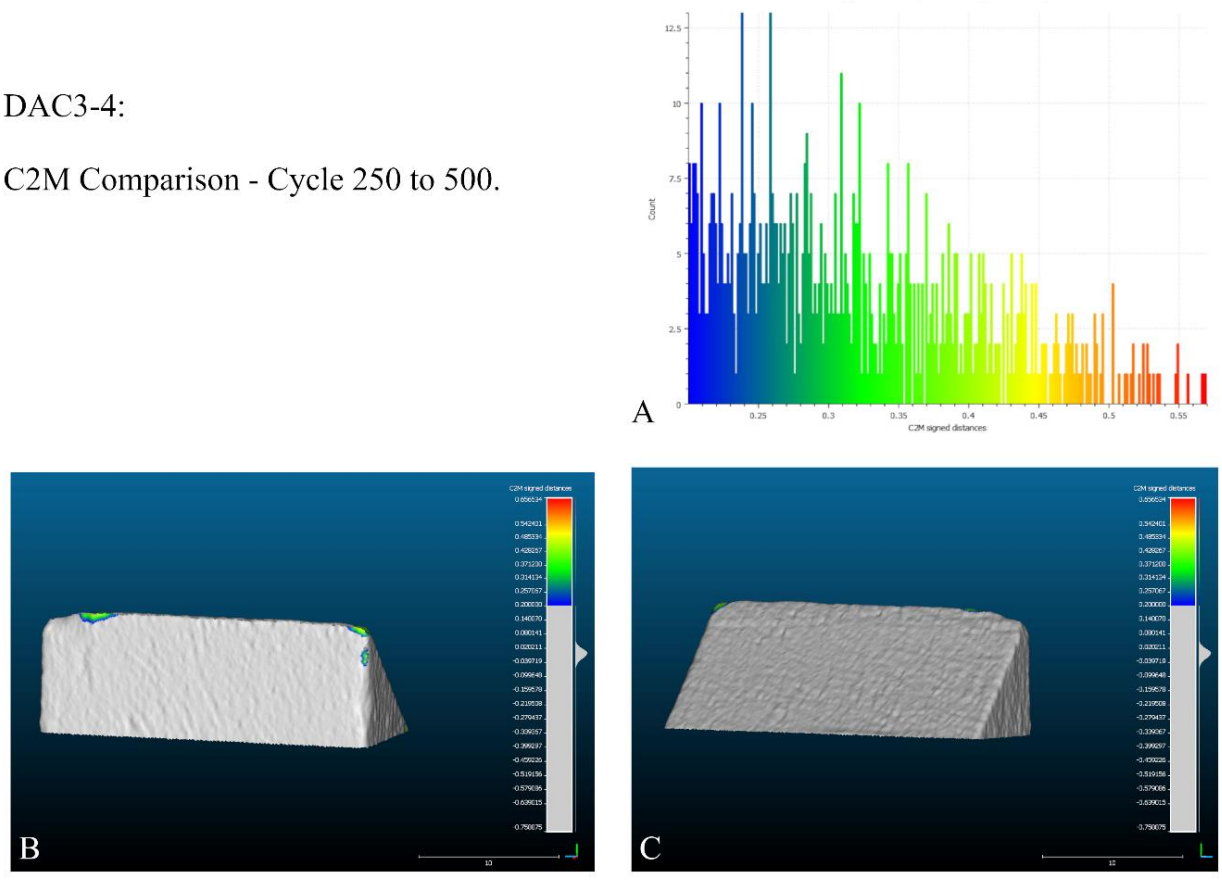

Figure 58: Cloud-to-Mesh edge reduction comparison, sample ID: DAC3-4, Cycle 250-500. A - Edge damage histogram, B - Back view, C - Front view.

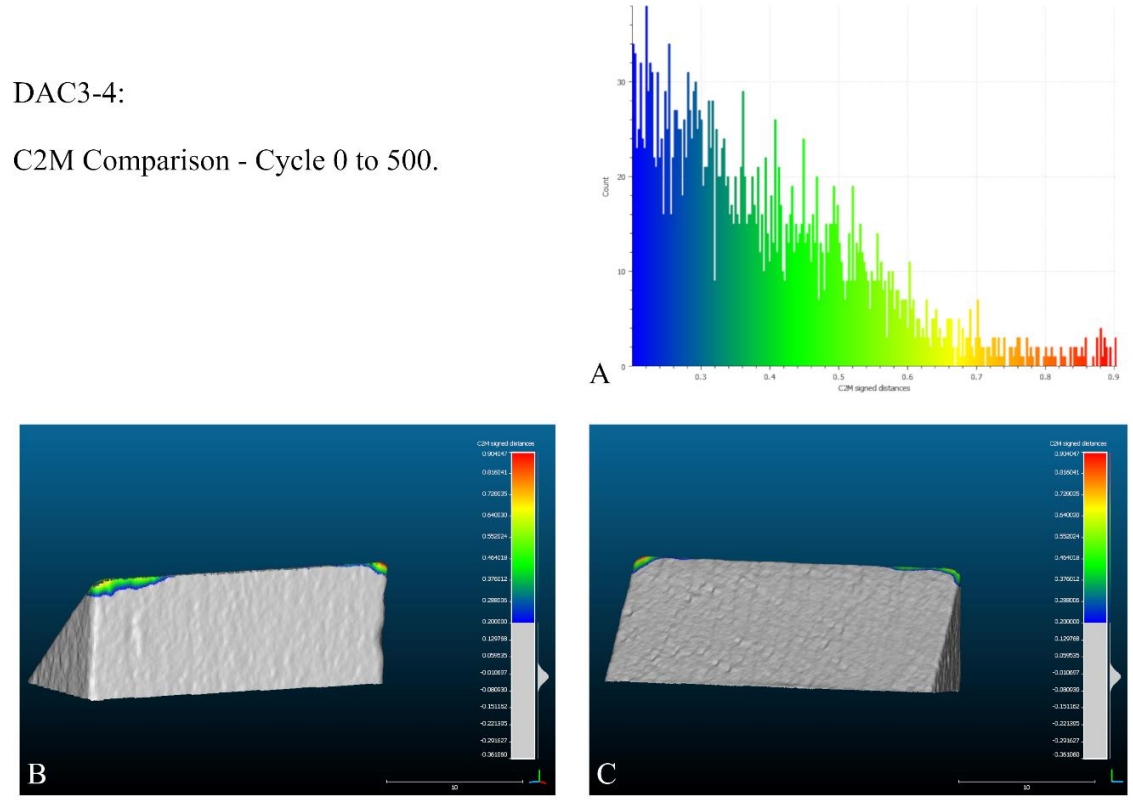

Figure 59: Cloud-to-Mesh edge reduction comparison, sample ID: DAC3-4, Cycle 0-500. A - Edge damage histogram, B - Back view, C - Front view.

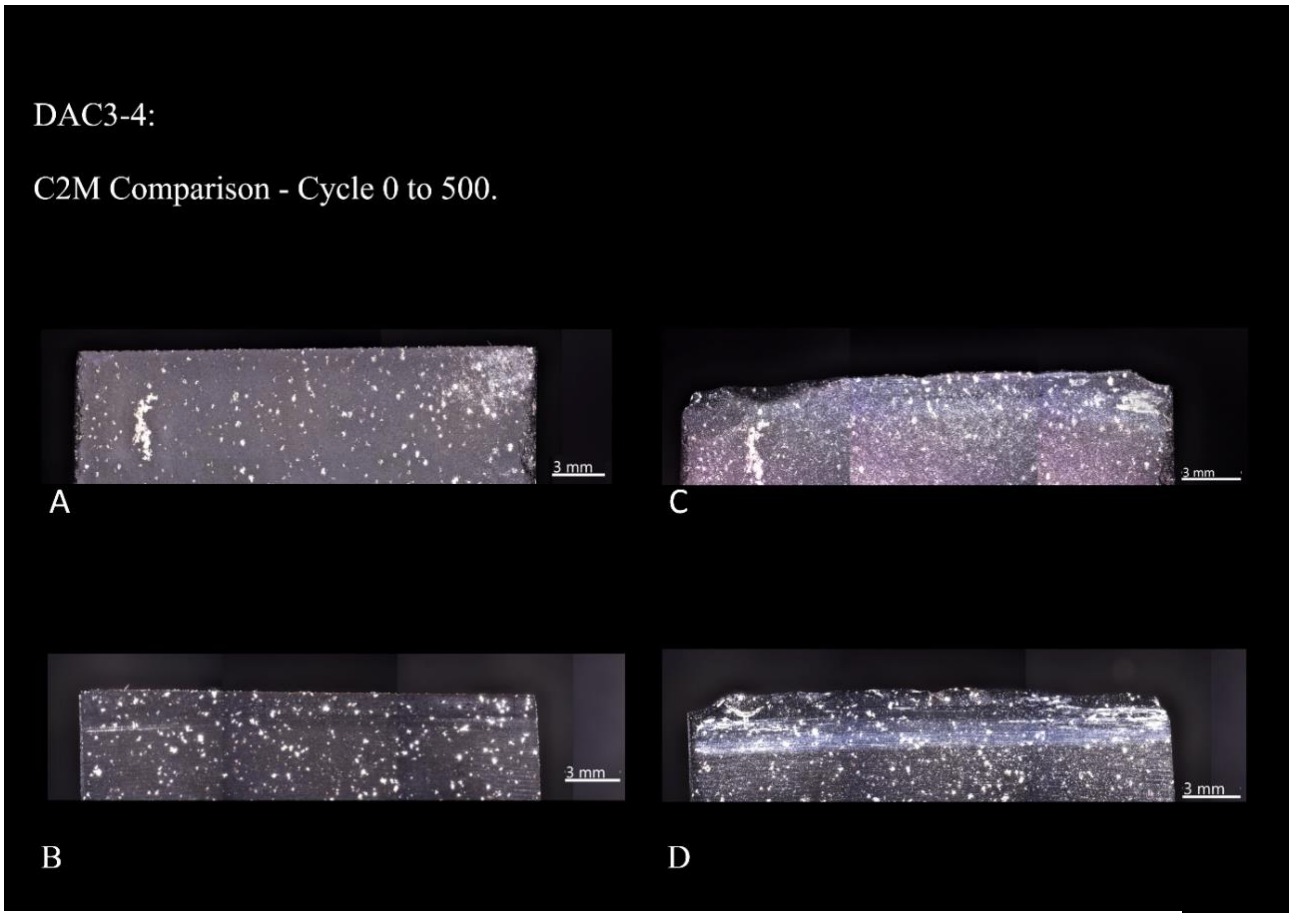

Figure 60: ZEISS Smart zoom images, A/B Cycle 0: A - Back view, B – Front view, C/D Cycle 500: C – Back View, D – Front view. Sample ID: DAC3-4.

4.2.3.c DAC3-2

From Figure 60 A, the results are the following:

The first cycle of sample DAC3-2 starts at 13.8 mm with an increase in depth as it goes through the motions and reaches step 20 with a depth approximately of 13.2 mm. All the cycles that come in the first stage (0 – 125) behave Similarly, an increase in steps 4 to 5 and then stabilizes until step 10 and then another pick in-depth on steps 11 to12 follow by a minimal penetration until the end. The deepest penetration occurs in step 11 at 11.7 mm. According to the previous cycles the next stage performs in the same way, increasing 1.05 mm in depth after the 250 strokes applied to the contact material.

From cycle 251 to 500 is possible to observe that sample DAC3-2 presents the same pattern of the experiment as cycle 0 to 125, and 126 to 250, with penetration from the first stroke to the last of 0.98 mm.

Although when data export and plot took place is visible by the graph that a machine error happened in the Z sensor because the depth goes from a maximum of 11.7 mm to 14.3 mm. Since the sample perform the 500 strokes into the pinewood perfectly without outliers or errors besides the unit number, and all the variables including position never change during the experiment (see table 8), it was possible to find the right unit value for cycle 251 -500, without changing the values that shows the penetration depth.

Once cycle 250 finishes in unit 12 mm, cycle 251 obligatory must start in the same unit. So, when the value was 14.0 mm pass to 12.0 mm and 13.0 mm pass to 11.0 mm. After the correction of the values is possible to observe that DAC3-2 reaches a penetration depth of 11.4 mm. From the observation of the cycle 0 to 500 in the new plot is visible the right continuous penetration from stroke 1 to 500 Figure 10-A.

Figure 60 B represents the sensors measure from Inotec, and the results are the following:

For force, DAC3-2 recorded values between a maximum of -70 N and -50 through all the experiment. It starts always with a constant value of approximately -58N, was it passes the first two steps force change often as a bimodal representation, the higher or lower pick frequently happen in step 4 and 12 to 13. In the last movements, the values tend to decrease proximal to the initial values.

As for friction, sample DAC3-2 cycle 1, start at 0 and goes higher as the linear movement is performed on the pinewood, reaching -50 N and then remain constant at between -20 and -40 until it stops at step 10. As with all the other samples, the first motion results in an increase of friction followed by decay at step 4. After this step in all cycles is visible that friction increase until it reaches point B.

As for velocity measures values are consistent with the previous sample, an increase from 1 to step 4 until it reaches 600 mm/s and decay as it stops in step 10, followed by another pick and a decrease of velocity until the end of the cycle. Values presented look homogenous in all the cycles.

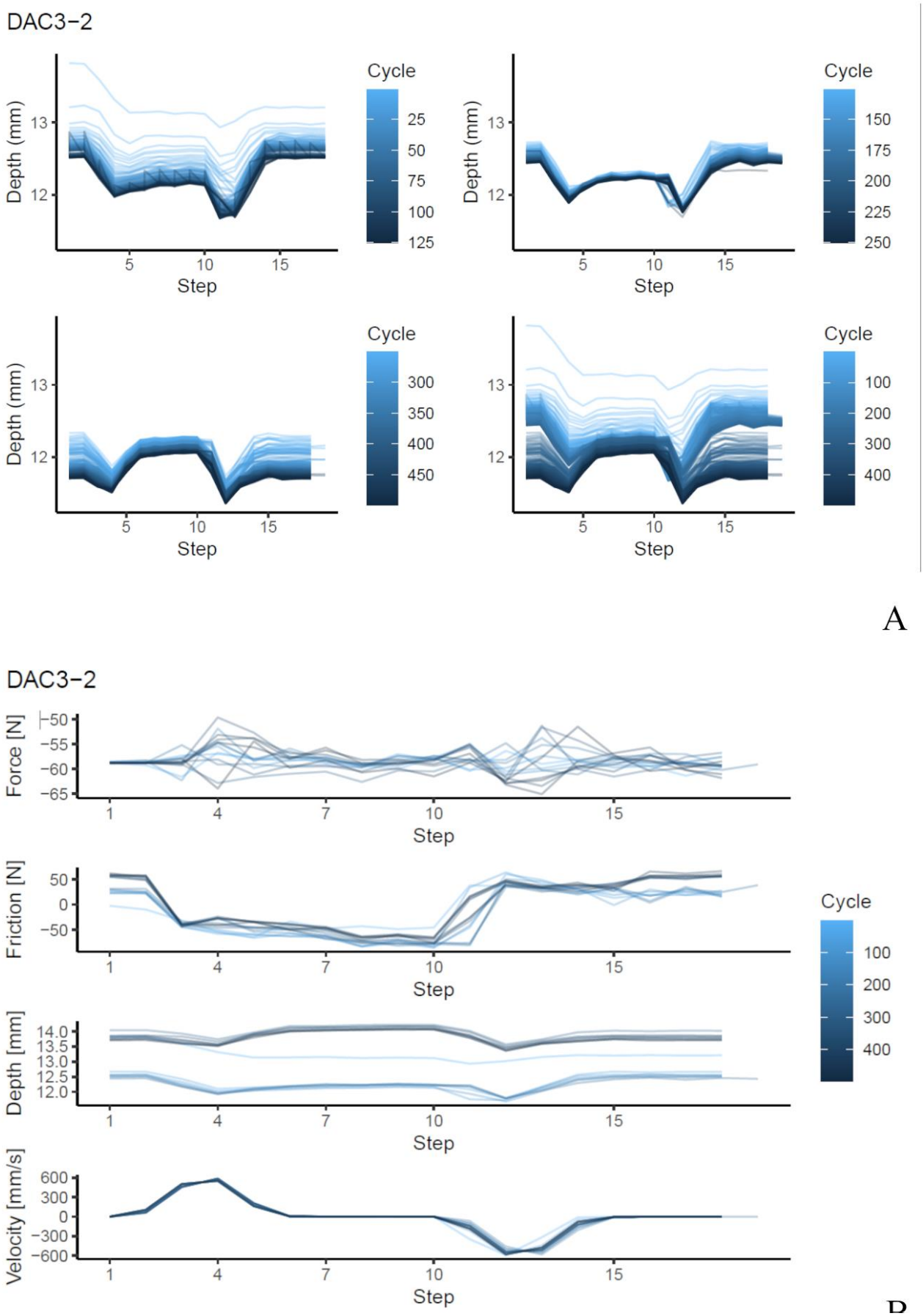

Figura 61: Graphic representation of the values recorded from Inotec from sample ID: DAC3-2. A - Penetration depth (mm) results, B - Sensors results.

4.2.3.d DAC3-2 Edge reduction, C2M Comparisons

From the 0 to 125 cycles graph Figure 61-A, is possible to see that the main damage in parts happens at an 0.3 mm penetration in the sample edge. But in concern to intrusive damage, once bigger damage is registered on the limits of the sample of approximately 0.7 mm. The next cycle representative of plus 250 strokes between dacite and pinewood, did not show representative damage in the edge Figure 62. The last cycle is when the sample is tested through more repetitions, shows a big removal in one edge of the sample Figure 63-B and C, then just some a minor abrasion of at least 0.3 mm is verified in the edge sample. The visual comparison between 0 and 500 cycles shows a better distribution of the damage in all the experiments.

DAC3-2:

C2M Comparison - Cycle 0 to 125.

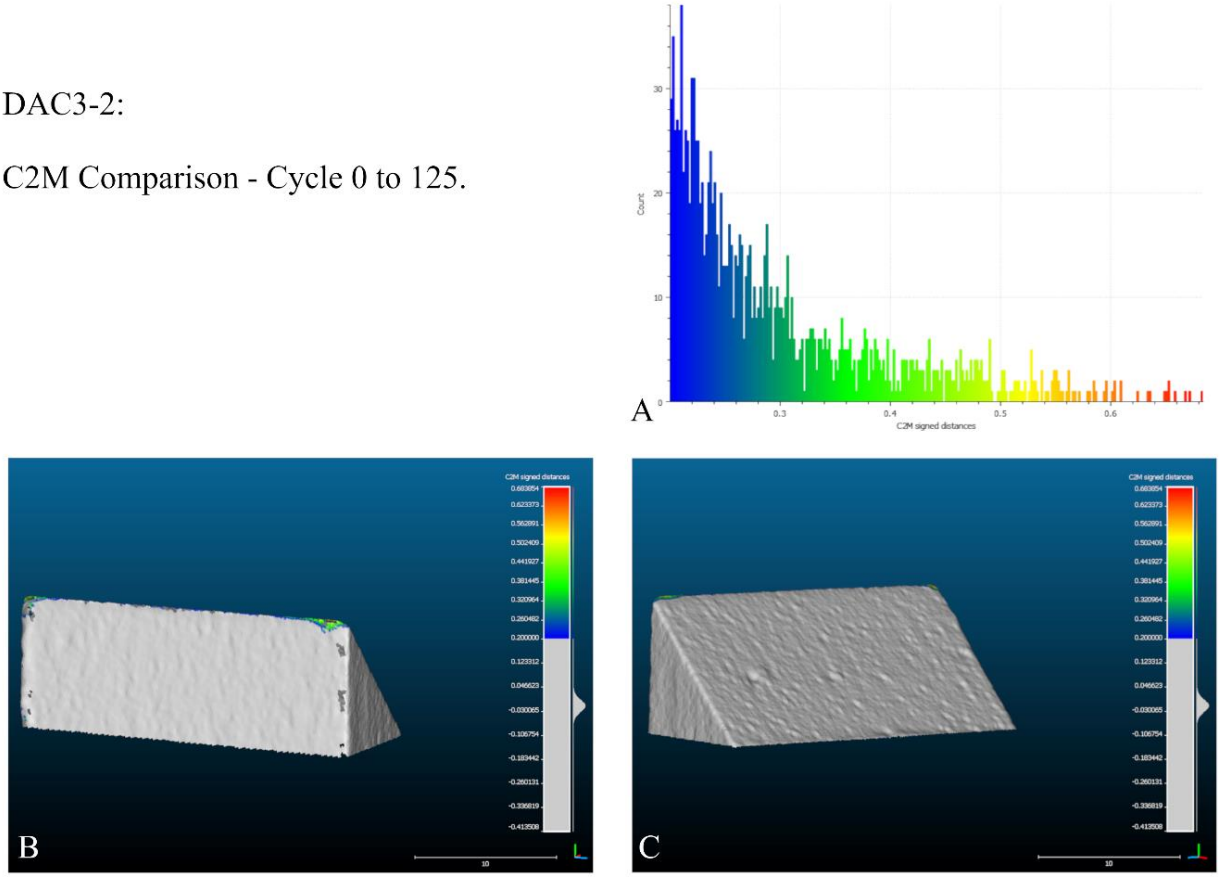

Figure 62: Cloud-to-Mesh edge reduction comparison, sample ID: DAC3-2, Cycle 0-125. A - Edge damage histogram, B - Back view, C - Front view.

DAC3-2:

C2M Comparison - Cycle 125 to 250.

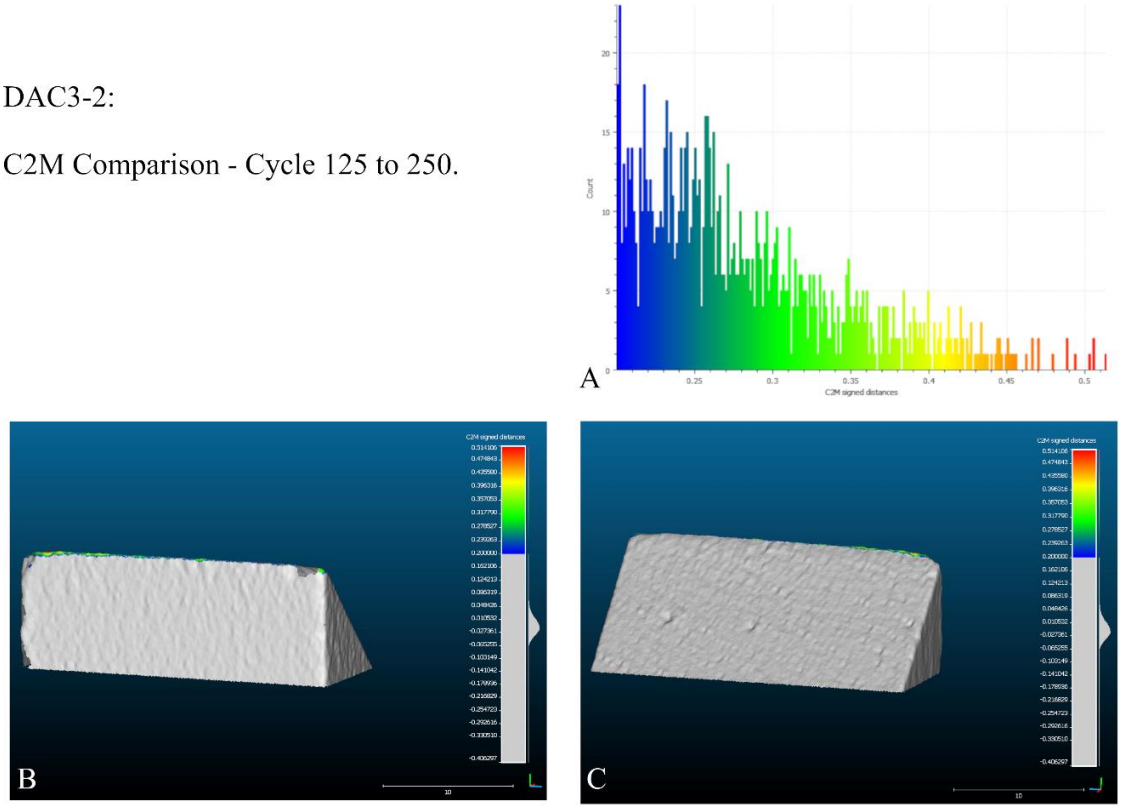

Figure 63: Cloud-to-Mesh edge reduction comparison, sample ID: DAC3-2, Cycle 125-250. A - Edge damage histogram, B - Back view, C - Front view.

DAC3-2:

C2M Comparison - Cycle 250 to 500.

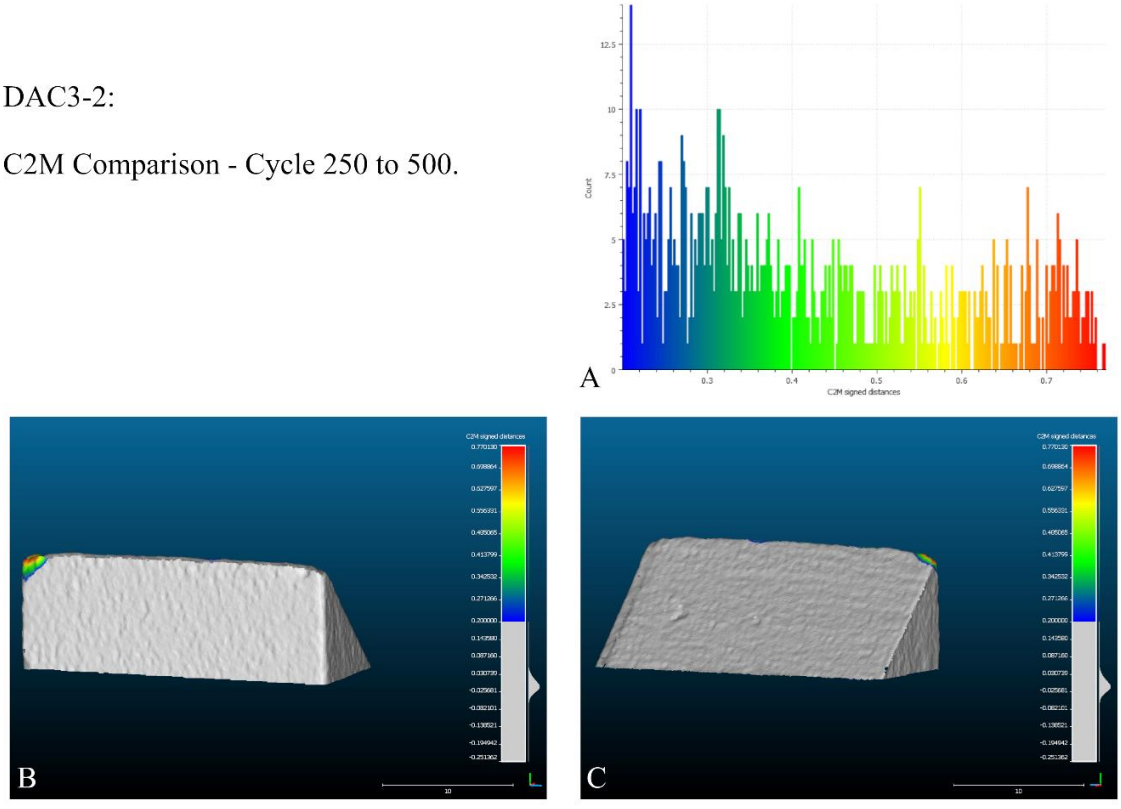

Figure 64: Cloud-to-Mesh edge reduction comparison, sample ID: DAC3-2, Cycle 250-500. A - Edge damage histogram, B - Back view, C - Front view.

DAC3-2:

C2M Comparison - Cycle 0 to 500.

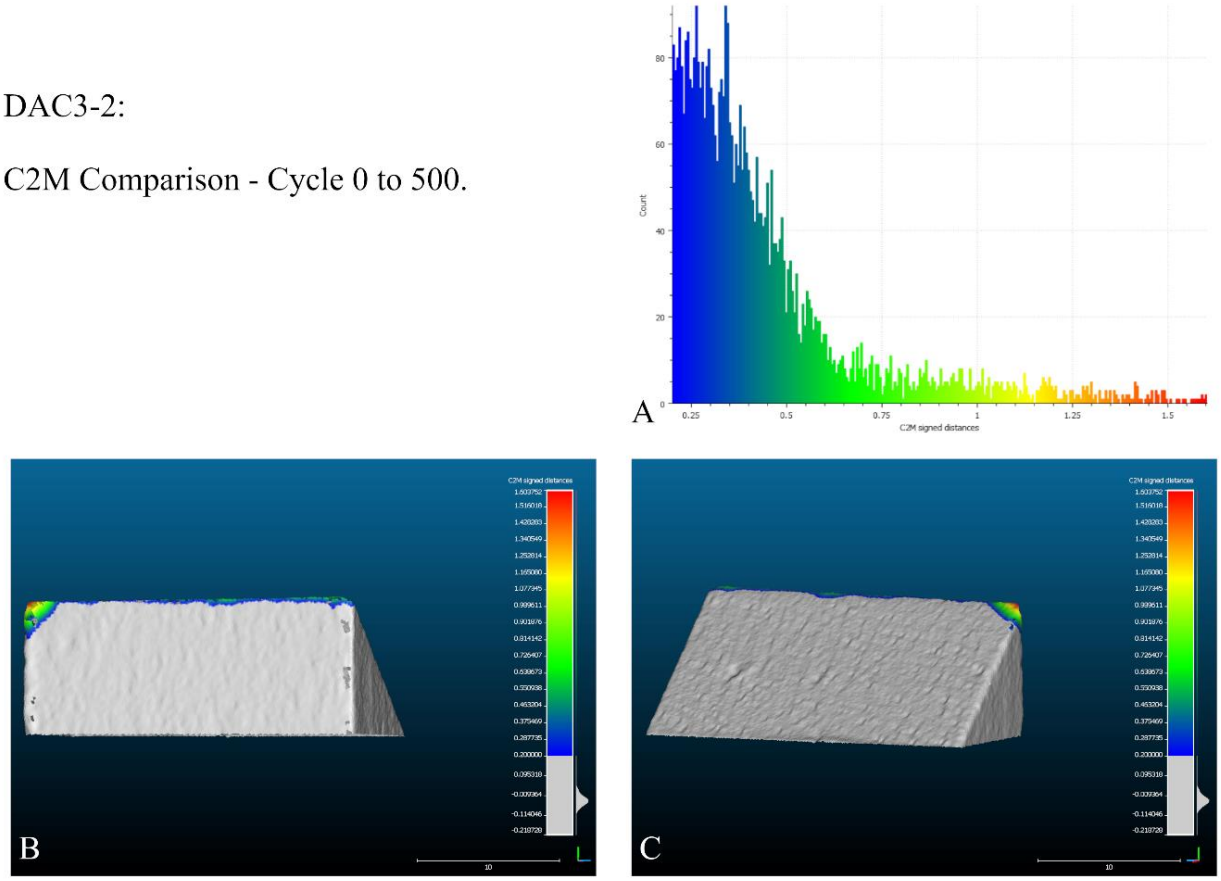

Figure 65: Cloud-to-Mesh edge reduction comparison, sample ID: DAC3-2, Cycle 250-500. A - Edge damage histogram, B - Back view, C - Front view.

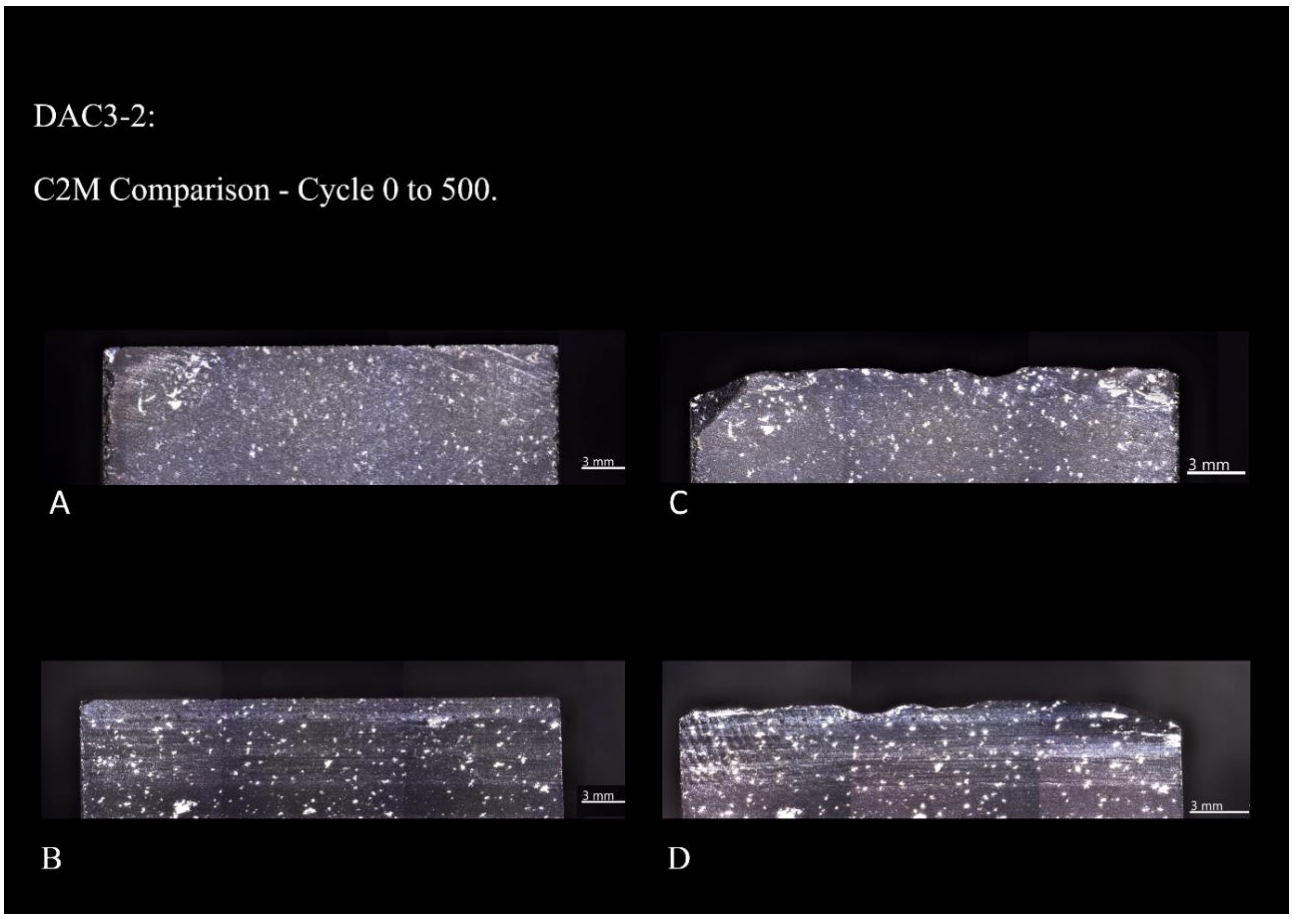

Figure 66: ZEISS Smart zoom images, A/B Cycle 0: A - Back view, B – Front view, C/D Cycle 500: C – Back View, D – Front view. Sample ID: DAC3-2.

4.2.3.e DAC3-6

From Figure 66 A, the results are the following:

Sample DAC3-6 starts its first contact with pinewood at 13.7 mm in steps 1 to 3, following with a slight decrease in depth at it reach 13.9 mm in step 5, the rest of the movement until step 10 didn't show major differences. After the stop and run from step 10 to 20 a significant increase in depth penetration occurs to approximately 12.7 mm. The rest of the cycle shows a regular increase in depth penetration at 11.9 mm in cycle 125. Cycle 126 to 250 represent once more a regular penetration into pinewood from approximately 12.5 mm to 11.6 mm. The last phase of 500 strokes represents an increase of 0.90 mm in-depth penetration. In sample DAC3-6 the same machine error in the Z sensor is visible, adjustment of the unit measure was applied taking into account the last stroke from cycle 250. DAC3-6 reach a total of 11.4 mm penetration by the end of the experiment.

Figure 66 B represents the sensors measure from Inotec, and the results are the following:

From DAC3-6 force sensor captures initial values of -59 N until step 2, after these, values represent a multimodal graphical representation with a range between -36 N to -76. From step 3 to 8, is possible to observe that in two cycles a stepped increase in force, but more frequently a decrease from the initial force, as the sample gets to its first stop in step 10 valued tend to stabilize near initial values. For the backward movement, the higher frequency is seen in the reduction of a force applied during the experiment.

Cycle 1 has a slight increase in friction approximately -20 N, and when it stops at point B step 10 no friction is applied from the contact from the DAC3-6 and pinewood. During the movement from point A to B (step 3 to 10) is possible to observe four picks when friction is higher (step, 3, 6, 8, and 10).

Velocity values represent a homogenous acceleration at 600mm/s as step 4, following with a reduction of velocity as it achieves the first stop during the cycle (step 10). From steps 10 to 20, representative of the linear movement of point B to A. The same representation of mirror effect values in negative units, as it represents a back movement step 10 to 20.

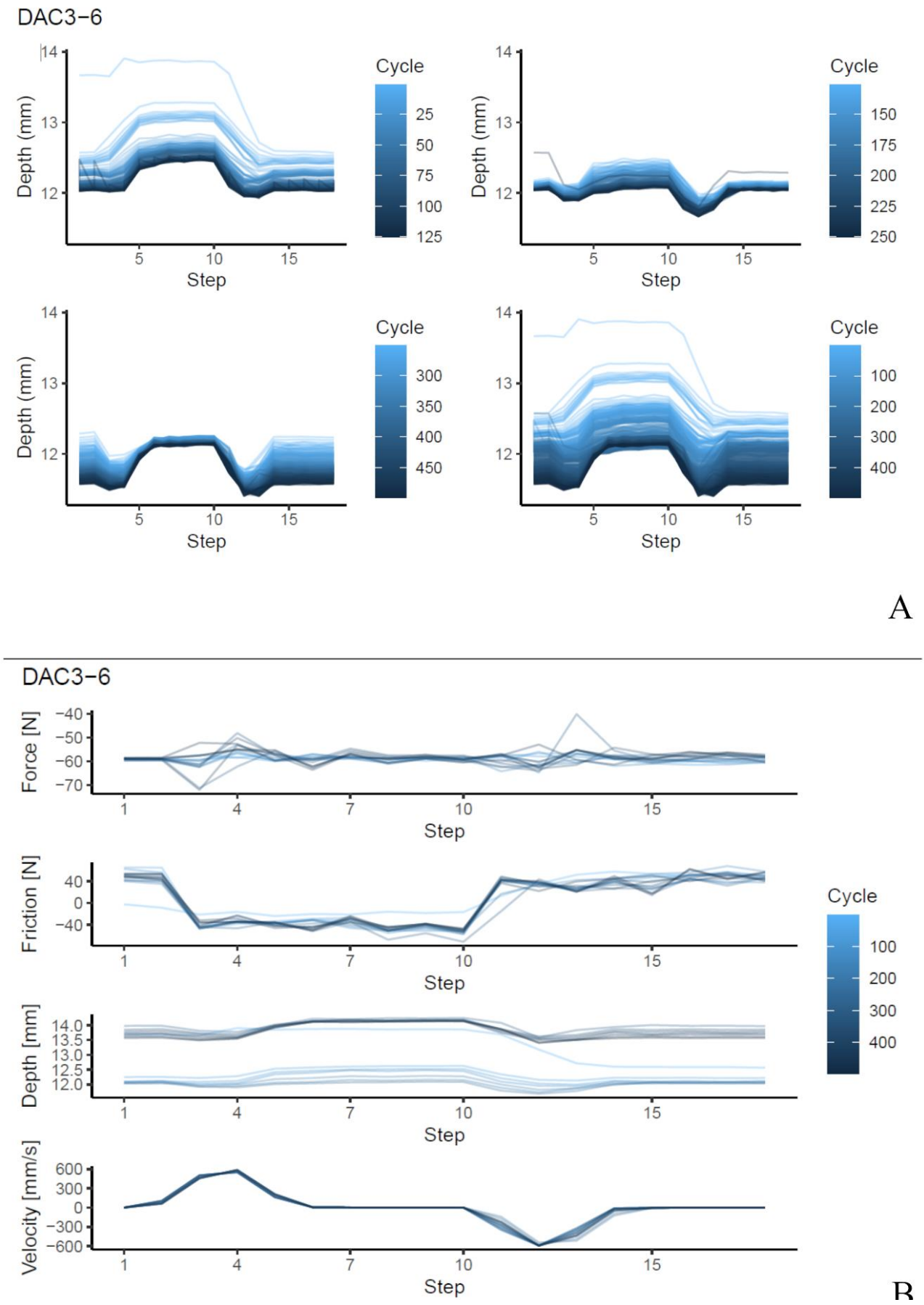

Figura 67: Graphic representation of the values recorded from Inotec from sample ID: DAC3-6. A - Penetration depth (mm) results, B - Sensors results.

4.2.3.f DAC3-6 Edge reduction, C2M Comparisons

DAC3-6 rapidly fracture in the first cycles, a small flake displacement occurs in the external extremity of the sample leaving a negative of 0.8 mm Figure 67-B, in these 250 strokes the rest of the edge shows a small reduction between 0.2 mm and 0.4 mm. In the next cycle (125-250) no major alterations are visible in the mesh comparisons.

In the last cycle, a higher reduction by parts can be seen in the graph Figure 68-A, but in terms of intrusive damage, no more than 0.4 mm is achieved, also the damage is more expressive in the external part of the sample.

DAC3-6:

C2M Comparison - Cycle 0 to 125.

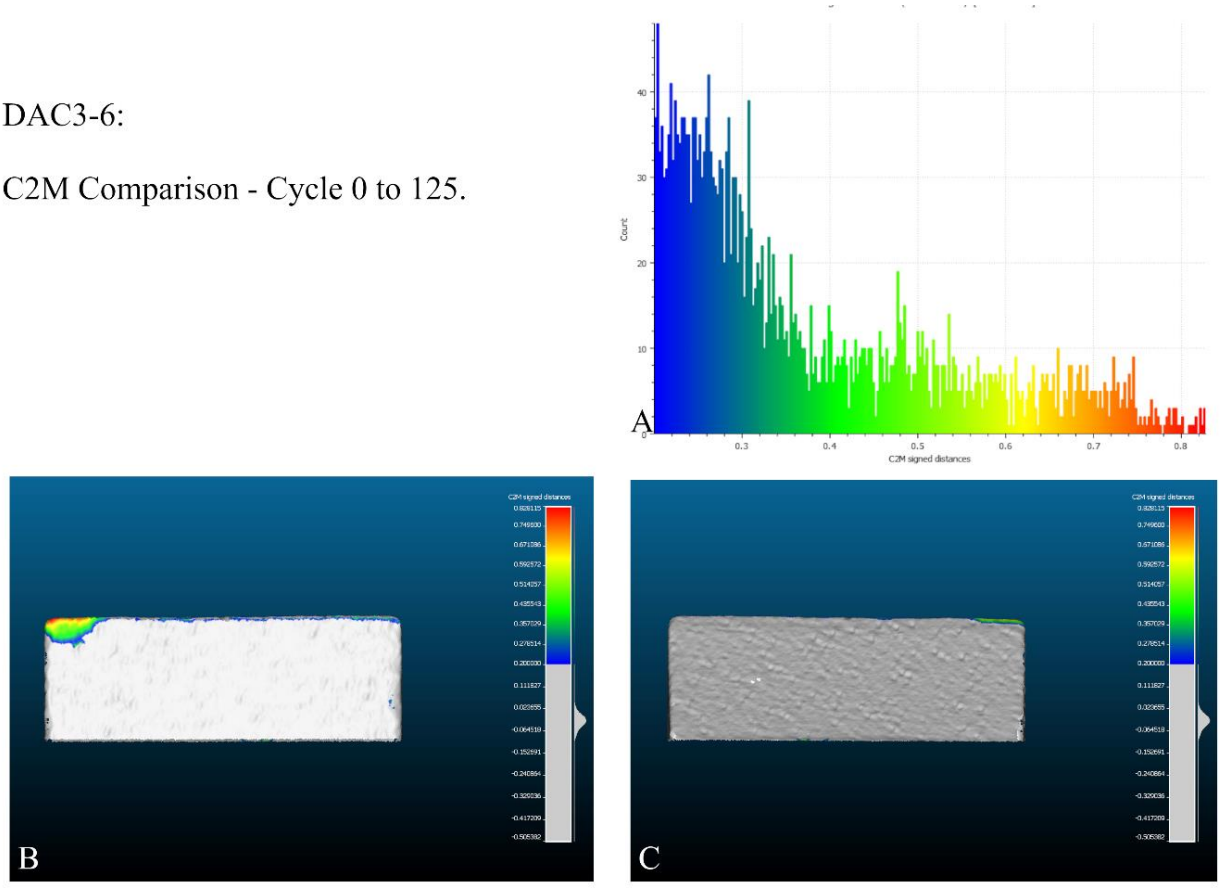

Figure 68: Cloud-to-Mesh edge reduction comparison, sample ID: DAC3-6, Cycle 0-125. A - Edge damage histogram, B - Back view, C - Front view.

DAC3-6:

C2M Comparison - Cycle 125 to 250.

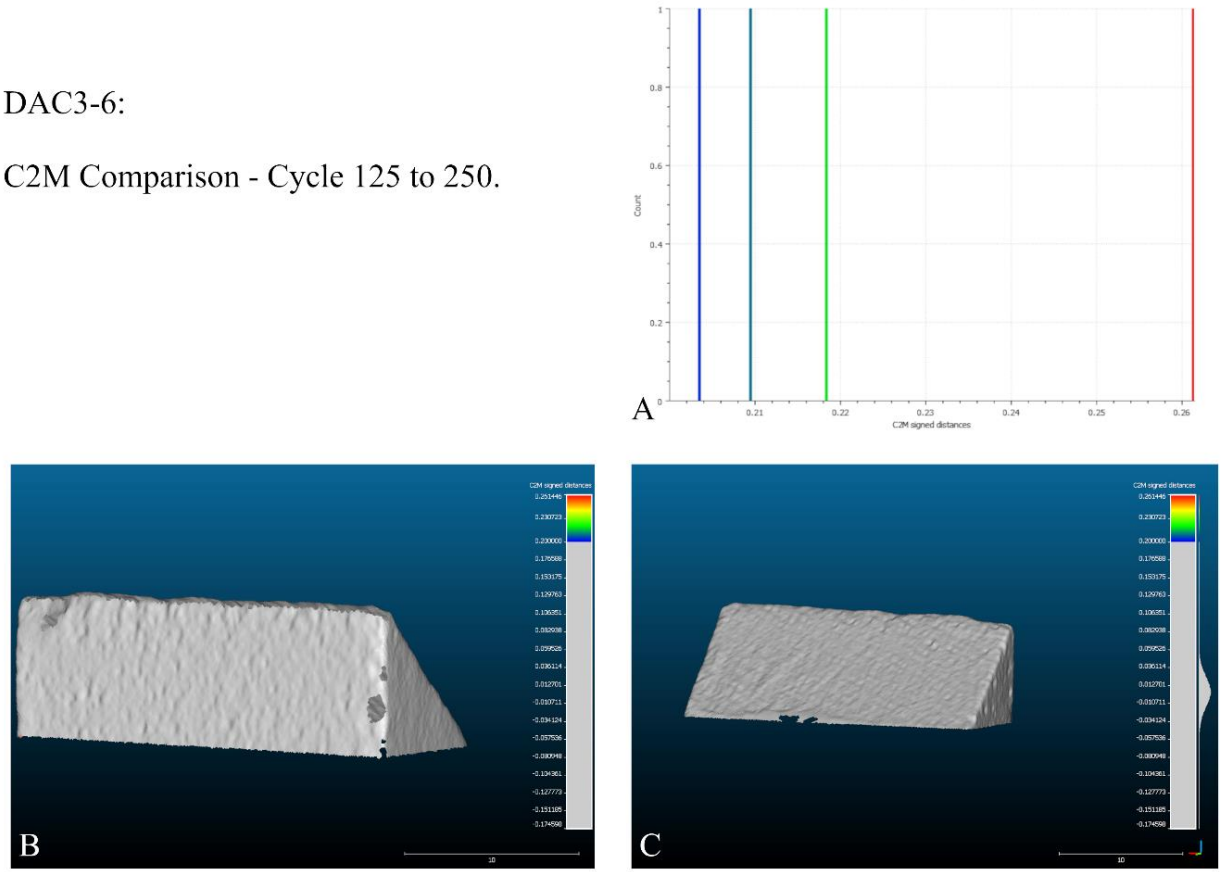

Figure 70: Cloud-to-Mesh edge reduction comparison, sample ID: DAC3-6, Cycle 125-250. A - Edge damage histogram, B - Back view, C - Front view.

DAC3-6:

C2M Comparison - Cycle 250 to 500.

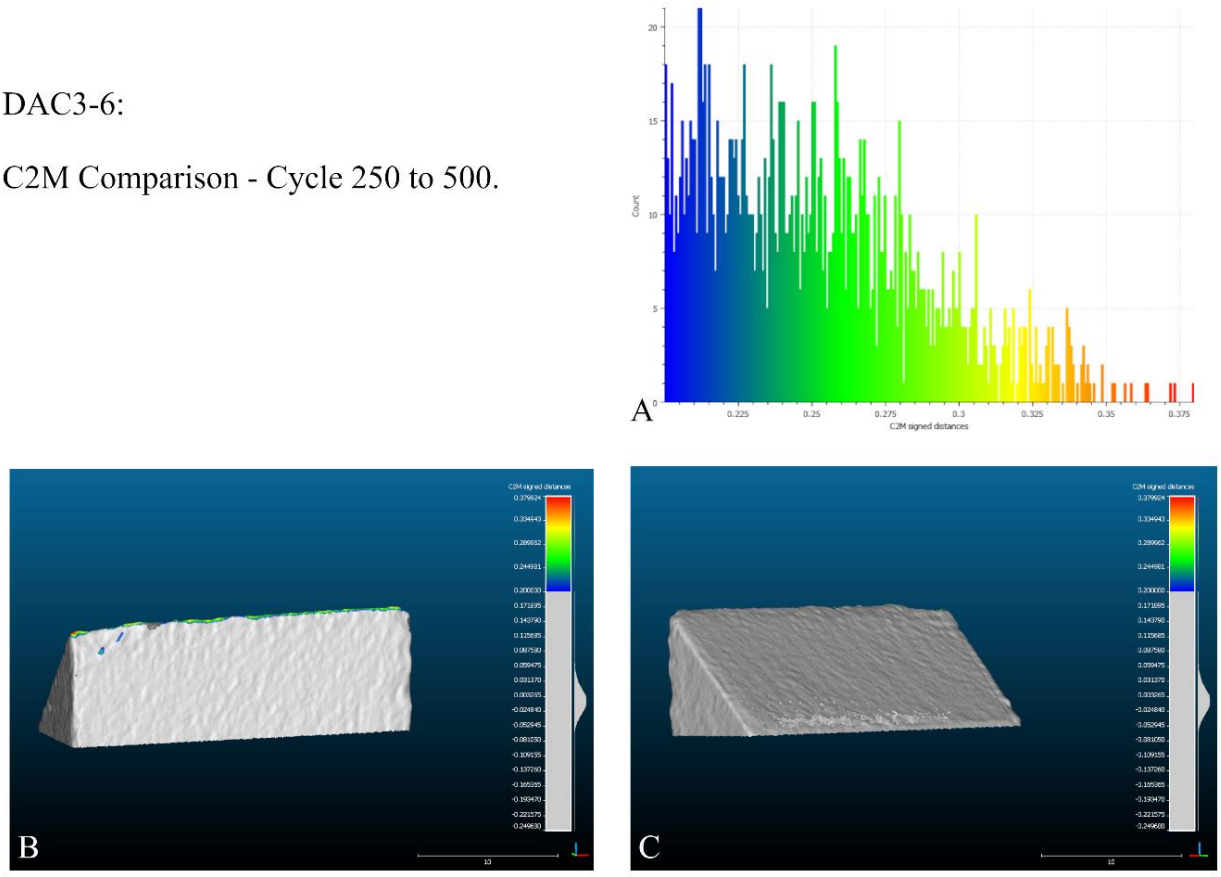

Figure 69: Cloud-to-Mesh edge reduction comparison, sample ID: DAC3-6, Cycle 250-500. A - Edge damage histogram, B - Back view, C - Front view.

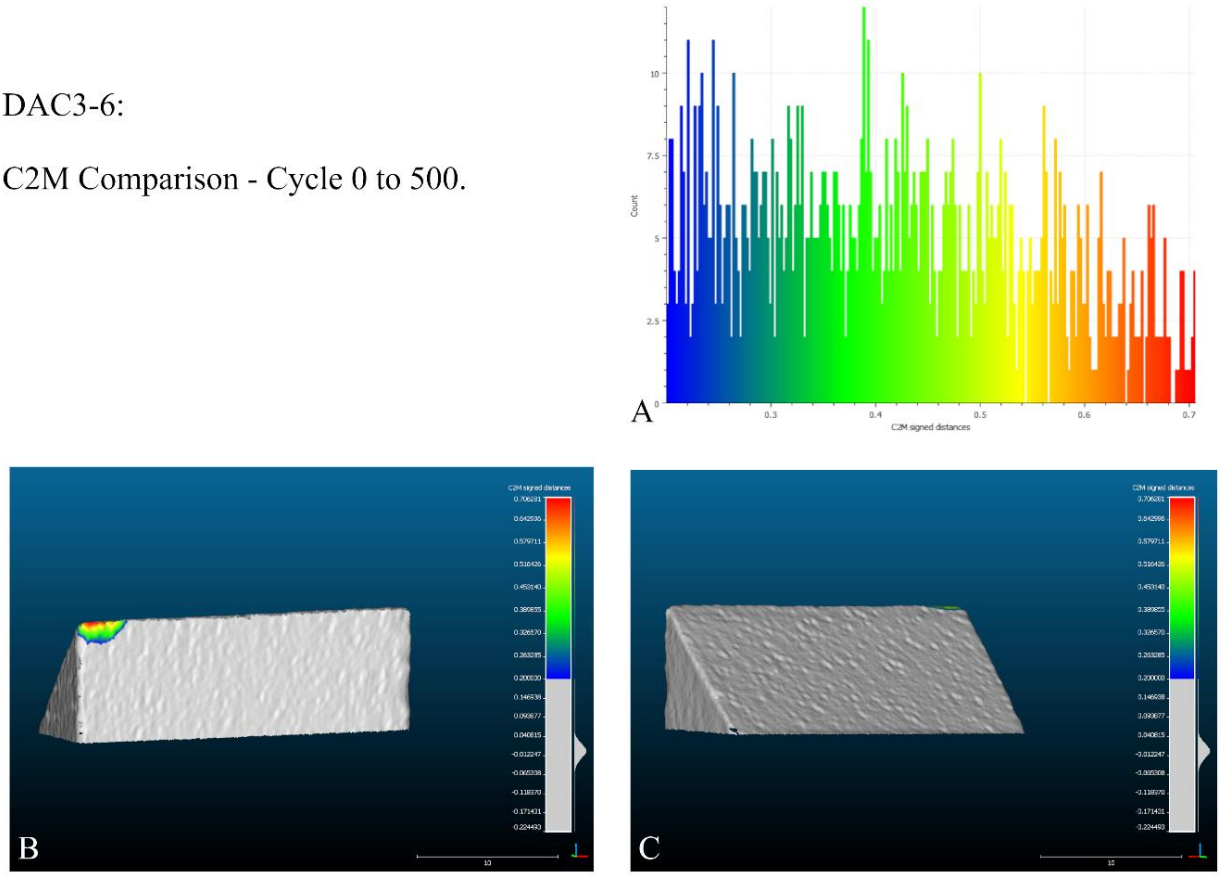

Figure 72: Cloud-to-Mesh edge reduction comparison, sample ID: DAC3-6, Cycle 0-500. A - Edge damage histogram, B - Back view, C - Front view.

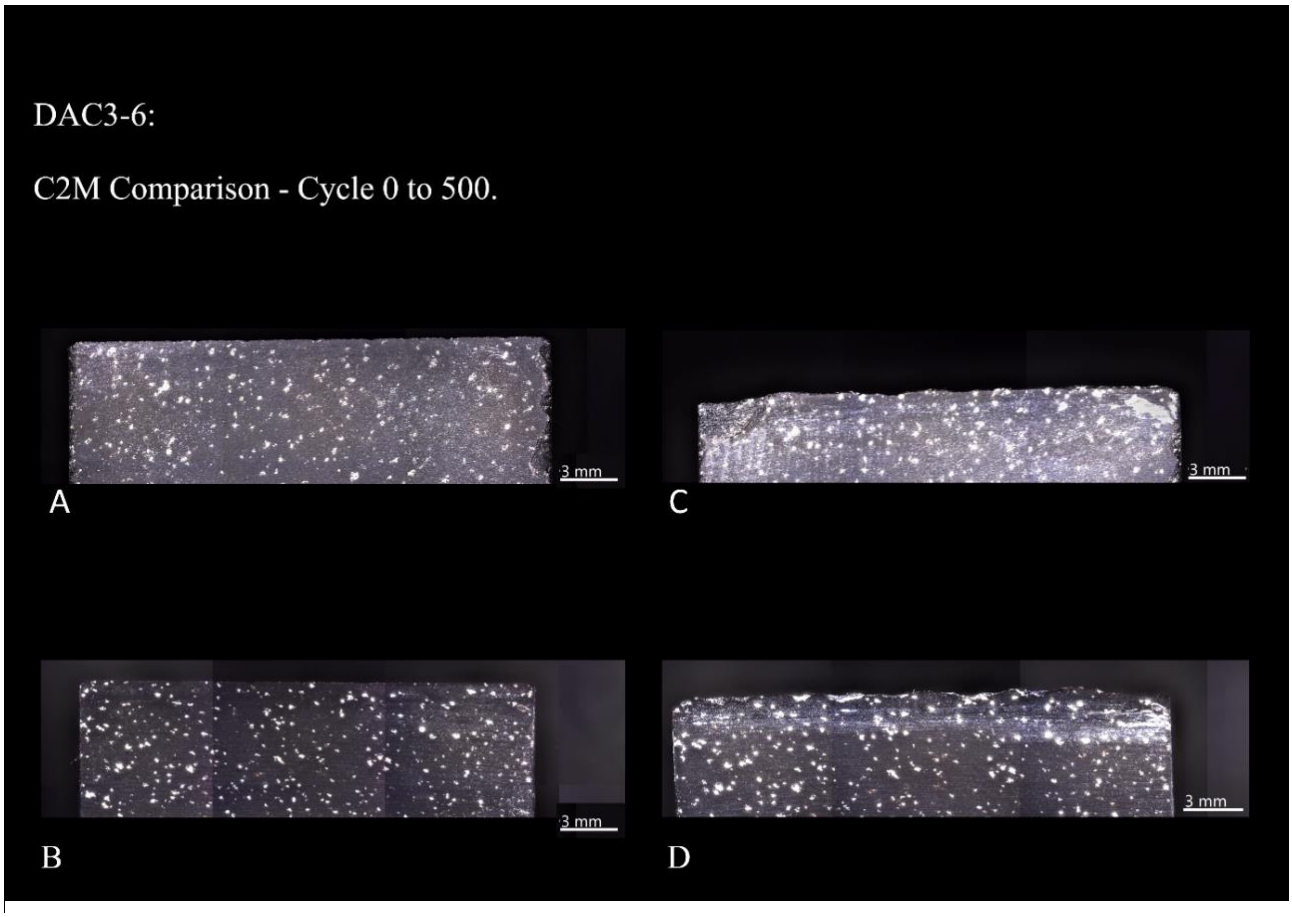

Figure 71: ZEISS Smart zoom images, A/B Cycle 0: A - Back view, B – Front view, C/D Cycle 500: C – Back View, D – Front view. Sample ID: DAC3-6.

4.2.4 OBSIDIAN

4.2.4.a OBS4-4

From Figure 72 A, the results are the following:

The first cycle begins with a depth penetration of approximately 14 mm. Throughout the movement, it is verified that the depth remains constant until step 11 is reached. From this step, the depth of the first cycle increases and reaches its maximum penetration depth. The performance between this interval of cycles is very similar. In all cycles, it is observed that the maximum penetration depth of the OBS4-4 sample is reached at step 11. From cycles 0-125, there is a maximum depth of 12.73 mm and a minimum depth of 14.28 mm.

From cycles 126 to 250, the OBS4-4 sample behaves similarly to cycles 0-125 mentioned above. All cycles in this range start with a penetration depth between 12.8 mm and 13 mm and register their maximum from step 11. The maximum registered depth from cycle 126 to 250 is 12.38 mm and the maximum is 13.25 mm. The maximum penetration depth achieved by OBS4-4 is recorded as 9.32 mm in the last cycles.

Figure 72 B represents the sensors measure from Inotec, and the results are the following:

The initial force exerted by OBS4-4 on the pinewood was approximately -60N. During the movements, it is observed that the force is practically constant in all steps and all cycles. The observed oscillations are verified in steps 4 and 13. In these steps, the applied force is greater in the final cycles than the initial cycles, with a maximum force of -82.84 N.

By observing the graph referring to friction, it can be concluded that the initial friction is 0 N in the first cycle and that it remains constant afterward. However, for the following cycles, the movement starts with an increase of friction followed by a decrease until step 7. After, step 8 is representative of high values, and step 9 a decrease in friction between contact material and OBS4-4.

The movement starts with a speed of 0 mm/s. Velocity increases in all cycles at step 4 and remains constant after step 6. From step 10 t0 20 all the values in negative represent the backward movement and are a mirror of the first ten steps.

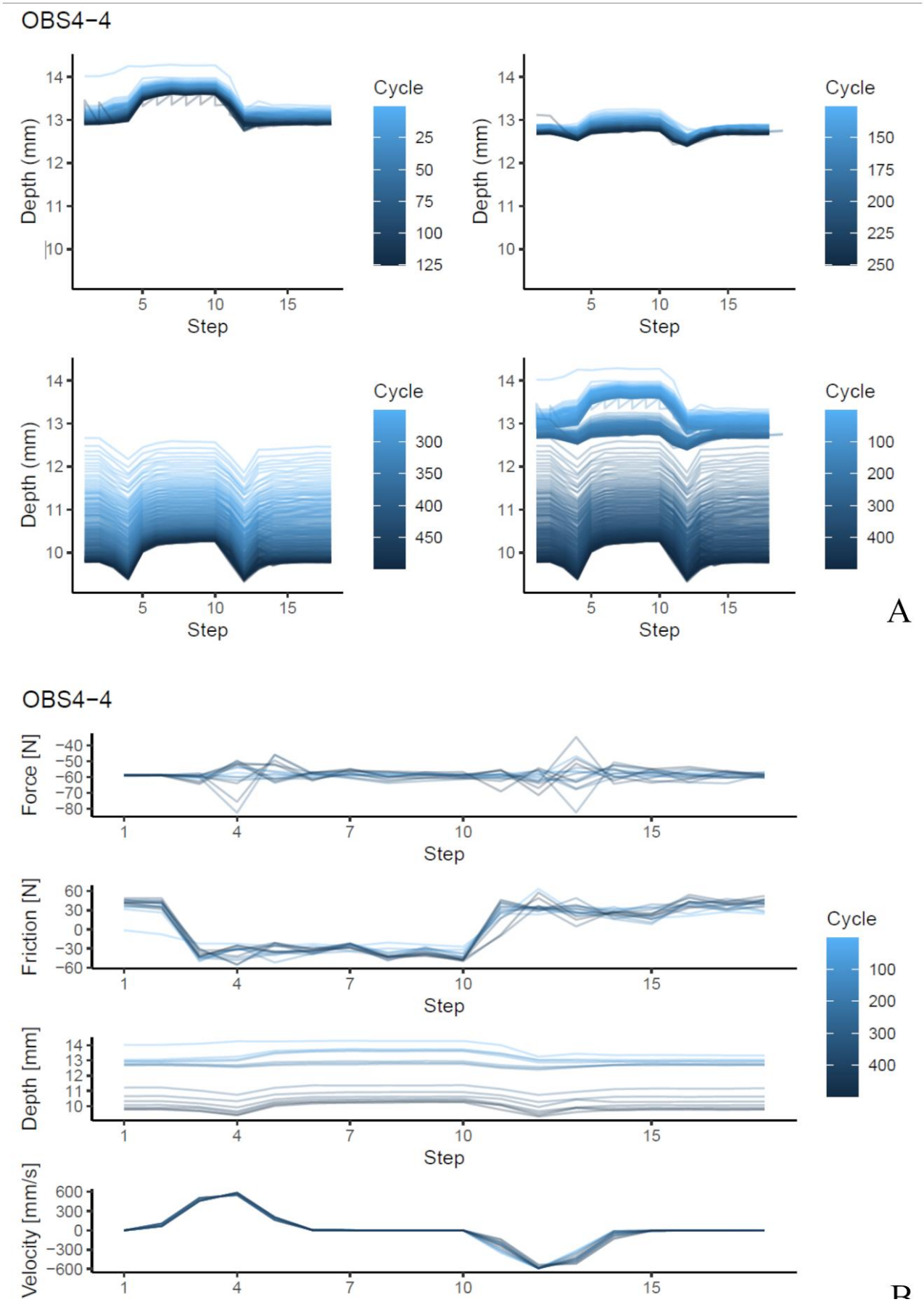

Figura 73: Graphic representation of the values recorded from Inotec from sample ID: OBS4-4. A - Penetration depth (mm) results, B - Sensors results

4.2.4.b OBS4-4 Edge reduction, C2M Comparisons

The damage visible from the comparison from mesh cycles 0 to 125, has a range in depth from 0.2 mm to 0.6 mm. From the histogram in Figure 73 is possible to see that the higher is the depth damage, the less is the correspondent area. The location of the edge damage can be seen in Figure 73-B and C, all the edge sample suffered a reduction, and is more expressive in the external side, leaving a wavy edge. The same pattern is seen in the next cycle (126 to 250), with the same reduction range (0.2 mm to 0.6 mm).

In the last phase of the experiment 500 strokes are applied to the contact material, OBS4-4 did not show high alterations in the edge sample in this phase, minor abrasions are visible in the external side of the sample Fig, 74-B.

Figure 64 is representative of the edge reduction through all stages (1000 strokes). In this sample, the damage is visible through all edges but in terms of quantitative damage is between 0.2 mm and 0.4 mm that more differences are verified from mesh 0 to 500.

OBS4-4:

C2M Comparison - Cycle 0 to 125.

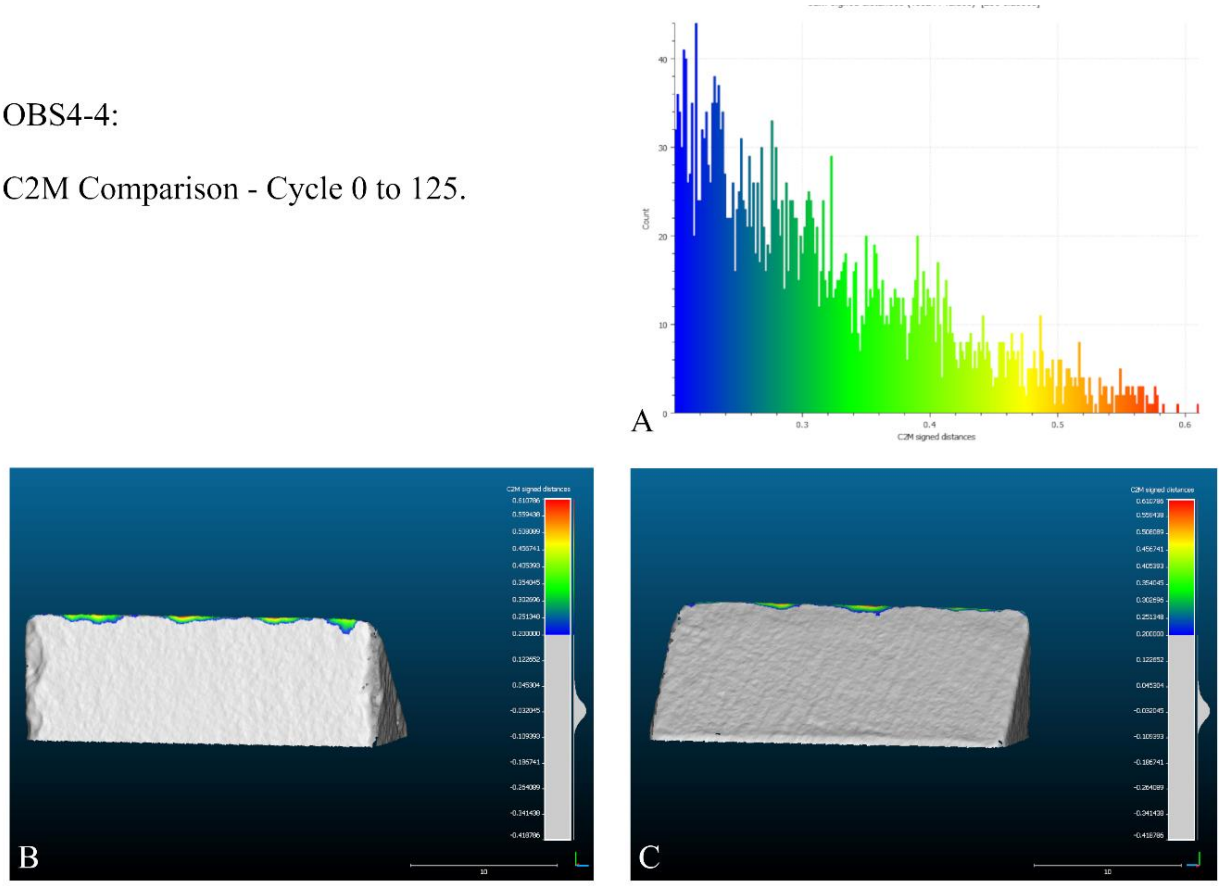

Figure 74: Cloud-to-Mesh edge reduction comparison, sample ID: OBS4-4, Cycle 0-125. A - Edge damage histogram, B - Back view, C - Front view.

OBS4-4:

C2M Comparison - Cycle 125 to 250.

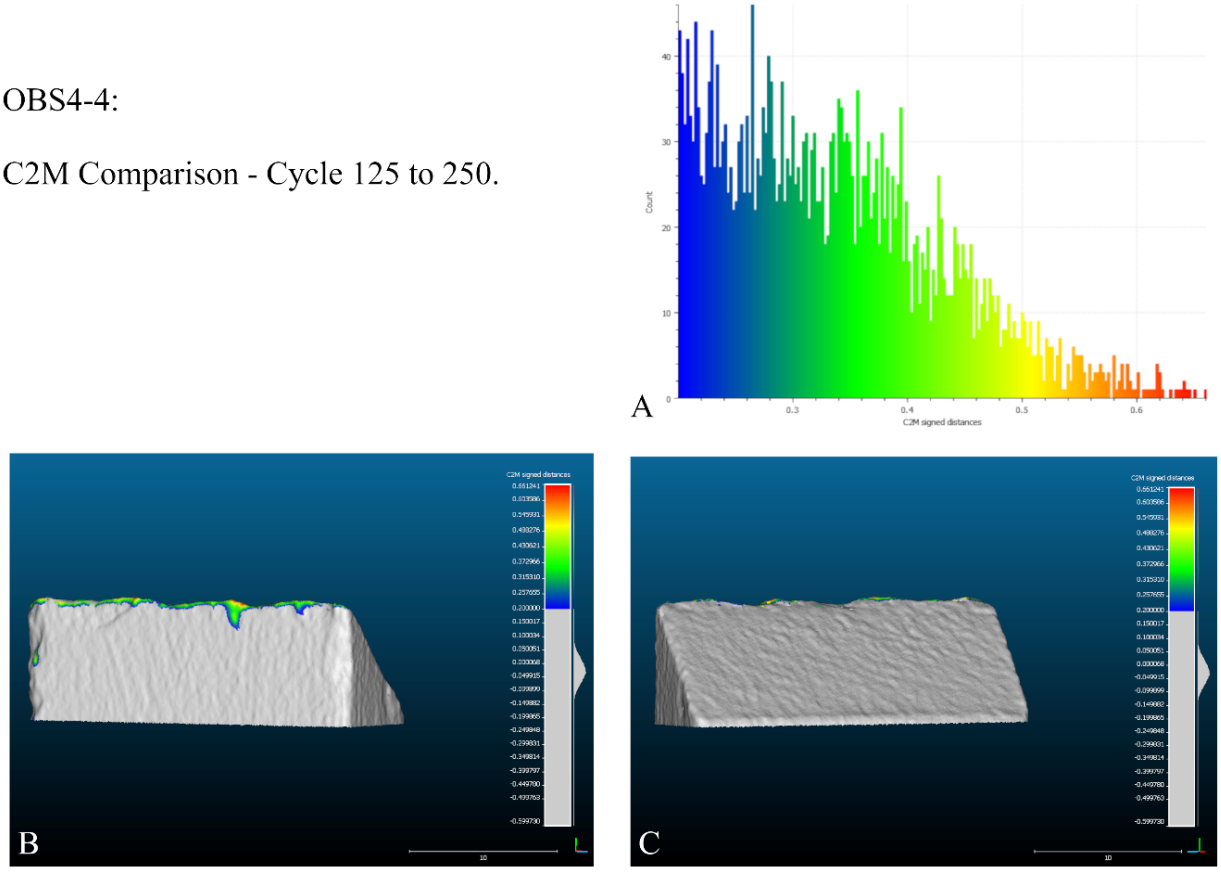

Figure 76: Cloud-to-Mesh edge reduction comparison, sample ID: OBS4-4, Cycle 0-125. A - Edge damage histogram, B - Back view, C - Front view.

OBS4-4:

C2M Comparison - Cycle 250 to 500.

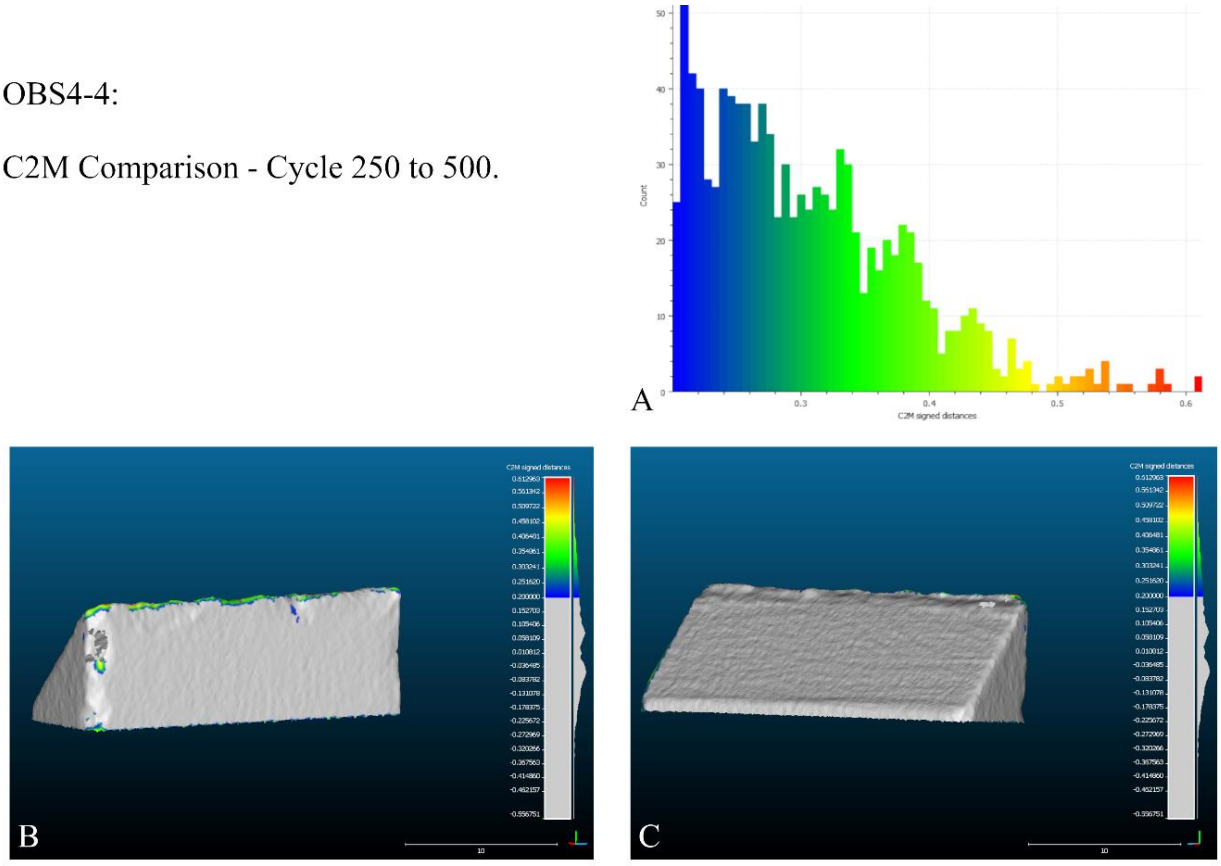

Figure 75: Cloud-to-Mesh edge reduction comparison, sample ID: OBS4-4, Cycle 250-500. A - Edge damage histogram, B - Back view, C - Front view.

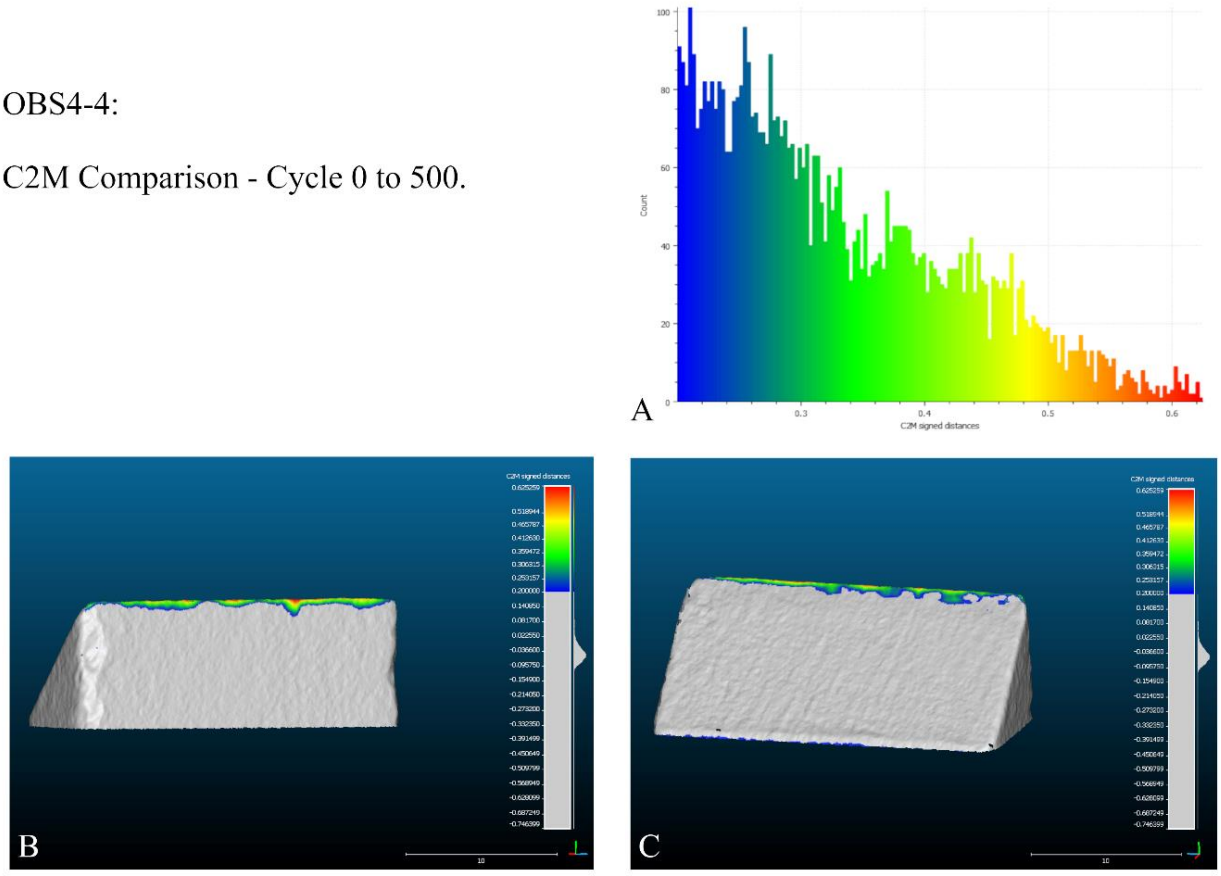

Figure 78: Cloud-to-Mesh edge reduction comparison, sample ID: OBS4-4, Cycle 0-500. A - Edge damage histogram, B - Back view, C - Front view.

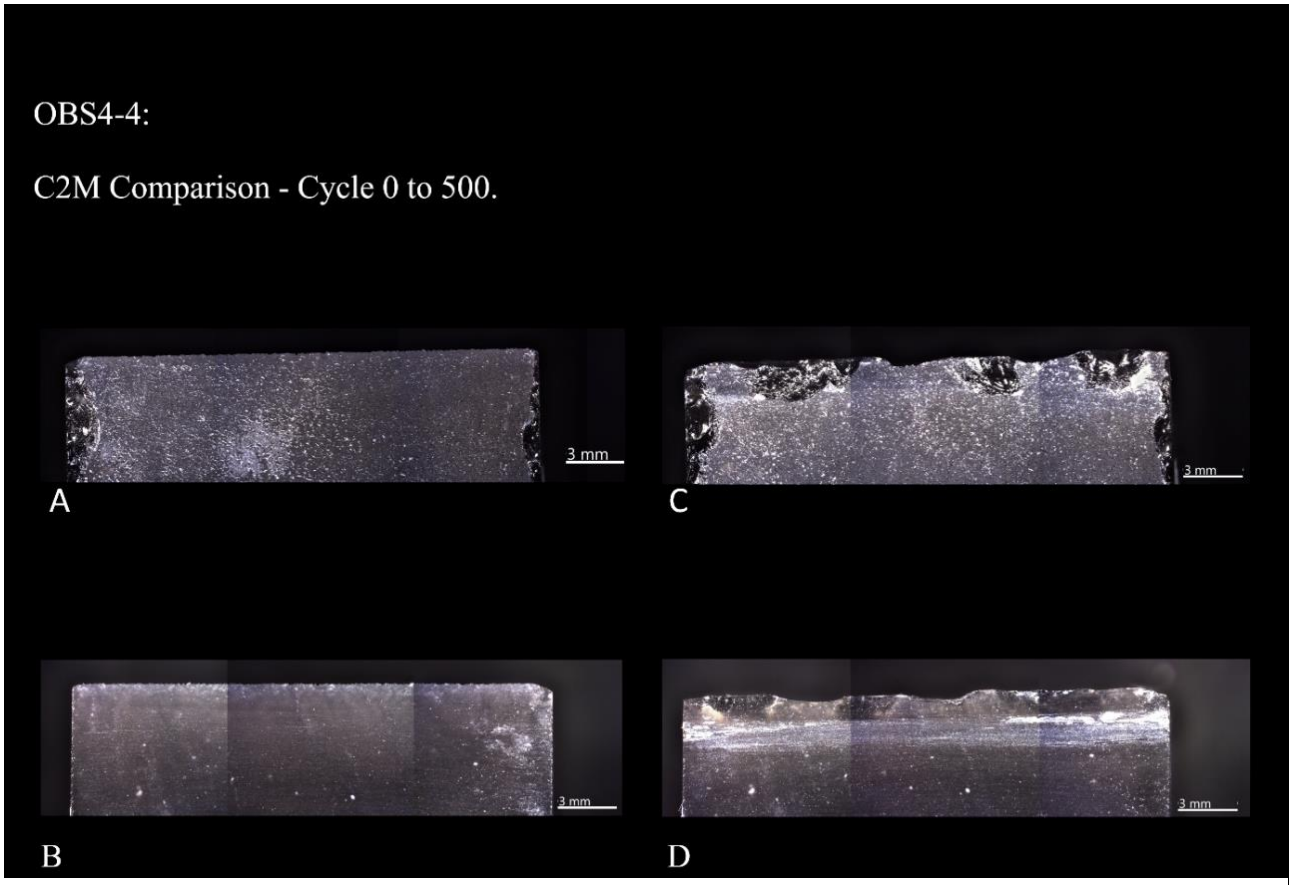

Figure 77 - ZEISS Smart zoom images, A/B Cycle 0: A - Back view, B – Front view, C/D Cycle 500: C – Back View, D – Front view. Sample ID: OBS4-4.

4.2.4.c OBS4-5

From Figure 78 A, the results are the following:

The penetration depth of the OBS4-5 sample in the first cycle starts at about 13.5 mm. In all steps of this cycle, a constant behavior is shown until step 10 is reached. After this step, the penetration depth into the pinewood increases. The first 125 cycles show the same behavior in all steps. The movement of these cycles starts with a penetration depth between 12.1 mm and 12.5 mm. The maximum penetration depth measured during these cycles was 11.9 mm.

As the cycles progress, the penetration depth increases significantly. For cycles 126-250, it is found that the movements start with a depth between 12.5 and 12.7 mm. From step 11 and for cycles 225-250, an increase in penetration depth is noted. In this series of cycles, a maximum penetration depth of 11.7 mm and a minimum penetration depth of 12.8 mm is recorded.

In the last cycle, 251-500, it is observed that the sample OBS4-5 starts the movements with a penetration depth between 12.4 and 11.5 mm. The graph for these cycles shows a slight decrease in the penetration depth from step 5 and after step 12 the penetration depth increases again. In these cycles, a maximum penetration depth of 9.3 mm and a minimum of 12.6 mm were recorded. In these 500 cycles, a maximum penetration depth of 9.31 mm was recorded in cycles 251-500 and a minimum of 14.2 mm was recorded in cycles 0-125.

Figure 78 B represents the sensors measure from Inotec, and the results are the following:

The initial force of the OBS4-5 sample on pinewood is -60N. The initial force is the same for all cycles, but in the first few cycles, a greater force is applied to the wood. From step 4 and step 5, the minimum peak values of applied force are recorded. During the measurement, the maximum force of -73.83 N was recorded for the 251-500 cycles and the minimum of -35.01.

The initial friction in the first cycle is zero. At the end of step 3, the friction decreases and later remains constant throughout the motion. In the remaining cycles, the initial friction in step 2 to step 3, increases significantly and several peaks are observed from this step onwards. The highest value that the friction reaches is -90 N between 126 and 250 cycles. Velocity starts at 0 mm/s. As the motion progresses, an increase in velocity is registered, peaking at step 4.

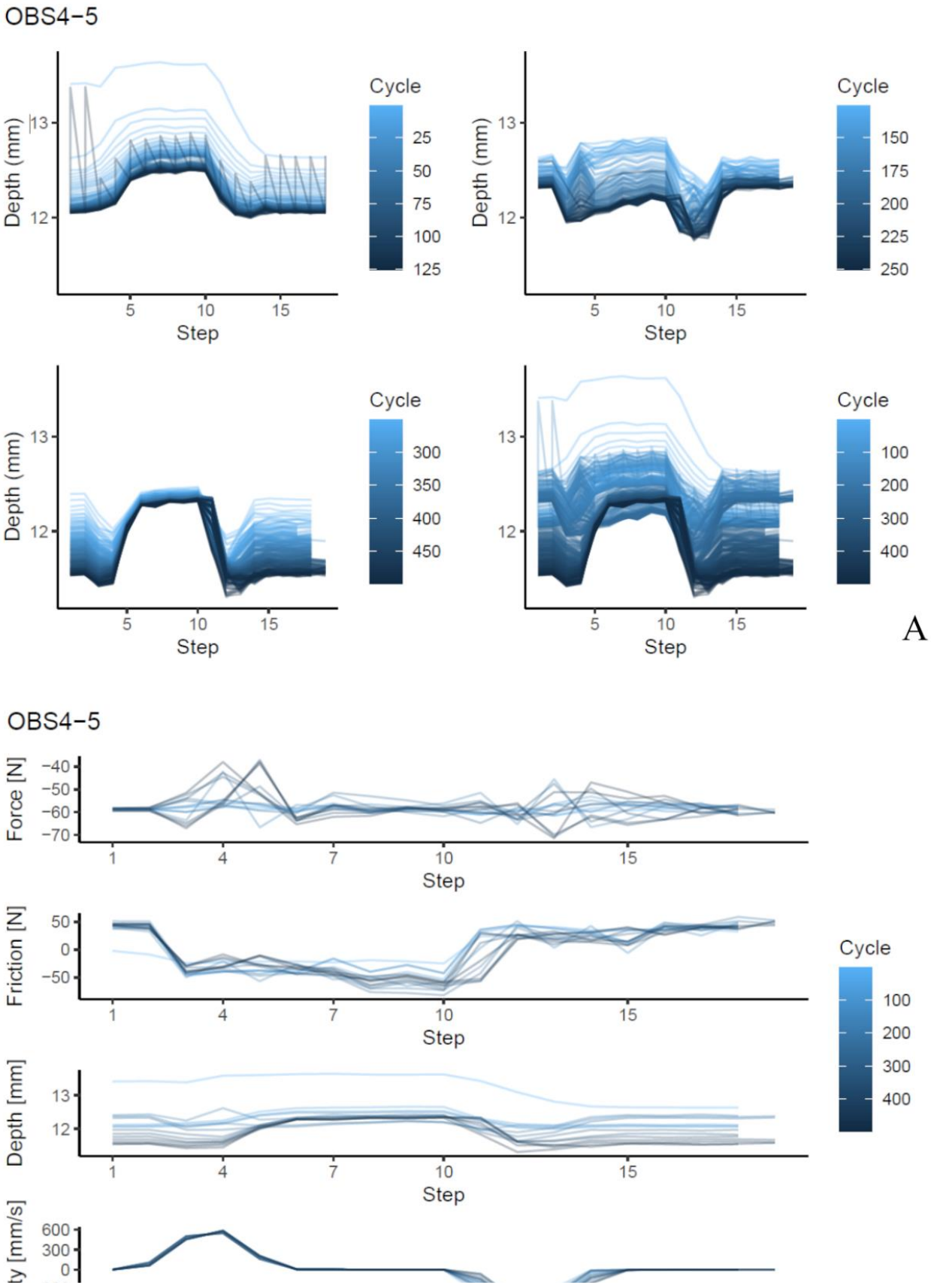

Figura 79: Graphic representation of the values recorded from Inotec from sample ID: OBS4-5. A - Penetration depth (mm) results, B - Sensors results.

4.2.4.d OBS4-5 Edge reduction, C2M Comparisons

Results from the first 250 strokes in OBS4-5 result in damage located at both extremities of the sample, removals can be seen reaching more than 0.6 mm in the external part of the sample. From the histogram, in Figure 79-A the data shows the edge damage is grouped and more incidents from 0.2 to 0.4 mm. In the cycle between 126 to 250 a big removal is visible starting in one corner of the sample where the damage is also bigger 1.0 mm, and move on to the mid-section of the sample with damage range from 0.2 mm to 0.7 mm. The last phase of 500 repetitions results in 0.2 mm to 1.00 mm of damage in the same corner as the previous cycle. The last figure 83 shows that most of the edges had a reduction of at least 1.00 mm, and a maxim of 1.98 mm.

OBS4-5:

C2M Comparison - Cycle 0 to 125.

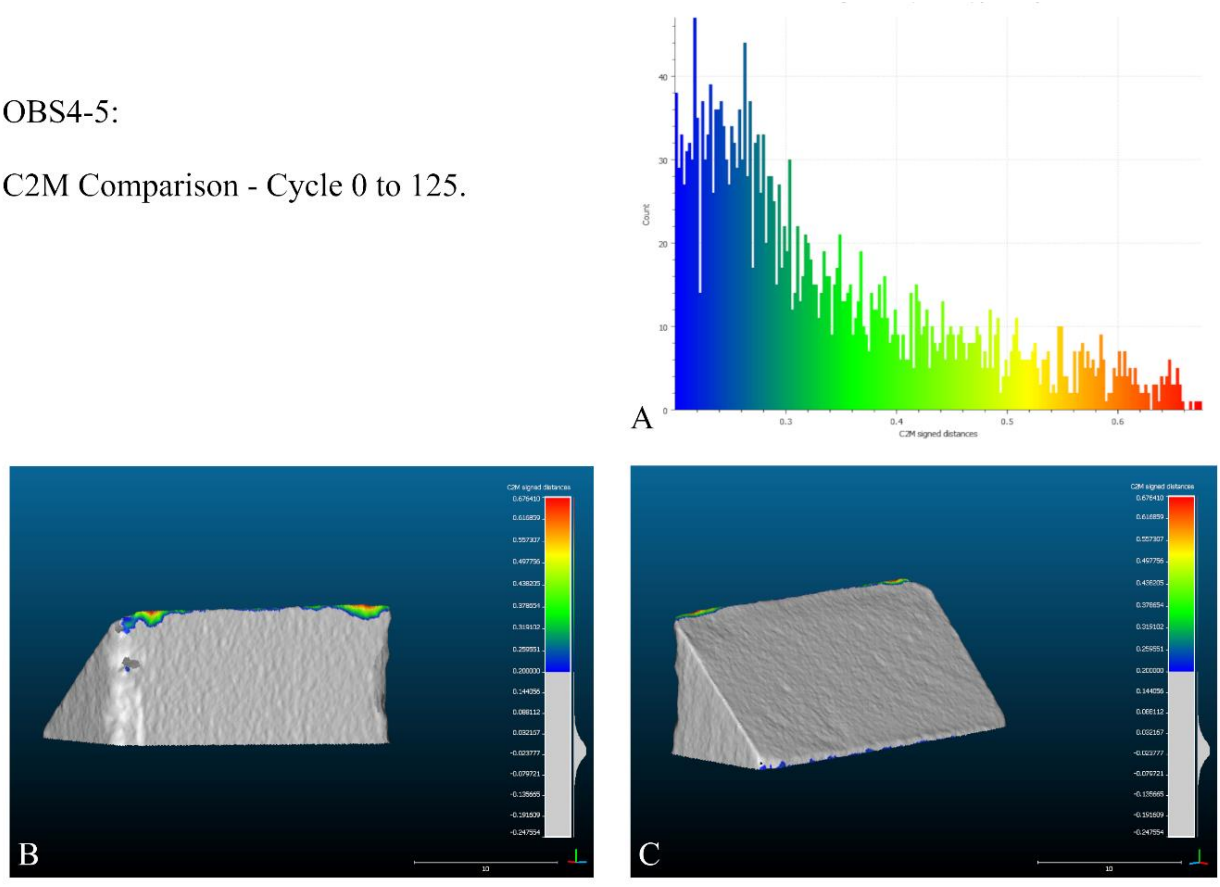

Figure 80: Cloud-to-Mesh edge reduction comparison, sample ID: OBS4-5, Cycle 0-125. A - Edge damage histogram, B - Back view, C - Front view.

OBS4-5:

C2M Comparison - Cycle 125 to 250.

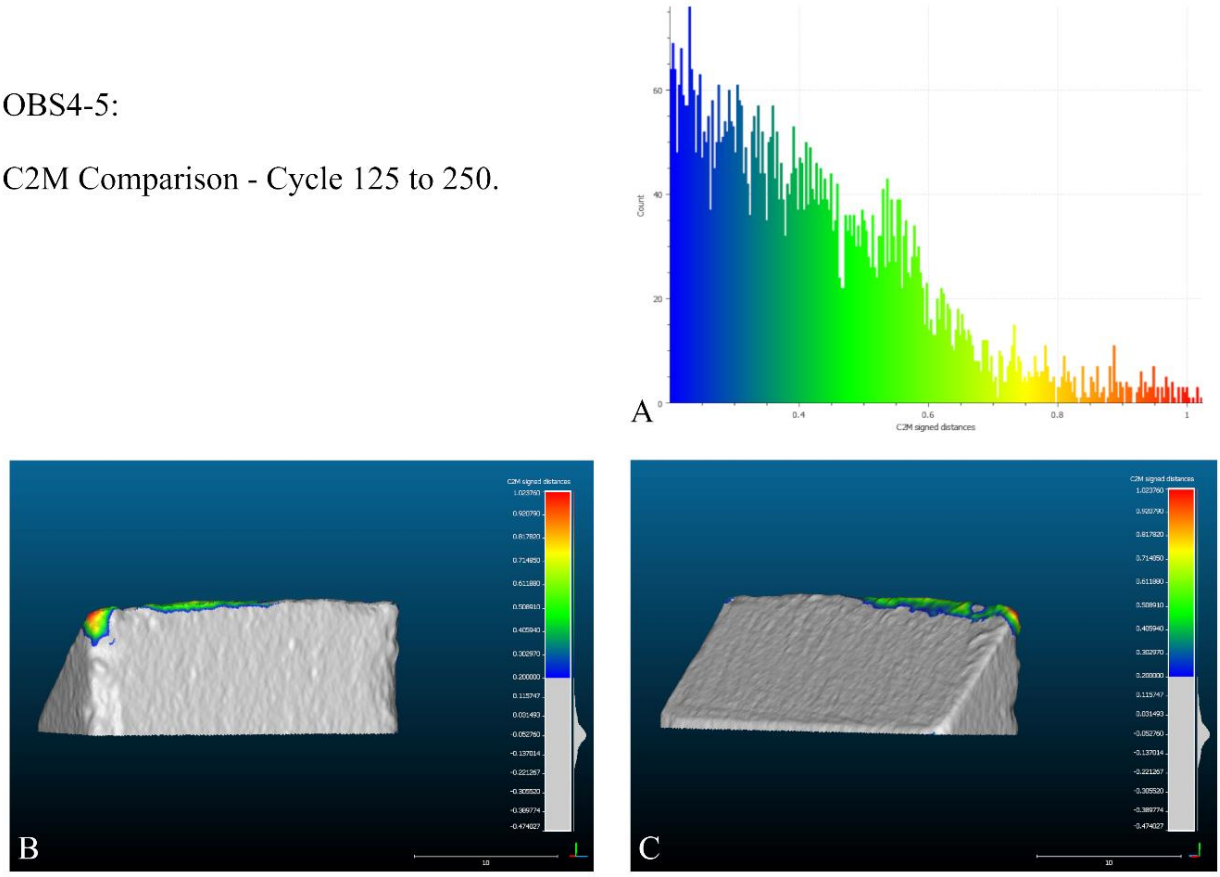

Figure 81: Cloud-to-Mesh edge reduction comparison, sample ID: OBS4-5, Cycle 125-250. A - Edge damage histogram, B - Back view, C - Front view.

OBS4-4:

C2M Comparison - Cycle 250 to 500.

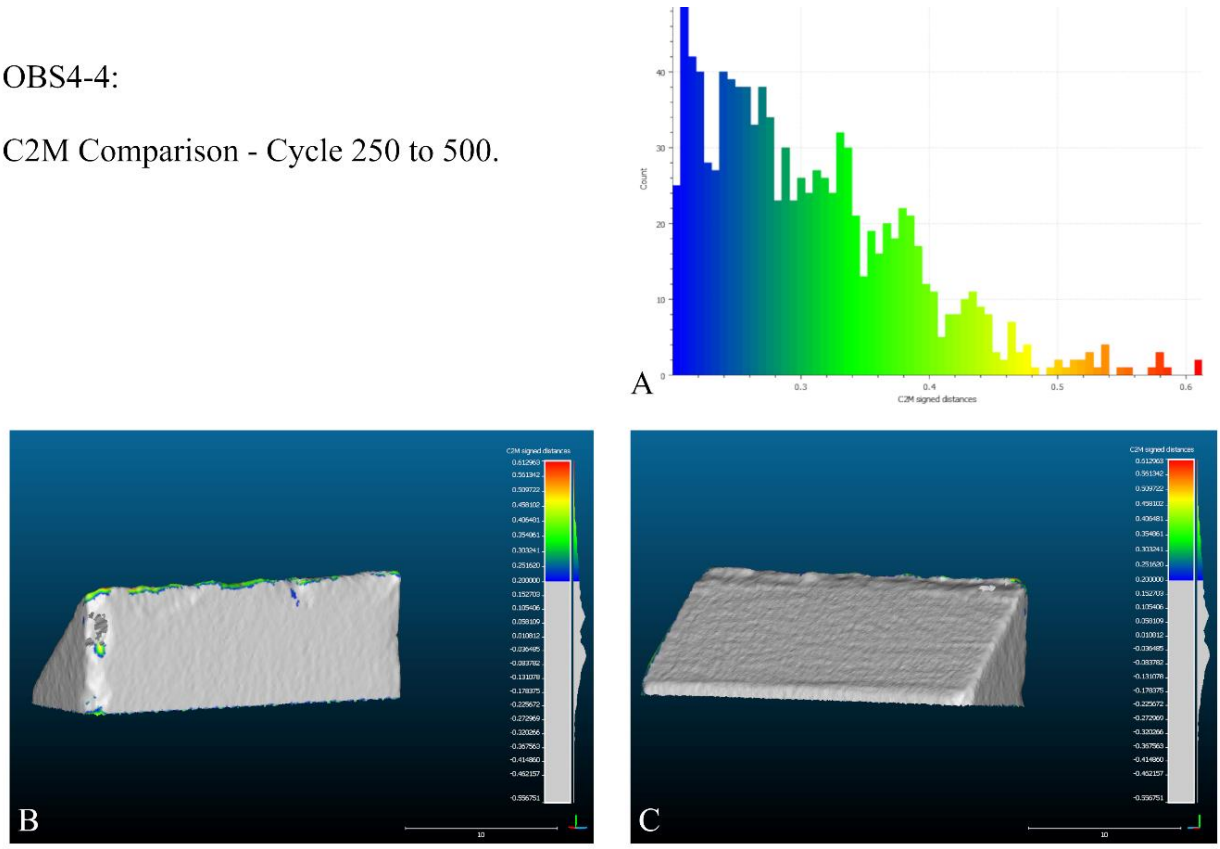

Figure 82: Cloud-to-Mesh edge reduction comparison, sample ID: OBS4-5, Cycle 250-500. A - Edge damage histogram, B - Back view, C - Front view.

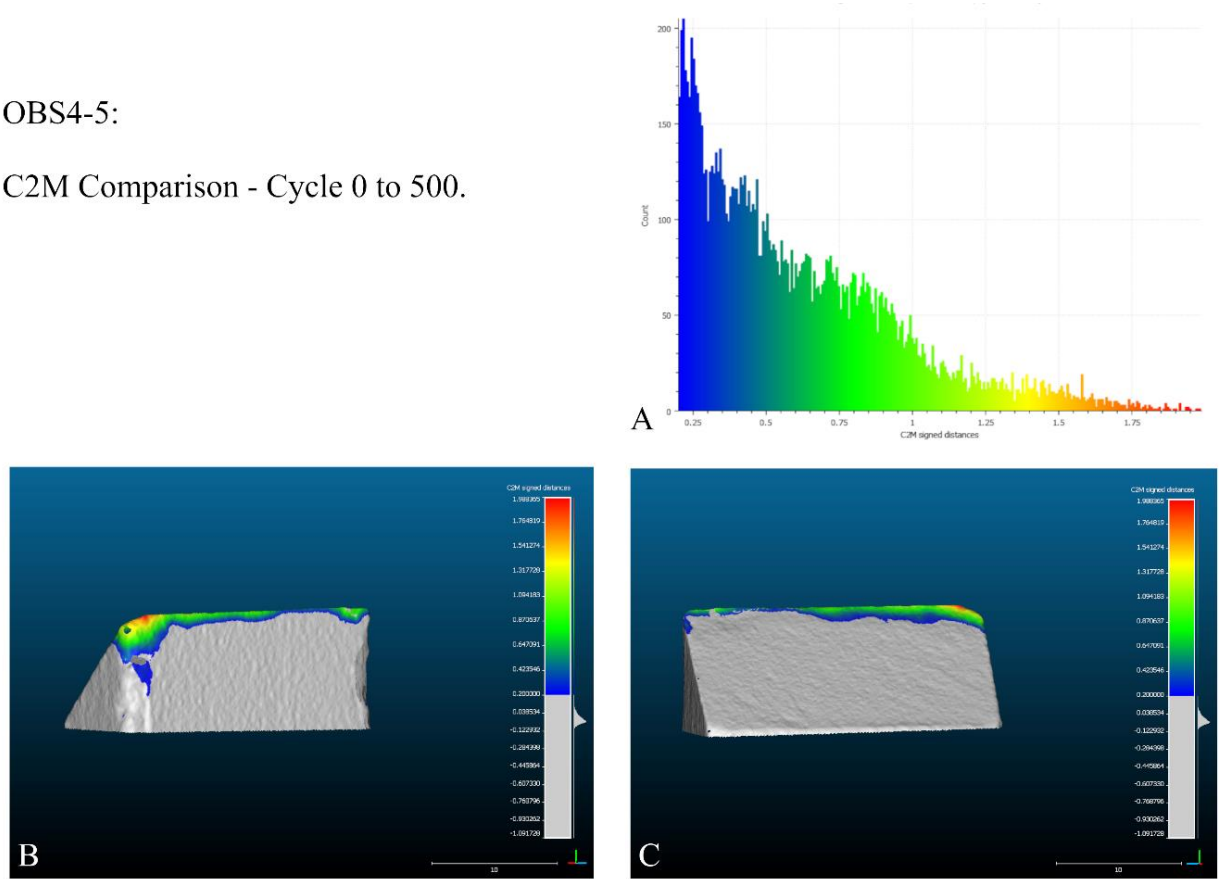

Figure 84: Cloud-to-Mesh edge reduction comparison, sample ID: OBS4-5, Cycle 0-500. A - Edge damage histogram, B - Back view, C - Front view.

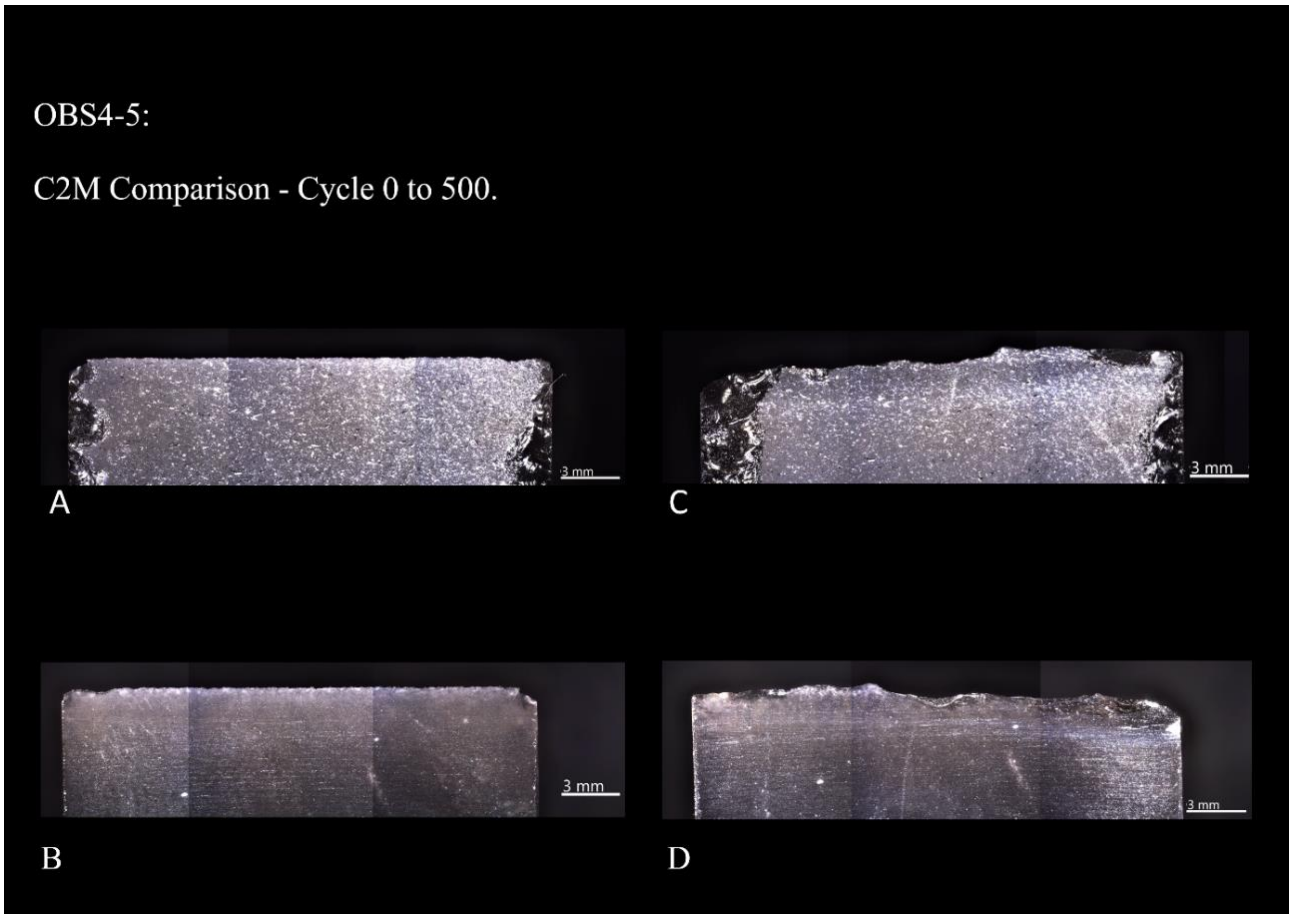

Figure 83: ZEISS Smart zoom images, A/B Cycle 0: A - Back view, B – Front view, C/D Cycle 500: C – Back View, D – Front view. Sample ID: OBS4-5.

4.2.4.e OBS4-6

From Figure 84 A, the results are the following:

The movement with the OBS4-6 sample starts with a penetration depth of about 13.8 mm. During the movement, and according to the graph, the penetration depth decreases slightly but increases from step 10.

Cycles 0-125 begin the motion with a penetration depth between 12.1 and 13 mm. As in the first cycle, the penetration depth increases during the first 10 steps and then decreases.

Cycles 126-250 start the movement with a depth penetration of 12.2 mm and 12.3 mm. From step 4, the penetration depth increases significantly. The maximum penetration depth found in these cycles is 12.7 mm and the minimum is 11.7 mm.

In the last cycles, the penetration depth ranges from 12.2 mm to 11.5 mm. As in the previous cycles, the penetration depth tends to be higher from step 4. The maximum is measured at 12.9 mm.

Figure 84 B represents the sensors measure from Inotec, and the results are the following:

The initial force exerted by the OBS4-6 on the wood is approximately -60N. During the measurement, it is found that the force is constant in all cycles. However, from step 4 onwards, the applied force decreases. The same behavior is observed at step 13. In step 13, the maximum applied force is also recorded, -71.3 N at cycle 126-250.

Friction begins the experiment at 0 N, as it goes in the first linear movement minor friction is registered at approximately -20 N from step 3 to 10. In the first cycle is visible that from stroke-to-stroke friction measured higher values. The other cycles present a performance with three high picks step 6, 8, and 10.

As in the previous obsidian samples, the initial velocity is 0 mm/s. According to the velocity diagram, the velocity increases in all cycles from step 3 and step 13. After an increase in velocity, there is a decrease and plateau from step 4. The maximum recorded velocity is -594.1 mm/s in cycles 125-250.

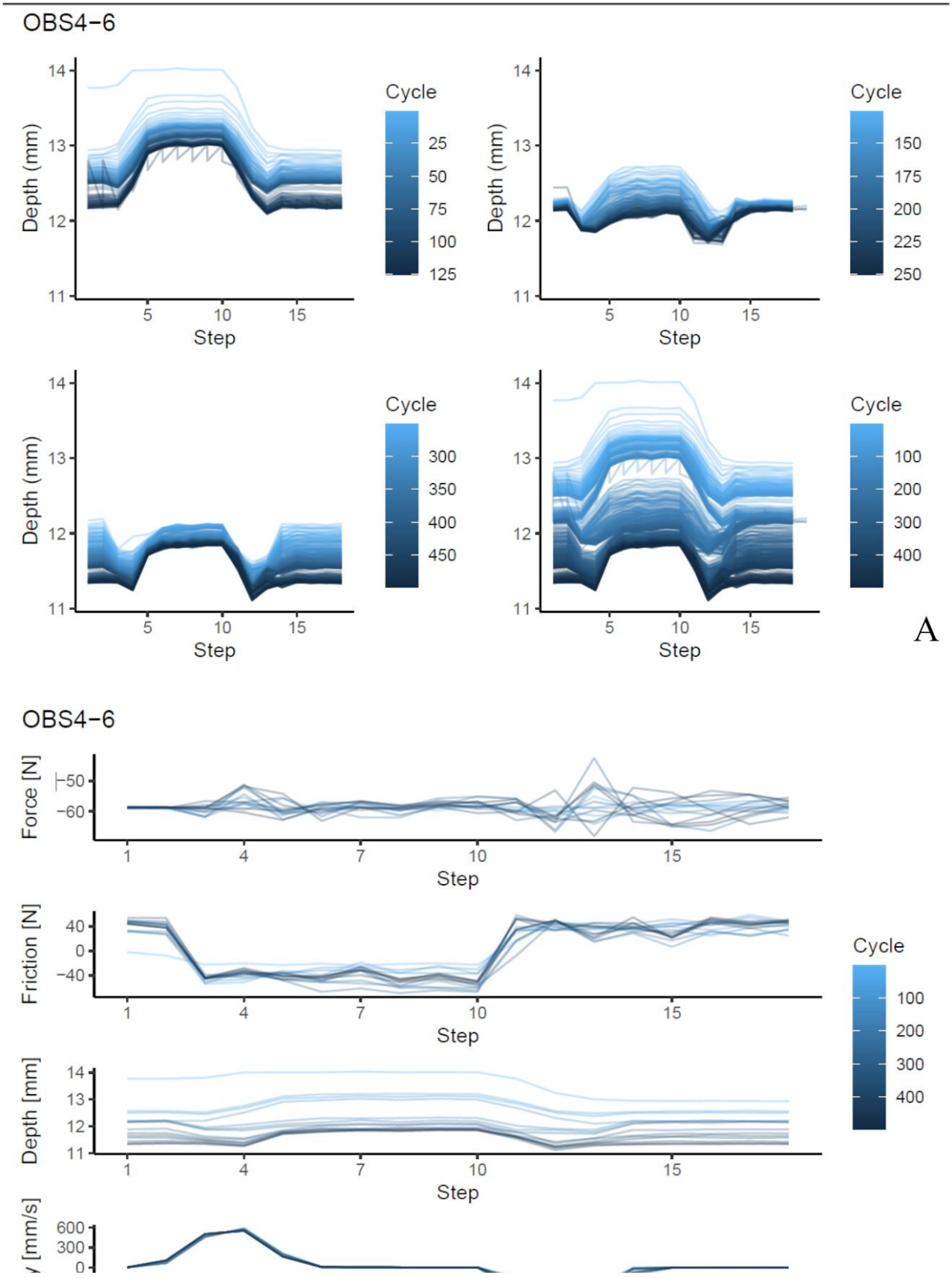

Figura 85: Graphic representation of the values recorded from Inotec from sample ID: OBS4-6. A - Penetration depth (mm) results, B - Sensors results.

4.2.4.f OBS4-6 Edge reduction, C2M Comparisons

Edge reduction at sample OBS4-6 occurs in the first cycle (0 to 125). From the data presented in the histogram Figure 85-A the damage is more expressive when is lower than 0.4 mm, but after that, a constant damage per part is visible until it reaches 1.16 mm. Damage is located mostly at one corner Figure 85-B. Next cycle 126 to 250 does not show major differences between meshes. It is at the last cycle that obsidian sample 4-6, breaks again. In the internal part Figure, 86-C is visible a detach starting in the edge and follow the ridge of the sample through the end, concerning the values presented the removal wasn't just superficial, as it reaches at least 0.8 mm in the ridge and 1.16 mm in the contact point. At the opposite corner, a small detachment also took place with values from 0.2 to 0.8 mm.

OBS4-6:

C2M Comparison - Cycle 0 to 125.

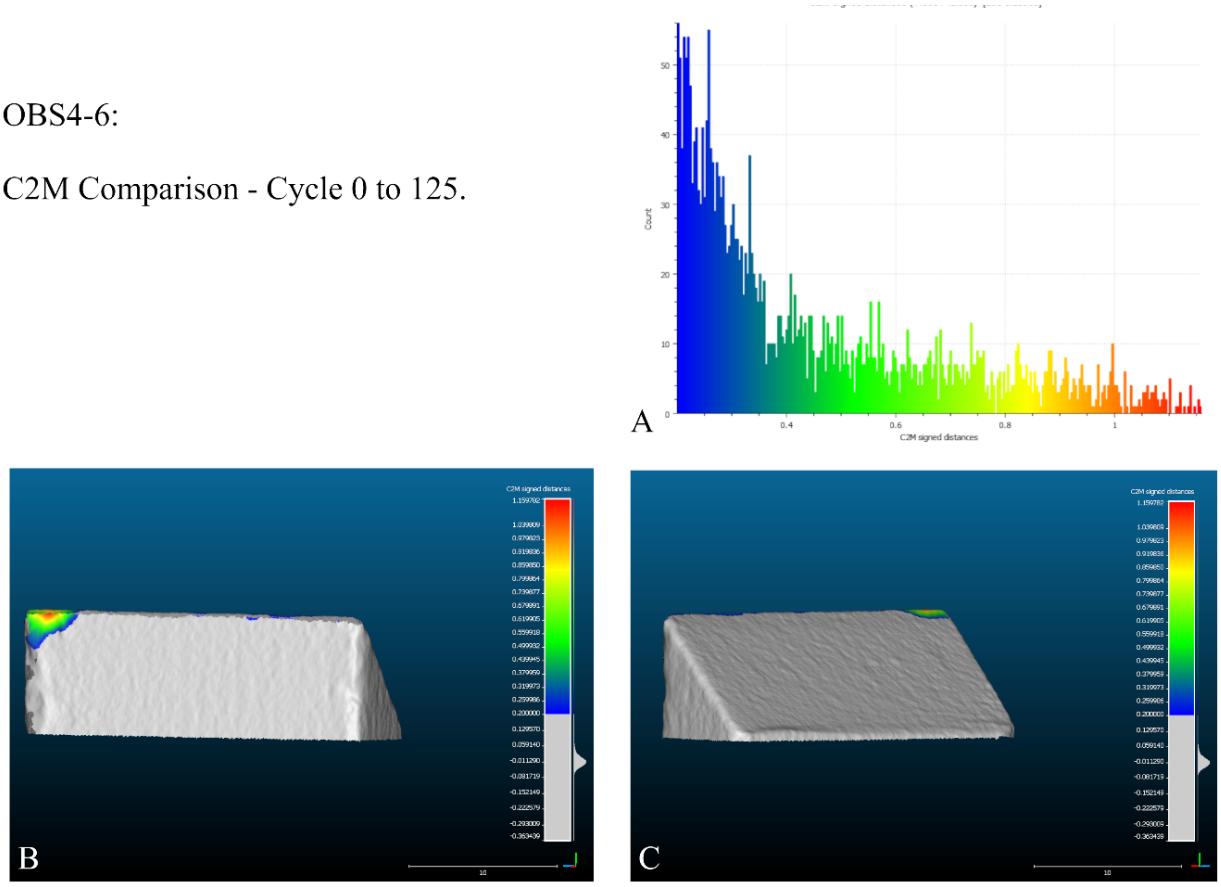

Figure 86: Cloud-to-Mesh edge reduction comparison, sample ID: OBS4-6, Cycle 0-125. A - Edge damage histogram, B - Back view, C - Front view.

OBS4-6:

C2M Comparison - Cycle 125 to 250.

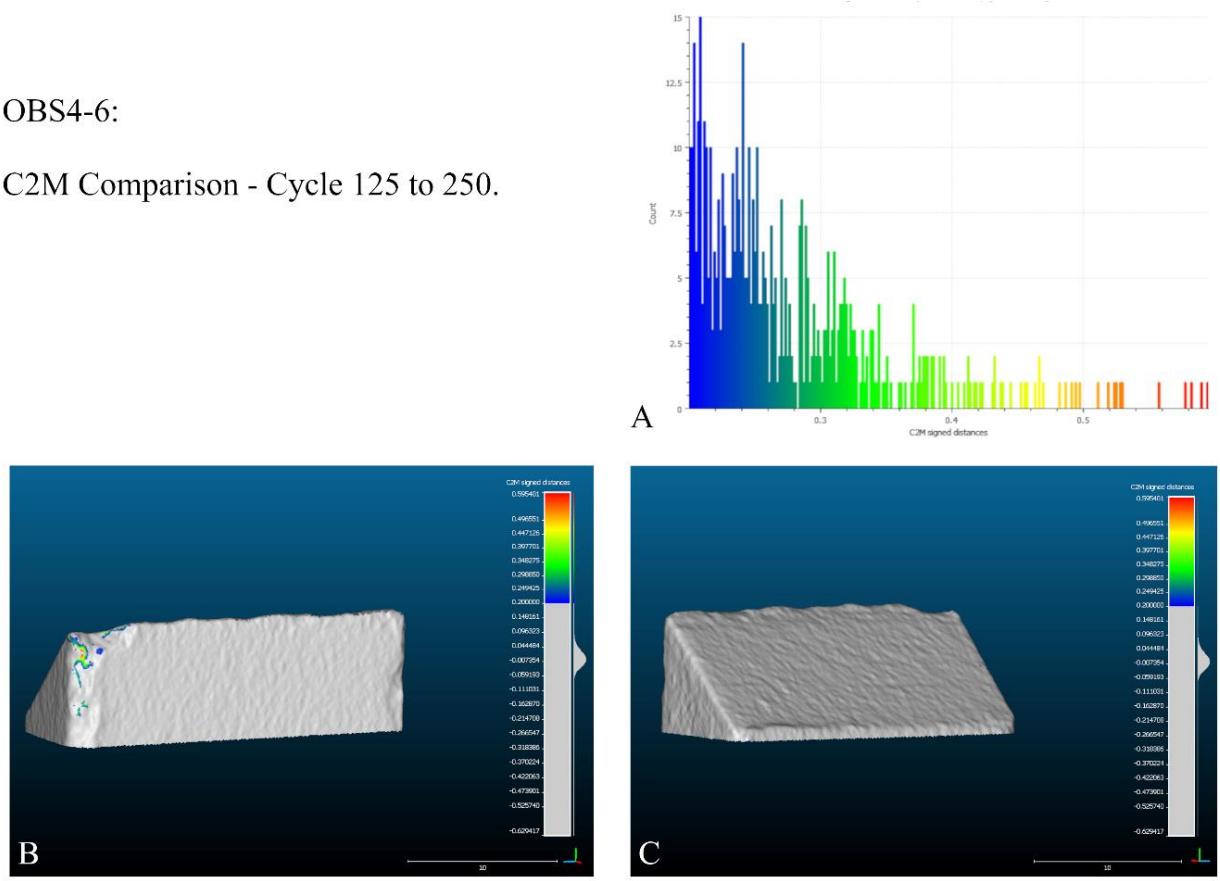

Figure 88: Cloud-to-Mesh edge reduction comparison, sample ID: OBS4-6, Cycle 125-250. A - Edge damage histogram, B - Back view, C - Front view.

OBS4-6:

C2M Comparison - Cycle 250 to 500.

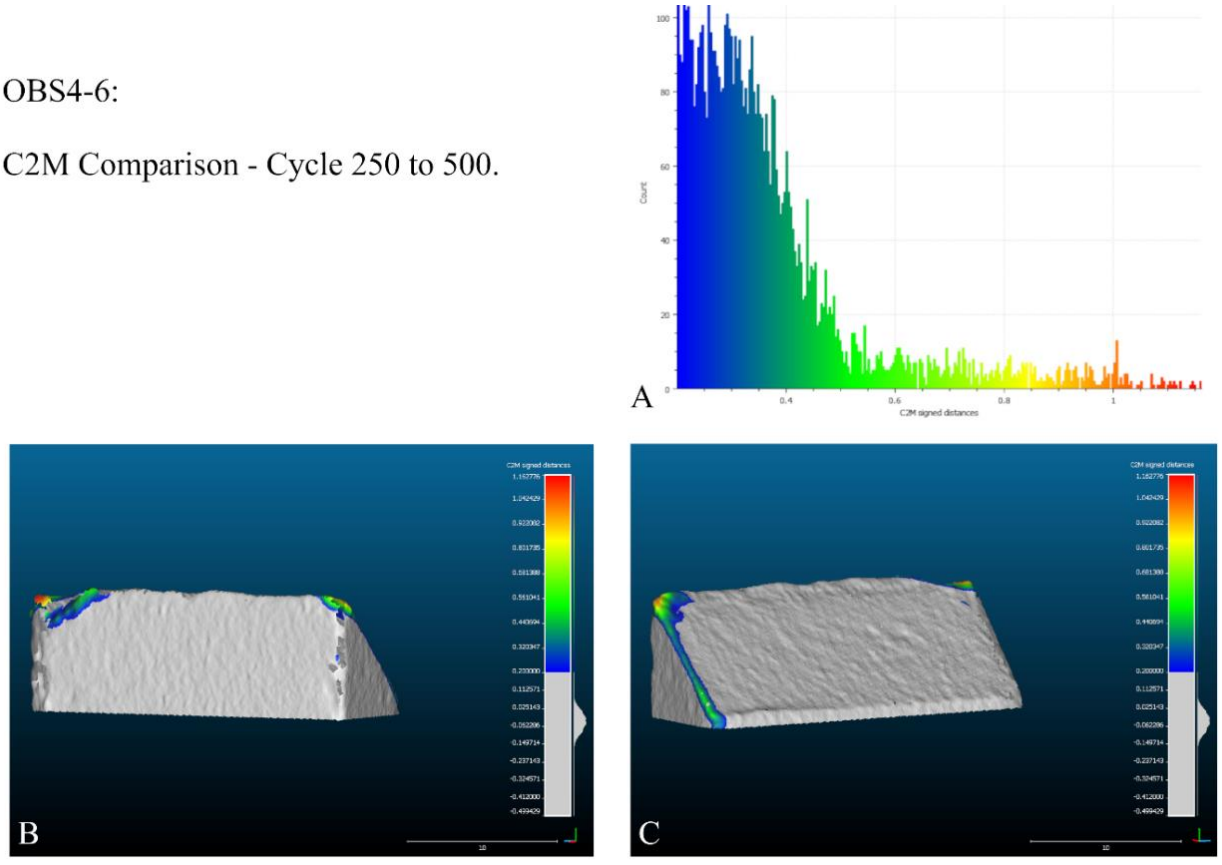

Figure 87: Cloud-to-Mesh edge reduction comparison, sample ID: OBS4-5, Cycle 0-500. A - Edge damage histogram, B - Back view, C - Front view.

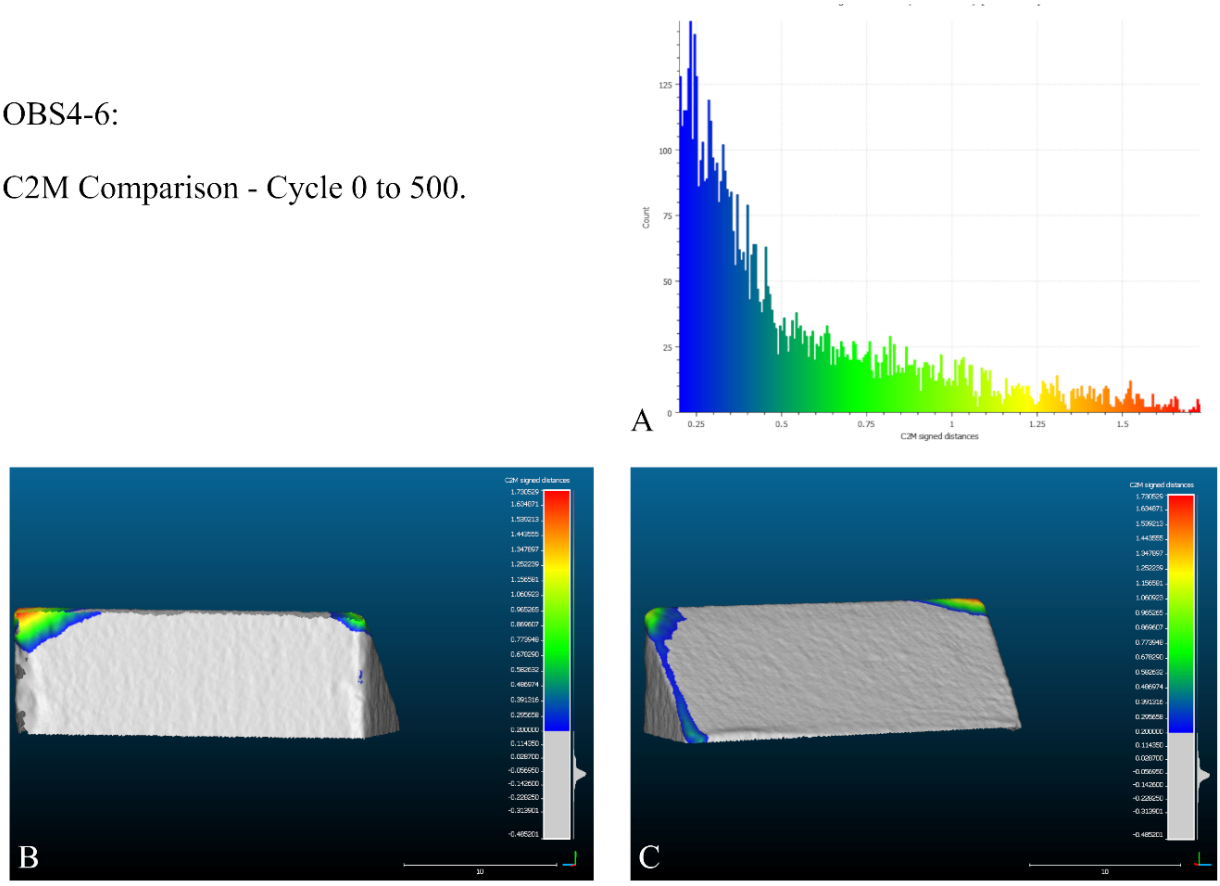

Figure 90: Cloud-to-Mesh edge reduction comparison, sample ID: OBS4-5, Cycle 0-500. A - Edge damage histogram, B - Back view, C - Front view.

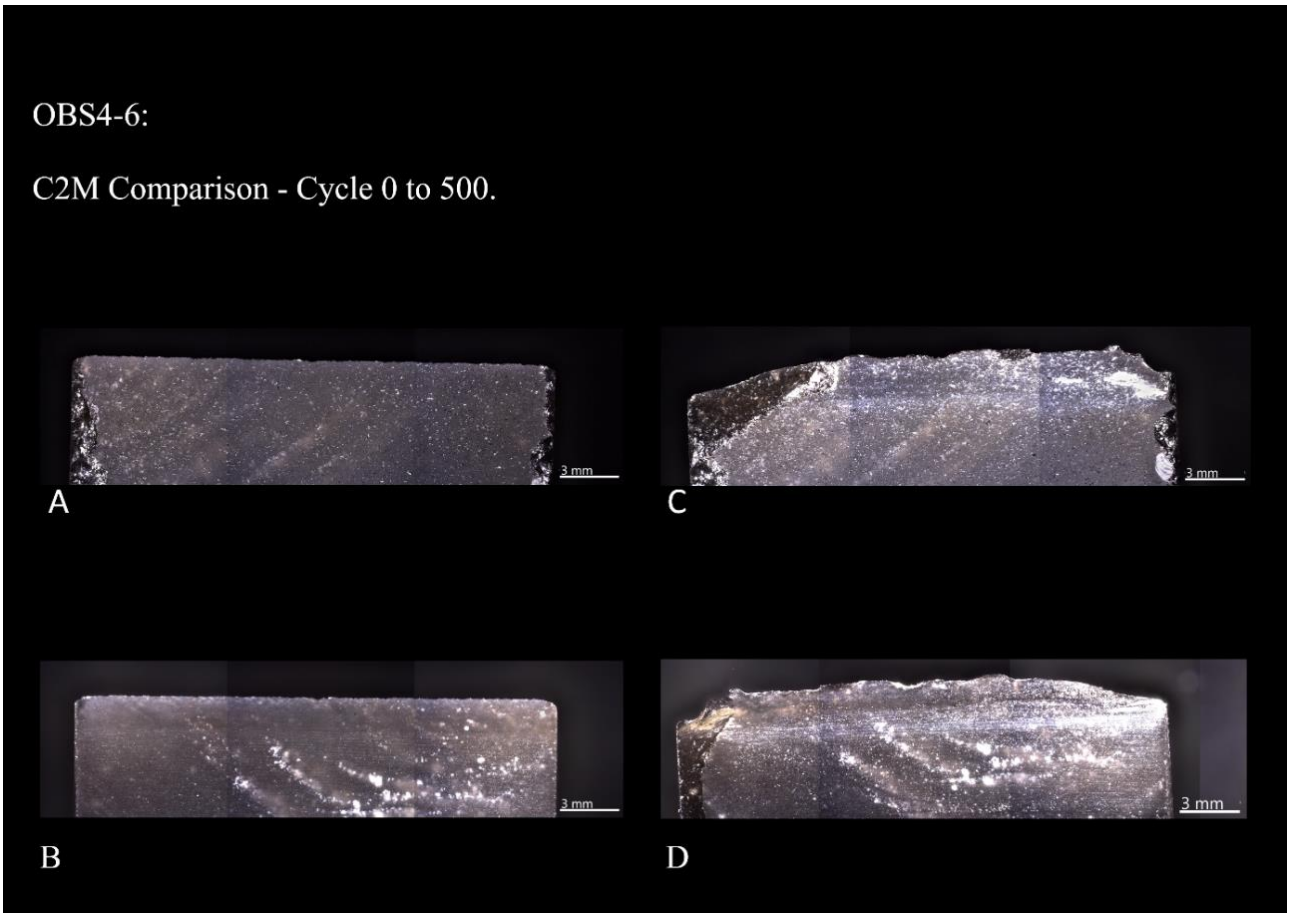

Figure 89 : ZEISS Smart zoom images, A/B Cycle 0: A - Back view, B – Front view, C/D Cycle 500: C – Back View, D – Front view. Sample ID: OBS4-6.

4.2.5 Worked Material

4.2.5.a Pinewood Plank

Pinewood analysis was done for a visual perspective of the result of 1000 strokes (500 cycles) applied, and to see if during the cutting motion there were any differences in the canyon created, as for a tentative quantification of material removed from cycle 0 to 500. Also, tridimensional scanning is a technique that results in a 3D model that can be used in the future analysis of this kind. Given the fact that pinewood is the passive sample (contact material) in this experimental design, it was not possible to obtain a scan between cycles, as done for the lithic samples. In this case, the strategy was focusing on understanding the result after the 1000 strokes (500 cycles) were applied to the pinewood. A tridimensional scan of the plank was used for GIS analysis and computation of Digital Elevation methods, such as slope and depth.

From the visual analysis is possible to see that all the samples have the sample longitudinal length, meaning that all samples were able to run along the entire similar and defined path length in all experiments. Second. what is also observable is the performance of the cut after 1000 strokes, from which it's possible to differentiate the quartzite sample with the "cleanest cut". By contrast, flint samples were the samples that cause more abrasion to the limits of the perform cut, while obsidian and dacite left a similar pattern on the pinewood.

In what concerns material removed from the pinewood, there is one sample that reaches a bigger remotion in-depth, sample FLT10-5 at -4.2 mm. All the other samples, based on the visualization of the graph, were removed between -3 and -0.6. The slope analysis shows that all the samples were cut in an alignment to the pinewood of about 85º, this allows to validate not only the material removal but also all the bidirectional linear movement, indicate that all the samples perform the cut in the same direction (perpendicular to the pinewood).

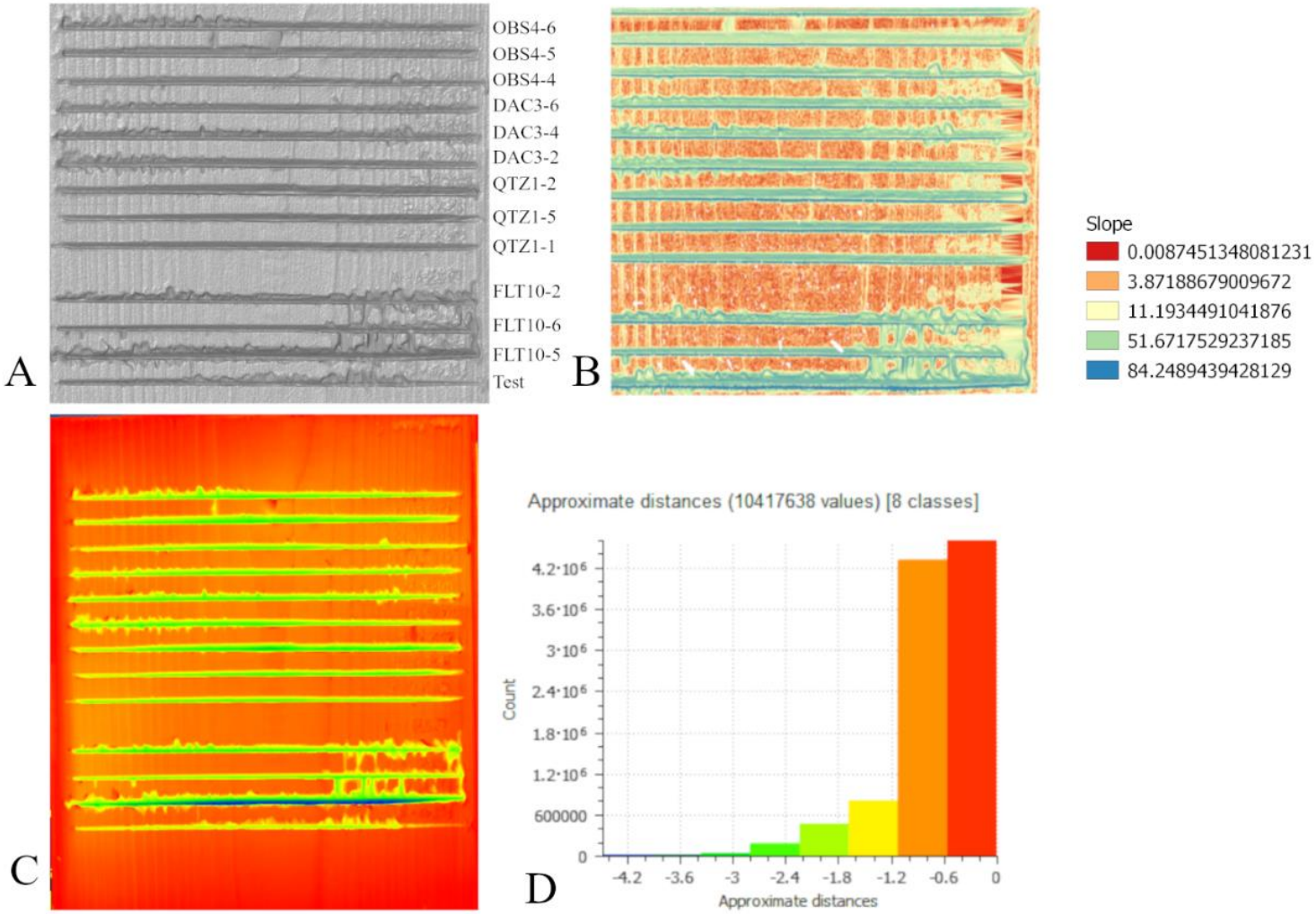

Figura 91 - Pinewood Plank, A - pinewood 3D scan, B - GIS slop analysis, C - Convex hull of pinewood 3D scan, D - Histogram representation of the values of distance (mm) from the convex hull.

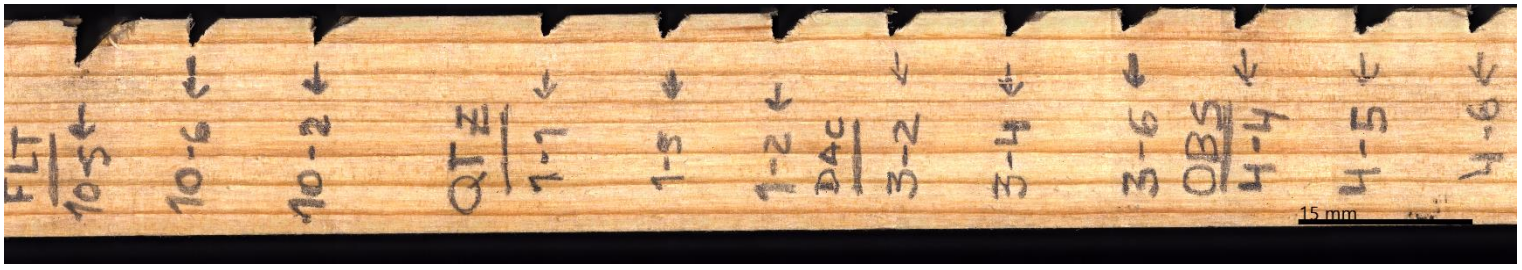

Figure 92: Section of the contact material (pinewood), after 1000 strokes.

Table 3: Sensors values of all lithic raw materials and cycles.

Raw material/Cycles	Force.min	Force.max	Friction.min	Velocity.min	Velocity.max	Depth.min	Depth.max
Dacite							
0-125							
DAC3-2	-63.350822	-53.99267	-96.859055	-593.6927	588.0226	11.671004	13.822058
DAC3-4	-67.36146	-53.08704	-67.79271	-593.9528	586.1683	11.849235	14.349834
DAC3-6	-64.6877	-53.216415	-61.970818	-592.17914	587.4256	11.926058	13.905796
125-250							
DAC3-2	-65.07583	-49.33515	-90.2609	-594.481	587.72504	11.694531	12.745763
DAC3-4	-68.05146	-50.24078	-89.9159	-592.40405	587.53204	12.393912	13.995679
DAC3-6	-65.33458	-52.957664	-59.38331	-593.036	587.4133	11.667163	12.572622
250-500							
DAC3-2	-70.94084	-41.65888	-85.689644	-593.1078	588.6025	11.358813	12.340616
DAC3-4	-65.50708	-49.98203	-92.28779	-593.488	588.4483	12.058962	13.003121
DAC3-6	-75.64149	-35.88011	-75.77086	-593.19696	587.8539	11.401066	12.309118
Flint							
0-125							
FLT10-2	-67.62021	-49.2489	-73.7871	-594.47754	588.0332	13.477121	16.003073
FLT10-5	-69.086464	-50.58578	-93.710915	-593.0669	586.89966	13.725261	15.454555
FLT10-6	-65.5502	-51.75016	-52.65579	-593.2471	587.52997	13.675325	15.590531
125-250							
FLT10-2	-67.57709	-51.879536	-66.28333	-592.7275	586.1221	13.4187355	14.995151
FLT10-5	-83.015884	-49.378277	-74.822105	-593.34393	587.68384	13.048447	14.800019
FLT10-6	-64.1702	-53.43204	-63.695824	-593.92755	585.29816	13.513228	15.0581455
250-500							
FLT10-2	-67.57709	-51.75016	-109.19284	-593.5853	588.1991	13.122966	14.469679
FLT10-5	-86.293396	-36.915115	-93.15029	-596.61523	587.81805	11.565756	14.236904
FLT10-6	-85.04276	-31.9126	-65.67958	-595.0058	586.2632	13.003889	14.551112
Obsidian							
0-125							
OBS4-4	-66.412704	-44.67764	-49.852654	-592.68835	588.7652	12.737312	14.285303
OBS4-5	-64.98958	-52.397038	-56.4508	-592.60956	588.0002	11.993662	13.639987
OBS4-6	-63.868324	-53.17329	-61.15144	-593.6028	587.3566	12.088155	14.031017
125-250							
OBS4-4	-69.04334	-48.81765	-55.7608	-595.1441	588.37823	12.387766	13.252028
OBS4-5	-72.5796	-36.268238	-90.04528	-593.92786	589.06195	11.753205	12.842561
OBS4-6	-71.28584	-42.17638	-73.22648	-594.10535	588.9109	11.684064	12.72963
250-500							
OBS4-4	-82.84338	-31.783224	-58.520805	-592.4001	590.4965	9.318673	12.661257
OBS4-5	-73.83023	-35.01761	-77.36649	-592.3014	586.49115	11.3030205	12.469199
OBS4-6	-71.02709	-39.502625	-86.6384	-593.72095	587.5351	11.103279	12.191867
Quatzite							
0-125							
QTZ1-2	-70.89772	-49.378277	-82.024	-593.5867	588.4967	12.059731	14.31296
QTZ1-5	-72.9246	-44.117012	-62.876446	-593.58386	589.6914	13.410285	14.705526
QZT1-1	-65.33458	-48.64515	-56.92518	-593.4887	587.3888	14.442022	15.963893
125-250							
QTZ1-2	-68.43959	-45.45389	-63.307697	-593.4113	584.8861	11.539637	13.004658
QTZ1-5	-69.172714	-50.542656	-68.65521	-593.0558	587.61975	13.232055	14.157776
QZT1-1	-66.412704	-51.362034	-63.048946	-593.2712	586.2932	14.279157	15.114995
250-500							
QTZ1-2	-92.33091	-29.583841	-75.16711	-596.3718	588.2321	10.746051	12.486868
QTZ1-5	-93.19341	-31.351973	-92.71904	-595.6911	592.1404	12.038988	13.905027
QZT1-1	-69.172714	-50.24078	-73.39898	-594.2624	589.3924	13.870457	14.892976

Chapter5 DISCUSSION

The experimental program developed in this thesis was conducted with the highest possible degree of control. The design included the largest possible range and number of variables within the scope of the research, as the discussion in this chapter indicates. This program is intended to contribute to and build on previous research by avoiding the limitations already on experimental studies of lithic raw material performance (Collins, 2007; Greiser, 1979; Jones, 1980; Keller, 1966).

In this chapter, data and results of the experimental program proposed here will be interpreted and discussed, starting with an examination of the relationship between edge damage and penetration depth within different cycles to address raw material efficiency, and edge durability to infer raw material strength over use.

5.1 STONE TOOLS EDGE EFFICIENCY AND DURABILITY

5.1.1 Edge Damage and Penetration Depth

Keller, (1966) indicated that four main factors are likely to affect stone tools edge damage: artifact material, cross-section of the edge, mode of use, and material upon which the artifact was used. But when studying archaeological artifacts, from those four only two are available to archaeologists to inquire about the artifact mode of use, which is the material of the tool and the cross-section of the edge. Knowledge of the material upon which artifact was used in majority became degraded and its evidence is lost during the formation of the archaeological record.

The type of experiment here presented has the purpose to test the performance (which includes efficiency and durability) of the lithics raw materials upon a known material, in this case, pinewood. On this specific experimental design, to understand tool efficiency and durability the edge was put under extreme stress to understand if it damages at performing a bidirectional movement against pinewood. Not only the expected damage was investigated, but also the location and quantification of the edge damage. As previously mentioned, to address this question, this thesis used tridimensional scanning data to gather information when comparing from stage to stage. this approach aims to give the differences of damage to the edge depends on the number of strokes applied in each stage.

The results of the second-generation experiments show that variation on edge damage exists in degrees of the number of parts and distance (mm) when comparing between 3D mashes from the different experimental cycles. Data variability is discussed within and between the four different raw materials. Taking into account, the graph below regarding the edge damage is possible to report variability between all lithic raw materials.

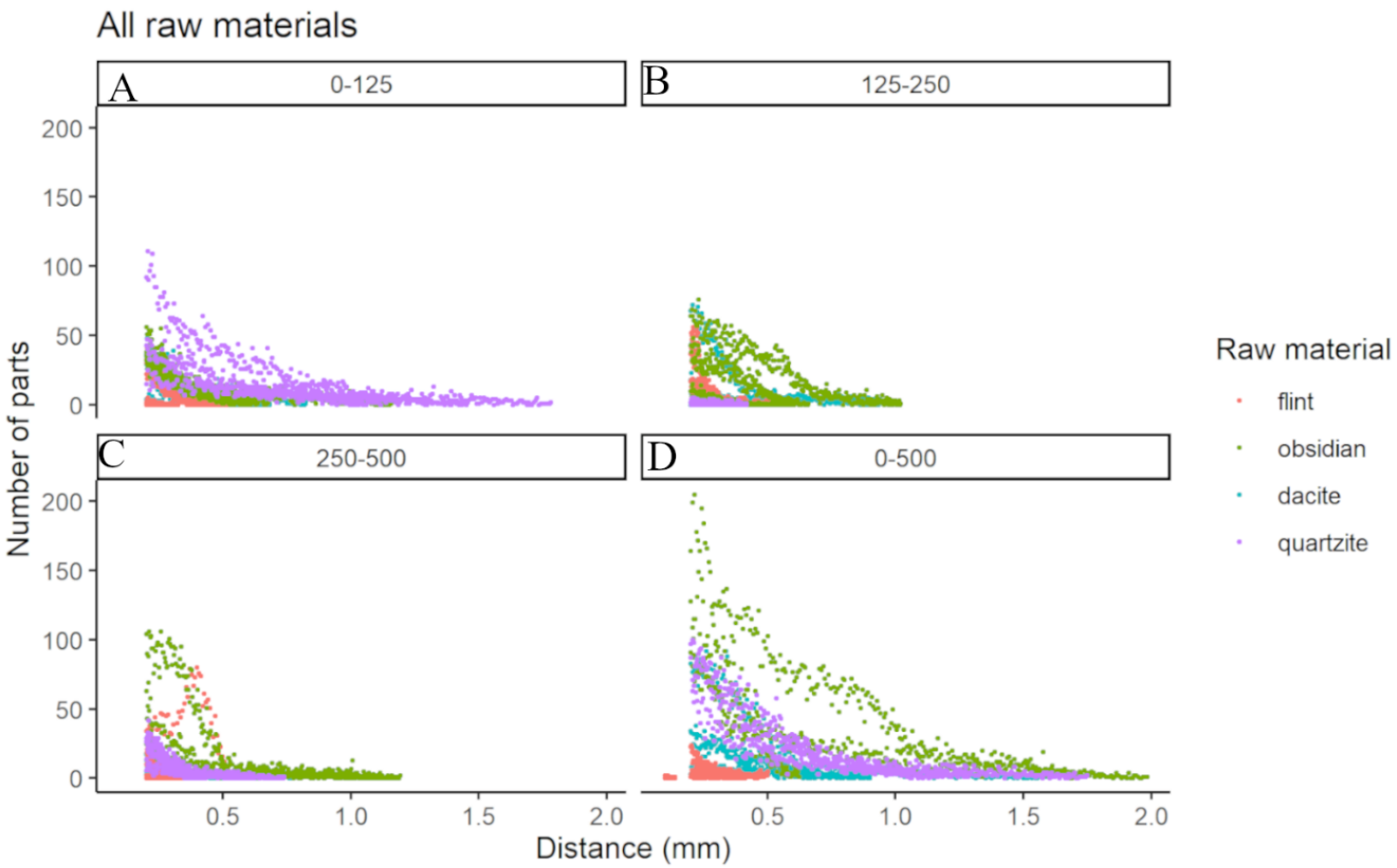

Figura 93: Plot comparison of edge damage between all lithic raw materials and cycles.

A general variability is demonstrated in Figure 92 (D), where is possible to distinguish four groups, being flint the one that shows a lower degree of damage. Quartzite and obsidian are the lithic raw materials that when performing a cutting action against pinewood displayed a high incidence of edge damage in distance and along the edge (number of parts). Dacite by the visual analysis of Figure 92 D shows a homogeneous pattern of edge damage through the 1000 strokes.

In the first 250 strokes (cycle 0 -125), quartzite (all three samples) shows the higher damage by distance and parts, which theoretically contradicts the data provided by force and friction, where

quartzite records a decrease in friction in the first 250 strokes and a stabilized force on the samples. One of the possible causes of this event is the way quartzite fractures, namely in the form of splinters instead of a regular conchoidal fracture, at least in the first 250 strokes.

In all samples quartzite result in a high incidence of edge reduction, in the three samples, a pattern of damage was catch by visual observation and photographed. Edge damage in the first 250 strokes is severely marked that debris of the edge stays carved into the pinewood (Figure 94), this is evidence of how degraded the edge finished when it performed the first 250 strokes. Besides, other lithic raw materials also display this brittle behaviour, such as obsidian and flint with high silica components, it seems that quartzite is the one that fractures at an early use stage.

Figure 94: Visual representation of the event of fragmentation of quartzite after the 250 strokes.

This effect can be explained by the HLC hardness measurements, not only do the ANOVA results show that quartzite is significantly different from the rest of the lithic raw materials but also when comparing the hardness values, quartzite is the more “fragile”, showing the lowest measure for hardness. These results are aligned with the first stage of quartzite edge modification (fragmentation) (Pedergnana et al., 2017). Fracturing at an early stage of use seems to occur more frequently in quartzite than in other lithic raw materials, possibly due to the larger quartz grain size (resulting in larger detached particles). Besides no petrological study was done to better characterize quartzite, a possible relation can be made from the fracture outcome after 250 strokes and the two deformation types that occur in quartzite: a) deformation through pressure among the grain borders, which is perpendicular to compressive forces, b)

plastic inter-crystalline deformation, where the exerted forces provoke dislocations in the grains interior (Pedergnana et al., 2017). It could be this tribology principle (the interaction of these two surfaces) and the fact that quartzite is a metamorphic rock very rich in quartz content, that causes the fragmentation in an earlier stage of use. The damage on the edges seems to have a direct relationship to the depth of penetration in all raw material since the deepest measures are all achieved in the first cycles when the edge is "clean".

Observation of Figure 94 comparing the absolute depth of penetration of all raw materials from cycles 0 to 125 shows that quartzite was the raw material that did not cut as deeply as the other three, probably due to the high fragmentation. Opposite relation can be seen on the dacite and flint, samples from these raw materials penetrate the deepest into the pinewood while the edge remaining without major damage.

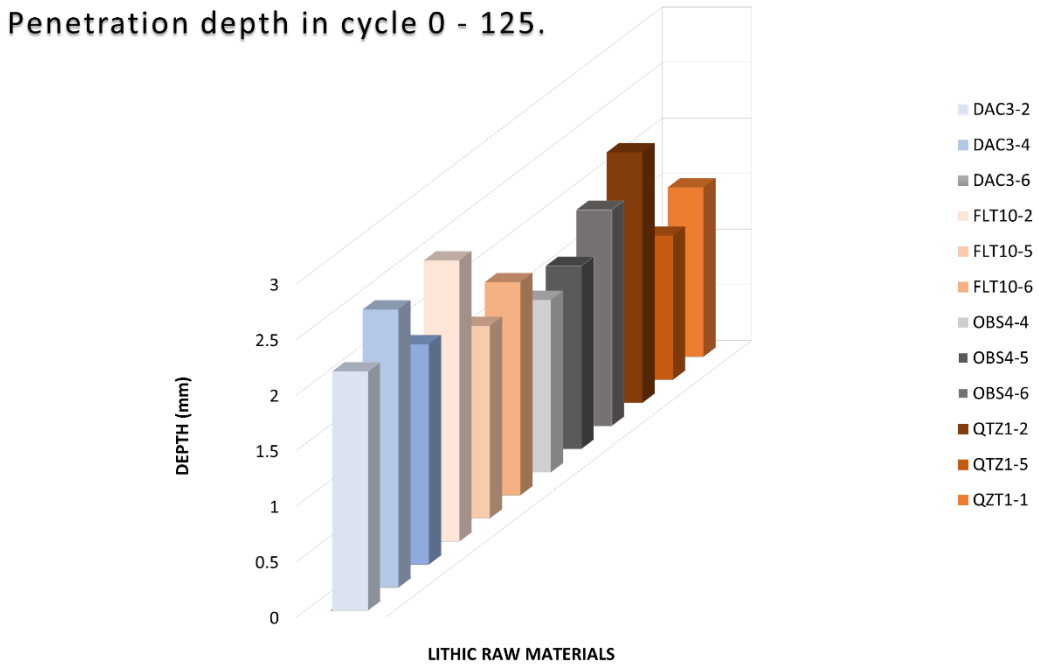

Figure 95: High frequencies of penetration depth in cycle 0-125, all lithic raw materials.

On the next stage is verified a contrast of the result from the first cycle, taking into account that the same number of strokes were applied to the samples. Here quartzite is off the equation, been replaced by obsidian and dacite in the highest values for edge reduction. This behave is evidenced by the data provided by friction and force. In these cases, obsidian has an increase

in friction which is related to an increase in force, the same for dacite, which means that a direct link is made between these two factors and the edge damage in this cycle. As for quartzite, the consequence of the high reduction in the last stage, and a continuing load it is subjected to, and contact material, resulting in a notch and dull edge. The residues from the contact material attached to the edge from the first cycles most likely contribute to this dull effected on the edge.

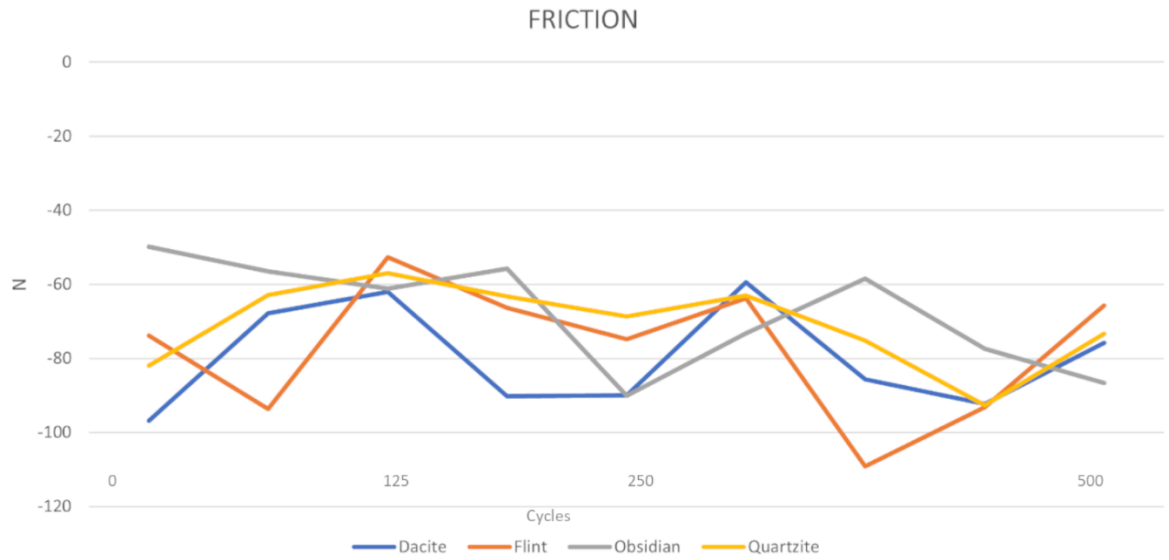

Figure 96: High frequencies for friction values, all lithic raw materials.

Looking at the values of penetration depth, the same correlation is registered as observed in the first cycle. Flint is the lithic raw material that does not reach a high reduction in mm in the edge sample, but for penetration depth, at this stage, all three samples (FLT10-2/5/6) record the deepest measures from contact with the contact material (pinewood), which corresponds with an increase in the highest measurements in flint for friction.

In cycle 250 to 500 is possible to see that obsidian have different behavior when comparing with the others raw materials. Obsidian samples not only continue to be reduced as the number of strokes increase, but at the same time, the sample's edges still showing what can be considered as a sharp edge. These aspects should be explored more in detail in further studies, for example with emphasis on quantitively measuring the edge angle and tip radius (Atkins, 2009; McCarthy et al., 2010; Schuldt et al., 2013). Even if these two variables were not used in this study due to experiment timing and goals, the tridimensional data gathered give that possibility in future analysis.

Still in the cycle 250 to 500, flint registered a different pattern, at least one sample, this is likely due to a detachment (i.e., fracture) on the edge (see appendix A, Figure 117). In all the other cycles flint have the most different performance, as it does not break as much as it would be expected, especially due to the fact that it is a siliceous rock, with a fine grain.

In general, to address which lithic raw material records fractures more on the edge after applied 1000 strokes, two groups can be distinguished. Obsidian and quartzite being the more breakable, while dacite and flint are the lowest, but it should be highlighted that flint is by far the less breakable lithic raw material in this experiment.

The modifications in the sense of microfracturing during the experiment can be visible in all lithic raw materials at different levels. In general, all samples show microfractures on the edge, where the damage does not reach the centimeter scale in all raw materials. However, microfracturing has an important role in performing a task, in this case, bidirectional movement in pinewood, as the continuous fracture helps to refresh the edge and remove more of the target material. Flint samples, for example, have no significant alteration. In this case, what likely happens is that the continuing use of the flint samples causes blunting through abrasion, finally resulting in a smoothed edge. However, sample FLT10-2 showed a different behavior, from the passage of 500 to 1000 strokes, a major detachment occurs and breaks the dullness of the edge (Figure 96 and Figure 15). This microfracture act as “self-resharpening”. These physical phenomena can happen in all lithic raw materials but are the recurrence of this event, that can dictate the performance of the edge, submitting the knapper to use different strategies to modify the edge, as different types of retouch.

Obsidian for example remains resilient in the first 250 stokes, besides some minor fractures that occur in the edge. It was after the first cycle where obsidian samples show edge scarring (almost identical to intentional retouch) Figures 114,115 and 116) that we see this raw material becoming highly reduced. This relation between an edge that results in a high reduction of the raw material, in this case, obsidian, could represent a problem for past hominins when the availability and accessibility of the outcrop were scarce, forcing a solution when dealing with this kind of problem.

For example, focusing on previous studies and considering Kalavan 2 (on which the author has been working), a Middle Paleolithic open-air site in Armenia with an abundance of obsidian artifacts that account for between 55% and 82% of the total assemblage and are geochemically consistent with volcanic origins at a distance of about 120-140 km from the site. It is possible

to find a possible solution in terms of reduction strategies for obsidian tools. In the Kalavan 2 assemblage, researchers encountered a technological feature that indicates a flaking practice associated with the retouched obsidian pieces, which they refer to as "shaping flakes" A broad term used to refer to all the by-products of tool modification, and their identification is based on the presence of retouching scars on the back of the pieces. They raise the question of whether these preliminary finds reflect continuous rejuvenation in the working of materials and movements associated with woodworking based on the preliminary use-wear studies (Malinsky-Buller et al., 2021).

This technological solution in this archaeological site could be related to the perception of the mechanics of obsidian seen in this experiment. In this experiment, the presence of a linear edge (in cycles 0 to 125) leads to a low reduction of the lithic raw material, while the presence of a denticulated or notched edge (cycle 125/250/500) leads to a high reduction of the raw material. So, the possible solution of shaping flakes could be introduced to economize this kind of lithic raw material, when this problem was noticed by the past human societies. Although these are only preliminary experimental results, more data must be added to this experimental design in order to draw more robust conclusions.

The durability of stone tools is still one of the most intriguing archaeological questions that most researchers are trying to tackle. In a sense, it is not possible to infer directly from the archaeological record how durable a tool is since archeologists only have access to a static past. Therefore, several current actualistic studies and control experiments attempt to assign units of measurement to archaeological artifacts by characterizing lithic raw materials, by measuring their performance and use-wear when performing different actions and activities (Braun et al., 2008; Dickson, 2002).

This study proposes a possible model for testing the durability of edge lithic raw materials. Considering durability as tool utility, that is, the ability of a stone tool to continue a task without breaking or becoming blunt (Collins, 2007). It is possible to use the penetration depth and edge damage of each sample in a simple linear regression and see which sample is closer to 0. This means that the samples that are close to 0 are the ones that have the least edge damage and continuously perform their function, in this case cutting pinewood (increasing the penetration).

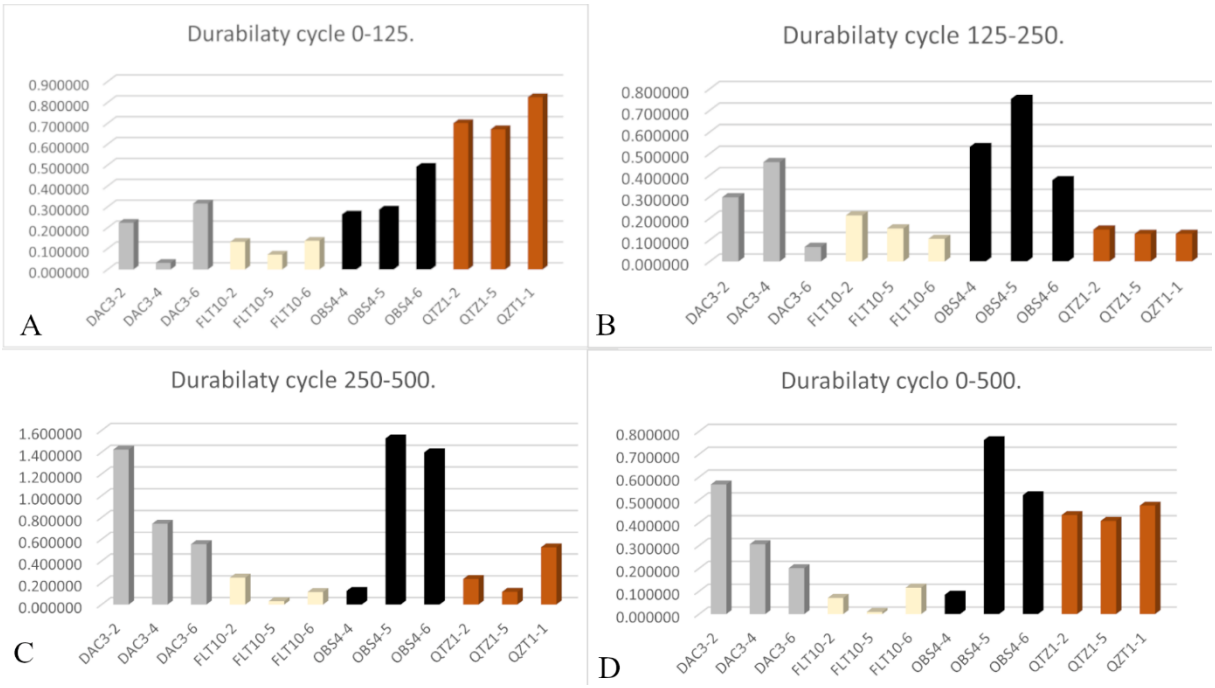

Figure 97: Frequencies for edge durability, all lithic raw materials. A - cycle 0-125; B - Cycle 125-250; C - cycle 250-500; D - Cycle 0-500.

From the above graph, flint is by far the most durable lithic raw material in this experiment in all cycles. Quartzite also had a similar penetration value when comparing to the other samples in the first cycle (see Figure 96-A), but the high fragmentation of the edge automatically identifies it as less durable. The fragmentation of the quartzite edge results in a notched edge, as mentioned earlier (Figures 111, 112, and 113). The effect of the fragmentation in edge morphology of the quartzite is evident in its durability over the next few cycles: not only does quartzite retain its function, but it does not fracture as much as it did in the first cycle with a less modified edge. This could indicate that the capacity of quartzite increases when the edge morphology changes to a notched edge, making it less fragile. Knowledge about these physical properties of quartzite may have led people in the past to retouch quartzite or not to retouch at all, not only to obtain sharp edges but also because it maintained the use of tools.

The opposite can be observed on the obsidian samples: When the edge morphology is a straight edge, obsidian is more durable (see Figure 96-A). On the other hand, when it breaks and turns into a notched edge in the next cycles, it is less and less durable. Sample OBS4-4 reacts differently, as three larger detachments act as self-sharpening, giving the sample a higher penetration depth (see a supplementary video in the supplementary material).

The behavior of dacite in the first cycle is similar to that is observed on flint, with no major damage to the edge and high values in penetration depth, but in the next cycle, the quartz composition leads to more damage to the edge and lower penetration into pinewood. Even though it is the second more durable lithic raw material used in the experiment.

There has, a logical predisposition to infer that some lithic raw materials are more efficient than others when undertaking some tasks. Two clarify this question two variables were measured specifically to attend how efficient each lithic raw material is, penetration depth, and duration (strokes). By analyzing the relation of these two variables, is possible to address at each cycle each sample perform the task of cutting wood in a bidirectional linear movement more efficiently. From the graphic above, if consider efficiency when a task is accomplished with results and does not fail when action occurs, is true to infer that all lithic raw materials are indeed efficient since all penetrate the pinewood at least 1 mm in the first 250 strokes. However, one can be more efficient than the other. As the graphic below shows that homogeneous dacite and flint are the groups that perform the task way more efficiently than obsidian, for example since they reached deeper into the pinewood. Following this, when more strokes are added to samples more variability is registered although one lithic raw material remains stable at an efficiency level, flint as a group can be observed in the next three graphics. If individual efficiency of samples rather than grouped was considered sample OBS4-4 is the one that even after 1000 strokes reach the deepest values into the pinewood, but this event is explained above, based on the "self-resharpening" phenomena.

When comparing data from similar studies on durability, raw material selection, or edge reduction experiments, interesting similarities between conclusions can be seen. In this study, durability was one of the main factors that had a greater impact on the performance of the lithic raw materials. This is also confirmed by Braun and colleagues (2009) who, after using mechanical testing in combination with atualistic experiments, concluded that Oldowan toolmakers were given more emphasis on durability when selecting different rock types. When investigating the variability of lithic raw materials, Key and colleagues (2020) found significant differences between chert, basalt, and quartzite after conducting control experiments on sharpness, durability, and functional performance. In terms of efficiency and durability, the experimental program conducted in this dissertation confirmed the same pattern, namely that significant differences exist between the quartzite, dacite, flint, and obsidian in the performance of a cutting motion in pinewood. Key and his colleagues found that quartzite was the sharpest

raw material in this experiment and required much less effort and energy to use than basalt. Sharpness was not measured (although it could be in future studies), but according to the sharpness principles Key lays out in his paper, the interesting similarity occurs in the first cycles of quartzite (Figure, 18-A). From the visual analysis of the graph, it appears that quartzite was the raw material that reached the deepest values in the first 250 strokes, which could be due to its sharpness, as Key and colleagues have shown in their experiments. The other assumptions can also be related to the results of this experiment. Chert, for example, can be compared to flint, both have the same behaviour, have sharper edges, and are durable. Basalt can be compared to the results of dacite. Both have been shown to have durable edges, but low sharpness as shown by the decrease in Figure 18 cycles 125-250 and 250-500.

The results of this dissertation experiment compared to an experiment by Pereira and colleagues (2017), which has similarities but only deals with edge reduction between fine-grained (flint) and coarse-grained (quartzite) material, have one main message in common. That quartzite edges have a high rate of edge reduction compared to flint (Figure 92). However, if obsidian as a lithic raw material is representative of fine-grain types, then the coarse-grain raw material quartzite exhibits a low rate of edge reduction in terms of distance (mm) and area compared to obsidian when all factors were strictly controlled in cutting wood. Pereira (2017) stated that the answer to the question of why people would use coarse-grained raw materials when they had available fine-grained ones is that in the past, hominins used different raw materials with different physical properties depending on the task.

To achieve this assumption, further experimental work needs to be done by testing the hardness/density ratio for each raw material, the continuous performance of each raw material (more strokes), the different contact materials, the different working movements (i.e., activities), the physical properties of the samples, the chemical properties of the samples, the different edge angles, and the different edge morphology.

.

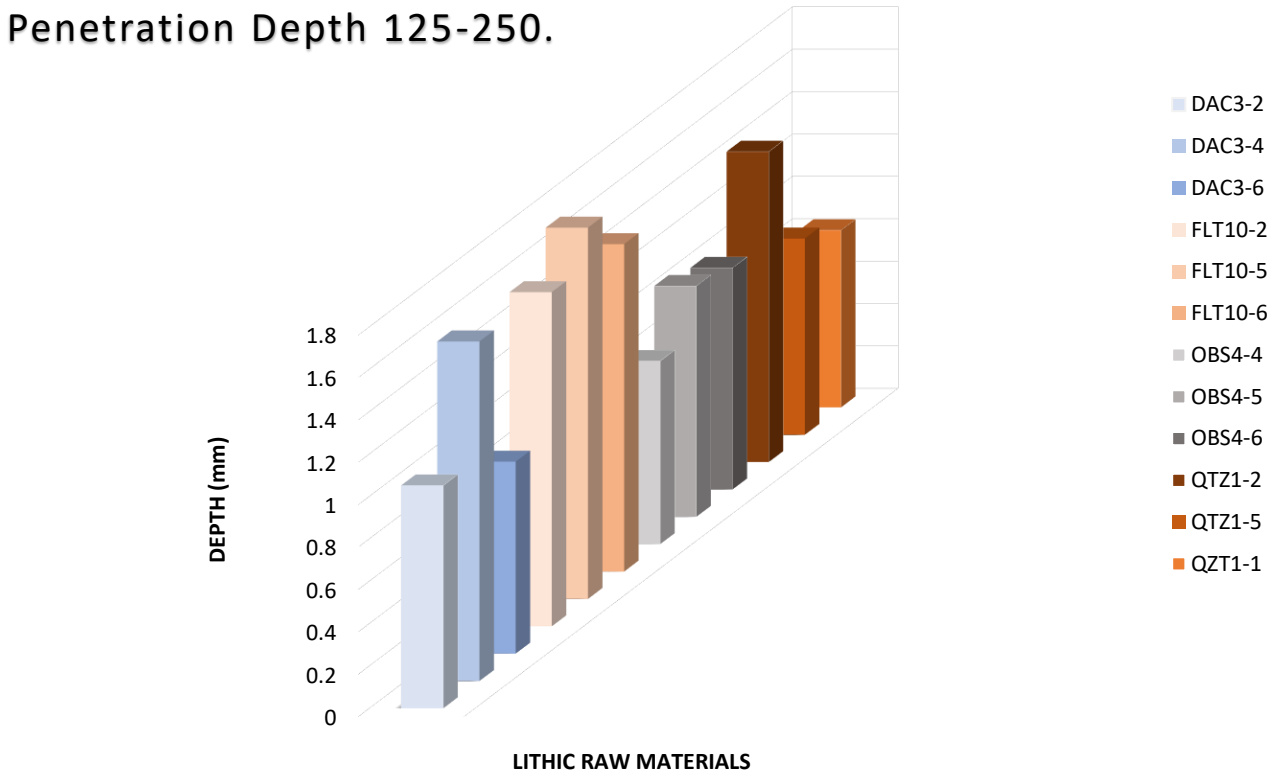

Figure 98: High frequencies of penetration depth in cycle 125-250, all lithic raw materials.

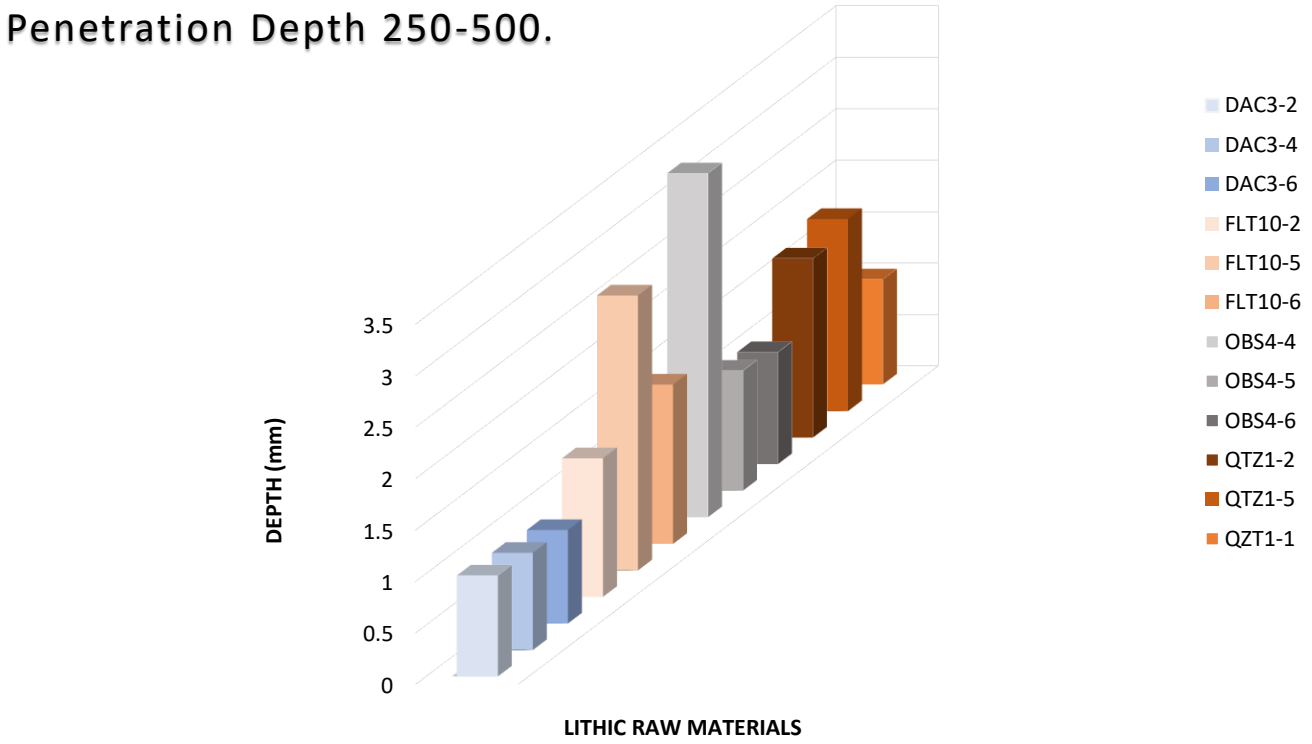

Figure 99: High frequencies of penetration depth in cycle 250-500, all lithic raw materials.

Chapter6 CONCLUSIONS

For every stone tool produced, a decision had to be made concerning which raw material to use. Assuming that tool use is a physical process, recognizing the mechanical properties of each lithic raw material is fundamental to understanding the performance and function of artifacts. Several research projects have a focus on functional studies to identify proportional differences between artifact use and lithic raw material types. These differences offer insights into the nature and organization of raw material acquisition and selection, raw material optimization, reduction strategies, typologies, and retouch sequences.

Here, is demonstrated that when bidirectional linear movement is performed edge durability and efficiency vary between flint, dacite, quartzite, and obsidian at different stages of use. In the controlled experiments conducted in this study, flint was revealed to be more efficient than dacite, obsidian, and quartzite in all cycles. In terms of functionality, all are excellent at performing a cut for a short period of time without altering the cutting edge. However, it is the continuous action that determines efficiency, with the durability of the edge having a major impact on the outcome. The brittle nature of obsidian, for example, is a disadvantage for some applications. These differences may have had an impact on raw material selection, manufacturing techniques, and tool performance throughout prehistory. So, according to the data presented in this thesis is possible to conclude that the nullification of the null hypothesis "*efficiency does not vary according to the different lithic raw materials* "was confirmed and replaced with the alternative hypothesis that "*efficiency does vary according to different lithic raw materials*".

Although much work remains to be done in this area of research, the relative success of these results in exploring some of the synthetic concepts on which lithic raw materials models are based indicates that it is possible to strengthen and extend these interpretive models through further experimentation. Experimentation with new contact materials, different lithic raw materials, different actions, different edges considering edge angle, retouch vs natural as well as questions arising from the analysis of the archaeological record. Using Kalavan 2 as a case study against which the results obtained here can be applied, the continuous development of this topic will lead to the clarification of research questions on the edge attrition on obsidian vs non-obsidian stone implements, to insights on the impact of raw material properties on

technology strategies, retouch intensity, reduction sequences, lithic procurement strategies, but also the recognition of performed activities through use-wear analysis.

Also, the introduction of novel analyses to characterize lithic raw materials along with conventional descriptive, qualitative, or petrological classifications needs to become more frequent, as this shows that it gives more practical data for archaeological interpretations.

References

Aldeias, V., Dibble, H. L., Sandgathe, D., Goldberg, P., & McPherron, S. J. P. (2016). How heat alters underlying deposits and implications for archaeological fire features: A controlled experiment. *Journal of Archaeological Science*, *67*, 64–79.

Aldeias, V., Gur-Arieh, S., Maria, R., Monteiro, P., & Cura, P. (2019). Shell we cook it? An experimental approach to the microarchaeological record of shellfish roasting. *Archaeological and Anthropological Sciences*, *11*(2), 389–407.

Ambrose, S. H. (2001). Paleolithic Technology and Human Evolution. *Science*.

Andrefsky, W. (1994). Raw-Material Availability and the Organization of Technology.

Andrefsky, W. (2005). *Lithics: Macroscopic approaches to analysis* (2nd ed). Cambridge University Press.

Ascher, R. (1961). Experimental Archeology1. *American Anthropologist*, *63*(4), 793–816.

Astruc, L., Vargiolu, R., & Zahouani, H. (2003). Wear assessments of prehistoric instruments. *Wear*, *255*(1–6), 341–347.

Atkins, T. (2009). *The science and engineering of cutting: The mechanics and processes of separating and puncturing biomaterials, metals and non-metals* (1. ed). Butterworth-Heinemann.

Benito-Calvo, A., Crittenden, A. N., Livengood, S. V., Sánchez-Romero, L., Martínez-Fernández, A., de la Torre, I., & Pante, M. (2018). 3D 360° surface morphometric analysis of pounding stone tools used by Hadza foragers of Tanzania: A new methodological approach for studying percussive stone artefacts. *Journal of Archaeological Science: Reports*, *20*, 611–621.

Bordes, F. (1971). Physical evolution and technological evolution in man: A parallelism. *World Archaeology*, *3*(1), 1–5

Brantingham, P. J., Olsen, J. W., Rech, J. A., & Krivoshapkin, A. I. (2000). Raw Material Quality and Prepared Core Technologies in Northeast Asia. *Journal of Archaeological Science*, *27*(3), 255–271.

Braun, D., Plummer, T., Ferraro, J., Ditchfield, P., & Bishop, L. (2009). Raw material quality and Oldowan hominin toolstone preferences: Evidence from Kanjera South, Kenya. *Journal of Archaeological Science*, *36*, 1605–1614.

Braun, D. R., Rogers, M. J., Harris, J. W. K., & Walker, S. J. (2008). Landscape-scale variation in hominin tool use: Evidence from the Developed Oldowan. *Journal of Human Evolution*, *55*(6), 1053–1063.

Calandra, I., Gneisinger, W., & Marreiros, J. (2020). A versatile mechanized setup for controlled experiments in archeology. *STAR: Science & Technology of Archaeological Research*, *6*(1), 30–40.

Caldwell, J. R. (1959). The New American Archeology: Its changing interests are bringing new kinds of understanding and a generalized view of its problems. *Science*, *129*(3345), 303–307.

Christenson, A. L. (1982). Maximizing Clarity in Economic Terminology. *American Antiquity*, *47*(2), 419–426.

Collins, S. (2008). Experimental investigations into edge performance and its implications for stone artefact reduction modelling. *Journal of Archaeological Science*, *35*(8), 2164–2170.

Collins, S. J. (2007). *AN EXPERIMENTAL EVALUATION OF THE PRINCIPLES AND FRAMEWORKS FOR INTERPRETING THE FUNCTION OF ARCHAEOLOGICAL STONE ARTEFACTS*. 336.

Costa, A. G. (2010). A Geometric Morphometric Assessment of Plan Shape in Bone and Stone Acheulean Bifaces from the Middle Pleistocene Site of Castel di Guido, Latium, Italy. In S. Lycett & P. Chauhan (Eds.), *New Perspectives on Old Stones: Analytical Approaches to Paleolithic Technologies* (pp. 23–41). Springer.

de la Torre, I. (2011). The Early Stone Age lithic assemblages of Gadeb (Ethiopia) and the Developed Oldowan/early Acheulean in East Africa. *Journal of Human Evolution*, *60*(6), 768–812.

Dibble, H. (1995). *Middle paleolithic scraper reduction: Background, clarification, and review of the evidence to date*.

Dibble, H. L., & Rezek, Z. (2009). Introducing a new experimental design for controlled studies of flake formation: Results for exterior platform angle, platform depth, angle of blow, velocity, and force. *Journal of Archaeological Science*, *36*(9), 1945–1954.

Dickson, D. B. (2002). Evidence of the Emergence of "Modern" Behavior in the Middle and Later Stone Age Lithic Assemblages at Shurmai Rockshelter (GnJm1) and Kakwa Lelash Rockshelter (GnJm2) in the Mukogodo Hills of North-Central Kenya. *African Archaeological Review*, 26.

Domanski, M., Webb, J. A., & Boland, J. (1994). MECHANICAL PROPERTIES OF STONE ARTEFACT MATERIALS AND THE EFFECT OF HEAT TREATMENT. *Archaeometry*, *36*(2), 177–208.

Domański, M., Webb, J., Glaisher, R., Gurba, J., Libera, J., & Zakościelna, A. (2009). Heat treatment of Polish flints. *Journal of Archaeological Science*, *36*(7), 1400–1408.

Doyle, J., & Walker, J. C. F. (1985). Indentation of wood by wedges. *Wood Science and Technology*, *19*(1), 47–55.

Eren, M. I., Lycett, S. J., Patten, R. J., Buchanan, B., Pargeter, J., & O'Brien, M. J. (2016). Test, Model, and Method Validation: The Role of Experimental Stone Artifact Replication in Hypothesis-driven Archaeology. *Ethnoarchaeology*, *8*(2), 103–136.

Eren, M. I., Lycett, S. J., Roos, C. I., & Sampson, C. G. (2011). Toolstone constraints on knapping skill: Levallois reduction with two different raw materials. *Journal of Archaeological Science*, *38*(10), 2731–2739.

Eren, M. I., Roos, C. I., Story, B. A., von Cramon-Taubadel, N., & Lycett, S. J. (2014). The role of raw material differences in stone tool shape variation: An experimental assessment. *Journal of Archaeological Science*, *49*, 472–487.

Evans, A. A. (2014). On the importance of blind testing in archaeological science: The example from lithic functional studies. *Journal of Archaeological Science*, *48*, 5–14.

Fiers, G., Halbrucker, É., De Kock, T., Laforce, B., Vandendriessche, H., Messiaen, L., Vincze, L., Crombé, P., & Cnudde, V. (2019). Preliminary characterization of flint raw material used on prehistoric sites in NW Belgium. *Geoarchaeology*, *34*(4), 400–412.

Foley, R., & Lahr, M. M. (2003). On stony ground: Lithic technology, human evolution, and the emergence of culture. *Evolutionary Anthropology: Issues, News, and Reviews*, *12*(3), 109–122.

Goldman-Neuman, T., & Hovers, E. (2012). Raw material selectivity in Late Pliocene Oldowan sites in the Makaamitalu Basin, Hadar, Ethiopia. *Journal of Human Evolution*, *62*(3), 353–366.

Goodman, M. E. (1944). The Physical Properties of Stone Tool Materials. *American Antiquity*, *9*(4), 415–433.

Goodyear, A. C. (2021). A Hypothesis for the Use of Cryptocrystalline Raw Materials Among Paleoindian Groups of North America. In C. J. Ellis & J. C. Lothrop, *Eastern Paleoindian Lithic Resource Use* (1st ed., pp. 1–9). Routledge.

Goudie, A. S. (2006). The Schmidt Hammer in geomorphological research. *Progress in Physical Geography: Earth and Environment*, *30*(6), 703–718.

Grace, R., Graham, I. D. G., & Newcomer, M. H. (1985). The quantification of microwear polishes. *World Archaeology*, *17*(1), 112–120.

Greiser, S. T. (1979). Raw material as a functional variable in use-wear studies. *Lithic Use-Wear Analysis*, 289–296.

Harmand, S. (2009). Variability in Raw Material Selectivity at the Late Pliocene sites of Lokalalei, West Turkana, Kenya. In E. Hovers & D. R. Braun (Eds.), *Interdisciplinary Approaches to the Oldowan* (pp. 85–97). Springer Netherlands.

Harmand, S., Lewis, J., Feibel, C., Lepre, C., Prat, S., Arnaud, L., Boës, X., Quinn, R., Brenet, M., Arroyo, A., Taylor, N., Clément, S., Daver, G., Brugal, J.-P., Leakey, L., Mortlock, R., Wright, J., Lokorodi, S., Kirwa, C., & Roche, H. (2015). 3.3-million-year-old stone tools from Lomekwi 3, West Turkana, Kenya. *Nature*, *521*, 310–315.

Hirata, S., Ohta, M., & Honma, Y. (2001). Hardness distribution on wood surface. *Journal of Wood Science*, *47*(1), 1–7.

Hiscock, P. D. (1986). *Raw material rationing as an explanation of assemblage differences: A case study of Lawn Hill, Northwest Queensland*.

Hovers, E., Braun, D. R., & Society for American Archaeology (Eds.). (2009). *Interdisciplinary approaches to the Oldowan*. Springer.

Iovita, R., Schönekeß, H., Gaudzinski-Windheuser, S., & Jäger, F. (2014). Projectile impact fractures and launching mechanisms: Results of a controlled ballistic experiment using replica Levallois points. *Journal of Archaeological Science*, *48*, 73–83.

Jones, P. R. (1980). Experimental butchery with modern stone tools and its relevance for Palaeolithic archaeology. *World Archaeology*, *12*(2), 153–165.

Keller, C. M. (1966). The Development of Edge Damage Patterns on Stone Tools. *Man*, *1*(4), 501.

Key, A. J. M., & Lycett, S. J. (2015). Edge Angle as a Variably Influential Factor in Flake Cutting Efficiency: An Experimental Investigation of Its Relationship with Tool Size and Loading: Edge angle as a factor in flake cutting efficiency. *Archaeometry*, *57*(5), 911–927.

Kuhn, S. L. (1990). A geometric index of reduction for unifacial stone tools. *Journal of Archaeological Science*, *17*(5), 583–593.

Kuhn, S. L. (1992). Blank Form and Reduction as Determinants of Mousterian Scraper Morphology. *American Antiquity*, *57*(1), 115–128.

Kuhn, T. S. (1962). Historical Structure of Scientific Discovery. *Science*.

Lerner, H. J. (2014). Intra-raw material variability and use-wear accrual: A continuing exploration. *Journal of Lithic Studies*, *1*(1), 165–186.

Lin, S. C., & Marreiros, J. (2021). Quina Retouch Does Not Maintain Edge Angle Over Reduction. *Lithic Technology*, *46*(1), 45–59.

Lin, S. C., Rezek, Z., & Dibble, H. L. (2018). Experimental Design and Experimental Inference in Stone Artifact Archaeology. *Journal of Archaeological Method and Theory*, *25*(3), 663–688.

Lin, S. C.-H. (2014). *EXPERIMENTATION AND SCIENTIFIC INFERENCE BUILDING IN THE STUDY OF HOMININ BEHAVIOR THROUGH STONE ARTIFACT ARCHAEOLOGY*. University of Pennsylvania.

Malinsky-Buller, A., Glauberman, P., Ollivier, V., Lauer, T., Timms, R., Frahm, E., Brittingham, A., Triller, B., Kindler, L., Knul, M. V., Krakovsky, M., Joannin, S., Hren, M. T., Bellier, O., Clark, A. A., Blockley, S. P. E., Arakelyan, D., Marreiros, J., Paixaco, E., … Gasparyan, B. (2021). Short-term occupations at high elevation during the Middle Paleolithic at Kalavan 2 (Republic of Armenia). *PLOS ONE*, *16*(2), e0245700.

Manninen, M. A., & Knutsson, K. (2014). Lithic raw material diversification as an adaptive strategy—Technology, mobility, and site structure in Late Mesolithic northernmost Europe. *Journal of Anthropological Archaeology*, *33*, 84–98.

Marreiros, J., Calandra, I., Gneisinger, W., Paixão, E., Pedergnana, A., & Schunk, L. (2020). Rethinking Use-Wear Analysis and Experimentation as Applied to the Study of Past Hominin Tool Use. *Journal of Paleolithic Archaeology*, *3*(3), 475–502.

Marreiros, J., Pereira, T., & Iovita, R. (2020). Controlled experiments in lithic technology and function. *Archaeological and Anthropological Sciences*, *12*(6), 110, s12520-020-01059–5.

Mcbrearty, S., & Brooks, A. S. (2000). The revolution that wasn't: A new interpretation of the origin of modern human behavior. *Journal of Human Evolution*, *39*(5), 453–563.

McCarthy, C. T., Annaidh, A. N., & Gilchrist, M. D. (2010). On the sharpness of straight edge blades in cutting soft solids: Part II – Analysis of blade geometry. *Engineering Fracture Mechanics*, *77*(3), 437–451.

McPherron, S. P., Braun, D. R., Dogandžić, T., Archer, W., Desta, D., & Lin, S. C. (2014). An experimental assessment of the influences on edge damage to lithic artifacts: A consideration of edge angle, substrate grain size, raw material properties, and exposed face. *Journal of Archaeological Science*, *49*, 70–82.

Miller, R. (1982). Review of Palaeolithic Reflections: Lithic Technology and Ethnographic Excavations Among Australian Aborigines. [Review of *Review of Palaeolithic Reflections: Lithic Technology and Ethnographic Excavations Among Australian Aborigines.*, by B. Hayden]. *Man*, *17*(3), 561–562.

Moník, M., & Hadraba, H. (2016). Mechanical characterization of raw material quality and its implication for Early Upper Palaeolithic Moravia. *Quaternary International*, *425*, 425–436.

Morrison, D. M. (1994). *Validity in lithic debitage analysis: An experimental assessment comparing quartzite to obsidian* [PhD Thesis]. Theses (Dept. of Archaeology)/Simon Fraser University.

Paixão, E., Pedergnana, A., Marreiros, J., Dubreuil, L., Prévost, M., Zaidner, Y., Carver, G., & Gneisinger, W. (2021). Using mechanical experiments to study ground stone tool use: Exploring the formation of percussive and grinding wear traces on limestone tools. *Journal of Archaeological Science: Reports*, *37*, 102971.

Pedergnana, A., García-Antón, M. D., & Ollé, A. (2017). Structural study of two quartzite varieties from the Utrillas facies formation (Olmos de Atapuerca, Burgos, Spain): From a petrographic characterisation to a functional analysis design. *Quaternary International*, *433*, 163–178

Pedergnana, A., Malinksky-Buller2, A., Gneisinger, W., & Marreiros, J. (2019). Using standardised samples and controlled experiments to evaluate the role of raw material in lithic edge durability and efficiency. *EAA 2019 Bern, Switzerland.*, 1.

Pereira, T., & Benedetti, M. M. (2013). A model for raw material management as a response to local and global environmental constraints. *Quaternary International*, *318*, 19–32.

Pereira, T., Marreiros, J., Paixão, E., & Martins, R. (2017). *MECHANICAL EXPERIMENTS TO TEST QUARTZITE VS CHERT EDGE REDUCTION*. 15.

Pfleging, J., Iovita, R., & Buchli, J. (2019). Influence of force and duration on stone tool wear: Results from experiments with a force-controlled robot. *Archaeological and Anthropological Sciences*, *11*(11), 5921–5935.

Popper, K. R. (1959). The logic of scientific discovery Hutchinson. *Hughes, John,(1987).“La Filosofía de La Investigación Social”, Breviarios, Fondo de Cultura Económica, México*.

Robinson, E., & Sellet, F. (2018). Lithic Technological Organization and Paleoenvironmental Change. In E. Robinson & F. Sellet (Eds.), *Lithic Technological Organization and Paleoenvironmental Change: Global and Diachronic Perspectives* (pp. 1–11). Springer International Publishing.

Schuldt, S., Arnold, G., Roschy, J., Schneider, Y., & Rohm, H. (2013). Defined abrasion procedures for cutting blades and comparative mechanical and geometrical wear characterization. *Wear*, *300*(1), 38–43.

Schunk, L. (2021). *Understanding Middle Palaeolithic asymmetric stone tool design and use: Usewear analysis and controlled experiments to assess Neanderthal technology.* Johannes Gutenberg University Mainz.

Semenov, S. A. (1964). *Prehistoric technology*.

Sillar, B. (2003). COMMENTS III: TECHNOLOGICAL CHOICES AND EXPERIMENTAL ARCHAEOLOGY. *Archaeometry*, *45*(1), 173–181. https://doi.org/10.1111/1475-4754.00102_3

Sonnenfeld, J. (1962). Interpreting the Function of Primitive Implements. *American Antiquity*, *28*(1), 56–65.

Stout, D., Quade, J., Semaw, S., Rogers, M. J., & Levin, N. E. (2005). Raw material selectivity of the earliest stone toolmakers at Gona, Afar, Ethiopia. *Journal of Human Evolution*, *48*(4), 365–380.

Yaşar, E., & Erdoğan, Y. (2004). Estimation of rock physicomechanical properties using hardness methods. *Engineering Geology*, *71*(3), 281–288.

Yonekura, K., Hasegawa, H., Hotta, A., & Suzuki, T. (2008). A Novel Approach to Studies of Prehistoric Exploitation of Stone Tool Materials Using Material Composition, Surface Morphology, Microstructure and Mechanical Properties*. *Archaeometry*, *50*(5), 727–746.

Yonekura, K., Hasegawa, H., & Suzuki, T. (2006). Mineral compositions, microstructures, and mechanical properties of primary materials from the Paleolithic age. *Materials Characterization*, *56*(2), 165–168.

Appendix A: Figures and Tables

Table 4 - Cloud-to-Mesh edge damage, all lithic raw materials, and cycles.

Raw material	cycle	ID	end.n	end.min	end.max	end.mean	end.median	end.sd	start.n	start. min	start.max	start.mean	start.median	start.sd
Flint	0-125	FLT10-2	224	0.2	0.5350	0.3675	0.3675	0.0973	224	0.2015	0.5365	0.3690	0.3690	0.0973
Flint	0-125	FLT10-5	256	0.2	0.3233	0.2617	0.2617	0.0358	256	0.2005	0.3238	0.2621	0.2621	0.0358
Flint	0-125	FLT10-6	132	0.2	0.4637	0.3319	0.3319	0.0770	132	0.2020	0.4658	0.3339	0.3339	0.0770
Flint	125-250	FLT10-2	184	0.2	0.5368	0.3684	0.3684	0.0980	184	0.2018	0.5386	0.3702	0.3702	0.0980
Flint	125-250	FLT10-5	256	0.2	0.4682	0.3341	0.3341	0.0779	256	0.2011	0.4692	0.3351	0.3351	0.0779
Flint	125-250	FLT10-6	256	0.2	0.3616	0.2808	0.2808	0.0469	256	0.2006	0.3623	0.2815	0.2815	0.0469
Flint	250-500	FLT10-2	48	0.2	0.5327	0.3664	0.3664	0.0991	48	0.2071	0.5398	0.3734	0.3734	0.0991
Flint	250-500	FLT10-5	256	0.2	0.2822	0.2411	0.2411	0.0239	256	0.2003	0.2826	0.2414	0.2414	0.0239
Flint	250-500	FLT10-6	256	0.2	0.3793	0.2897	0.2897	0.0521	256	0.2007	0.3800	0.2904	0.2904	0.0521
Flint	0-500	FLT10-2	256	0.2	0.4040	0.3020	0.3020	0.0592	256	0.2008	0.4048	0.3028	0.3028	0.0592
Flint	0-500	FLT10-5	256	0.1	0.1377	0.1188	0.1188	0.0109	256	0.1001	0.1378	0.1190	0.1190	0.0109
Flint	0-500	FLT10-6	176	0.2	0.5001	0.3500	0.3500	0.0874	176	0.2017	0.5018	0.3518	0.3518	0.0874
Obsidian	0-125	OBS4-4	256	0.2	0.6092	0.4046	0.4046	0.1188	256	0.2016	0.6108	0.4062	0.4062	0.1188
Obsidian	0-125	OBS4-5	200	0.2	0.6740	0.4370	0.4370	0.1379	200	0.2024	0.6764	0.4394	0.4394	0.1379
Obsidian	0-125	OBS4-6	256	0.2	1.1560	0.6780	0.6780	0.2776	256	0.2037	1.1598	0.6818	0.6818	0.2776
Obsidian	125-250	OBS4-4	196	0.2	0.6589	0.4294	0.4294	0.1335	196	0.2024	0.6612	0.4318	0.4318	0.1335
Obsidian	125-250	OBS4-5	256	0.2	1.0205	0.6103	0.6103	0.2383	256	0.2032	1.0238	0.6135	0.6135	0.2383
Obsidian	125-250	OBS4-6	256	0.2	0.5939	0.3969	0.3969	0.1144	256	0.2015	0.5954	0.3985	0.3985	0.1144
Obsidian	250-500	OBS4-4	68	0.2	0.6069	0.4034	0.4034	0.1201	68	0.2061	0.6130	0.4095	0.4095	0.1201

Raw material	cycle	ID	end.n	end.min	end.max	end.mean	end.median	end.sd	start.n	start. min	start.max	start.mean	start.median	start.sd
Obsidian	250-500	OBS4-5	256	0.2	1.1921	0.6960	0.6960	0.2881	256	0.2039	1.1960	0.6999	0.6999	0.2881
Obsidian	250-500	OBS4-6	256	0.2	1.1590	0.6795	0.6795	0.2785	256	0.2038	1.1628	0.6833	0.6833	0.2785
Obsidian	0-500	OBS4-4	144	0.2	0.6223	0.4112	0.4112	0.1232	144	0.2030	0.6253	0.4141	0.4141	0.1232
Obsidian	0-500	OBS4-5	256	0.2	1.9814	1.0907	1.0907	0.5173	256	0.2070	1.9884	1.0977	1.0977	0.5173
Obsidian	0-500	OBS4-6	256	0.2	1.7246	0.9623	0.9623	0.4427	256	0.2060	1.7305	0.9683	0.9683	0.4427
Dacite	0-125	DAC3-2	256	0.2	0.6820	0.4410	0.4410	0.1399	256	0.2019	0.6839	0.4429	0.4429	0.1399
Dacite	0-125	DAC3-4	224	0.2	0.2798	0.2399	0.2399	0.0232	224	0.2004	0.2801	0.2402	0.2402	0.0232
Dacite	0-125	DAC3-6	248	0.2	0.8256	0.5128	0.5128	0.1817	248	0.2025	0.8281	0.5153	0.5153	0.1817
Dacite	125-250	DAC3-2	240	0.2	0.5128	0.3564	0.3564	0.0909	240	0.2013	0.5141	0.3577	0.3577	0.0909
Dacite	125-250	DAC3-4	248	0.2	0.9376	0.5688	0.5688	0.2142	248	0.2030	0.9406	0.5718	0.5718	0.2142
Dacite	125-250	DAC3-6	256	0.2	0.2612	0.2306	0.2306	0.0178	256	0.2002	0.2614	0.2308	0.2308	0.0178
Dacite	250-500	DAC3-2	256	0.2	0.7679	0.4840	0.4840	0.1649	256	0.2022	0.7701	0.4862	0.4862	0.1649
Dacite	250-500	DAC3-4	255	0.2	0.5686	0.3850	0.3850	0.1066	255	0.2029	0.5701	0.3865	0.3865	0.1066
Dacite	250-500	DAC3-6	256	0.2	0.3792	0.2896	0.2896	0.0520	256	0.2007	0.3799	0.2903	0.2903	0.0520
Dacite	0-500	DAC3-2	256	0.2	1.5983	0.8991	0.8991	0.4060	256	0.2055	1.6038	0.9046	0.9046	0.4060
Dacite	0-500	DAC3-4	256	0.2	0.9013	0.5506	0.5506	0.2036	256	0.2028	0.9040	0.5534	0.5534	0.2036
Dacite	0-500	DAC3-6	232	0.2	0.7041	0.4520	0.4520	0.1465	232	0.2022	0.7063	0.4542	0.4542	0.1465
Quartzite	0-125	QTZ1-1	236	0.2	1.7811	0.9905	0.9905	0.4593	236	0.2067	1.7878	0.9973	0.9973	0.4593
Quartzite	0-125	QTZ1-2	256	0.2	1.0704	0.6352	0.6352	0.2527	256	0.2034	1.0738	0.6386	0.6386	0.2527
Quartzite	0-125	QTZ1-5	256	0.2	1.4560	0.8280	0.8280	0.3647	256	0.2049	1.4609	0.8329	0.8329	0.3647

Raw material	cycle	ID	end.n	end.min	end.max	end.mean	end.median	end.sd	start.n	start. min	start.max	start.mean	start.median	start.sd
Quartzite	125-250	QTZ1-1	256	0.2	0.4169	0.3085	0.3085	0.0630	256	0.2009	0.4178	0.3093	0.3093	0.0630
Quartzite	125-250	QTZ1-2	256	0.2	0.3187	0.2593	0.2593	0.0345	256	0.2005	0.3192	0.2598	0.2598	0.0345
Quartzite	125-250	QTZ1-5	256	0.2	0.3073	0.2536	0.2536	0.0311	256	0.2004	0.3077	0.2541	0.2541	0.0311
Quartzite	250-500	QTZ1-1	256	0.2	0.6104	0.4052	0.4052	0.1192	256	0.2016	0.6120	0.4068	0.4068	0.1192
Quartzite	250-500	QTZ1-2	136	0.2	0.4195	0.3098	0.3098	0.0641	136	0.2016	0.4211	0.3114	0.3114	0.0641
Quartzite	250-500	QTZ1-5	192	0.2	0.7387	0.4693	0.4693	0.1567	192	0.2028	0.7415	0.4722	0.4722	0.1567
Quartzite	0-500	QTZ1-1	256	0.2	1.7487	0.9743	0.9743	0.4497	256	0.2061	1.7547	0.9804	0.9804	0.4497
Quartzite	0-500	QTZ1-2	196	0.2	1.2886	0.7443	0.7443	0.3167	196	0.2056	1.2942	0.7499	0.7499	0.3167
Quartzite	0-500	QTZ1-5	168	0.2	1.1946	0.6973	0.6973	0.2897	168	0.2060	1.2005	0.7032	0.7032	0.2897

Table 5 - Inotec Force sensor summary statistics, all lithic raw materials, and cycles.

Raw_material	CycleGroup	Sample	Force.n	Force.min	Force.max	Force.mean	Force.median	Force.sd
Dacite	0-125	DAC3-2	2775	-63.350822	-53.99267	-58.66883017	-58.607056	1.533210804
Dacite	0-125	DAC3-4	2808	-67.36146	-53.08704	-58.49288571	-58.65018	2.069380257
Dacite	0-125	DAC3-6	2808	-64.6877	-53.216415	-58.78100061	-58.82268	1.663956898
Dacite	125-250	DAC3-2	2322	-65.07583	-49.33515	-58.42692254	-58.56393	1.788694027
Dacite	125-250	DAC3-4	2256	-68.05146	-50.24078	-58.04340973	-58.262054	2.751931231
Dacite	125-250	DAC3-6	2248	-65.33458	-52.957664	-58.96778816	-58.952057	1.700102618
Dacite	250-500	DAC3-2	4488	-70.94084	-41.65888	-58.56445985	-58.779556	2.722505923
Dacite	250-500	DAC3-4	4482	-65.50708	-49.98203	-58.23438313	-58.262054	1.812133754
Dacite	250-500	DAC3-6	4482	-75.64149	-35.88011	-58.95872575	-58.779556	3.482434398
Flint	0-125	FLT10-2	2812	-67.62021	-49.2489	-59.00962921	-58.865807	2.272849382
Flint	0-125	FLT10-5	2808	-69.086464	-50.58578	-58.64929111	-58.82268	2.661938313
Flint	0-125	FLT10-6	2774	-65.5502	-51.75016	-58.71591087	-58.82268	1.960303455
Flint	125-250	FLT10-2	2266	-67.57709	-51.879536	-58.89307931	-58.82268	2.041055388
Flint	125-250	FLT10-5	2310	-83.015884	-49.378277	-58.59988793	-58.65018	3.181127391
Flint	125-250	FLT10-6	2255	-64.1702	-53.43204	-58.60260055	-58.65018	1.690600108
Flint	250-500	FLT10-2	4530	-67.57709	-51.75016	-58.98891855	-58.82268	1.896650578
Flint	250-500	FLT10-5	4504	-86.293396	-36.915115	-59.42211607	-58.865807	7.154448062
Flint	250-500	FLT10-6	4481	-85.04276	-31.9126	-58.78301215	-58.73643	7.380632491
Obsidian	0-125	OBS4-4	2807	-66.412704	-44.67764	-58.30066357	-58.693306	2.326507864
Obsidian	0-125	OBS4-5	2808	-64.98958	-52.397038	-58.66570847	-58.82268	1.829911493

Raw_material	CycleGroup	Sample	Force.n	Force.min	Force.max	Force.mean	Force.median	Force.sd
Obsidian	0-125	OBS4-6	2808	-63.868324	-53.17329	-58.66724415	-58.73643	1.419048198
Obsidian	125-250	OBS4-4	2246	-69.04334	-48.81765	-58.95706901	-58.90893	2.793664392
Obsidian	125-250	OBS4-5	2286	-72.5796	-36.268238	-57.7283682	-58.003304	4.714584435
Obsidian	125-250	OBS4-6	2252	-71.28584	-42.17638	-58.80996706	-58.82268	3.693886444
Obsidian	250-500	OBS4-4	4482	-82.84338	-31.783224	-58.51483133	-58.73643	5.322781319
Obsidian	250-500	OBS4-5	4525	-73.83023	-35.01761	-57.93383769	-58.607056	5.561231105
Obsidian	250-500	OBS4-6	4482	-71.02709	-39.502625	-58.3783549	-58.693306	3.516130514
Quartzite	0-125	QTZ1-2	2805	-70.89772	-49.378277	-58.81115145	-58.82268	2.221878879
Quartzite	0-125	QTZ1-5	2806	-72.9246	-44.117012	-58.91503402	-58.779556	3.247551041
Quartzite	0-125	QZT1-1	2807	-65.33458	-48.64515	-58.56857124	-58.779556	2.222409767
Quartzite	125-250	QTZ1-2	2248	-68.43959	-45.45389	-58.85665673	-58.952057	2.539064878
Quartzite	125-250	QTZ1-5	2243	-69.172714	-50.542656	-58.95942132	-58.865807	2.497163109
Quartzite	125-250	QZT1-1	2246	-66.412704	-51.362034	-59.03730922	-58.952057	1.89947795
Quartzite	250-500	QTZ1-2	4488	-92.33091	-29.583841	-58.52378534	-58.73643	7.347321337
Quartzite	250-500	QTZ1-5	4476	-93.19341	-31.351973	-58.86405405	-58.73643	7.323929191
Quartzite	250-500	QZT1-1	4482	-69.172714	-50.24078	-58.77129208	-58.73643	2.601761994

Table 6 - Inotec Friction sensor summary statistics, all lithic raw materials, and cycles.

Raw_material	CycleGroup	Sample	Friction.n	Friction.min	Friction.max	Friction.mean	Friction.median	Friction.sd
Dacite	0-125	DAC3-2	2775	-96.859055	73.87335	-13.16631315	9.875656	49.76586399
Dacite	0-125	DAC3-4	2808	-67.79271	83.102135	9.872998654	36.742615	50.88612228
Dacite	0-125	DAC3-6	2808	-61.970818	73.22648	8.232800022	31.2225975	44.99387957
Dacite	125-250	DAC3-2	2322	-90.2609	74.865234	-14.32226192	5.7572055	46.74963521
Dacite	125-250	DAC3-4	2256	-89.9159	66.240204	-4.877288238	23.7835125	45.36332289
Dacite	125-250	DAC3-6	2248	-59.38331	51.620785	1.313129628	26.7375835	38.94045658
Dacite	250-500	DAC3-2	4488	-85.689644	75.81399	-0.894300392	22.4897575	50.69425616
Dacite	250-500	DAC3-4	4482	-92.28779	76.63336	11.7722474	33.9610425	46.10291537
Dacite	250-500	DAC3-6	4482	-75.77086	64.3427	4.854589028	28.5057145	42.99354702
Flint	0-125	FLT10-2	2812	-73.7871	124.89039	22.00239112	33.831667	65.33639029
Flint	0-125	FLT10-5	2808	-93.710915	93.840294	-7.211281017	18.1125565	53.96971704
Flint	0-125	FLT10-6	2774	-52.65579	74.735855	4.715175271	26.4141445	40.72536101
Flint	125-250	FLT10-2	2266	-66.28333	129.7204	25.83465764	35.599798	67.66597212
Flint	125-250	FLT10-5	2310	-74.822105	123.20851	20.15892782	43.189822	61.21177492
Flint	125-250	FLT10-6	2255	-63.695824	104.10407	12.98089485	32.731976	53.88819336
Flint	250-500	FLT10-2	4530	-109.19284	82.800255	-4.392299601	31.9126	64.87705761
Flint	250-500	FLT10-5	4504	-93.15029	150.07547	20.27690374	33.745417	76.79750962
Flint	250-500	FLT10-6	4481	-65.67958	108.02846	1.119463457	16.38755	48.98649364
Obsidian	0-125	OBS4-4	2807	-49.852654	63.437073	2.226098777	21.993818	32.95860838
Obsidian	0-125	OBS4-5	2808	-56.4508	53.475166	4.179866753	31.481348	38.87590762

Raw_material	CycleGroup	Sample	Friction.n	Friction.min	Friction.max	Friction.mean	Friction.median	Friction.sd
Obsidian	0-125	OBS4-6	2808	-61.15144	58.82268	6.592493726	30.446344	38.67297072
Obsidian	125-250	OBS4-4	2246	-55.7608	53.43204	2.297498232	25.0772645	37.83080041
Obsidian	125-250	OBS4-5	2286	-90.04528	63.56645	-4.128995759	4.72220235	44.79258181
Obsidian	125-250	OBS4-6	2252	-73.22648	70.25085	-6.261302277	14.72723275	41.27895375
Obsidian	250-500	OBS4-4	4482	-58.520805	57.701427	3.587093227	18.6084955	36.25139937
Obsidian	250-500	OBS4-5	4525	-77.36649	55.5883	-2.437299109	13.800043	39.46604732
Obsidian	250-500	OBS4-6	4482	-86.6384	63.8252	2.797129676	27.7941495	44.16907315
Quartzite	0-125	QTZ1-2	2805	-82.024	78.142746	-4.594187431	22.856321	44.07311791
Quartzite	0-125	QTZ1-5	2806	-62.876446	61.927692	-3.300578976	17.9184935	38.93667599
Quartzite	0-125	QZT1-1	2807	-56.92518	62.445194	1.057664251	26.220081	40.59576136
Quartzite	125-250	QTZ1-2	2248	-63.307697	74.735855	4.511813676	24.495075	44.99377741
Quartzite	125-250	QTZ1-5	2243	-68.65521	64.6877	-2.350079493	30.058218	45.48923345
Quartzite	125-250	QZT1-1	2246	-63.048946	88.10465	-2.625564074	24.883202	40.06845641
Quartzite	250-500	QTZ1-2	4488	-75.16711	85.12901	8.119728541	24.128513	48.19263076
Quartzite	250-500	QTZ1-5	4476	-92.71904	84.13714	0.931651264	19.7944365	42.56114623
Quartzite	250-500	QZT1-1	4482	-73.39898	70.63897	5.991247243	37.389492	49.80081624

Table 7 - Inotec Depth sensor summary statistics, all lithic raw materials, and cycles.

Raw_material	CycleGroup	Sample	Depth.n	Depth.min	Depth.max	Depth. Difference	Depth.mean	Depth.median	Depth.sd
Dacite	0-125	DAC3-2	2775	11.671004	13.822058	2.151054	12.3443984	12.327844	0.301465326
Dacite	0-125	DAC3-4	2808	11.849235	14.349834	2.500599	12.41639619	12.22221175	0.51050359
Dacite	0-125	DAC3-6	2808	11.926058	13.905796	1.979738	12.30809992	12.254093	0.267978048
Dacite	125-250	DAC3-2	2322	11.694531	12.745763	1.051232	12.29021706	12.254862	0.217826455
Dacite	125-250	DAC3-4	2256	12.393912	13.995679	1.601767	12.91760003	12.947041	0.172930873
Dacite	125-250	DAC3-6	2248	11.667163	12.572622	0.905459	12.06713288	12.07279	0.139442348
Dacite	250-500	DAC3-2	4488	11.358813	12.340616	0.981803	11.88163134	11.854324	0.208886247
Dacite	250-500	DAC3-4	4482	12.058962	13.003121	0.944159	12.42087196	12.403899	0.179418562
Dacite	250-500	DAC3-6	4482	11.401066	12.309118	0.908052	11.87373512	11.8378065	0.229562483
Flint	0-125	FLT10-2	2812	13.477121	16.003073	2.525952	14.22032305	14.0417725	0.658747154
Flint	0-125	FLT10-5	2808	13.725261	15.454555	1.729294	14.38753192	14.42973	0.234290677
Flint	0-125	FLT10-6	2774	13.675325	15.590531	1.915206	14.38014077	14.32102575	0.352866987
Flint	125-250	FLT10-2	2266	13.4187355	14.995151	1.5764155	14.12921189	13.7632885	0.562427431
Flint	125-250	FLT10-5	2310	13.048447	14.800019	1.751572	13.6382009	13.589283	0.250397606
Flint	125-250	FLT10-6	2255	13.513228	15.0581455	1.5449175	14.13622377	13.966486	0.41918306
Flint	250-500	FLT10-2	4530	13.122966	14.469679	1.346713	13.55458212	13.397225	0.285274728
Flint	250-500	FLT10-5	4504	11.565756	14.236904	2.671148	12.73234476	12.3336055	0.818431595
Flint	250-500	FLT10-6	4481	13.003889	14.551112	1.547223	13.74321398	13.596966	0.517065606
Obsidian	0-125	OBS4-4	2807	12.737312	14.285303	1.547991	13.248128	13.126807	0.322841545
Obsidian	0-125	OBS4-5	2808	11.993662	13.639987	1.646325	12.33926836	12.240265	0.28297589

Raw_material	CycleGroup	Sample	Depth.n	Depth.min	Depth.max	Depth. Difference	Depth.mean	Depth.median	Depth.sd
Obsidian	0-125	OBS4-6	2808	12.088155	14.031017	1.942862	12.68959405	12.639747	0.362607922
Obsidian	125-250	OBS4-4	2246	12.387766	13.252028	0.864262	12.75748687	12.749988	0.135208785
Obsidian	125-250	OBS4-5	2286	11.753205	12.842561	1.089356	12.28913881	12.324002	0.207425307
Obsidian	125-250	OBS4-6	2252	11.684064	12.72963	1.045566	12.1356787	12.161138	0.169947433
Obsidian	250-500	OBS4-4	4482	9.318673	12.661257	3.342584	10.45000682	10.358093	0.593237063
Obsidian	250-500	OBS4-5	4525	11.3030205	12.469199	1.1661785	11.91864346	11.852307	0.316894823
Obsidian	250-500	OBS4-6	4482	11.103279	12.191867	1.088588	11.67290969	11.6809915	0.233425272
Quartzite	0-125	QTZ1-2	2805	12.059731	14.31296	2.253229	13.00565949	13.036923	0.309505334
Quartzite	0-125	QTZ1-5	2806	13.410285	14.705526	1.295241	13.78526507	13.769434	0.169625041
Quartzite	0-125	QZT1-1	2807	14.442022	15.963893	1.521871	14.9074657	14.906804	0.186891674
Quartzite	125-250	QTZ1-2	2248	11.539637	13.004658	1.465021	12.12039894	12.171892	0.213336567
Quartzite	125-250	QTZ1-5	2243	13.232055	14.157776	0.925721	13.53649343	13.530129	0.120011666
Quartzite	125-250	QZT1-1	2246	14.279157	15.114995	0.835838	14.71128437	14.7477795	0.158040869
Quartzite	250-500	QTZ1-2	4488	10.746051	12.486868	1.740817	11.75553641	11.612234	0.431303032
Quartzite	250-500	QTZ1-5	4476	12.038988	13.905027	1.866039	13.11486362	13.163682	0.449961339
Quartzite	250-500	QZT1-1	4482	13.870457	14.892976	1.022519	14.35568976	14.32141	0.239413979

Table 8 - Inotec Position sensor summary statistics, all lithic raw materials, and cycles.

Raw_material	CycleGroup	Sample	Position.n	Position.min	Position.max	Position.mean	Position.median	Position.sd
Dacite	0-125	DAC3-2	2775	259.9998	389.9975	322.8371669	317.4225	58.05007333
Dacite	0-125	DAC3-4	2808	259.9998	389.9946	321.1610786	301.43415	58.03453473
Dacite	0-125	DAC3-6	2808	259.9997	389.9934	320.8892463	307.34515	58.00932611
Dacite	125-250	DAC3-2	2322	259.9998	389.9956	322.6852095	299.8323	58.41482238
Dacite	125-250	DAC3-4	2256	259.9998	389.9951	322.1403954	299.8023	58.14370661
Dacite	125-250	DAC3-6	2248	259.9995	389.9966	322.0427277	308.574	58.09624949
Dacite	250-500	DAC3-2	4488	259.9999	389.9925	323.4730907	299.81935	58.20124417
Dacite	250-500	DAC3-4	4482	259.9998	389.9961	320.9453377	301.39205	58.01787704
Dacite	250-500	DAC3-6	4482	259.9999	389.9959	321.6159278	307.31935	58.0607231
Flint	0-125	FLT10-2	2812	259.9998	389.9984	320.829768	297.16995	58.02409569
Flint	0-125	FLT10-5	2808	259.9997	389.9964	322.5403944	301.4045	58.15516902
Flint	0-125	FLT10-6	2774	259.9996	389.9973	321.7755824	305.5868	57.99475044
Flint	125-250	FLT10-2	2266	259.9983	389.9953	320.8319039	297.15835	58.08066079
Flint	125-250	FLT10-5	2310	259.9997	389.9984	320.7740087	297.1699	58.23355394
Flint	125-250	FLT10-6	2255	259.9993	389.9969	320.5052977	297.1957	58.0352132
Flint	250-500	FLT10-2	4530	259.9998	389.9929	322.4244087	297.2161	58.2504618
Flint	250-500	FLT10-5	4504	259.9997	389.9949	321.4549609	297.15635	58.09128473
Flint	250-500	FLT10-6	4481	259.9998	389.9943	321.0882331	305.6456	58.02874692

Raw_material	CycleGroup	Sample	Position.n	Position.min	Position.max	Position.mean	Position.median	Position.sd
Obsidian	0-125	OBS4-4	2807	259.9998	389.9963	320.8101053	305.5959	58.01726236
Obsidian	0-125	OBS4-5	2808	259.9999	389.9944	321.092473	301.44375	58.03059821
Obsidian	0-125	OBS4-6	2808	259.9999	389.9956	320.6764707	301.43255	57.9972816
Obsidian	125-250	OBS4-4	2246	259.9999	389.9976	321.8859799	298.5289	58.0816583
Obsidian	125-250	OBS4-5	2286	259.9999	389.9956	322.1941759	297.20945	58.25167521
Obsidian	125-250	OBS4-6	2252	259.9998	389.9951	322.5014376	299.78675	58.15510817
Obsidian	250-500	OBS4-4	4482	259.9998	389.9945	322.744893	307.3205	58.14026636
Obsidian	250-500	OBS4-5	4525	259.9997	389.9969	322.7058187	299.7898	58.22226582
Obsidian	250-500	OBS4-6	4482	259.9998	389.9938	322.5661742	307.30615	58.13221558
Quartzite	0-125	QTZ1-2	2805	259.9999	389.9968	320.3558291	305.5969	57.9890988
Quartzite	0-125	QTZ1-5	2806	259.9998	389.9958	321.8726062	308.5586	58.08246862
Quartzite	0-125	QZT1-1	2807	259.9998	389.9954	321.3564206	305.5985	58.04657534
Quartzite	125-250	QTZ1-2	2248	259.9998	389.9965	321.1826806	305.8755	58.03141423
Quartzite	125-250	QTZ1-5	2243	259.9998	389.9928	320.9145355	317.4069	57.99199705
Quartzite	125-250	QZT1-1	2246	259.9998	389.9958	322.4332129	305.57725	58.12643109
Quartzite	250-500	QTZ1-2	4488	259.9998	389.9969	321.3974095	297.1992	58.06268288
Quartzite	250-500	QTZ1-5	4476	259.9996	389.9967	321.3160774	305.60285	58.03490642
Quartzite	250-500	QZT1-1	4482	259.9999	389.9958	321.0099345	307.48285	58.01437288

Table 9 - Inotec Velocity sensor summary statistics, all lithic raw materials, and cycles.

Raw_material	CycleGroup	Sample	Velocity.n	Velocity.min	Velocity.max	Velocity.mean	Velocity.median	Velocity.sd
Dacite	0-125	DAC3-2	2775	-593.6927	588.0226	1.992736579	0.03695164	257.871945
Dacite	0-125	DAC3-4	2808	-593.9528	586.1683	2.658236393	0.00382351	255.2800408
Dacite	0-125	DAC3-6	2808	-592.17914	587.4256	2.992166624	0.018323567	254.8575312
Dacite	125-250	DAC3-2	2322	-594.481	587.72504	0.284545779	0.001897656	253.0572617
Dacite	125-250	DAC3-4	2256	-592.40405	587.53204	1.406156458	0.003435144	256.1158928
Dacite	125-250	DAC3-6	2248	-593.036	587.4133	1.812553797	0.006502744	256.2898101
Dacite	250-500	DAC3-2	4488	-593.1078	588.6025	-0.126252814	0.007093027	257.3810176
Dacite	250-500	DAC3-4	4482	-593.488	588.4483	2.626729726	0.003836358	255.1294236
Dacite	250-500	DAC3-6	4482	-593.19696	587.8539	2.14614844	0.02349838	255.7665005
Flint	0-125	FLT10-2	2812	-594.47754	588.0332	2.677169905	0.001997708	255.0176382
Flint	0-125	FLT10-5	2808	-593.0669	586.89966	0.668188204	0.00675629	257.1172786
Flint	0-125	FLT10-6	2774	-593.2471	587.52997	2.637451331	0.004554867	257.2687736
Flint	125-250	FLT10-2	2266	-592.7275	586.1221	2.038899672	0.001974658	254.7733159
Flint	125-250	FLT10-5	2310	-593.34393	587.68384	0.933866084	9.72E-04	253.2849633
Flint	125-250	FLT10-6	2255	-593.92755	585.29816	2.185393405	4.95E-04	255.5610163
Flint	250-500	FLT10-2	4530	-593.5853	588.1991	0.561712945	0.003627855	255.336703
Flint	250-500	FLT10-5	4504	-596.61523	587.81805	1.823755702	0.003881771	254.8463814

Raw_material	CycleGroup	Sample	Velocity.n	Velocity.min	Velocity.max	Velocity.mean	Velocity.median	Velocity.sd
Flint	250-500	FLT10-6	4481	-595.0058	586.2632	2.629807166	0.00535877	255.2901463
Obsidian	0-125	OBS4-4	2807	-592.68835	588.7652	2.624791801	0.00369341	255.6856706
Obsidian	0-125	OBS4-5	2808	-592.60956	588.0002	2.645374703	0.005406157	255.4348746
Obsidian	0-125	OBS4-6	2808	-593.6028	587.3566	3.028150816	0.003531422	254.9404848
Obsidian	125-250	OBS4-4	2246	-595.1441	588.37823	1.880372312	0.0039544	256.3840011
Obsidian	125-250	OBS4-5	2286	-593.92786	589.06195	0.592095445	0.002877376	255.0773695
Obsidian	125-250	OBS4-6	2252	-594.10535	588.9109	0.881016135	0.008707697	256.4456458
Obsidian	250-500	OBS4-4	4482	-592.4001	590.4965	0.901962345	0.014596119	256.9996451
Obsidian	250-500	OBS4-5	4525	-592.3014	586.49115	0.675777755	0.004148477	255.254072
Obsidian	250-500	OBS4-6	4482	-593.72095	587.5351	1.021977234	0.014574174	256.5913111
Quartzite	0-125	QTZ1-2	2805	-593.5867	588.4967	2.588104873	7.10E-04	255.6554011
Quartzite	0-125	QTZ1-5	2806	-593.58386	589.6914	2.041267448	0.006204501	256.3105084
Quartzite	0-125	QZT1-1	2807	-593.4887	587.3888	2.472868527	0.004829307	255.6345502
Quartzite	125-250	QTZ1-2	2248	-593.4113	584.8861	2.63447867	0.004623628	255.5405393
Quartzite	125-250	QTZ1-5	2243	-593.0558	587.61975	3.072488979	0.03198832	255.1545651
Quartzite	125-250	QZT1-1	2246	-593.2712	586.2932	1.170863594	0.002828397	256.8668133
Quartzite	250-500	QTZ1-2	4488	-596.3718	588.2321	2.27430269	0.004262965	255.4605042
Quartzite	250-500	QTZ1-5	4476	-595.6911	592.1404	2.601941664	0.003451091	255.4824853
Quartzite	250-500	QZT1-1	4482	-594.2624	589.3924	2.80191698	0.006795231	255.1307189

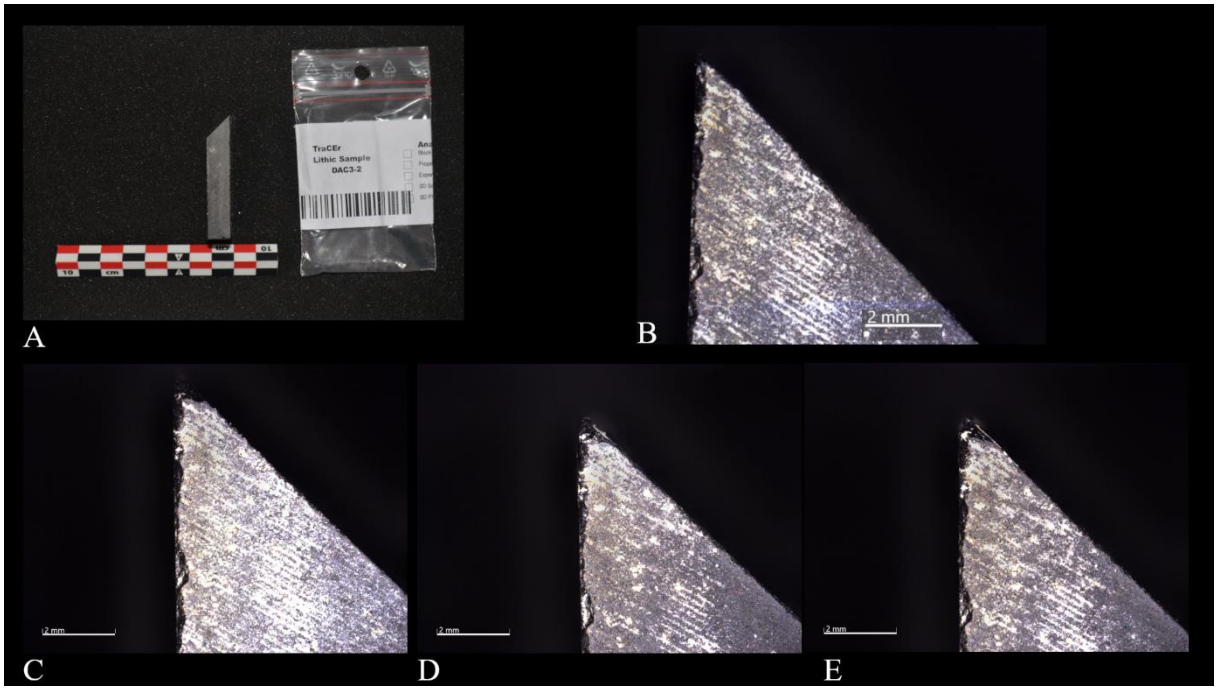

Figure 100: ZEISS Smart zoom DAC3-2 images: Profile view, A – Sample profile and ID; B – Profile view cycle 0; C – Profile view cycle 125; D - Profile view cycle 250; E – Profile view cycle 500.

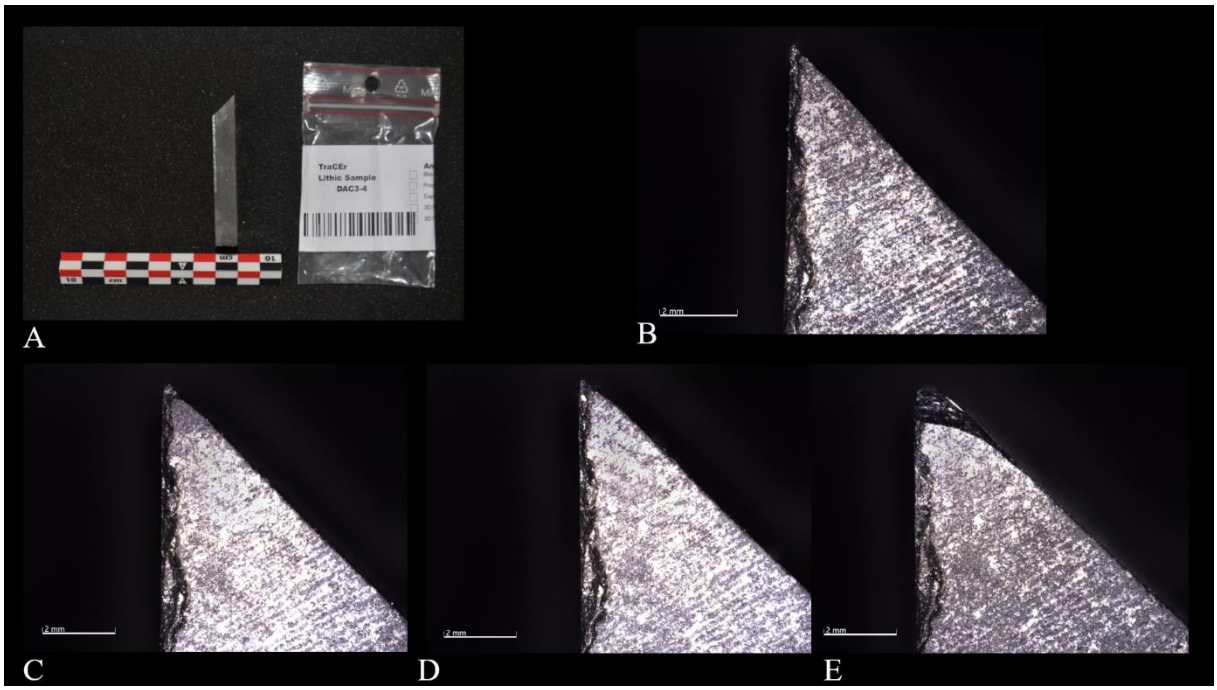

Figure 101: ZEISS Smart zoom DAC3-4 images: Profile view, A – Sample profile and ID; B – Profile view cycle 0; C – Profile view cycle 125; D - Profile view cycle 250; E – Profile view cycle 500.

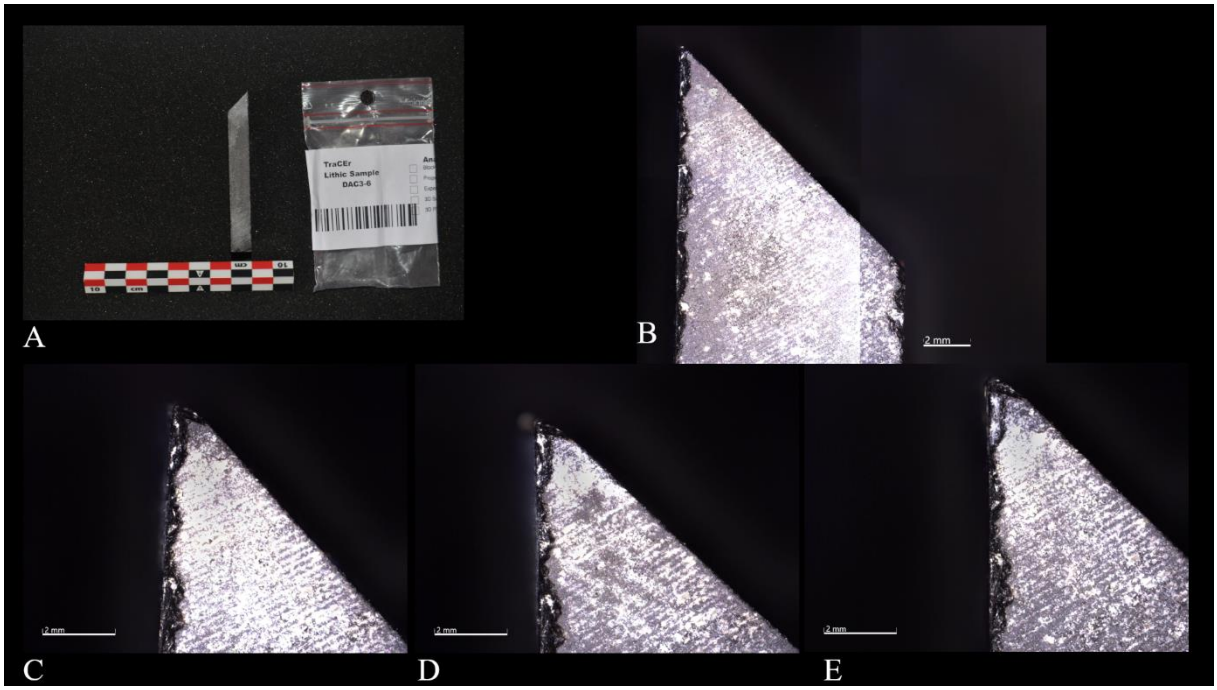

Figure 102: ZEISS Smart zoom DAC3-6 images: Profile view, A – Sample profile and ID; B – Profile view cycle 0; C – Profile view cycle 125; D - Profile view cycle 250; E – Profile view cycle 500.

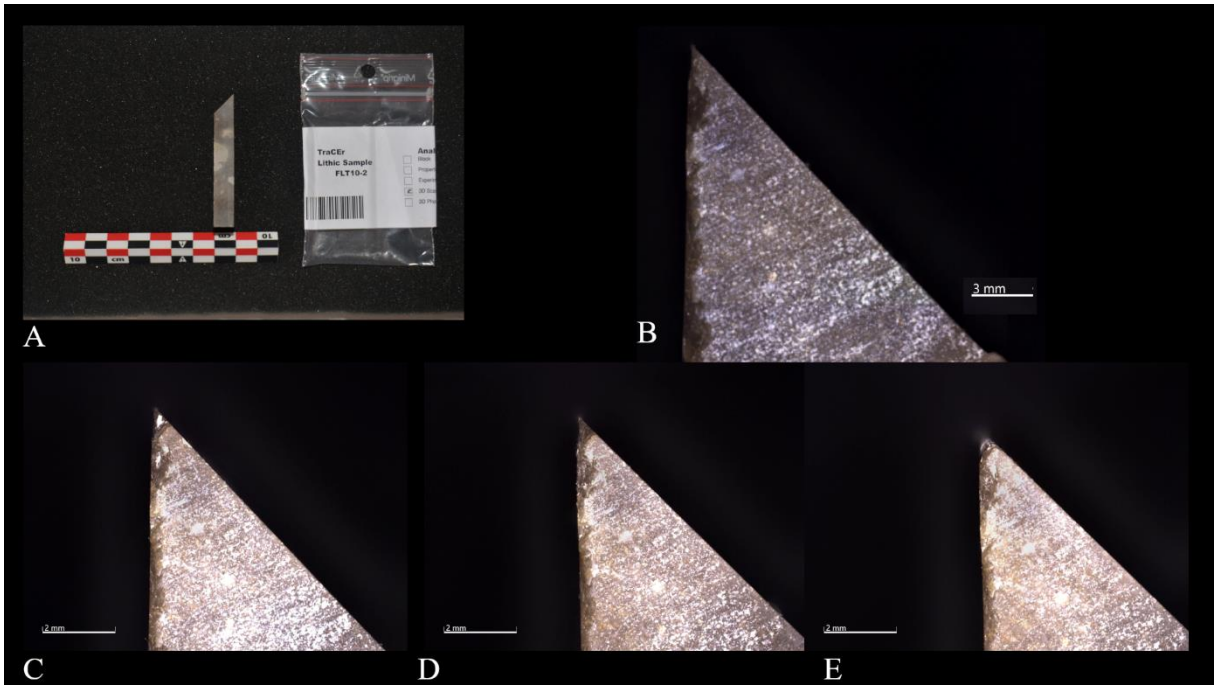

Figure 103. ZEISS Smart zoom FLT10-2 images: Profile view, A – Sample profile and ID; B – Profile view cycle 0; C – Profile view cycle 125; D - Profile view cycle 250; E – Profile view cycle 500.

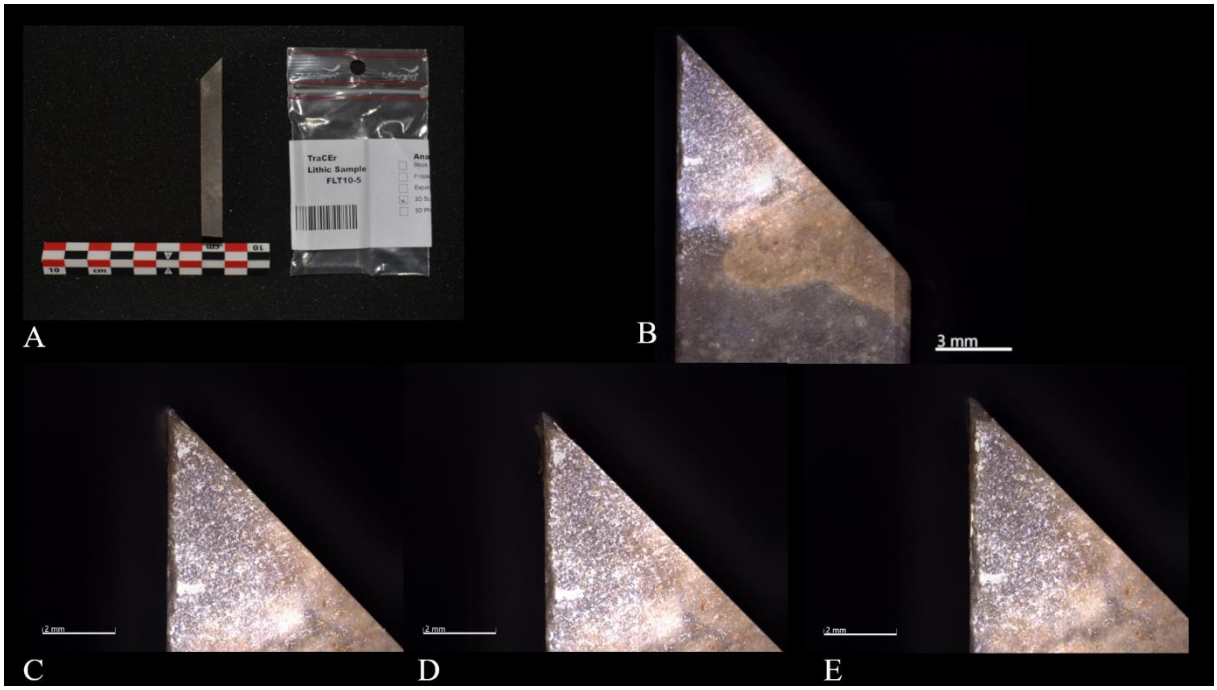

Figure 104: ZEISS Smart zoom FLT10-5 images: Profile view, A – Sample profile and ID; B – Profile view cycle 0; C – Profile view cycle 125; D - Profile view cycle 250; E – Profile view cycle 500.

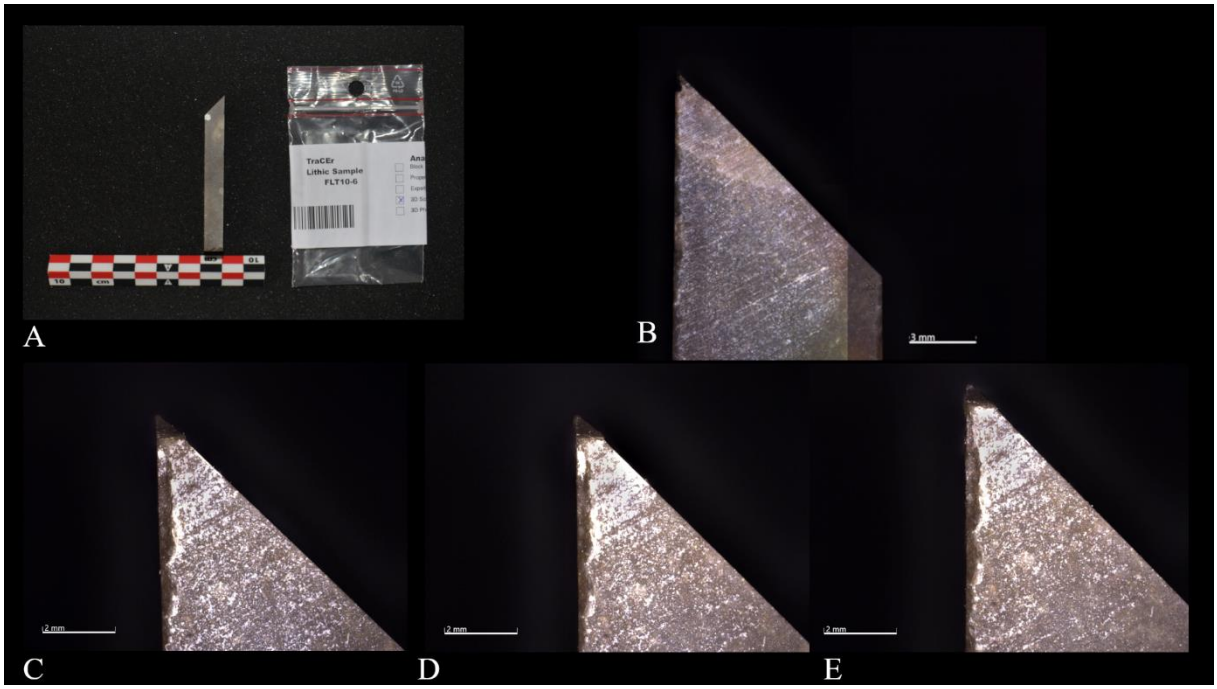

Figure 105: ZEISS Smart zoom FLT10-6 images: Profile view, A – Sample profile and ID; B – Profile view cycle 0; C – Profile view cycle 125; D - Profile view cycle 250; E – Profile view cycle 500.

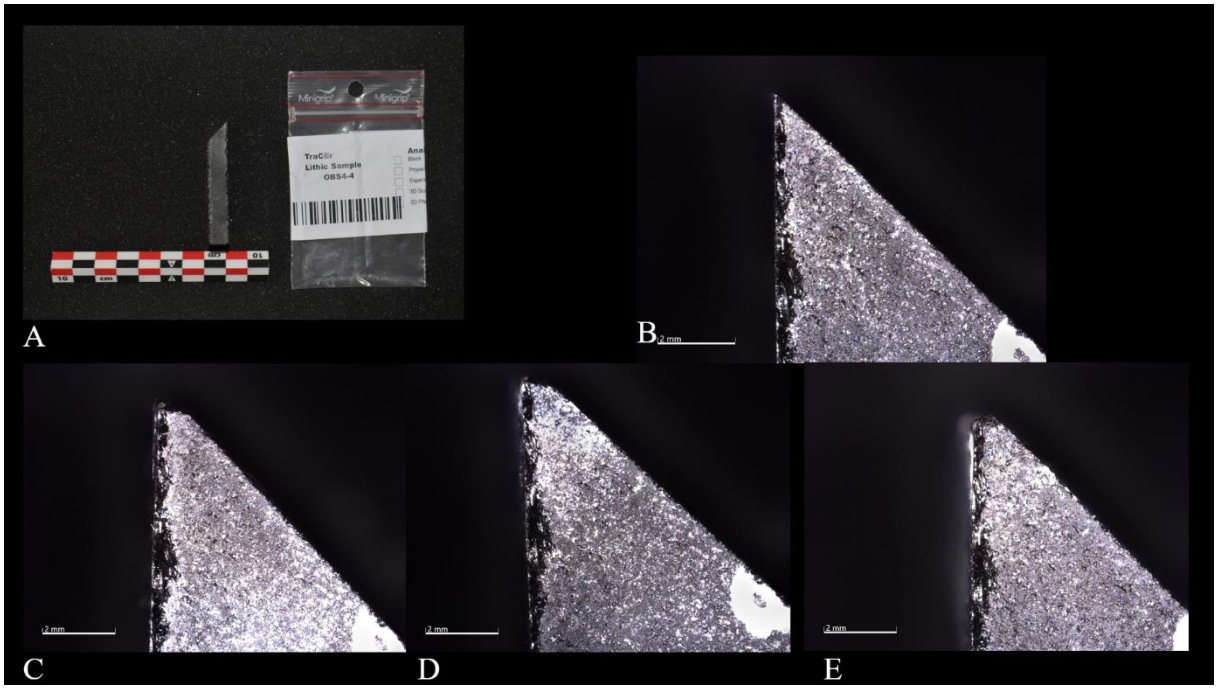

Figure 106: ZEISS Smart zoom OBS4-4 images: Profile view, A – Sample profile and ID; B – Profile view cycle 0; C – Profile view cycle 125; D - Profile view cycle 250; E – Profile view cycle 500.

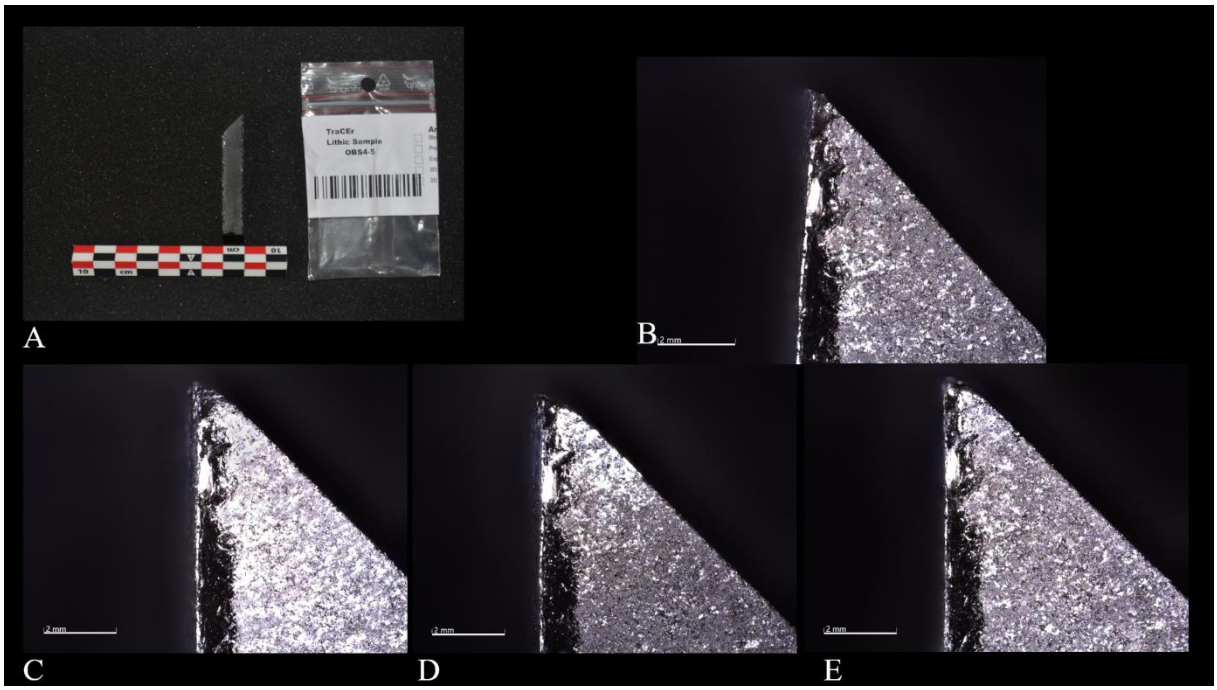

Figure 107: ZEISS Smart zoom OBS4-5 images: Profile view, A – Sample profile and ID; B – Profile view cycle 0; C – Profile view cycle 125; D - Profile view cycle 250; E – Profile view cycle 500.

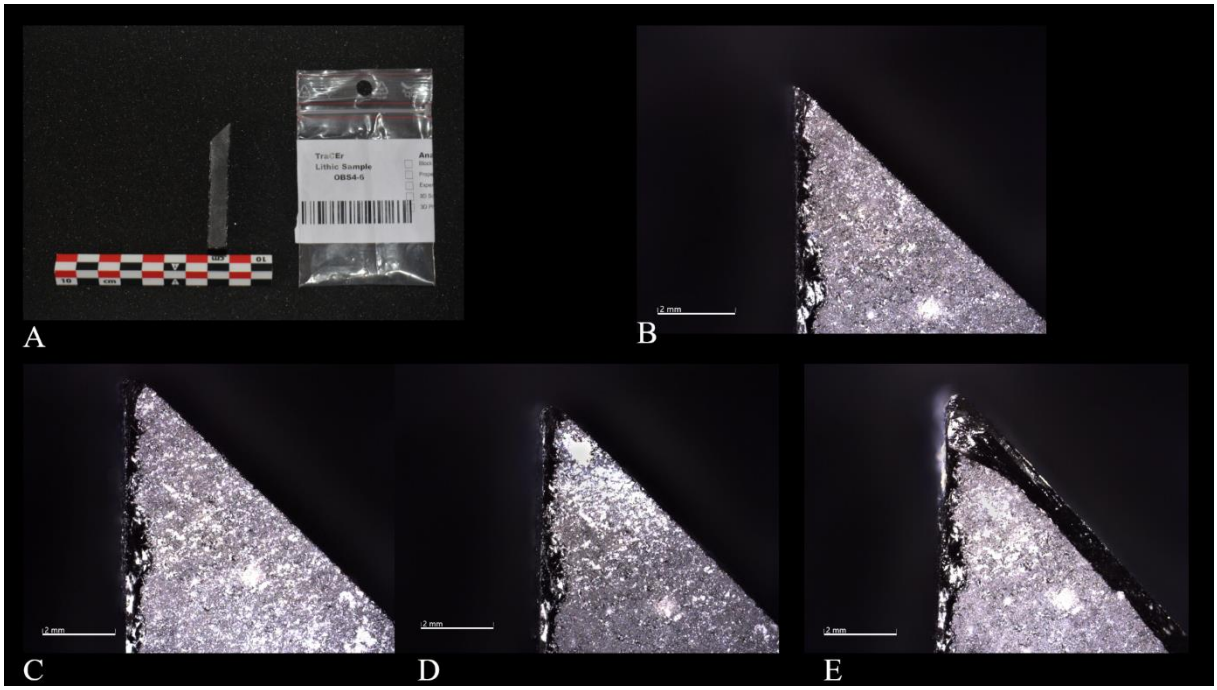

Figure 108: ZEISS Smart zoom OBS4-6 images: Profile view, A – Sample profile and ID; B – Profile view cycle 0; C – Profile view cycle 125; D - Profile view cycle 250; E – Profile view cycle 500.

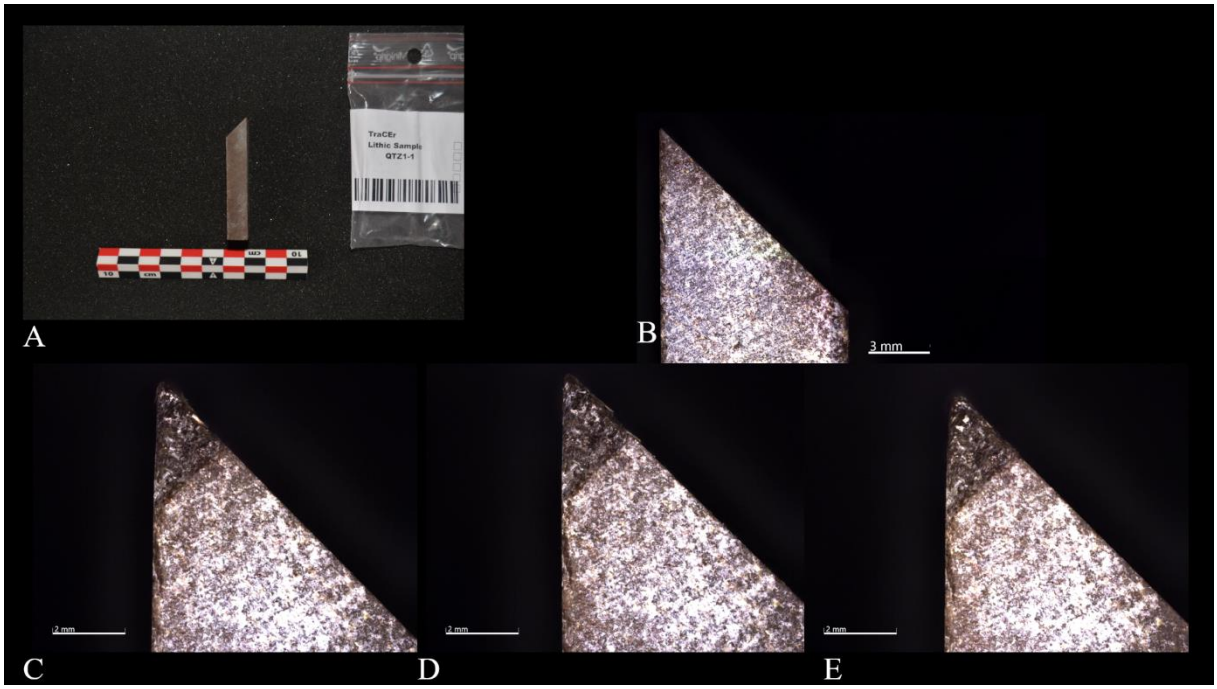

Figure 109: ZEISS Smart zoom QTZ1-1 images: Profile view, A – Sample profile and ID; B – Profile view cycle 0; C – Profile view cycle 125; D - Profile view cycle 250; E – Profile view cycle 500.

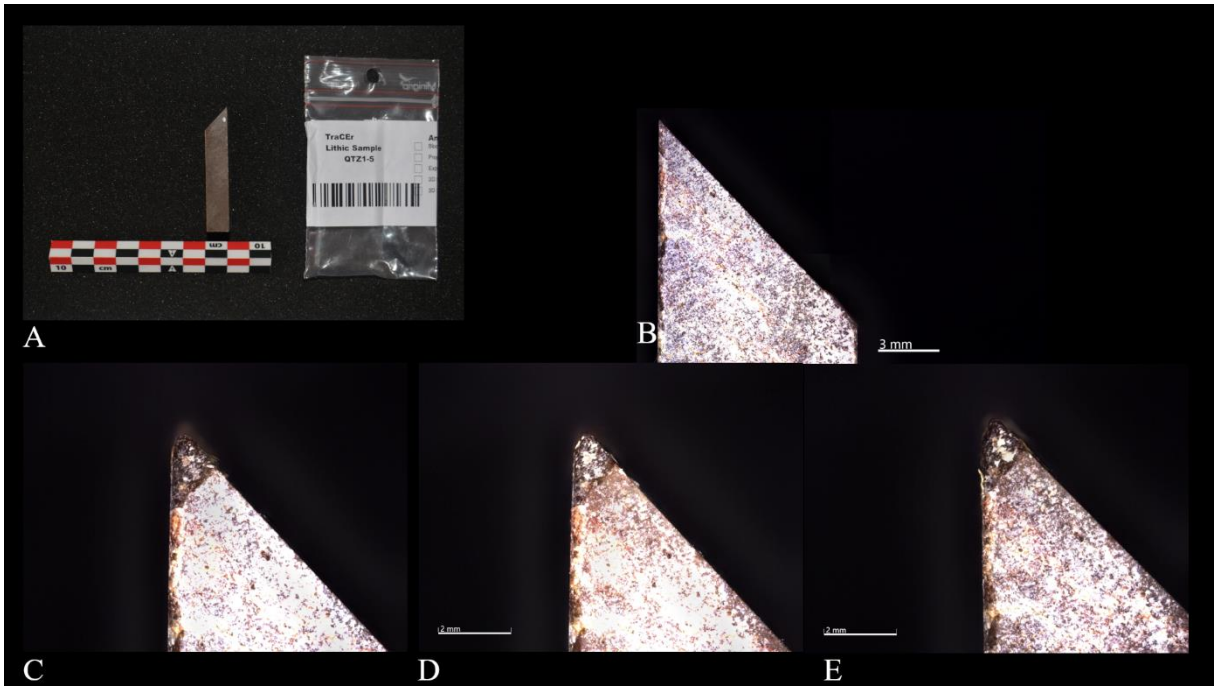

Figure 110: ZEISS Smart zoom QTZ1-5 images: Profile view, A – Sample profile and ID; B – Profile view cycle 0; C – Profile view cycle 125; D - Profile view cycle 250; E – Profile view cycle 500.

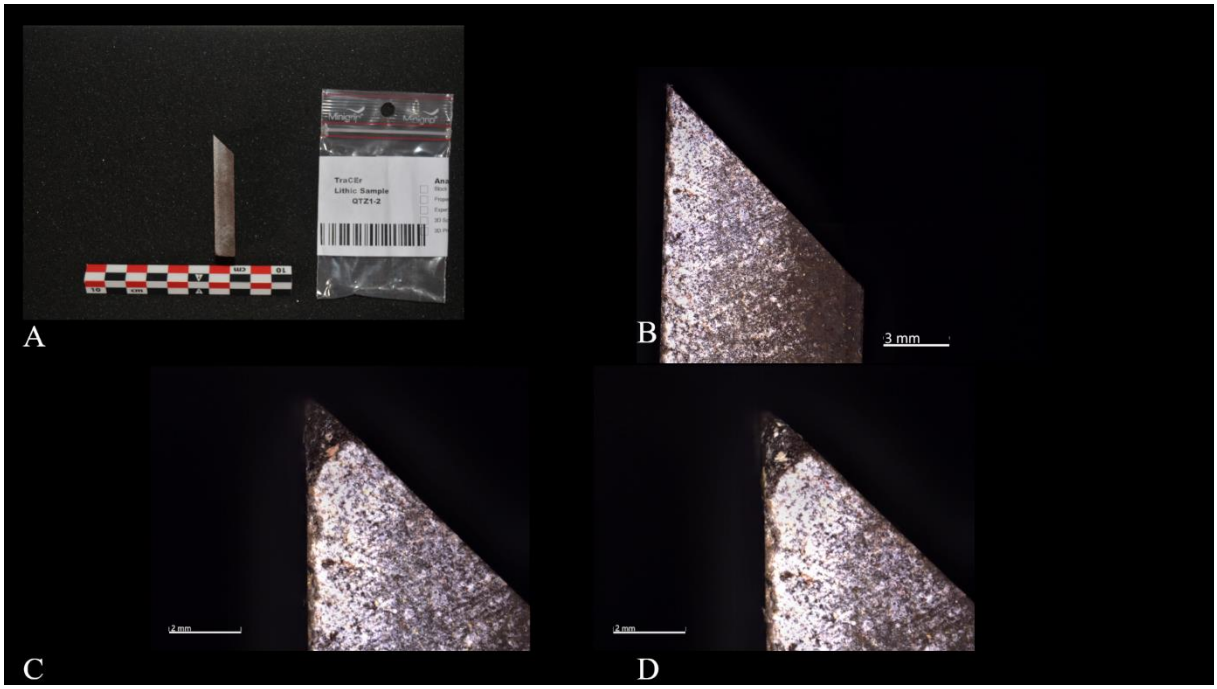

Figure 111: ZEISS Smart zoom QTZ1-1 images: Profile view, A – Sample profile and ID; B – Profile view cycle 0; C – Profile view cycle 125: D – Profile view cycle 500.

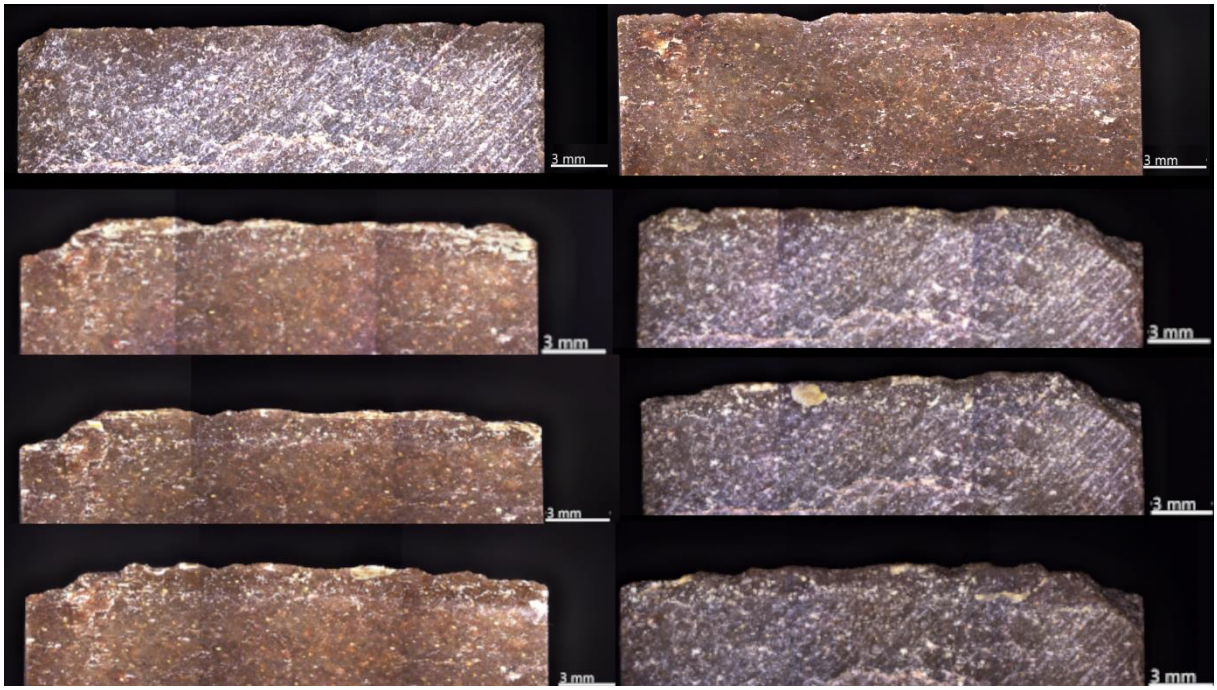

Figure 112: ZEISS Smart zoom QTZ1-1 images: Left - Back view; Right – Front view: Top to bottom (cycle 0/125/250/500).

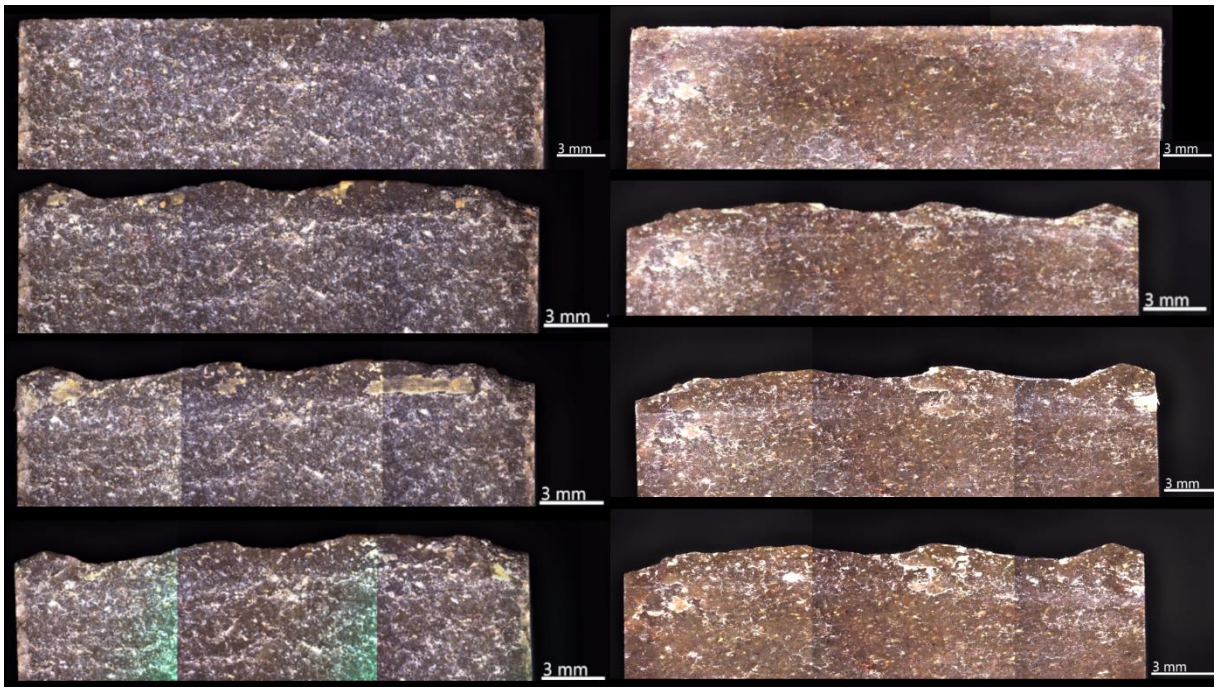

Figure 113: ZEISS Smart zoom QTZ1-2 images: Left - Back view; Right – Front view: Top to bottom (cycle 0/125/250/500).

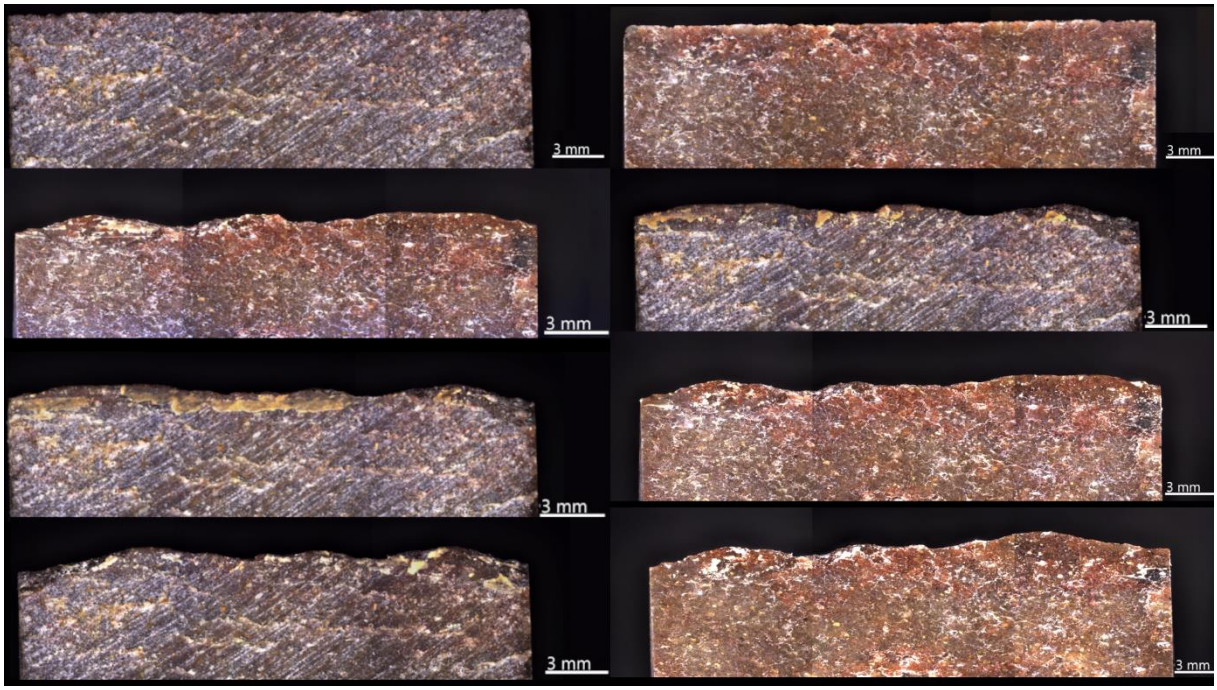

Figure 114: ZEISS Smart zoom QTZ1-5 images: Left - Back view; Right – Front view: Top to bottom (cycle 0/125/250/500).

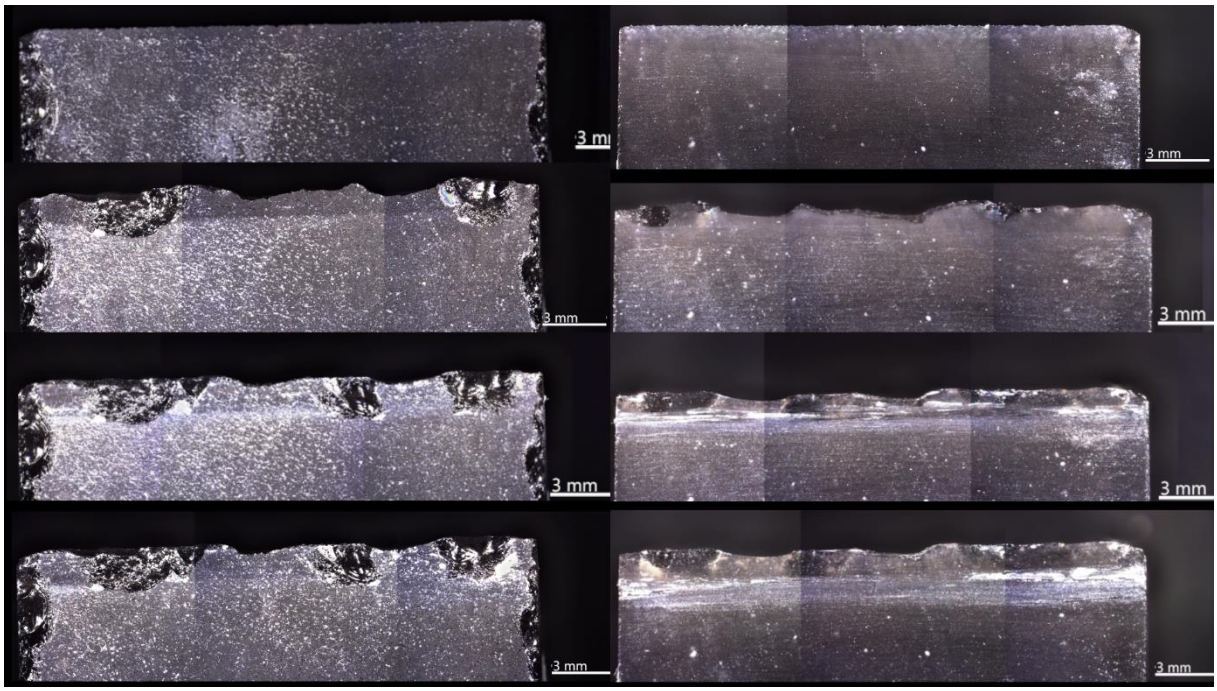

Figure 115: ZEISS Smart zoom OBS4-4 images: Left - Back view; Right – Front view: Top to bottom (cycle 0/125/250/500).

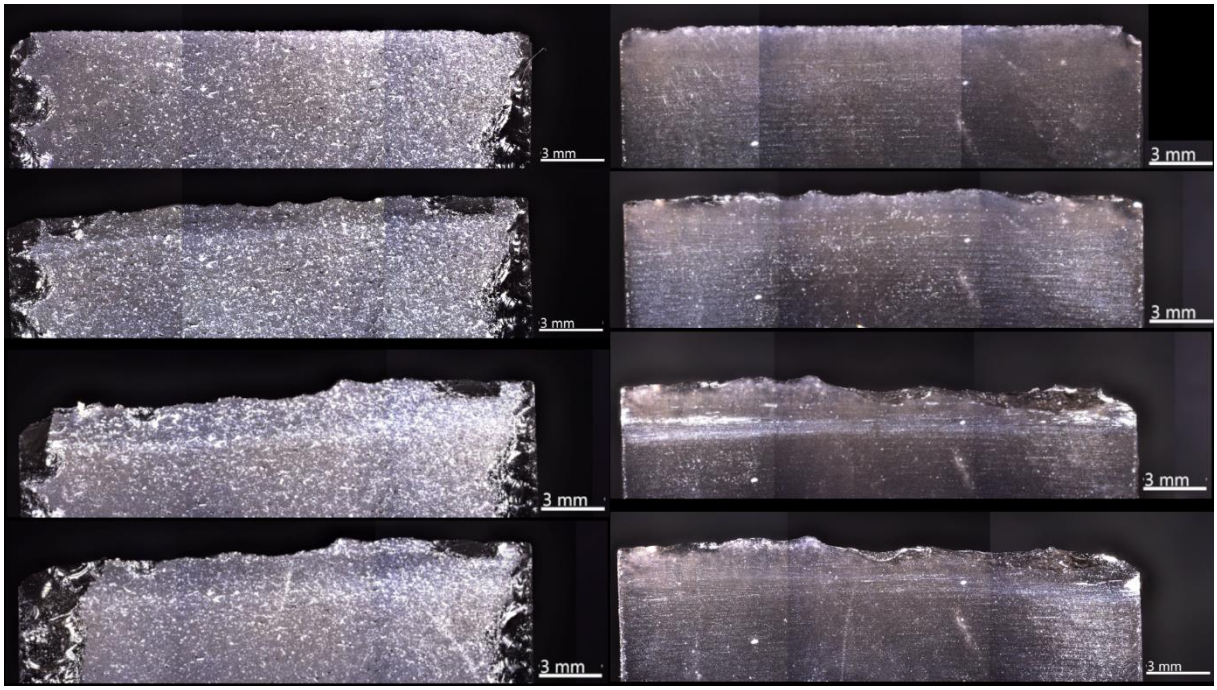

Figure 116: ZEISS Smart zoom OBS4-5 images: Left - Back view; Right – Front view: Top to bottom (cycle 0/125/250/500).

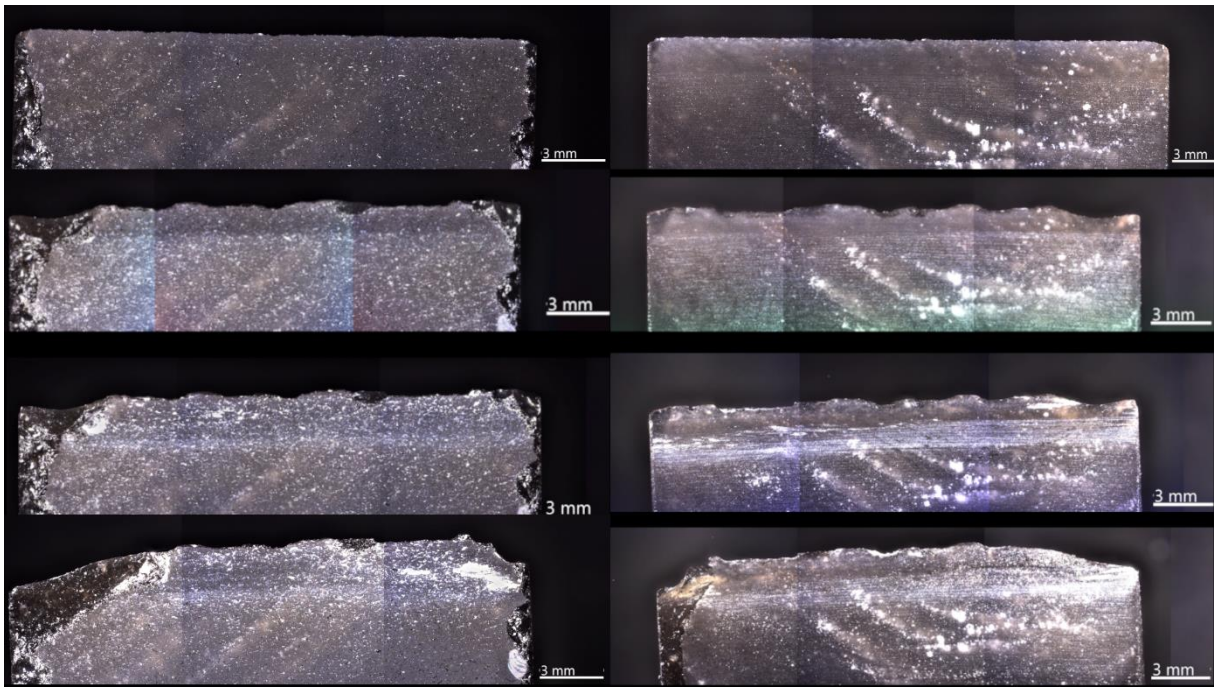

Figure 117: ZEISS Smart zoom OBS4-6 images: Left - Back view; Right – Front view: Top to bottom (cycle 0/125/250/500).

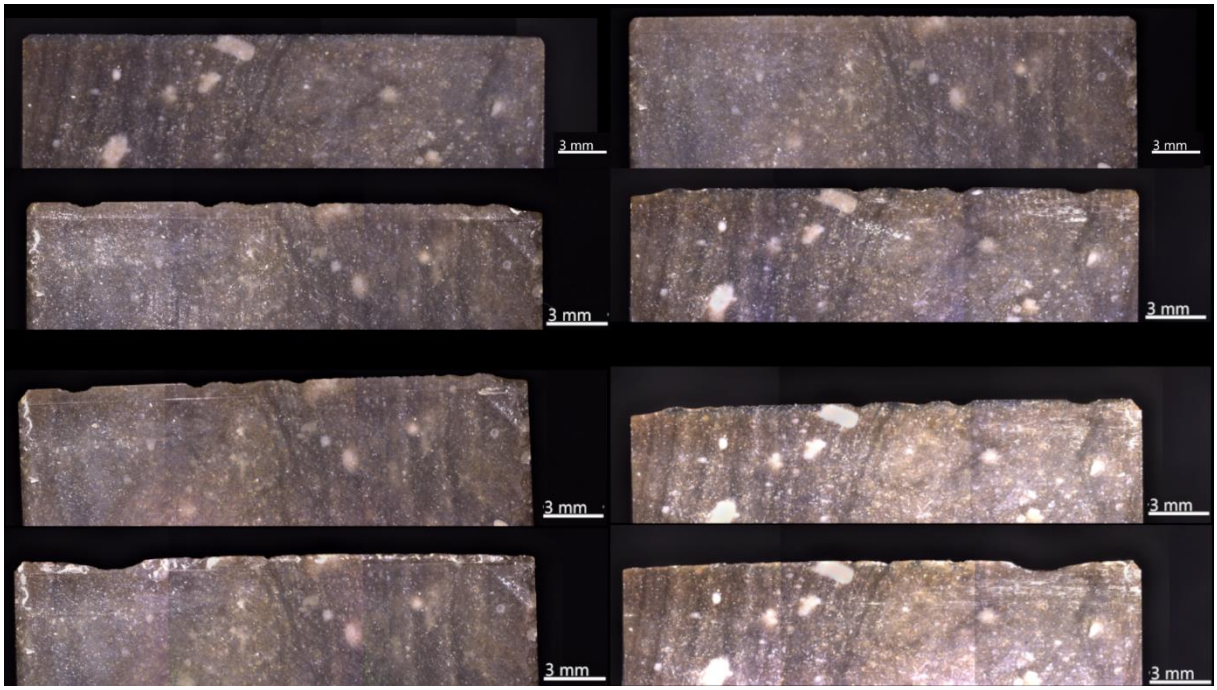

Figure 118: ZEISS Smart zoom FLT10-2 images: Left - Back view; Right – Front view: Top to bottom (cycle 0/125/250/500).

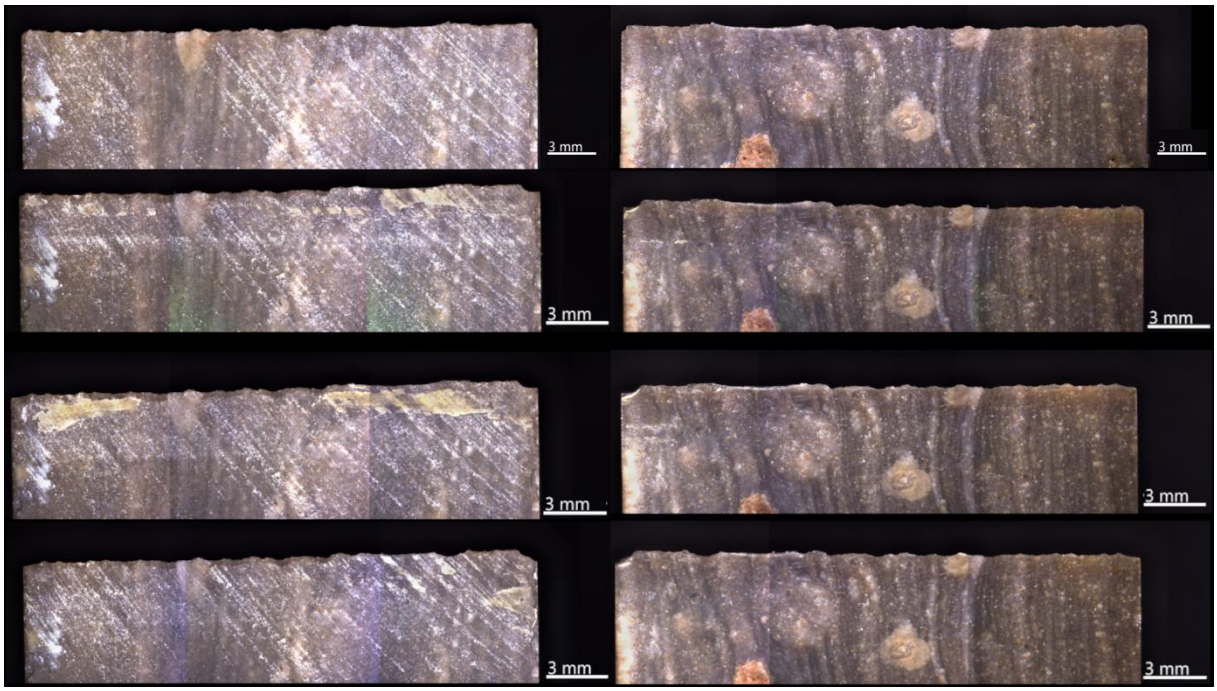

Figure 119: ZEISS Smart zoom FLT10-5 images: Left - Back view; Right – Front view: Top to bottom (cycle 0/125/250/500).

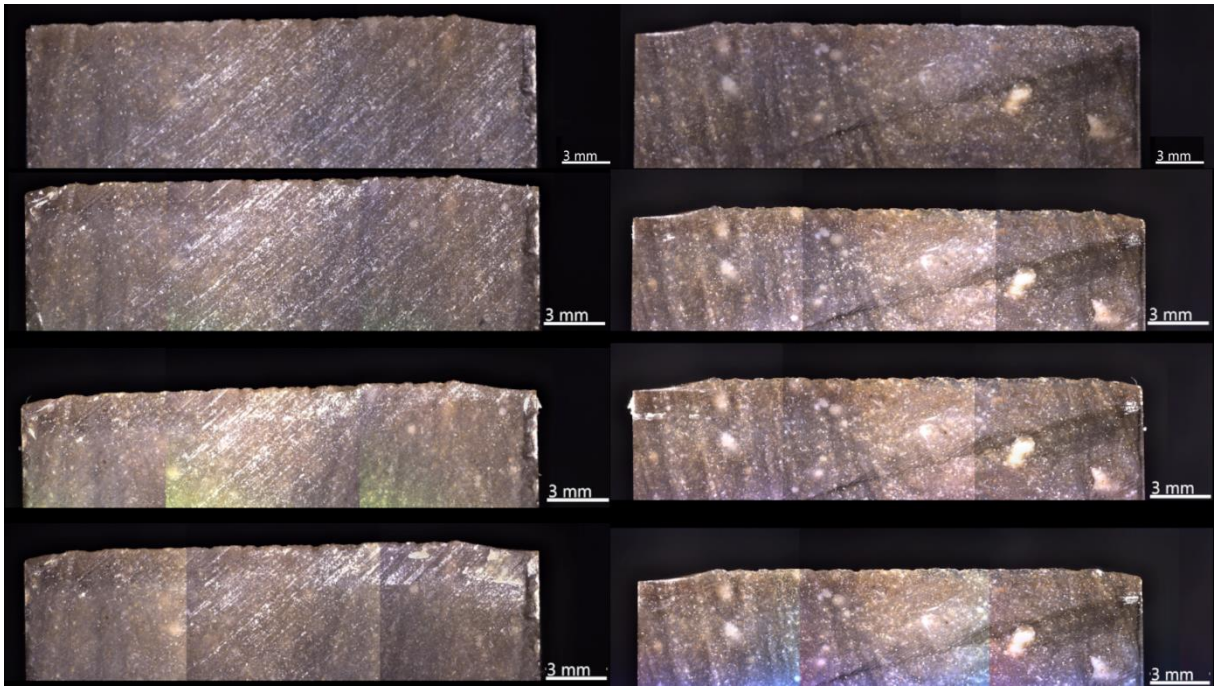

Figure 120: ZEISS Smart zoom FLT10-6 images: Left - Back view; Right – Front view: Top to bottom (cycle 0/125/250/500).

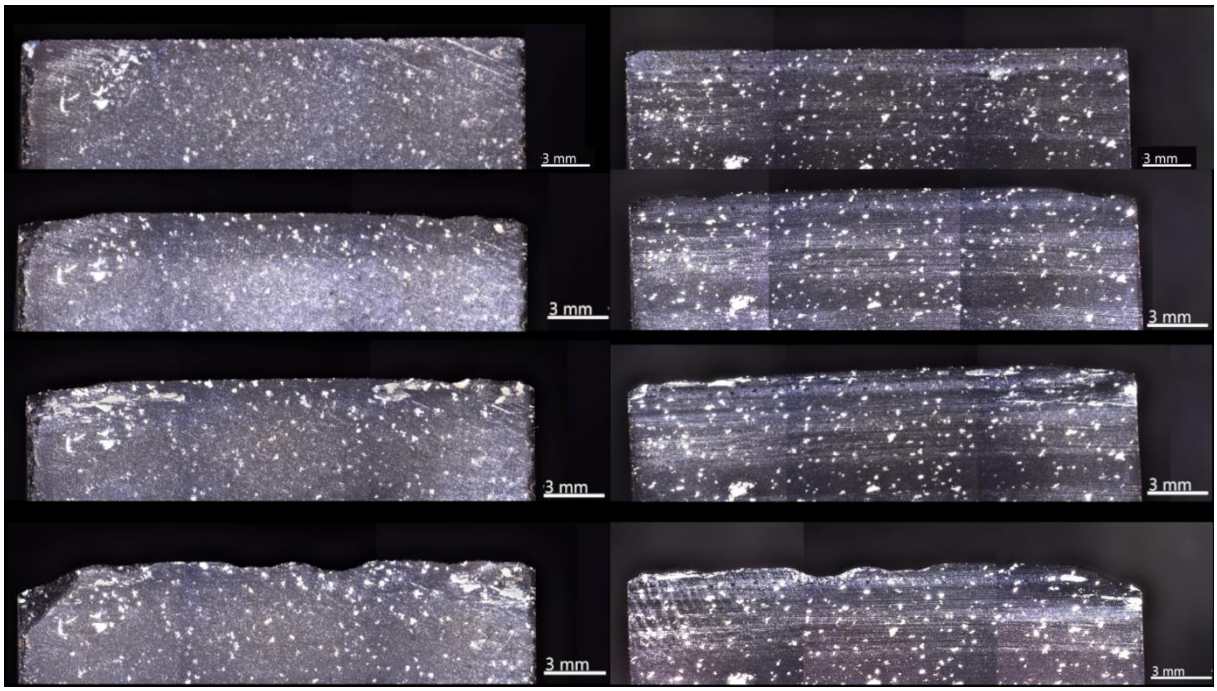

Figure 121: ZEISS Smart zoom DAC3-2 images: Left - Back view; Right – Front view: Top to bottom (cycle 0/125/250/500).

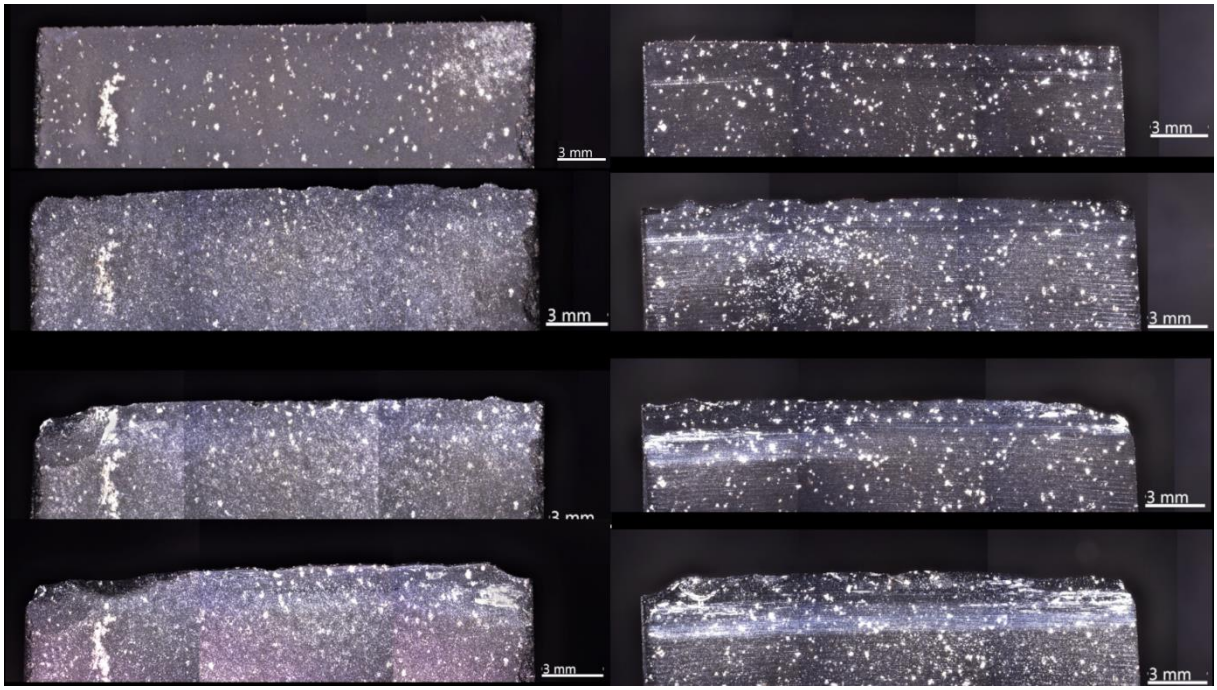

Figure 122: ZEISS Smart zoom DAC3-4 images: Left - Back view; Right – Front view: Top to bottom (cycle 0/125/250/500).

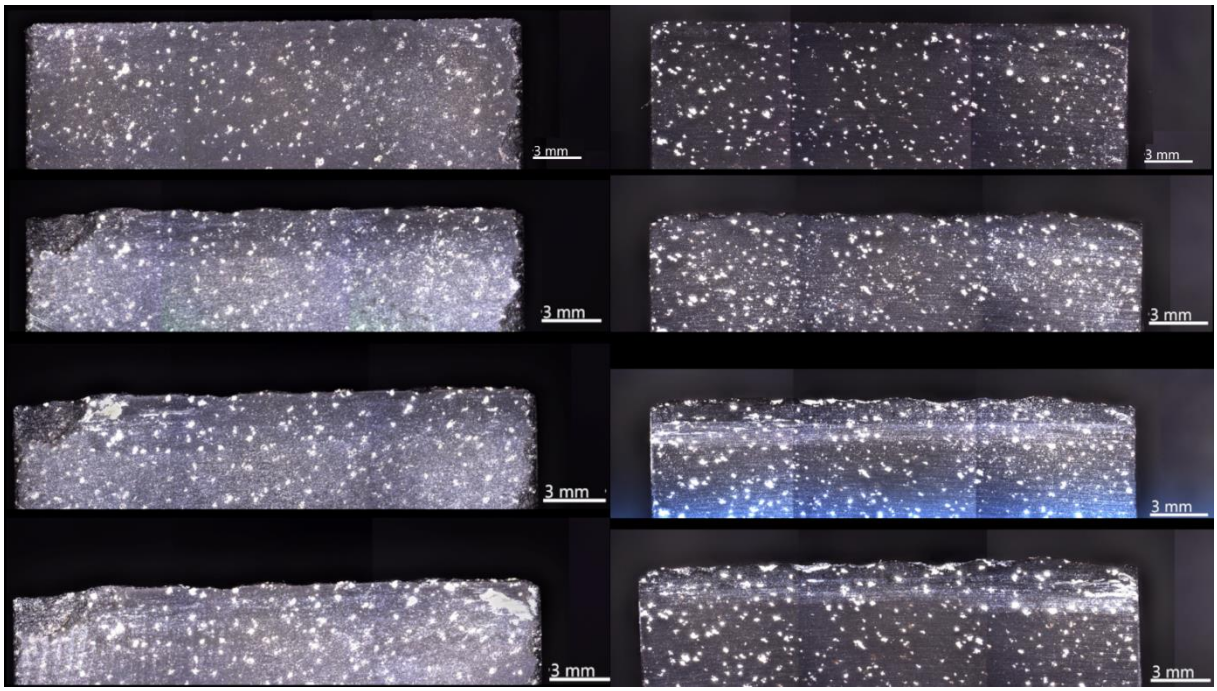

Figure 123: ZEISS Smart zoom DAC3-6 images: Left - Back view; Right – Front view: Top to bottom (cycle 0/125/250/500).

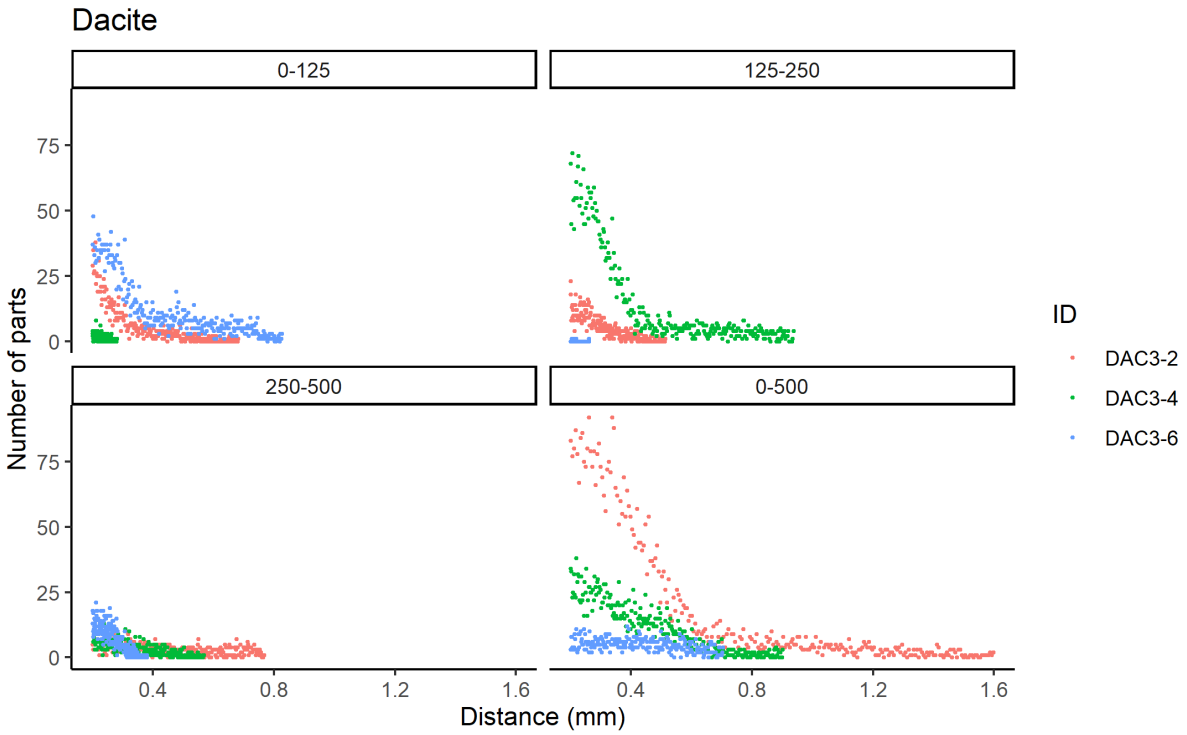

Figure 124: Plot edge damage, Dacite all cycles.

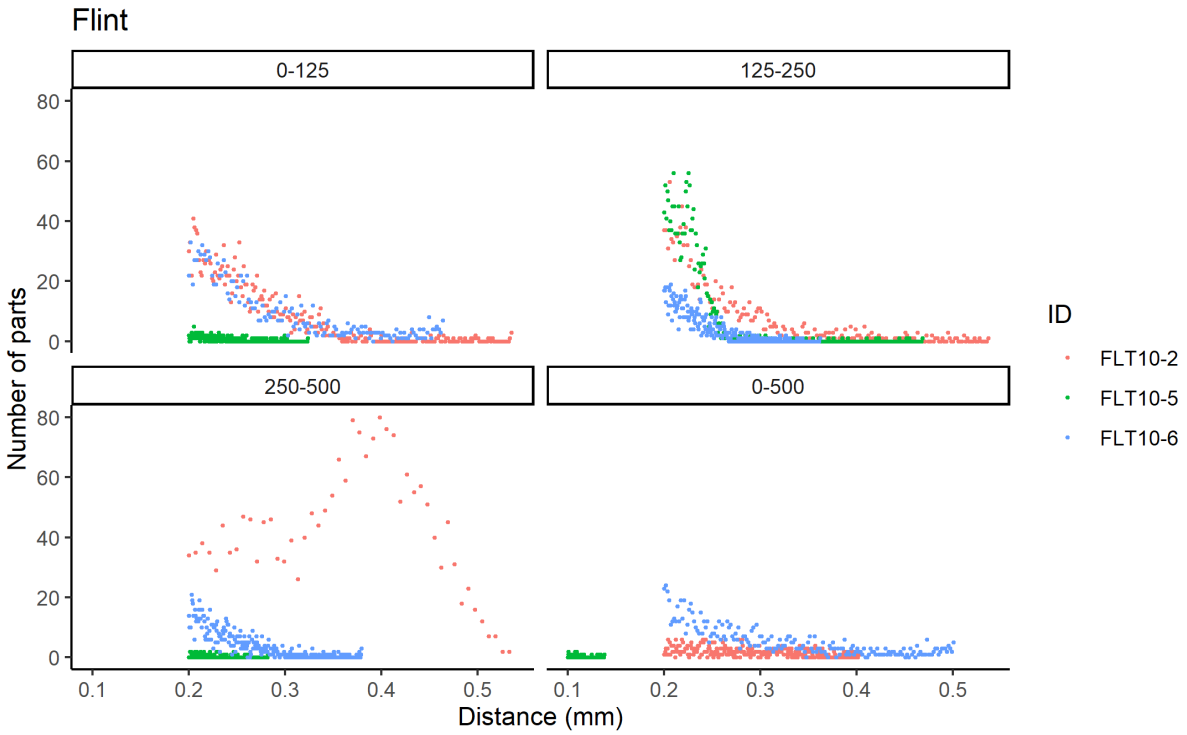

Figure 125: Plot edge damage, Flint all cycles.

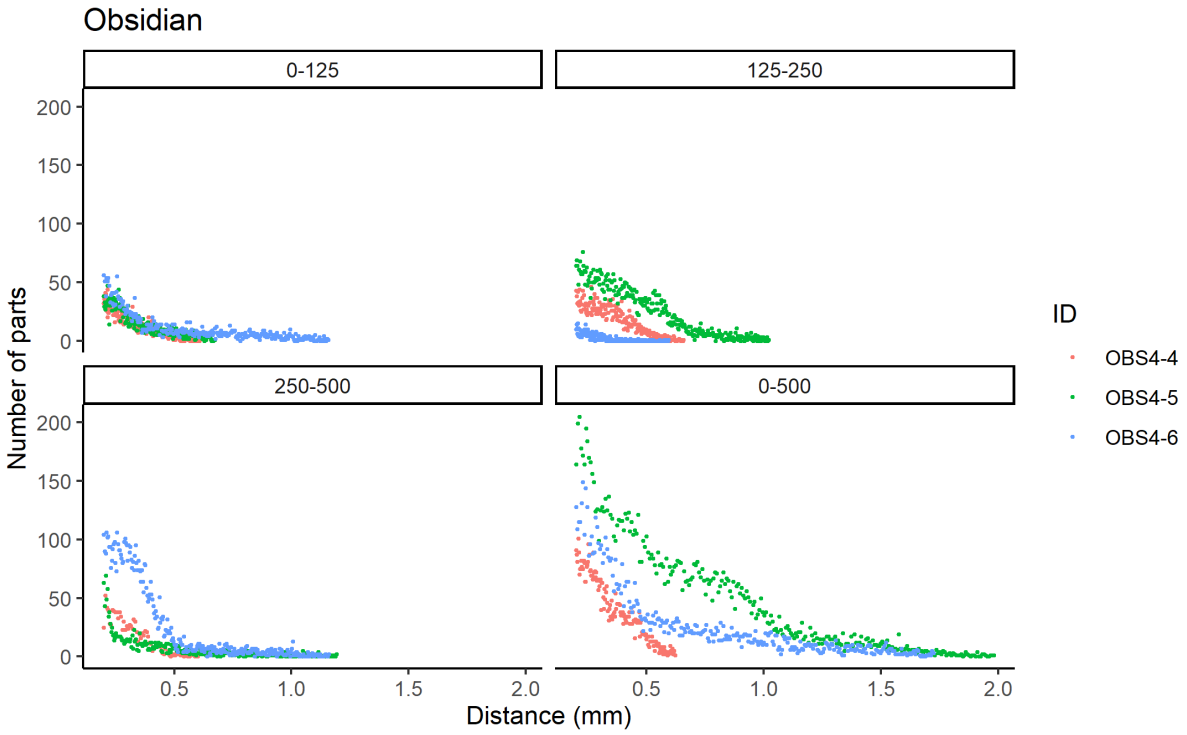

Figure 126: Plot edge damage, Obsidian all cycles.

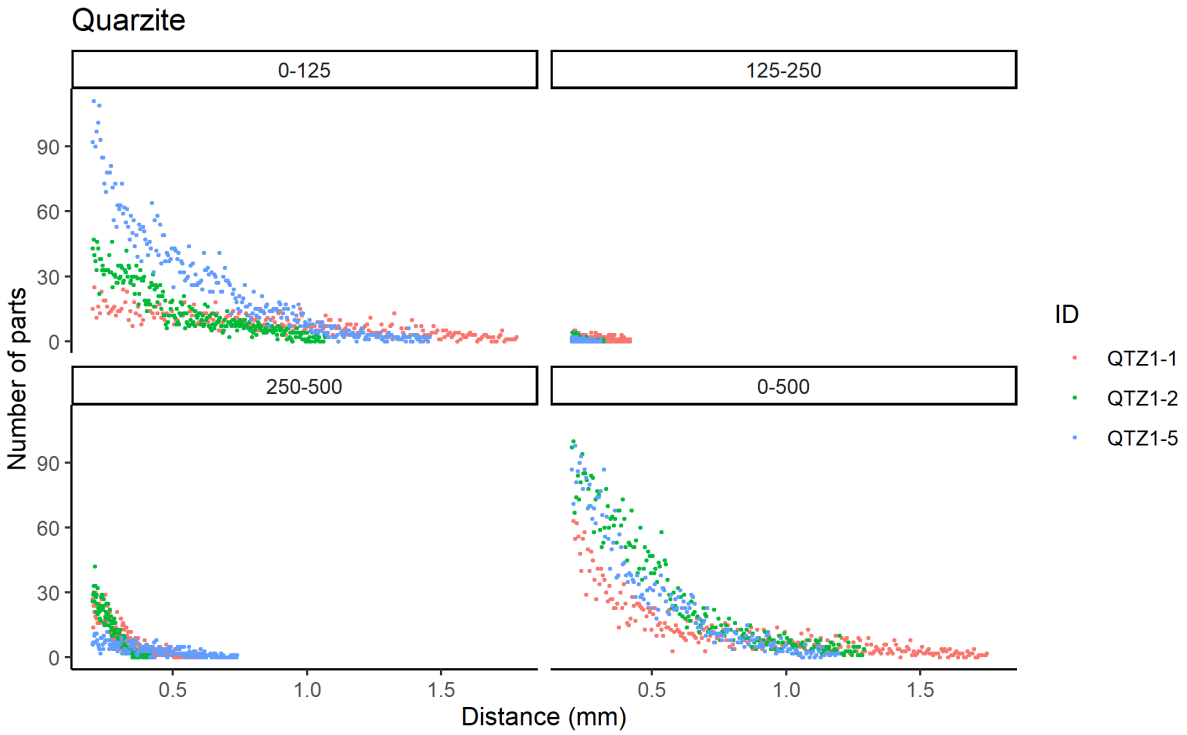

Figure 127: Plot edge damage, Quartzite all cycles.

Appendix B: R Scripts

Equotip hardness measurements

João Marreiros and David Nora

2021-07-14

Goal of the script

This script reads the csv file (measurements have been generated with the Equotip Leeb C rebound) and formats the data for a statistical analysis.
The script will:

5. Read in the original csv file and organise the data
6. Plot the data
7. Write an XLSX-file and save an R object ready for further analysis in R

Imported files are in: '../analysis/raw_data'

Figures are saved in: '../analysis/plots'

Tables are saved in: '../analysis/derived_data'

Load packages

```
library(tidyverse)
```

```
## ── Attaching packages ─────────────────────────────────────── tidyverse
1.3.1 ──
```

```
## ✓ ggplot2 3.3.5     ✓ purrr   0.3.4
## ✓ tibble  3.1.2     ✓ dplyr   1.0.7
## ✓ tidyr   1.1.3     ✓ stringr 1.4.0
## ✓ readr   1.4.0     ✓ forcats 0.5.1
```

```
## ── Conflicts ────────────────────────────────────────── tidyverse_confl
icts() ──
## x dplyr::filter() masks stats::filter()
## x dplyr::lag()    masks stats::lag()
```

```
library(AICcmodavg)
library(ggplot2)
library(utils)
library(qwraps2)
library(kableExtra)
```

```
##
## Attaching package: 'kableExtra'

## The following object is masked from 'package:dplyr':
##
##     group_rows

library(doBy)

##
## Attaching package: 'doBy'

## The following object is masked from 'package:dplyr':
##
##     order_by
```

Read in original xlsx-file

```
# List all CSV files in dir_in

imp_data <- read_csv("../raw_data/data.csv")

##
## ── Column specification ────────────────────────────────────────
────────
## cols(
##   ID = col_character(),
##   rawmaterial = col_character(),
##   Date = col_character(),
##   Time = col_time(format = ""),
##   M1 = col_double(),
##   M2 = col_double(),
##   M3 = col_double(),
##   M4 = col_double(),
##   M5 = col_double(),
##   M6 = col_double(),
##   M7 = col_double(),
##   M8 = col_double(),
##   M9 = col_double(),
##   M10 = col_double()
## )
```

Organize data

```
# organizing data
longdata <- imp_data %>%
  gather("M1", "M2","M3", "M4", "M5","M6","M7", "M8", "M9", "M10", key = M
easurment, value = HLC)

longdata
```

```
## # A tibble: 230 x 6
##    ID     rawmaterial Date       Time     Measurment   HLC
##    <chr>  <chr>       <chr>      <time>   <chr>      <dbl>
##  1 QTZ3-6 quartzite   09/06/2021 14:27:34 M1           876
##  2 QTZ3-5 quartzite   09/06/2021 14:22:10 M1           919
##  3 QTZ3-4 quartzite   09/06/2021 14:18:29 M1           913
##  4 QTZ3-3 quartzite   09/06/2021 14:15:35 M1           822
##  5 QTZ3-2 quartzite   09/06/2021 14:12:22 M1           863
##  6 QTZ3-1 quartzite   09/06/2021 14:05:18 M1           910
##  7 OBS4-6 obsidian    09/06/2021 13:59:22 M1           927
##  8 OBS4-5 obsidian    09/06/2021 13:51:50 M1           969
##  9 OBS4-4 obsidian    09/06/2021 13:48:41 M1           966
## 10 OBS4-3 obsidian    09/06/2021 13:43:07 M1           957
## # … with 220 more rows

write_csv(longdata, "../derived_data/longdata.csv")
```

Data analysis - descriptive stats

```
# descriptive statistics

nminmaxmeanmedsd <- function(x){
    y <- x[!is.na(x)]
    n_test <- length(y)
    min_test <- min(y)
    max_test <- max(y)
    mean_test <- mean(y)
    med_test <- median(y)
    sd_test <- sd(y)
    out <- c(n_test, min_test, max_test, mean_test, med_test, sd_test)
    names(out) <- c("n", "min", "max", "mean", "median", "sd")
    return(out)
}

num.var <- 6:length(longdata)
stats <- summaryBy(.~rawmaterial, data=longdata[c("rawmaterial", names(lon
gdata)[num.var])], FUN=nminmaxmeanmedsd)

stats

## # A tibble: 4 x 7
##   rawmaterial HLC.n HLC.min HLC.max HLC.mean HLC.median HLC.sd
##   <chr>       <dbl>   <dbl>   <dbl>    <dbl>      <dbl>  <dbl>
## 1 dacite         60     865     979     958.        963    18.5
## 2 flint          50     900     972     954.        960.   17.5
## 3 obsidian       60     893     970     952.        958.   16.0
## 4 quartzite      60     735     939     886.        894    37.7

write_csv(stats, "../derived_data/stats.csv")
```

ANOVA analysis

```r
# anova
#longdata$rawmaterial <- as.factor(longdata$rawmaterial)

anova <- aov(HLC ~ rawmaterial, data = longdata)
anovafactor <- summary(aov(HLC ~ factor(rawmaterial), data = longdata))
one <- oneway.test(HLC ~ rawmaterial, data = longdata)
tuk <- TukeyHSD(aov(HLC ~ factor(rawmaterial), data = longdata))

anova
```

```
## Call:
##    aov(formula = HLC ~ rawmaterial, data = longdata)
##
## Terms:
##                 rawmaterial Residuals
## Sum of Squares     213345.5  134127.6
## Deg. of Freedom           3       226
##
## Residual standard error: 24.36155
## Estimated effects may be unbalanced
```

```r
anovafactor
```

```
##                       Df Sum Sq Mean Sq F value Pr(>F)
## factor(rawmaterial)   3 213345   71115   119.8 <2e-16 ***
## Residuals           226 134128     593
## ---
## Signif. codes:  0 '***' 0.001 '**' 0.01 '*' 0.05 '.' 0.1 ' ' 1
```

```r
one
```

```
##
##  One-way analysis of means (not assuming equal variances)
##
## data:  HLC and rawmaterial
## F = 62.731, num df = 3.00, denom df = 122.33, p-value < 2.2e-16
```

```r
tuk
```

```
##   Tukey multiple comparisons of means
##     95% family-wise confidence level
##
## Fit: aov(formula = HLC ~ factor(rawmaterial), data = longdata)
##
## $`factor(rawmaterial)`
##                            diff       lwr        upr     p adj
## flint-dacite          -4.556667 -16.63054   7.517202 0.7628076
## obsidian-dacite       -5.800000 -17.31198   5.711983 0.5613191
## quartzite-dacite     -72.566667 -84.07865 -61.054684 0.0000000
## obsidian-flint        -1.243333 -13.31720  10.830536 0.9933580
## quartzite-flint      -68.010000 -80.08387 -55.936131 0.0000000
## quartzite-obsidian   -66.766667 -78.27865 -55.254684 0.0000000
```

Data analysis - plot

```
# boxplot
data_plot <- ggplot (longdata, aes(rawmaterial, HLC, color = rawmaterial))
+
             theme_classic() +
             theme(legend.title = element_blank()) +
             geom_boxplot() +
             geom_jitter() + labs(x="Raw material", y="Leeb Rebound Hardne
ss in HLC", title="")

print(data_plot)
```

Session Info() and RStudio version

```
sessionInfo()
```

```
## R version 4.0.4 (2021-02-15)
## Platform: x86_64-apple-darwin17.0 (64-bit)
## Running under: macOS Catalina 10.15.7
##
## Matrix products: default
## BLAS:   /Library/Frameworks/R.framework/Versions/4.0/Resources/lib/libR
blas.dylib
## LAPACK: /Library/Frameworks/R.framework/Versions/4.0/Resources/lib/libR
lapack.dylib
##
## locale:
## [1] en_US.UTF-8/en_US.UTF-8/en_US.UTF-8/C/en_US.UTF-8/en_US.UTF-8
##
## attached base packages:
## [1] stats     graphics  grDevices utils     datasets  methods   base
##
## other attached packages:
##  [1] doBy_4.6.10      kableExtra_1.3.4 qwraps2_0.5.2    AICcmodavg_2.3-
1
##  [5] forcats_0.5.1    stringr_1.4.0    dplyr_1.0.7      purrr_0.3.4
##  [9] readr_1.4.0      tidyr_1.1.3      tibble_3.1.2     ggplot2_3.3.5
## [13] tidyverse_1.3.1
##
## loaded via a namespace (and not attached):
##  [1] httr_1.4.2           VGAM_1.1-5           jsonlite_1.7.2
##  [4] viridisLite_0.4.0    splines_4.0.4        modelr_0.1.8
##  [7] microbenchmark_1.4-7 assertthat_0.2.1     highr_0.9
## [10] sp_1.4-5             stats4_4.0.4         cellranger_1.1.0
## [13] yaml_2.2.1           pillar_1.6.1         backports_1.2.1
## [16] lattice_0.20-44      glue_1.4.2           digest_0.6.27
## [19] rvest_1.0.0          colorspace_2.0-2     htmltools_0.5.1.1
## [22] Matrix_1.3-4         plyr_1.8.6           pkgconfig_2.0.3
## [25] broom_0.7.8          raster_3.4-13        curry_0.1.1
## [28] haven_2.4.1          xtable_1.8-4         scales_1.1.1
```

```
## [31] webshot_0.5.2        svglite_2.0.0        farver_2.1.0
## [34] generics_0.1.0       ellipsis_0.3.2       withr_2.4.2
## [37] cli_2.5.0            survival_3.2-11      magrittr_2.0.1
## [40] crayon_1.4.1         readxl_1.3.1         evaluate_0.14
## [43] fs_1.5.0             fansi_0.5.0          nlme_3.1-152
## [46] MASS_7.3-54          xml2_1.3.2           tools_4.0.4
## [49] hms_1.1.0            lifecycle_1.0.0      munsell_0.5.0
## [52] reprex_2.0.0         Deriv_4.1.3          compiler_4.0.4
## [55] systemfonts_1.0.2    rlang_0.4.11         grid_4.0.4
## [58] rstudioapi_0.13      labeling_0.4.2       rmarkdown_2.9
## [61] gtable_0.3.0         codetools_0.2-18     DBI_1.1.1
## [64] R6_2.5.0             lubridate_1.7.10     knitr_1.33
## [67] utf8_1.2.1           stringi_1.6.2        parallel_4.0.4
## [70] unmarked_1.1.1       Rcpp_1.0.6           vctrs_0.3.8
## [73] dbplyr_2.1.1         tidyselect_1.1.1     xfun_0.24
```

Import SMARTTESTER datasets

Joao Marreiros and David Nora

2021-07-14 16:08:08

Goal of the script

This script imports and merges all single TXT-files (strokes + sensors) produced with the Inotec Smarttester. The experiment involved 12 samples (3 samples from each 4 raw materials) which have been used in four cycles (0-250, 250-500, and 500-1000 strokes) respectively. The script will:

8. Read in the original TXT-files

9. Format and merge the data for each sample
10. Combine the data from the 12 samples into one
11. Write an XLSX-file and save an R object ready for further analysis in R

This script is an adapted from...

```
dir_in <- "analysis_inotec/raw_data/"
dir_out <- "analysis_inotec/derived_data/"
```

Raw data must be located in “analysis_inotec/raw_data/”.
Formatted data will be saved in “analysis_inotec/derived_data/”. The knit directory for this script is the project directory.

Load packages

```
library(tidyverse)
library(R.utils)
library(openxlsx)
library(tools)
```

List all files and get names of the files

```
# List all CSV files in dir_in
TXT_files <- list.files(dir_in, pattern = "\\.txt$", recursive = TRUE, ful
l.names = TRUE)

# Extract sample names from paths
samples_names <- dirname(dirname(dirname(TXT_files))) %>% # Path of folder
```

```
3 levels higher
                  basename() %>%                                  # Name of folder
3 levels higher
                  unique()                                        # Unique names
```

Define sensors

```
sensors <- data.frame(mess = paste0("Messung", 1:5),
                      meas = c("Force", "Friction", "Depth", "Position", "
Velocity"),
                      unit = c("N", "N", "mm", "mm", "mm/s"))
```

Merge all files and format the data

```
# Create named list, 1 element for each sample
sampl <- vector(mode = "list", length = length(samples_names))
names(sampl) <- samples_names

# For each sample
for (s in seq_along(samples_names)) {

  # Gets information through the path name and defines the cycle, raw mate
rial and
  # contact material
  folder <- paste0(samples_names[s], "/") %>%
            grep(TXT_files, value = TRUE) %>%
            dirname() %>%
            dirname() %>%
            unique() %>%
            basename() %>%
            strsplit(., "_")

  cycles <- sapply(folder, FUN = function(x) x[[3]])
  # Defines the number of the first stroke per cycle based on the name fro
m the folders
  cycle_start <- gsub("-.*$", "", x = cycles) %>%
                 # Converts into numeric
                 as.numeric()

  # Orders the cycles
  order_cycles <- order(cycle_start)
  cycle_start <- cycle_start[order_cycles]
  cycle_start[1] <- 1
  cycles <- cycles[order_cycles]

  # Takes the information about the contact material
  cont_mat <- sapply(folder, FUN = function(x) x[[2]]) %>%
              unique()

  # Takes the information about the raw material
```

```
  raw_mat <- ifelse(grepl("FLT", names(sampl)[s]), "Flint", "Lydite")


  # Create named list, 1 element for each sensor ("Messung")
  sampl[[s]] <- vector(mode = "list", length = nrow(sensors))
  names(sampl[[s]]) <- sensors [["meas"]]

  # For each sensor ("Messung")
  for (m in seq_along(sampl[[s]])) {

    # Extract file names of all strokes for the given sensor
    # Paste sample name and slash to avoid partial matching
    s_m <- paste0(samples_names[[s]], "/") %>%
           # Extract sample "s" from all files
           grep(TXT_files, value = TRUE) %>%
           # Extract sensor "m" from sample "s"
           grep(sensors[["mess"]][m], ., value = TRUE)

    # Create named list, 1 element for each stroke bin
    sampl[[s]][[m]] <- vector(mode = "list", length = length(cycles))
    names(sampl[[s]][[m]]) <- cycles

    # For each cycle
    for (cy in seq_along(sampl[[s]][[m]])) {

      # Extract file names of all strokes for each cycle
      s_m_cy <- grep(cycles[cy], s_m, value = TRUE)

      # Create named list, 1 element for each stroke
      sampl[[s]][[m]][[cy]] <- vector(mode = "list", length = length(s_m_c
y))
      names(sampl[[s]][[m]][[cy]]) <- paste0("Stroke", seq_along(s_m_cy))

      # For each stroke
      for (st in seq_along(s_m_cy)) {

        # Read in TXT file
        sampl[[s]][[m]][[cy]][[st]] <- read.table(s_m_cy[st], skip = 4, se
p = ";") %>%

          # Add columns Step based on V2 and Stroke based on "st"
          mutate(Step = V2/100000+1, Stroke = st -1 + cycle_start[cy]) %>%

          # Select columns stroke, step, V1
          select(Stroke, Step, V1)

        # Rename column V1 based on "m"
        names(sampl[[s]][[m]][[cy]][[st]])[3] <- sensors[m, "meas"]
      }
```

```
      # rbind all files per cycle
      sampl[[s]][[m]][[cy]] <- do.call(rbind, sampl[[s]][[m]][[cy]])
    }

    # rbind all cycles per sensor
    sampl[[s]][[m]] <- do.call(rbind, sampl[[s]][[m]])
  }

  # rbind all sensors per sample
  sampl[[s]] <- full_join(sampl[[s]][[1]], sampl[[s]][[2]]) %>%
    full_join(sampl[[s]][[3]]) %>%
    full_join(sampl[[s]][[4]]) %>%
    full_join(sampl[[s]][[5]]) %>%
    mutate(Sample = names(sampl)[s], Raw_material = raw_mat,
           Contact_material = cont_mat) %>%

    select(Sample, Raw_material, Contact_material, everything())
}

# rbind all samples
sampl <- do.call(rbind, sampl)
```

Save data

Format name of output file

```
file_out <- "sampl"
```

Write to XLSX

```
write.xlsx(list(data = sampl, units = sensors), file = paste0(dir_out, fil
e_out, ".xlsx"))
```

Save R object

```
saveObject(sampl, file = paste0(dir_out, file_out, ".Rbin"))
```

```
Warning in gzfile(file, "wb"): cannot open compressed file 'analysis_inote
c/
derived_data/sampl.Rbin.tmp', probable reason 'No such file or directory'

Error in gzfile(file, "wb"): cannot open the connection
```

Session Info() and RStudio version

```
sessionInfo()
```

```
R version 4.0.4 (2021-02-15)
Platform: x86_64-apple-darwin17.0 (64-bit)
Running under: macOS Catalina 10.15.7

Matrix products: default
BLAS:   /Library/Frameworks/R.framework/Versions/4.0/Resources/lib/libRbla
s.dylib
LAPACK: /Library/Frameworks/R.framework/Versions/4.0/Resources/lib/libRlap
ack.dylib

locale:
[1] en_US.UTF-8/en_US.UTF-8/en_US.UTF-8/C/en_US.UTF-8/en_US.UTF-8

attached base packages:
[1] tools     stats     graphics  grDevices utils     datasets  methods
[8] base

other attached packages:
 [1] openxlsx_4.2.4    R.utils_2.10.1    R.oo_1.24.0       R.methodsS3_1.8
.1
 [5] forcats_0.5.1     stringr_1.4.0     dplyr_1.0.7       purrr_0.3.4
 [9] readr_1.4.0       tidyr_1.1.3       tibble_3.1.2      ggplot2_3.3.5
[13] tidyverse_1.3.1

loaded via a namespace (and not attached):
 [1] tidyselect_1.1.1  xfun_0.24         haven_2.4.1       colorspace_2.0-
2
 [5] vctrs_0.3.8       generics_0.1.0    htmltools_0.5.1.1 yaml_2.2.1
 [9] utf8_1.2.1        rlang_0.4.11      pillar_1.6.1      glue_1.4.2
[13] withr_2.4.2       DBI_1.1.1         dbplyr_2.1.1      modelr_0.1.8
[17] readxl_1.3.1      lifecycle_1.0.0   munsell_0.5.0     gtable_0.3.0
[21] cellranger_1.1.0  zip_2.2.0         rvest_1.0.0       evaluate_0.14
[25] knitr_1.33        fansi_0.5.0       broom_0.7.8       Rcpp_1.0.6
[29] scales_1.1.1      backports_1.2.1   jsonlite_1.7.2    fs_1.5.0
[33] hms_1.1.0         digest_0.6.27     stringi_1.6.2     grid_4.0.4
[37] cli_2.5.0         magrittr_2.0.1    crayon_1.4.1      pkgconfig_2.0.3
[41] ellipsis_0.3.2    xml2_1.3.2        reprex_2.0.0      lubridate_1.7.1
0
[45] assertthat_0.2.1  rmarkdown_2.9     httr_1.4.2        rstudioapi_0.13
[49] R6_2.5.0          compiler_4.0.4
```

END OF SCRIPT

Plots_inotec_data

João Marreiros and David Nora

2021-09-27 20:11:00

Goal of the script

This script plots all sensor data in order to visualizes the measurements recorded throughout the tool function experiment. In this study the variable of interest is the *Penetration depth*

```
dir_in <- "../derived_data"
dir_out <- "../plots"
```

Raw data must be located in ~/../derived_data.
Formatted data will be saved in ~/../plots. The knit directory for this script is the project directory.

Load packages

```
library(R.utils)
library(ggplot2)
library(tools)
library(tidyverse)
library(patchwork)
library(doBy)
library(ggrepel)
library(openxlsx)
library(readxl)
```

Get name, path and information of the file

```
data_file <- list.files(dir_in, pattern = "\\.Rbin$", full.names = TRUE)
md5_in <- md5sum(data_file)
info_in <- data.frame(file = basename(names(md5_in)), checksum = md5_in, r
ow.names = NULL)
info_in
```

```
        file                            checksum
1 sampl.Rbin dc6531b4df62a2e1d84ed75fcb7d1b59
```

Load data into R object

```
imp_data <- loadObject(data_file)
str(imp_data)

'data.frame':   114706 obs. of  10 variables:
 $ Sample          : chr  "DAC3-2" "DAC3-2" "DAC3-2" "DAC3-2" ...
 $ Raw_material    : chr  "Dacite" "Dacite" "Dacite" "Dacite" ...
 $ Contact_material: chr  "wood" "wood" "wood" "wood" ...
 $ Stroke          : num  1 1 1 1 1 1 1 1 1 ...
 $ Step            : num  1 2 3 4 5 6 7 8 9 10 ...
 $ Force           : num  -58.8 -59.3 -61.6 -56.7 -58 ...
 $ Friction        : num  -2.46 -9.88 -31.78 -53.99 -64.34 ...
 $ Depth           : num  13.8 13.8 13.6 13.3 13.1 ...
 $ Position        : num  260 263 297 356 387 ...
 $ Velocity        : num  -0.0031 106.7299 502.972 551.2161 162.7834 ...

# replace "stroke" by "cycle"
colnames(imp_data)[colnames(imp_data) == "Stroke"] <- "Cycle"
```

The imported file is: “~/../derived_data/sampl.Rbin”

Plot each of the selected numeric variable

Plot showing the absolut penetration depths

```
# calculates the absolute depths reached per sample
abs.depth <- function(x) {
  noNA <- x[!is.na(x)]
  out <- abs(min(noNA) - max(noNA))
}

# Define grouping variable and compute the summary statistics
depth <- summaryBy(Depth ~ Sample+Raw_material+Contact_material,
                   data=imp_data,
                   FUN=abs.depth)

str(depth)

'data.frame':   12 obs. of  4 variables:
 $ Sample          : chr  "DAC3-2" "DAC3-4" "DAC3-6" "FLT10-2" ...
 $ Raw_material    : chr  "Dacite" "Dacite" "Dacite" "Flint" ...
 $ Contact_material: chr  "wood" "wood" "wood" "wood" ...
 $ Depth.abs.depth : num  2.94 2.5 2.91 2.88 3.89 ...

depth[["Contact_material"]] <- factor(depth[["Contact_material"]])

# plots all depth points in one facet plot (contact material together)
p3 <- ggplot(data = depth, aes(x = Contact_material,
                               y = Depth.abs.depth, colour =
                                 Raw_material)) +
```

```
       geom_point() + labs(y = "Absolute depth (mm)") +
       facet_wrap(~Raw_material, strip.position = "bottom") +
       # avoids overplotting of the labels (sample IDs)
       geom_text_repel(aes(label=Sample), size = 2,
                       nudge_x = -0.4,
                       segment.size = 0.1, force = 2,
                       seed = 123) +
       scale_y_continuous(trans = "reverse") +
       scale_x_discrete(position ="top") +
       # removes the "_" between "Contact_material in the legend
       labs(x = "Contact material") +
         theme_classic() +
       theme(legend.position = "none")

print(p3)
```

```
# save to PDF
file_out <- paste0(file_path_sans_ext(info_in[["file"]]),
                   "_depth_a_plot_", ".pdf")
ggsave(filename = file_out, plot = p3, path = dir_out,
       device = "pdf",
       width = 25, height = 17, units = "cm")


depth[["Raw_material"]] <- factor(depth[["Raw_material"]])

# plots all depth points in one facet plot (contact material separated)
p4 <- ggplot(data = depth, aes(x = Contact_material,
                               y = Depth.abs.depth, colour =
                                 Raw_material)) +
       geom_point() + labs(y = "Absolute depth (mm)") +
       # avoids overplotting of the labels (sample IDs)
       geom_text_repel(aes(label=Sample), size = 2,
                       nudge_x = -0.4,
                       segment.size = 0.1, force = 2,
                       seed = 123) +
       scale_y_continuous(trans = "reverse") +
       scale_x_discrete(position ="top") +
       # removes the "_" between "Contact_material in the legend
       labs(x = "Contact material") +
         theme_classic() +
       theme(axis.text.x = element_blank(), axis.ticks = element_blank())
+
       theme(legend.position = "none")

print(p4)
```

```
# save to PDF
file_out <- paste0(file_path_sans_ext(info_in[["file"]]),
                   "_depth_b_plot_", ".pdf")
ggsave(filename = file_out, plot = p4, path = dir_out,
       device = "pdf",
       width = 25, height = 17, units = "cm")
```

All sensor data

```
sp <- split(imp_data, imp_data[["Sample"]])

for (i in seq_along(sp)) {
  # creates a sequence of every ~ 50th strokes
  seq_st <- seq(1, length(unique(sp[[i]][["Cycle"]])), by = 40) %>%
            c(max(unique(sp[[i]][["Cycle"]])))
  dat_i_all <- sp[[i]] %>%
               filter(Cycle %in% seq_st)
  range_force_all <- range(dat_i_all[["Force"]])
  range_friction_all <- range(dat_i_all[["Friction"]])
  range_depth_all <- range(dat_i_all[["Depth"]])
  range_velocity_all <- range(dat_i_all[["Velocity"]])


    p1b <- ggplot(data = dat_i_all) +
        geom_line(aes(x = Step, y = Force, colour = Cycle, group = Cycle),
alpha = 0.3) +
        labs(x = "Step", y = "Force [N]") +
        scale_colour_continuous(trans = "reverse") +
        coord_cartesian(ylim = range_force_all) +
        scale_x_continuous(breaks=c(1, 4, 7, 10, 15, 20, 25)) +
          theme_classic()
  print(p1b)

    p2b <- ggplot(data = dat_i_all) +
        geom_line(aes(x = Step, y = Friction, colour = Cycle, group = Cycl
e), alpha = 0.3) +
        labs(x = "Step", y = "Friction [N]") +
        scale_colour_continuous(trans = "reverse") +
        coord_cartesian(ylim = range_friction_all) +
        scale_x_continuous(breaks=c(1, 4, 7, 10, 15, 20, 25)) +
          theme_classic()
  print(p2b)

  p3b <- ggplot(data = dat_i_all) +
        geom_line(aes(x = Step, y = Depth, colour = Cycle, group = Cycle),
alpha = 0.3) +
        labs(x = "Step", y = "Depth [mm]") +
        scale_colour_continuous(trans = "reverse") +
        coord_cartesian(ylim = range_depth_all) +
        scale_x_continuous(breaks=c(1, 4, 7, 10, 15, 20, 25)) +
          theme_classic()
```

```
  print(p3b)

    p4b <- ggplot(data = dat_i_all) +
        geom_line(aes(x = Step, y = Velocity, colour = Cycle, group = Cycl
e), alpha = 0.3) +
        labs(x = "Step", y = "Velocity [mm/s]") +
        scale_colour_continuous(trans = "reverse") +
        coord_cartesian(ylim = range_velocity_all) +
        scale_x_continuous(breaks=c(1, 4, 7, 10, 15, 20, 25)) +
          theme_classic()
  print(p4b)

  # patchwork plot
  pb <- p1b + p2b + p3b + p4b + plot_annotation(title = names(sp)[i]) + pl
ot_layout(ncol = 1, guides = "collect")
  print(pb)
  # save to PDF
  file_out <- paste0(file_path_sans_ext(info_in[["file"]]), "_sensors_plot
_",
                     names(sp)[i], ".pdf")
  ggsave(filename = file_out, plot = pb, path = dir_out, device = "pdf")
}
```

Penetration depth plots showing the strokes as lines

```
# plots all strokes per sample divided by 40
# splits the data in the individual 24 samples
sp <- split(imp_data, imp_data[["Sample"]])


for (i in seq_along(sp)) {
  # creates a sequence of every ~ 50th cycles
  seq_st <- seq(1, length(unique(sp[[i]][["Cycle"]])), by = 40) %>%
            c(max(unique(sp[[i]][["Cycle"]])))
  dat_i_all <- sp[[i]] %>%
               filter(Cycle %in% 1:500)
  range_depth <- range(dat_i_all[["Depth"]])
  p1 <- ggplot(data = dat_i_all, aes(x = Step, y = Depth, colour = Cycle))
+
        geom_line(aes(group = Cycle), alpha = 0.3) +
        labs(x = "Step", y = "Depth (mm)") + ylab(NULL) +
        # reverses the legend starting with 0 going to 2000 strokes
        scale_colour_continuous(trans = "reverse") +
        coord_cartesian(ylim = range_depth) +
        # changes the 'Step-number' in the x-legend
        theme_classic()

# plots only the first 125 cycles per sample
  dat_i_250 <- sp[[i]] %>%
```

```
              # takes only the first 50 cycles per sample
              filter(Cycle %in% 1:125)
  range_depth <- range(dat_i_all[["Depth"]])
  p2 <- ggplot(data = dat_i_250) +
        geom_line(aes(x = Step, y = Depth, colour = Cycle, group = Cycle),
alpha = 0.3) +
        labs(x = "Step", y = "Depth (mm)") +
        scale_colour_continuous(trans = "reverse") +
        coord_cartesian(ylim = range_depth) +
          theme_classic()

# plots only between 125 to 205 cycles per sample
  dat_i_500 <- sp[[i]] %>%
              # takes only the first 50 cycles per sample
              filter(Cycle %in% 126:250)
  range_depth <- range(dat_i_all[["Depth"]])
  p3 <- ggplot(data = dat_i_500) +
        geom_line(aes(x = Step, y = Depth, colour = Cycle, group = Cycle),
alpha = 0.3) +
        labs(x = "Step", y = "Depth (mm)") +
        scale_colour_continuous(trans = "reverse") +
        coord_cartesian(ylim = range_depth) +
          theme_classic()

  # plots only between 250 to 500 cycles per sample
  dat_i_500 <- sp[[i]] %>%
              # takes only the first 50 cycles per sample
              filter(Cycle %in% 251:500)
  range_depth <- range(dat_i_all[["Depth"]])
  p4 <- ggplot(data = dat_i_500) +
        geom_line(aes(x = Step, y = Depth, colour = Cycle, group = Cycle),
alpha = 0.3) +
        labs(x = "Step", y = "Depth (mm)") +
        scale_colour_continuous(trans = "reverse") +
        coord_cartesian(ylim = range_depth) +
          theme_classic()

  # patchwork plot
  p <- p2 + p3 + p4 + p1 +plot_annotation(title = names(sp)[i])
  print(p)

  # save to PDF
  file_out <- paste0(file_path_sans_ext(info_in[["file"]]), "_depth_plot_"
,
                names(sp)[i], ".pdf")
  ggsave(filename = file_out, plot = p, path = dir_out,
         device = "pdf")
}
```

Penetration depth plots showing the strokes as lines (Fixed dataset)

```
imp_data2 <- read_excel("../derived_data/sampl_edited.xlsx")
# replace "stroke" by "cycle"
colnames(imp_data2)[colnames(imp_data2) == "Stroke"] <- "Cycle"

# plots all strokes per sample divided by 40
# splits the data in the individual 24 samples
sp <- split(imp_data2, imp_data2[["Sample"]])


for (i in seq_along(sp)) {
  # creates a sequence of every ~ 50th cycles
  seq_st <- seq(1, length(unique(sp[[i]][["Cycle"]])), by = 40) %>%
            c(max(unique(sp[[i]][["Cycle"]])))
  dat_i_all <- sp[[i]] %>%
               filter(Cycle %in% 1:500)
  range_depth <- range(dat_i_all[["Depth"]])
  p1 <- ggplot(data = dat_i_all, aes(x = Step, y = Depth, colour = Cycle))
+
        geom_line(aes(group = Cycle), alpha = 0.3) +
        labs(x = "Step", y = "Depth (mm)") + ylab(NULL) +
        # reverses the legend starting with 0 going to 2000 strokes
        scale_colour_continuous(trans = "reverse") +
        coord_cartesian(ylim = range_depth) +
        # changes the 'Step-number' in the x-legend
        theme_classic()

# plots only the first 125 cycles per sample
  dat_i_250 <- sp[[i]] %>%
               # takes only the first 50 cycles per sample
               filter(Cycle %in% 1:125)
  range_depth <- range(dat_i_all[["Depth"]])
  p2 <- ggplot(data = dat_i_250) +
        geom_line(aes(x = Step, y = Depth, colour = Cycle, group = Cycle),
alpha = 0.3) +
        labs(x = "Step", y = "Depth (mm)") +
        scale_colour_continuous(trans = "reverse") +
        coord_cartesian(ylim = range_depth) +
          theme_classic()

# plots only between 125 to 205 cycles per sample
  dat_i_500 <- sp[[i]] %>%
               # takes only the first 50 cycles per sample
               filter(Cycle %in% 126:250)
  range_depth <- range(dat_i_all[["Depth"]])
  p3 <- ggplot(data = dat_i_500) +
        geom_line(aes(x = Step, y = Depth, colour = Cycle, group = Cycle),
alpha = 0.3) +
        labs(x = "Step", y = "Depth (mm)") +
```

```
        scale_colour_continuous(trans = "reverse") +
        coord_cartesian(ylim = range_depth) +
          theme_classic()

  # plots only between 250 to 500 cycles per sample
  dat_i_500 <- sp[[i]] %>%
              # takes only the first 50 cycles per sample
              filter(Cycle %in% 251:500)
  range_depth <- range(dat_i_all[["Depth"]])
  p4 <- ggplot(data = dat_i_500) +
        geom_line(aes(x = Step, y = Depth, colour = Cycle, group = Cycle),
alpha = 0.3) +
        labs(x = "Step", y = "Depth (mm)") +
        scale_colour_continuous(trans = "reverse") +
        coord_cartesian(ylim = range_depth) +
          theme_classic()

  # patchwork plot
  p <- p2 + p3 + p4 + p1 +plot_annotation(title = names(sp)[i])
  print(p)

  # save to PDF
  file_out <- paste0(file_path_sans_ext(info_in[["file"]]), "_fixed_data_d
epth_plot_",
                     names(sp)[i], ".pdf")
  ggsave(filename = file_out, plot = p, path = dir_out,
         device = "pdf")
}
```

Summarize the Penetration depth data

```
imp_data2 <- read_excel("../derived_data/sampl_edited.xlsx")
# replace "stroke" by "cycle"
colnames(imp_data2)[colnames(imp_data2) == "Stroke"] <- "Cycle"


nminmaxmeanmedsd <- function(x){
    y <- x[!is.na(x)]
    n_test <- length(y)
    min_test <- min(y)
    max_test <- max(y)
    mean_test <- mean(y)
    med_test <- median(y)
    sd_test <- sd(y)
    out <- c(n_test, min_test, max_test, mean_test, med_test, sd_test)
    names(out) <- c("n", "min", "max", "mean", "median", "sd")
    return(out)
}

num.var <- 7:length(imp_data2)
```

```
stats <- summaryBy(.~Raw_material + CycleGroup + Sample, data=imp_data2[c(
"Raw_material", "CycleGroup", "Sample", names(imp_data2)[num.var])], FUN=n
minmaxmeanmedsd)

write_csv(stats, "../derived_data/depth_stats.csv")
```

The files will be saved as “~/../plots.[ext]”.

```
# Save data ## Write to
XLSX (summary
statistics)
r
write.xlsx(list(depth
= depth, depth_good =
depth_good), file =
paste0(dir_out,
file_out, ".xlsx"))
Error in
buildWorkbook(x,
asTable = asTable,
...): object
'depth_good' not
found
```

Session Info() and RStudio version

```
sessionInfo()

R version 4.0.4 (2021-02-15)
Platform: x86_64-apple-darwin17.0 (64-bit)
Running under: macOS Catalina 10.15.7

Matrix products: default
BLAS:   /Library/Frameworks/R.framework/Versions/4.0/Resources/lib/libRbla
s.dylib
LAPACK: /Library/Frameworks/R.framework/Versions/4.0/Resources/lib/libRlap
ack.dylib

locale:
[1] en_US.UTF-8/en_US.UTF-8/en_US.UTF-8/C/en_US.UTF-8/en_US.UTF-8

attached base packages:
[1] tools     stats     graphics  grDevices utils     datasets  methods
[8] base

other attached packages:
 [1] readxl_1.3.1      openxlsx_4.2.4    ggrepel_0.9.1     doBy_4.6.11
 [5] patchwork_1.1.1   forcats_0.5.1     stringr_1.4.0     dplyr_1.0.7
 [9] purrr_0.3.4       readr_2.0.1       tidyr_1.1.3       tibble_3.1.4
```

```
[13] tidyverse_1.3.1   ggplot2_3.3.5     R.utils_2.10.1    R.oo_1.24.0
[17] R.methodsS3_1.8.1

loaded via a namespace (and not attached):
 [1] httr_1.4.2           bit64_4.0.5          vroom_1.5.4
 [4] jsonlite_1.7.2       modelr_0.1.8         microbenchmark_1.4-7
 [7] assertthat_0.2.1     highr_0.9            cellranger_1.1.0
[10] yaml_2.2.1           pillar_1.6.2         backports_1.2.1
[13] lattice_0.20-44      glue_1.4.2           digest_0.6.27
[16] rvest_1.0.1          colorspace_2.0-2     htmltools_0.5.2
[19] Matrix_1.3-4         pkgconfig_2.0.3      broom_0.7.9
[22] curry_0.1.1          haven_2.4.3          scales_1.1.1
[25] tzdb_0.1.2           generics_0.1.0       farver_2.1.0
[28] ellipsis_0.3.2       withr_2.4.2          cli_3.0.1
[31] magrittr_2.0.1       crayon_1.4.1         evaluate_0.14
[34] fs_1.5.0             fansi_0.5.0          MASS_7.3-54
[37] xml2_1.3.2           hms_1.1.0            lifecycle_1.0.0
[40] munsell_0.5.0        reprex_2.0.1         zip_2.2.0
[43] Deriv_4.1.3          compiler_4.0.4       rlang_0.4.11
[46] grid_4.0.4           rstudioapi_0.13      labeling_0.4.2
[49] rmarkdown_2.10       gtable_0.3.0         DBI_1.1.1
[52] R6_2.5.1             lubridate_1.7.10     knitr_1.33
[55] bit_4.0.4            fastmap_1.1.0        utf8_1.2.2
[58] stringi_1.7.4        parallel_4.0.4       Rcpp_1.0.7
[61] vctrs_0.3.8          dbplyr_2.1.1         tidyselect_1.1.1
[64] xfun_0.25
```

END OF SCRIPT

Plots 3D data

Joao Marreiros and David Nora

2021-09-27 15:18:39

Goal of the script

This script reads and plots all the 3D edge reduction data

```
dir_in <- "../raw_data"
dir_out <- "../plots"
```

Raw data must be located in ~/../raw_data.
Formatted data will be saved in ~/../plots. The knit directory for this script is the project directory.

Load packages

```
library(R.utils)
library(ggplot2)
library(tools)
library(tidyverse)
```

```
Warning: package 'readr' was built under R version 4.1.1
```

```
library(patchwork)
library(doBy)
library(ggrepel)
library(openxlsx)
library(flextable)
```

```
Warning: package 'flextable' was built under R version 4.1.1
```

```
library(janitor)
```

Get name, path and information of the file

```
data_file <- list.files(dir_in, pattern = "\\.csv$", full.names = TRUE)
md5_in <- md5sum(data_file)
info_in <- data.frame(file = basename(names(md5_in)), checksum = md5_in, r
ow.names = NULL)
info_in
```

```
        file                             checksum
1 3dedge.csv 52ee9086fd16a8f24cda909b13913408
```

Load data db

```
imp_data <- read_csv("../raw_data/3dedge.csv")
str(imp_data)
```

```
spec_tbl_df [10,915 x 8] (S3: spec_tbl_df/tbl_df/tbl/data.frame)
 $ ID          : chr [1:10915] "DAC3-2" "DAC3-2" "DAC3-2" "DAC3-2" ...
 $ raw.material: chr [1:10915] "dacite" "dacite" "dacite" "dacite" ...
 $ cycle       : chr [1:10915] "0-125" "0-125" "0-125" "0-125" ...
 $ class       : num [1:10915] 1 2 3 4 5 6 7 8 9 10 ...
 $ value       : num [1:10915] 29 35 26 27 26 38 22 26 25 19 ...
 $ end         : num [1:10915] 0.2 0.202 0.204 0.206 0.208 ...
 $ start       : num [1:10915] 0.202 0.204 0.206 0.208 0.209 ...
 $ ...8        : logi [1:10915] NA NA NA NA NA NA ...
 - attr(*, "spec")=
  .. cols(
  ..   ID = col_character(),
  ..   raw.material = col_character(),
  ..   cycle = col_character(),
  ..   class = col_double(),
  ..   value = col_double(),
  ..   end = col_double(),
  ..   start = col_double(),
  ..   ...8 = col_logical()
  .. )
 - attr(*, "problems")=<externalptr>
```

Summarize data

```
# General overview

nminmaxmeanmedsd <- function(x){
    y <- x[!is.na(x)]
    n_test <- length(y)
    min_test <- min(y)
    max_test <- max(y)
    mean_test <- mean(y)
    med_test <- median(y)
    sd_test <- sd(y)
    out <- c(n_test, min_test, max_test, mean_test, med_test, sd_test)
    names(out) <- c("n", "min", "max", "mean", "median", "sd")
    return(out)
}

num.var <- 6:length(imp_data)

stats <- summaryBy(.~raw.material + cycle + ID, data=imp_data[c("raw.mater
ial","cycle", "ID", names(imp_data)[num.var])], FUN=nminmaxmeanmedsd)
```

```
write_csv(stats, "../derived_data/stats.csv")


# Summarizin number of parts per cycle, per raw material

imp_data$cycle <- factor(imp_data$cycle, levels = c("0-125", "125-250", "2
50-500", "0-500"))
imp_data$raw.material <- factor(imp_data$raw.material, levels = c("flint",
"obsidian", "dacite", "quartzite"))

parts <- imp_data %>%
  group_by(raw.material, cycle) %>%
  summarize(total = n()) %>%
  pivot_wider(names_from = "cycle",
              values_from = "total",
              values_fill = 0) %>%
  adorn_totals(where = c("row", "col"), fill = "") %>%
  rename("Raw material" = raw.material)

print(parts)
```

```
 Raw material 0-125 125-250 250-500 0-500 Total
        flint   612     696     560   688  2556
     obsidian   712     708     580   656  2656
       dacite   728     744     767   744  2983
    quartzite   748     768     584   620  2720
        Total  2800    2916    2491  2708 10915
```

```
write_csv(parts, "../derived_data/parts.csv")
```

Plots summarized data

Plot Max distance between samples

```
# gets new order
stats$cycle <- factor(stats$cycle, levels = c("0-125", "125-250", "250-500
", "0-500"))
stats$raw.material <- factor(stats$raw.material, levels = c("flint", "obsi
dian", "dacite", "quartzite"))



stats.plot <- ggplot(data = stats) +
              geom_point(mapping = aes(x = raw.material, y = end.max, colo
ur = raw.material)) +
              theme_classic() +
              labs(colour = "Raw material", x = "Raw material", y = "Maxim
um distance (mm)", title = "Max distance") +
              facet_wrap(~ cycle)
```

```
print(stats.plot)
```

```
ggsave("../plots/endmax.png")
```

Plot distance intervals and number of counts

```
# filter db, only observations where distance is > 0.2 mm

# gets new order
imp_data$cycle <- factor(imp_data$cycle, levels = c("0-125", "125-250", "2
50-500", "0-500"))
imp_data$raw.material <- factor(imp_data$raw.material, levels = c("flint",
"obsidian", "dacite", "quartzite"))

counts.plot <-ggplot(data = imp_data) +
              geom_point(mapping = aes(x = end, y = value, colour = raw.ma
terial), size = 0.5) +
              theme_classic() +
              labs(colour = "Raw material", x = "Distance (mm)", y = "Numb
er of parts", title = "All raw materials") +
              facet_wrap(~ cycle)

print(counts.plot)
```

```
ggsave("../plots/counts.png")

# Flint
imp_data$cycle <- factor(imp_data$cycle, levels = c("0-125", "125-250", "2
50-500", "0-500"))
imp_data$raw.material <- factor(imp_data$raw.material, levels = c("flint",
"obsidian", "dacite", "quartzite"))

counts.plot.flt <-ggplot(subset(imp_data, raw.material=="flint")) +
              geom_point(mapping = aes(x = end, y = value, colour = ID), s
ize = 0.5) +
              theme_classic() +
              labs(colour = "ID", x = "Distance (mm)", y = "Number of part
s", title = "Flint") +
              facet_wrap(~ cycle)

print(counts.plot.flt)
```

```
ggsave("../plots/flt.png")

# Quartzite
```

```
imp_data$cycle <- factor(imp_data$cycle, levels = c("0-125", "125-250", "250-500", "0-500"))
imp_data$raw.material <- factor(imp_data$raw.material, levels = c("flint", "obsidian", "dacite", "quartzite"))


counts.plot.qrtz <-ggplot(subset(imp_data, raw.material=="quartzite")) +
              geom_point(mapping = aes(x = end, y = value, colour = ID), size = 0.5) +
              theme_classic() +
              labs(colour = "ID", x = "Distance (mm)", y = "Number of parts", title =  "Quarzite") +
              facet_wrap(~ cycle)

print(counts.plot.qrtz)
```

```
ggsave("../plots/qrtz.png")

# Obsidian
imp_data$cycle <- factor(imp_data$cycle, levels = c("0-125", "125-250", "250-500", "0-500"))
imp_data$raw.material <- factor(imp_data$raw.material, levels = c("flint", "obsidian", "dacite", "quartzite"))


counts.plot.obs <-ggplot(subset(imp_data, raw.material=="obsidian")) +
              geom_point(mapping = aes(x = end, y = value, colour = ID), size = 0.5) +
              theme_classic() +
              labs(colour = "ID", x = "Distance (mm)", y = "Number of parts", title = "Obsidian") +
              facet_wrap(~ cycle)

print(counts.plot.obs)
```

```
ggsave("../plots/obs.png")

# Dacite
imp_data$cycle <- factor(imp_data$cycle, levels = c("0-125", "125-250", "250-500", "0-500"))
imp_data$raw.material <- factor(imp_data$raw.material, levels = c("flint", "obsidian", "dacite", "quartzite"))


counts.plot.dac <-ggplot(subset(imp_data, raw.material=="dacite")) +
              geom_point(mapping = aes(x = end, y = value, colour = ID), size = 0.5) +
```

```
              theme_classic() +
              labs(colour = "ID", x = "Distance (mm)", y = "Number of part
s", title = "Dacite") +
              facet_wrap(~ cycle)

print(counts.plot.dac)
```

```
ggsave("../plots/dac.png")
```

Session Info() and RStudio version

```
sessionInfo()
```

```
R version 4.1.0 (2021-05-18)
Platform: x86_64-w64-mingw32/x64 (64-bit)
Running under: Windows 10 x64 (build 19043)

Matrix products: default

locale:
[1] LC_COLLATE=English_United States.1252
[2] LC_CTYPE=English_United States.1252
[3] LC_MONETARY=English_United States.1252
[4] LC_NUMERIC=C
[5] LC_TIME=English_United States.1252

attached base packages:
[1] tools     stats     graphics  grDevices utils     datasets  methods
[8] base

other attached packages:
 [1] janitor_2.1.0     flextable_0.6.8   openxlsx_4.2.4    ggrepel_0.9.1
 [5] doBy_4.6.11       patchwork_1.1.1   forcats_0.5.1     stringr_1.4.0
 [9] dplyr_1.0.7       purrr_0.3.4       readr_2.0.1       tidyr_1.1.3
[13] tibble_3.1.2      tidyverse_1.3.1   ggplot2_3.3.5     R.utils_2.10.1
[17] R.oo_1.24.0       R.methodsS3_1.8.1

loaded via a namespace (and not attached):
 [1] fs_1.5.0             lubridate_1.7.10     bit64_4.0.5
 [4] httr_1.4.2           Deriv_4.1.3          backports_1.2.1
 [7] utf8_1.2.1           R6_2.5.1             DBI_1.1.1
[10] colorspace_2.0-2     withr_2.4.2          tidyselect_1.1.1
[13] bit_4.0.4            compiler_4.1.0       cli_3.0.1
[16] rvest_1.0.1          xml2_1.3.2           microbenchmark_1.4-7
[19] officer_0.4.0        labeling_0.4.2       scales_1.1.1
[22] systemfonts_1.0.2    digest_0.6.27        rmarkdown_2.11
[25] base64enc_0.1-3      pkgconfig_2.0.3      htmltools_0.5.2
```

```
[28] highr_0.9            dbplyr_2.1.1        fastmap_1.1.0
[31] rlang_0.4.11         readxl_1.3.1        rstudioapi_0.13
[34] farver_2.1.0         generics_0.1.0      jsonlite_1.7.2
[37] vroom_1.5.5          zip_2.2.0           magrittr_2.0.1
[40] Matrix_1.3-3         Rcpp_1.0.7          munsell_0.5.0
[43] fansi_0.5.0          gdtools_0.2.3       lifecycle_1.0.0
[46] stringi_1.7.4        yaml_2.2.1          snakecase_0.11.0
[49] MASS_7.3-54          grid_4.1.0          parallel_4.1.0
[52] crayon_1.4.1         lattice_0.20-44     haven_2.4.3
[55] hms_1.1.0            knitr_1.34          pillar_1.6.2
[58] uuid_0.1-4           curry_0.1.1         reprex_2.0.1
[61] glue_1.4.2           evaluate_0.14       data.table_1.14.0
[64] modelr_0.1.8         vctrs_0.3.8         tzdb_0.1.2
[67] cellranger_1.1.0     gtable_0.3.0        assertthat_0.2.1
[70] xfun_0.26            broom_0.7.9         ellipsis_0.3.2
```

END OF SCRIPT

Appendix C: Workflows

CloudCompare Version 2.12 alpha [Windows 64-bit] *Complied with MSVC 1916 and 5.15.2*
License: GNU GPL (General Public Licence).

Nora, 2021. The role of lithic raw materials on tool performance and use: The efficiency and durability on stone tools edge.

CloudCompare workflow

1. **Import** the two .stl files (before and after
2. **Align** 3D models
    a. **Select the two meshes**.
    b. Registration **and Match Bounding-box centers**
    c. Registration and **Align** (points pair picking)
    d. Registration and **Fine registration** (ICP)
3. **Compare** the two meshes[1]
    a. **Select the two** meshes
    b. Compute **Cloud/Mesh distance**
    c. Compute
    d. Select only the "**registered**" mesh
    e. In **Properties/SF display params/Display ranges**
        i. Set displayed values to 0.2 mm (3D Scanner accuracy and baby powder layer)
        ii. Make the Color Scale visible
        iii. In the Parameters bar **unselect "show NaN/ out of range values in grey"**
4. Get **comparison** data
    a. Select only the "registered" mesh
    b. Show Histogram
    c. Export Histogram to a .CSV file
    d. Export Histogram to image to .PNG

[1] Combinations: 0-250, 250-500, 500-1000 and 0-1000

GOM Inspect Workflow

Mesh Treatment

1. **Import** the stage 0 .stl file (alternative: ply) import STL as target element type: mesh → ok
2. **Eliminate Mesh Errors**
    a. RMC (right mouse click) **Select all points of Element**
    b. **Operations → Mesh → Other → Eliminate Mesh Errors → Apply**
3. **Align 3D model**
    a. RMC on the Left back of the screen X, Y, Z icon to establish Matrix
    b. RMC **Select all points of Element**
    c. **Operations → Alignment → Manual Alignment →** Set Matrix (Settings[2])
    d. Change Rotation values until your object is aligned
    e. Change Translation to set your object to the 0/0/0 (zero) point[3] → **Ok**
4. **Cut 3D model**
    a. RMC → **Select/Deselect Trough Surface** (Ctrl+Shift+Space) → Close the select area LMC
    b. **Delete** select 3D area (Ctrl+Del)
5. **Export Mesh** as a .stl file. (File → Export → .stl).
6. **Close Project.**

Aligned Cut

1. **Cut 3D Models aligned**
    a. **Import** the stage 0 (zero) .stl file **aligned cut** (add Part)
    b. RMC **Select all points of Element → Operations → CAD → Actual Mesh to CAD**
2. **Import** mesh stg250_rawdata .stl file (second 3D model)
    a. **Operations → Alignment → Initial Alignment → Prealignment**[4] (At this stage both 3D models are overlap).

---

[2] Coordinate System: Global coordinate system

Part choice: Part.

[3] Note: Check always different position by RMC on the left back X / Y / Z Icon.

[4] Search Time: Long

b. **Cut the mesh** at the same line as the stage 0 (zero) → RMC → **Select/Deselect Trough Surface** (Ctrl+Shift+Space) → Close the select area LMC

7. **Export Mesh** as a .stl file. (File → Export → .stl)
8. **Repeat the aligned cut for the others 3D's models.**

Appendix D: Hardness Reports